UNIVERSITA' DEGLI STUDI DI MILANO-BICOCCA

SCUOLA DI DOTTORATO DI SCIENZE

Facoltà di Scienze Matematiche, Fisiche e Naturali
Corso di Dottorato di Ricerca in Biotecnologie Industriali, XXV ciclo

Nuclear Magnetic Resonance Characterization of β-amyloid peptides and their interactions with anti-amyloidogenic compounds

Tutor: Prof. Francesco Nicotra

Co-Tutor: Dr.ssa Cristina Airoldi

Erika Sironi

Dipartimento di Biotecnologie e Bioscienze

INDEX

Riassunto

Il morbo di Alzheimer è una malattia neurodegenerativa che colpisce più di 30 milioni di persone al mondo. Nonostante l'intensa attività di ricerca, non esiste ancora una vera e propria cura per questa patologia, ma la terapia è limitata all'uso di farmaci palliativi, che hanno il solo scopo di alleviarne i sintomi. Ne deriva che il morbo di Alzheimer ha un forte impatto sociale ed economico non solo sulla vita dei pazienti, ma anche su quella dei loro familiari e, dato l'incremento progressivo dell'aspettativa di vita nei Paesi industrializzati, e il conseguente maggior numero di persone che potranno sviluppare la malattia in futuro, la ricerca di terapie efficaci e metodi di diagnosi per questa patologia rappresentano un obiettivo di primaria importanza. I meccanismi genetici e molecolari che portano allo sviluppo del morbo di Alzheimer non sono stati ancora del tutto chiariti, tuttavia una caratteristica dominante della patologia è rappresentata dall'accumulo di peptidi β-amiloidi (Aβ) in forma di aggregati oligomerici e fibrillari nel cervello.[1,2,3,4]

Tra le diverse strategie per lo sviluppo di una terapia contro il morbo di Alzheimer c'è la possibilità di utilizzare piccole molecole in grado di legare i peptidi amiloidi ed inibirne il processo di aggregazione. Ligandi degli aggregati amiloidi rappresenterebbero inoltre dei potenziali strumenti per una diagnosi

[1] J. Hardy, D. Allsop , **"**Amyloid deposition as the central event in the aetiology of Alzheimer's disease", *Trends. Pharmacol. Sci*.,**1991,** 12**,** 383-388.

[2] C. J. Pike, D. Burdick, A.J. Walencewicz, C.G. Glabe , C.W. Cotman, "Neurodegeneration induced by beta-amyloid peptides in vitro: the role of peptide assembly state", *J. Neurosci.*, **1993**, 13**,** 1676-1687.

[3] D. J. Selkoe, "Towards a comprehensive theory for Alzheimer's disease. Hypothesis: Alzheimer's disease is caused by the cerebral accumulation and citotoxicity of amyloid beta-protein" *Ann. N. Y. Acad. Sci.*, **2000**, 924, 17-25.

[4] K. Ono, M. Yamada, "Antioxidant compounds have potent anti-fibrillogenic and fibril-destabilizing effects for alpha-synuclein fibrils *in vitro", J. Neurochem*., **2006**, 97, 105-115.

precoce della malattia, che allo stato attuale può essere eseguita con certezza solo *post mortem*.

Molte piccole molecole, sia composti naturali che di sintesi, dotate di attività anti-amiloidogenica sono già note. Si tratta in genere di molecole caratterizzate dalla presenza di strutture aromatiche ed idrofobiche, che sono probabilmente essenziali per l'interazione con i residui idrofobici dei peptidi Aβ, ma il cui meccanismo d'azione a livello molecolare non è ancora stato spiegato. Molte di queste molecole sono inoltre scarsamente stabili o solubili in condizioni fisiologiche, e alcune di esse possiedono proprietà farmacologiche non correlate con il morbo di Alzheimer (come l'attività antibiotica delle tetracicline), che rendono ancora più difficile la valutazione della loro attività come anti-amiloidogenici. L'obiettivo di questa tesi è stato rappresentato dallo studio, condotto principalmente tramite l'uso della spettroscopia di risonanza magnetica nucleare (NMR), dell'interazione tra i peptidi β-amiloidi e piccole molecole già note per la loro attività anti-amiloidogenica (tetraciclina, curcumina, acido rosmarinico), in modo da ottenere maggiori dettagli riguardo al loro possibile meccanismo d'azione. Le informazioni ricavate sono state poi utilizzate per la progettazione e sintesi di nuovi ligandi dei peptidi Aβ, potenzialmente utilizzabili come strumenti per la terapia e la diagnosi del morbo di Alzheimer.

1. STUDIO DELL'INTERAZIONE TRA TETRACICLINA E PEPTIDI β-AMILOIDI, E SVILUPPO DI COMPOSTI TRICICLICI GLICOFUSI QUALI NUOVI LIGANDI DEGLI Aβ [5,6]

La tetraciclina (**1**) (**Figura 1**) rappresenta un candidato di particolare interesse per la progettazione di composti con specifica attività anti-amiloidogenica. E' stata già dimostrata infatti la sua capacità di inibire l'aggregazione dei peptidi Aβ e di destabilizzarne eventuali aggregati preformati.[7]

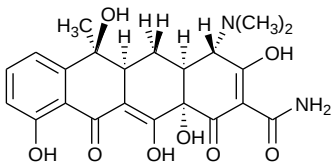

1

Figura 1. Struttura della tetraciclina

Poiché il meccanismo d'azione della tetraciclina come composto anti-amiloidogenico non è ancora stato chiarito, sono stati effettuati esperimenti NMR per l'identificazione del sito di legame tra tetraciclina e peptidi Aβ. Esperimenti STD (*Saturation Transfer Difference*)-NMR[8] e trNOESY hanno dimostrato l'interazione diretta tra la tetraciclina e forme oligomeriche dei peptidi Aβ1-40 e Aβ1-42, ma non hanno evidenziato uno specifico sito di legame della tetraciclina, se non un maggior contributo all'interazione da parte

[5] C. Airoldi, L. Colombo, C. Manzoni, E. Sironi, A. Natalello, S. M. Doglia, G. Forloni, F. Tagliavini, E. Del Favero, L. Cantù, F. Nicotra, M. Salmona , "Tetracycline prevents Aβ peptide toxicity through an atypical supramolecular interaction", *Org. Biomol. Chem*., **2011**, 9,463

[6] a) C. Airoldi, F. Cardona, E. Sironi, L. Colombo, M. Salmona, A. Silva, F. Nicotra, B. La Ferla, "cis-glyco-fused benzopyran compounds as new amyloid β peptide ligands", *Chem. Commun*., 2011, **47**, 10266-10268; b) Patent n° RM2011A000264

[7] G. Forloni, M. Salmona, G. Marcon, F. Tagliavini, "Tetracyclines and prion infectivity", *Infectious disorders: drug targets,* **2009**, 9, 23-30.

[8] a) B. Meyer, T. Peters, "NMR Spectroscopy techniques for screening and identifying ligand binding to protein receptors", *Angew. Chem. Int. Ed.,* **2003**, 42, 864; b) M. Mayer, T. L. James, "Detecting ligand binding to a small RNA target via saturation transfer difference NMR experiments in D2O and H2O", *JACS*, **2002**, 124, 13376-13377.

della porzione aromatica. Non si è osservata invece interazione tra tetraciclina e forme monomeriche del peptide. Analisi di *Dynamic Light Scattering* (DLS) hanno mostrato che l'aggiunta di tetraciclina ad una soluzione fresca di peptide Aβ1-40 genera l'immediata formazione di grandi aggregati, più grandi di quelli formati dal peptide da solo, ma che risultano stabili nel tempo, a differenza di quelli formati dal solo peptide, che continuano invece ad accrescersi. Analisi di Microscopia a Forza Atomica (AFM), eseguite per chiarire la natura degli aggregati formati dalla co-incubazione dei peptidi Aβ con la tetraciclina, hanno mostrato anch'esse che la codissoluzione di tetraciclina e peptidi Aβ genera immediatamente grossi aggregati, con aspetto differente da quello degli aggregati oligomerici generati dal solo peptide. Si è quindi ipotizzato che la tetraciclina, quando co-disciolta con i peptidi Aβ, generi immediatamente grossi complessi supramolecolari capaci di rallentare la formazione di aggregati fibrillari e la progressione della cascata amiloide.

La tetraciclina tuttavia, così come numerosi altri composti anti-amiloidogenici, presenta alcuni difetti, quali la scarsa solubilità in acqua in condizioni fisiologiche e l'instabilità alle alte temperature, e possiede inoltre un'attività antibiotica che non consente di valutare in modo corretto le sue proprietà terapeutiche nei confronti del morbo di Alzheimer. Queste sono le ragioni per cui sono state progettate e sintetizzate nuove molecole tricicliche glicofuse (**Figura 2**), quali mimetici della tetraciclina e nuovi potenziali ligandi degli Aβ.[6]

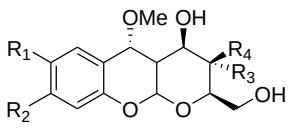

Figura 2. Struttura generale delle molecole tricicliche glicofuse progettate.

E‘ stata generata una piccola libreria di queste molecole utilizzando *O*-idrossibenzaldeidi diversamente sostituite (composti **2**-**8**) e utilizzando sia il glucale che il galattale come zuccheri (composti **9**-**10**) (**Schema 1**).

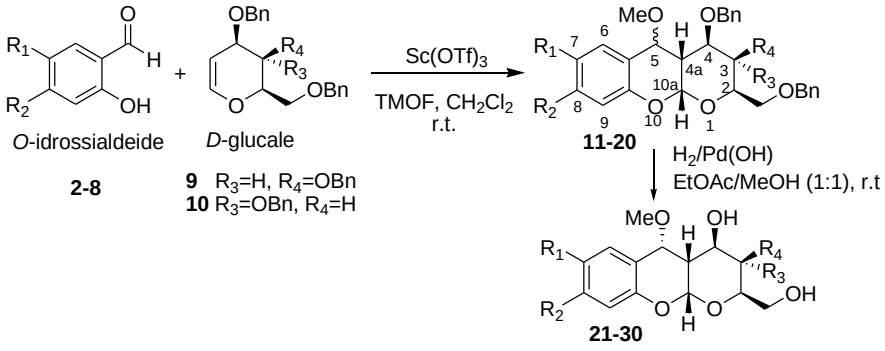

Schema 1. Procedura sintetica per la produzione dei composti triciclici glicofusi.

Sono stati ottenuti i composti **11**-**20** (resa 21-91%), ma a differenza di quanto già riportato in letteratura,[9] le reazioni hanno fornito una miscela di diastereoisomeri al C5, presenti in proporzioni diverse, che sono stati poi deprotetti generando i composti finali **21**-**30** (**Tabella 1**).

[9] J. S. Yadav, B. V. S. Reddy, L. Chandraiah, B. Jagannadh, S. K. Kumar and A. C. Kunwar, “Sc(OTf)3-catalyzed synthesis of pyrano[3,2-*b*]-1-benzopyrans from D-glycals”, *Tetrahedron Letters*, **2002**, 43, 4527-4530.

O-idrossibenzaldeidi	D-glucale	Prodotti protetti	C5 R/S (resa%)	Composti deprotetti C5 R (resa%)
2 R_1,R_2= H,H	**9**	**11**R_1,R_2,R_3,R_4= H,H,H,OBn	92/8 (59%)	**21** R_1,R_2,R_3,R_4= H,H,H,OH (97%)
3 R_1,R_2= NO_2,H	**9**	**12** R_1,R_2,R_3,R_4= NO_2,H,H,OBn	100/0 (40%)	**22** R_1,R_2,R_3,R_4= NH_2,H,H,OH (94%)
4 R_1,R_2= OBn,H	**9**	**13** R_1,R_2,R_3,R_4= OBn,H,H,OBn	100/0 (35%)	**23** R_1,R_2,R_3,R_4= OH,H,H,OH (100%)
5 R_1,R_2= OMe,H	**9**	**14** R_1,R_2,R_3,R_4= OMe,H,H,OBn	85/15 (73%)	**24** R_1,R_2,R_3,R_4= OMe,H,H,OH (96%)
6 R_1,R_2= CH_3,H	**9**	**15** R_1,R_2,R_3,R_4= CH_3,H,H,OBn	95/5 (91%)	**25** R_1,R_2,R_3,R_4= CH_3,H,H,OH (95%)
7 R_1,R_2= H, OMe	**9**	**16** R_1,R_2,R_3,R_4= H,OMe,H,OBn	53/47 (64%)	**26** R_1,R_2,R_3,R_4= H,OMe,H,OH (97%)
8 R_1,R_2= H,CH_3	**9**	**17** R_1,R_2,R_3,R_4= H,CH_3,H,OBn	100/0 (45%)	**27** R_1,R_2,R_3,R_4= H,CH_3,H,OH (97%)
6	**10**	**18** R_1,R_2,R_3,R_4= CH_3,H,OBn,H	100/0 (66%)	**28** R_1,R_2,R_3,R_4= CH_3,H,OH,H (98%)
7	**10**	**19** R_1,R_2,R_3,R_4= H,OMe,OBn,H	100/0 (37%)	**29** R_1,R_2,R_3,R_4= H,OMe,OH,H (97%)
8	**10**	**20** R_1,R_2,R_3,R_4= H, CH_3, OBn,H	100/0 (21%)	**30** R_1,R_2,R_3,R_4= H, CH_3, OH,H (98%)

Tabella 1. Composti triciclici glicofusi sintetizzati

I composti **21**-**30** conservano una struttura aromatica che sembra giocare un ruolo chiave nell'interazione della tetraciclina con i peptidi Aβ, ma possiedono anche una componente zuccherina che aumenta la loro solubilità in acqua e ne permette l'opportuna funzionalizzazione per la coniugazione a nanoparticelle, fluorofori, supporti polimerici e altre strutture che possano risultare utili per applicazioni diagnostiche e terapeutiche. Sono inoltre chimicamente stabili e, a differenza della tetraciclina, non presentano attività antibiotica.

Esperimenti STD-NMR e trNOESY hanno mostrato che tutte le molecole sintetizzate sono ligandi di forme oligomeriche dei peptidi Aβ, con l'eccezione

del composto **22,** che presenta un'ammina come sostituente sull'anello aromatico.

I composti **25**, **27**, **28** e **30**, che presentano un gruppo metile come sostituente sull'anello aromatico, si sono rivelati i ligandi con la maggiore affinità, seguiti dai composti **24**, **26** e **29**, che presentano un gruppo *O*-metile come sostituente, e dal composto **21**, che non presenta sostituenti sull'anello aromatico. Infine il composto **23**, che ha un gruppo ossidrile in posizione 7, è quello meno affine. Si può concludere che minore è la polarità dei sostituenti sull'anello aromatico, maggiore risulta essere l'affinità del composto per l'Aβ1-42. Inoltre, la posizione dei sostituenti sull'anello aromatico (posizione 7 o 8), così come la natura dell'entità zuccherina, risultano non rilevanti ai fini dell'interazione, come dimostrato dall'uguale affinità dei composti **25**, **27**, **28**, **30** e dei composti **24**, **26** e **29**.

Per verificare che solo la polarità del sostituente sull'anello aromatico fosse responsabile della diversa affinità, è stata effettuata un'analisi conformazionale di tutti i composti tramite simulazioni di dinamica e meccanica molecolare, utilizzando il campo di forza MM3*[[10,11]] implementato nel programma MacroModel.[[12]] Le simulazioni dimostrano che i composti **21**-**30** presentano tutti la stessa conformazione tridimensionale, e quindi le differenze di affinità per il peptide sono effettivamente dovute alla natura dei sostituenti sull'anello aromatico e non a differenze conformazionali.

[10] N. L. Allinger, Y. H. Yuh and J. H. Lii, "Molecular mechanics force-field development for amino acid zwitterions", *J. Am. Chem. Soc*., **1989**, 111, 8551–8566.
[11] M. Martın-Pastor, J. F. Espinosa, J. L. Asensio and J. Jimenez- Barbero, *Carbohydr. Res*., "A comparison of the geometry and of the energy results obtained by application of different molecular mechanics force fields to methyl α lactoside and the C-analog of lactose", **1997**, 298, 15–49.
[12] MacroModel, **2008**, 9.6 ed. Schrödinger, LLC, New York

E’ stato sintetizzato in seguito un derivato fluorescente (composto **31**) di uno dei composti triciclici che hanno maggiore affinità di legame, coniugando la cumarina, un piccolo fluoroforo, al composto **27**. (**Figura 3**).

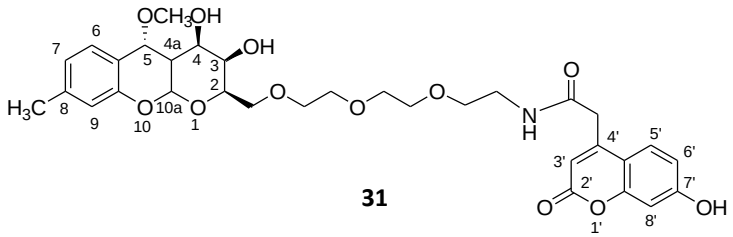

31

Figura 3. Derivato fluorescente del composto **30**

Esperimenti STD-NMR hanno confermato che questo derivato conserva le proprietà di legame all’Aβ1-42. Inoltre, esperimenti di microscopia di fluorescenza, effettuati in collaborazione con l’istituto di Ricerche Farmacologiche M. Negri, hanno mostrato che questa molecola è in grado di legare placche amiloidi presenti in sezioni di cervello di topi transgenici portatori del morbo di Alzheimer. Ulteriori esperimenti hanno dimostrato inoltre che il composto **31**, grazie ad un opportuno bilanciamento delle sue proprietà di idrofilia/idrofobicità, è in grado di attraversare, probabilmente tramite un meccanismo di diffusione, un modello cellulare *in vitro* di barriera emato-encefalica. Esso rappresenta quindi un candidato molto promettente per lo sviluppo di strumenti diagnostici e terapeutici per la cura del morbo di Alzheimer.[[13]]

[[13]] C. Airoldi, F. Cardona, E. Sironi, L. Colombo, M. Salmona, I. Cambianica, F. Ornaghi, G. Sancini, F.Nicotra, B.a La Ferla, “Fluorescent Amyloid β peptide ligand derivatives as potential diagnostic tools for Alzheimer disease”, **2012**, submitted

2. STUDIO DELL'INTERAZIONE TRA DERIVATI DELLA CURCUMINA E FORME OLIGOMERICHE DEL PEPTIDE Aβ [14]

Un'altra piccola molecola di interesse per lo sviluppo di potenziali farmaci contro il morbo di Alzheimer è la curcumina (**32**) (**Figura 4**), un composto naturale con ampia varietà di effetti biologici.[15,16,17]

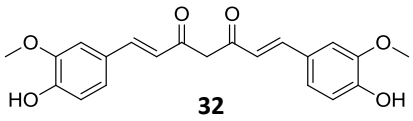

32

Figura 4. Struttura della curcumina

Nel 2001 Lim et al.[18] dimostrarono che la curcumina è in grado di bloccare la patogenesi dell'Alzheimer; nonostante ciò, gli effetti diretti della curcumina sulla formazione e la destabilizzazione degli aggregati amiloidi rimane poco chiara. Nel 2007, Reinke et al.[19] studiarono la correlazione struttura-attività di inibitori dell'aggregazione dei peptidi β-amiloidi basati sulla struttura della curcumina: la coplanarità dei due anelli aromatici e la distanza tra essi (da 8 a 16 Å) si rivelarono elementi fondamentali ai fini dell'interazione. Sulla base di queste informazioni sono stati sintetizzati una serie di derivati della curcumina

[14] C. Airoldi, C. Zona, E. Sironi, L. Colombo, M. Messa, D. Aurilia, M. Gregori, M. Masserini, M. Salmona, F. Nicotra, B. La Ferla, "Curcumin derivative sas new ligands of Aβ peptides", *Journal of Biotechnology*, **2011**, 56, 4, 317–324.

[15] A. Goel, A.B. Kunnumakkara, B.B. Aggarwal, "Curcumina s curecumin: from kitchen to clinic", *Biochem. Pharmacol.*, **2008**, 75, 787-809.

[16] B.L. Zhao, X. J. Li, R.G. He, S.J. Cheng, ; W.J. Xin, "Scavenging effect of extracts of green tea and natural antioxidants on active oxygen radicals", *Cell. Biophys.*, **1989**, 14, 175-185.

[17] T. Thomas, G. Nadackal, K. Thomas, "Aspirin and non-steroidal anti-inflammatory drugs inhibit amyloid-beta aggregation", *NeuroReport*, **2001**, 12, 3263-3267.

[18] G.P. Lim, T. Chu, F. Yang, W. Beech, S.A. Frautschy, G.M. Cole, "The curry spice curcumin reduces oxidative damage and amyloid pathology in an Alzheimer transgenic mouse", *J. Neurosci.*, **2001**, 21, 8370-8377.

[19] A.A. Reinke, J.E. Gestwicki, "Structure –activity relationships of amyloid-beta aggregation inhibitors based on curcumin: influence of linker lenght and flexibility", *Chem. Biol. Drug. Des.*, **2007**, 70, 206-215.

(**Schema 2**, molecole **33**-**37**) che rispettano questi parametri e sono inoltre stabili e solubili in condizioni fisiologiche, a differenza della molecola capostipite.[20]

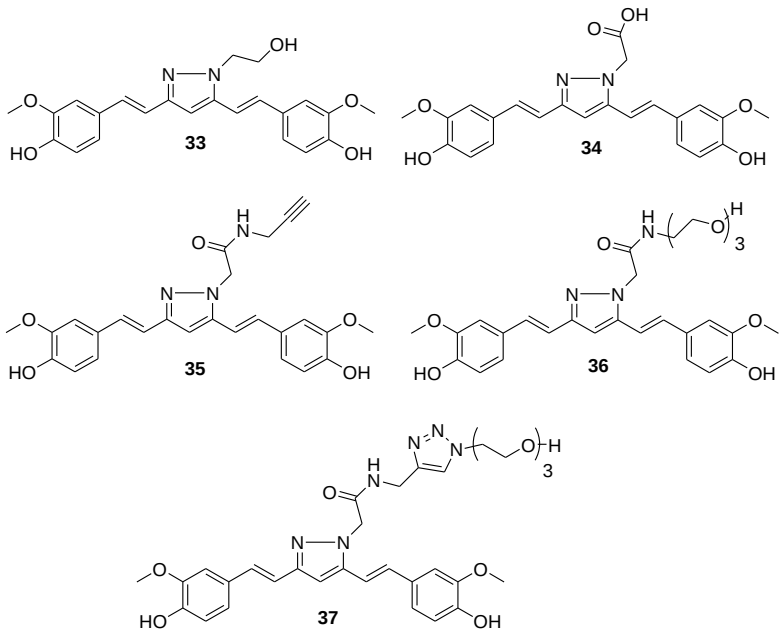

Schema 2. Derivati della curcumina

La capacità di queste molecole di interagire *in vitro* con forme oligomeriche del peptide Aβ è stata confermata attraverso esperimenti STD-NMR, i quali hanno mostrato che la porzione maggiormente coinvolta nell'interazione è rappresentata dal sistema aromatico della curcumina, mentre le diverse catene presenti sull'anello pirazolico non contribuiscono in modo significativo al

[20] a) M. Bernabe-Pineda, M.T. Ramirez-Silva, M. Romero-Romo, E. Gonzalez-Vergara, A. Rojas-Hernandez, "Determination of acidity constants of curcumin in aqueous solution and apparent rate constant of its decomposition", *Spectrochim. Acta A Mol Biomol Spectrosc*, **2004**, 60, 1091-7. b) Y.J. Wang, M.H. Pan, A.L. Cheng, L.I. Lin, Y.S. Ho, C.Y. Hsieh, J.K. Lin, "Stability of curcumin in buffer solutions and characterization of ist degradation products" , *J. Pharm. Biomed. Anal.*, **1997**, 15, 1867-76. c) H.H. Tonnesen, J. Karlsen, *Z. Lebensm. ,* "Studies on curcumin and curcuminoids. VI. Kinetics of curcumin degradation in aqueous solution", *Unters Forsch*, **1985**, 180, 402-4.

legame. Gli esperimenti STD hanno consentito di classificare i composti **33**-**37** in base alla loro affinità di legame: il composto **34** è quello che presenta la maggiore affinità, mentre i composti **33** e **35** sono quelli che presentano l'affinità minore.

Esperimenti di microscopia di fluorescenza analoghi a quelli effettuati per il composto **31** hanno inoltre dimostrato che anche queste molecole sono in grado di legare depositi amiloidi presenti in sezioni di cervelli di topi esprimenti la malattia di Alzheimer.

I dati raccolti riguardanti queste molecole sono di particolare interesse per la futura produzione di nanoparticelle opportunamente funzionalizzate per l'attraversamento della barriera emato-encefalica e volte alla terapia e alla diagnosi del morbo di Alzheimer.

3. STUDIO DELL'INTERAZIONE DELL'ACIDO ROSMARINICO E DI ALCUNI SUOI DERIVATI CON FORME OLIGOMERICHE DEI PEPTIDI Aβ [21]

L'acido rosmarinico (**38**) (**Figura 5**) è un composto con proprietà antiossidanti naturalmente presente in molte erbe *Lamiaceae* e comunemente usato come spezia.

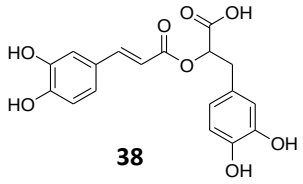

38

Figura 5. Struttura dell'acido rosmarinico

[21] C. Airoldi, E. Sironi, et al. Natural compounds against Alzheimer's Disease: the interaction *of Salvia sclareoides* extract and its major component rosmarinic acid with Aβ1-42 peptide investigated by NMR, Chemistry an Asian Journal, **2012**, in press.

Come riportato in letteratura,[22] l'acido rosmarinico riduce una serie di eventi causati dall'accumulo dell'Aβ, tra cui la formazione di specie reattive dell'ossigeno, la frammentazione del DNA, l'attivazione della caspasi 3 e l'iperfosforilazione della proteina *tau*. Non sono tuttavia disponibili informazioni circa il meccanismo molecolare con cui l'acido rosmarinico esercita il suo effetto biologico.

Per cercare di colmare questa lacuna si è sfruttata ancora una volta la spettroscopia NMR. In particolare, esperimenti STD e trNOESY hanno rivelato l'interazione diretta tra aggregati oligomerici del peptide Aβ e l'acido rosmarinico presente in estratti di *Salvia sclareoides*. Ulteriori esperimenti condotti poi su campioni contenenti l'acido rosmarinico in forma pura hanno evidenziato che i protoni aromatici rappresentano la porzione della molecola maggiormente coinvolta nel legame e che l'acido rosmarinico, quando lega i peptidi Aβ, adotta una conformazione diversa rispetto a quella che possiede in soluzione in assenza del peptide, e cioè una conformazione in cui le due entità aromatiche si avvicinano l'una all'altra.

Per analizzare in maggior dettaglio quale sia il contributo delle due porzioni aromatiche dell'acido rosmarinico nel riconoscimento e nel legame dell'Aβ1-42, la sua struttura è stata suddivisa in due parti, corrispondenti al metil caffeato (**39**) e all'acido deidrocaffeico (**40**), secondo lo **schema 3**.

[22] T. Iuvone, D. De Filippis, G. Esposito, A. D'Amico, A.A. Izzo, "The spice sage and its active ingredient rosmarinic acid protect PC12 cells from amyloid-β-peptide induced neurotoxicity", *J. Pharmacology and Experimental Therapeutics*, **2006**, 317, 1143-1149.

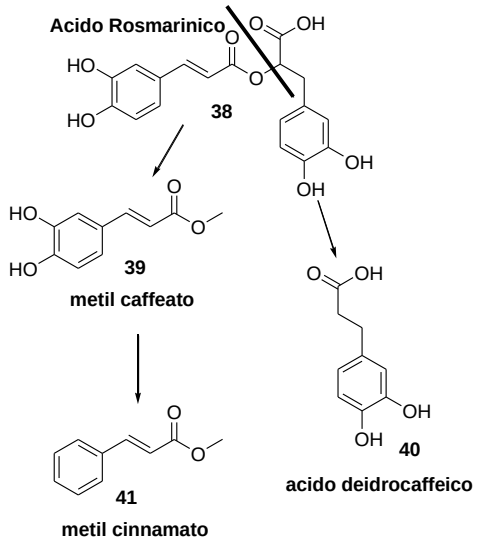

Schema 3. Struttura dei derivati dell'acido rosmarinico usati per le analisi NMR

Il metil caffeato e l'acido deidrocaffeico sono stati preparati a partire dall'acido caffeico, rispettivamente tramite esterificazione del metile e idrogenazione. Esperimenti STD-NMR e trNOESY hanno mostrato che mentre il metil caffeato mantiene le proprietà di legame, l'acido deidrocaffeico non è più un ligando degli Aβ. Si può quindi supporre che la presenza di doppi legami coniugati, che rendono planare la struttura del metil caffeato, sia una caratteristica molecolare importante per l'interazione.

Per analizzare il ruolo giocato nell'interazione dai gruppi ossidrilici del metil caffeato, è stato testato anche il metil cinnamato (**41**), che si è mostrato essere un altro ligando dei peptidi Aβ. Alla luce di questo risultato parrebbe che i gruppi ossidrilici non siano quindi determinanti per l'interazione. In realtà, un'attenta osservazione dei campioni NMR ha mostrato che la presenza del metil cinnamato sembra favorire l'aggregazione del peptide, poiché si osserva

la formazione di un precipitato sul fondo del tubo e la conseguente diminuzione dell'intensità dei segnali ^{1}H.

Ciò è stato in seguito confermato tramite il saggio della tioflavina T,[23] che ha permesso di monitorare nel tempo l'aggregazione del peptide Aβ incubato in condizioni fisiologiche da solo o in presenza di concentrazioni equimolari di acido rosmarinico, metil caffeato o metil cinnamato. Mentre l'acido rosmarinico e il metil caffeato non solo inibiscono l'aggregazione del peptide, ma esercitano attività disgregante, il metil cinnamato incrementa invece la velocità di aggregazione del peptide.

Le informazioni ottenute sono utili per la progettazione di nuovi ligandi dei peptidi Aβ, volti alla terapia e diagnosi del morbo di Alzheimer.

[23] H. LeVine, *Protein Sci*., "Thioflavin T interaction with synthetic Alzheimer's disease beta-amyloid peptides: detection of amyloid aggregation in solution", **1993**, 2, 404–410.

Introduction

1. NEURODEGENERATIVE DISORDERS

In their natural life cycle intracellular proteins are continuously synthesized and degraded. This process of turnover allows a strict control of their concentration in the cell, as a consequence of the needs of maximum economy of materials and energy, and to allow proper regulation of the metabolic processes involving the individual protein species.

Recently it was discovered that a large number of disorders, including Alzheimer's Disease (AD), Parkinsson Disease (PD), type II diabetes, and even some forms of cancer, are associated with protein misfolding and aggregation phenomena. It is now believed that the aggregation of proteins in aberrant forms is the result of a lack of ability of the proteins to be folded, or to remain in their active conformation.[24] A large number of clinically different Neurodegenerative Disorders (NDDs) have been proved to have a similar pathogenic molecular mechanism, including pathological aggregation of proteins, the formation of insoluble fibrillar structures, and their deposition in the form of histopathological inclusions in the nervous system.[25] The majority of histopathological deposits formed by aggregation-prone proteins displays properties of amyloid. However, relatively recent studies revealed that there are proteins that produce non amyloid inclusions, and the common term “amyloidosis of the nervous system” failed to include all of the disorders characterized by metabolic alterations, aggregation, and deposition of proteins in tissues of the nervous system. A more general term was then necessary for this group of disorders. Historically, pathological protein inclusions were first

[24] M. Dumoulin, R. Bader, “Methods to Study Protein Aggregation and Amyloid Formation”; *Protein and Peptide Letters*, **2006**, 13(3), 211-21.

identified in PD, (α-synuclein deposition in the form of Lewy bodies) and various dementias (tau protein depositions). The disorders were consequently termed synucleinopathies and tauopathies, respectively. More recently, several types of pathological inclusions formed by different proteins proved to occur simultaneously in the nervous system of some patients. The term "proteinopathy" (or proteopathy) consequently came to be broadly used to designate the group of disorders characterized by protein pathology. Thus, the NDD forms whose pathogenesis is based on the structural changes and/or metabolic alterations of certain proteins, that result in their aggregation or lead to aggregation of pathogenic peptides with the subsequent formation of characteristic histopatological protein or peptide deposits, are now classified as proteinopathies.[26] Proteinopathies include AD, which is characterized by extracellular amyloid plaques and intracellular neurofibrillary tangles; PD, which is characterized by Lewy bodies; prion diseases; trinucleotide repeat disorders, such as Huntington's disease; motor neuron disease, including amyotrophic lateral sclerosis and several rare NDDs. (**Table 1**)

[25] J.L. Cummings, "Toward a molecular neuropsychiatry of neurodegenerative diseases". *Ann. Neurol*., **2003**, 54,147–154.
[26] K. A. Jellinger, " Basic mechanisms of neurodegeneration: A critical update", *J. Cell Mol. Med*., **2010**, 14, 57–87.

Protein	Gene	Localization	Histopathological structure	Disease
β-amyloid (Aβ)	β-amyloid precursor protein gene (APP), chromosome 21	Outside cell	Senile plaques	Alzheimer's disease
Tau protein	MAPT (microtubule-associated protein tau), chromosome 17	Cytoplasm (neurons, oligodendrocytes or astrocytes)	Neurofibrillary tangles Pick bodies Tau-positive inclusions	Alzheimer's disease Pick's disease Frontotemporal lobar degeneration Corticobasal degeneration Progressive supranuclear palsy
α-synuclein	NCA(PARK1), chromosome 4	Cytoplasm (neurons or oligodendrocytes)	Lewy bodies, Lewy neurites	Parkinson's disease Dementia with Lewy bodies Multiplen system atrophy
Superoxide dismutase 1	ALS1 (SOD1), chromosome 21	Cytoplasm (neurons)	Deposits in motoneurons	Amyotrophic lateral sclerosis
Protease-resistant prion protein PrP^{Sc}	Prion protein gene PRN P, chromosome 20	Outside cells	Prion plaques	Prion diseases (Creutzfeld-Jakob disease, fatal familial insomnia, Gerstmann-Straussler-Scheinker syndrome)
Huntingtin	Htt (IT15), chromosome 4	Nucleus	Neuronal deposits	Huntington's disease
Ataxin	Ataxin-I, chromosome 6	Nucleus (neurons)	Neuronal deposits	Spinocerebellar ataxia type I
TDP-43 (transactive response-DNA-binding protein 43)	TARDBP, chromosome 1	Cytoplasm (neurons, glial cells)	Ubiquitin-positive, tau-and FUS-negative inclusions	Frontotemporal lobar degeneration with ubiquitin-positive inclusions
FUS/TLS (fused in sarcoma/translocated in liposarcoma)	FUS/TLS, chromosome 16	Cytoplasm (neurons, glial cells)	TDP-43-negative inclusions	Frontotemporal lobar degeneration with ubiquitin- positive inclusions

Table 1. Major protein components of pathological protein deposits in neurodegenerative disorders classified as proteinopathies.

Amyloid pathological inclusions in tissues of various parts of the nervous system were described in classical works on NDD nosology and are still used to verify the diagnosis by autopsy. Modern studies on the molecular mechanisms of formation of pathogenic inclusions indicate that protein aggregation is a cascade process and that the principal steps of the formation of protein/peptide deposits are similar in different NDDs.[27] They are shown in **Fig. 1**. According to a commonly accepted hypothesis, a conformational change of a key protein and a consequent change in its aggregation properties are essential to trigger pathogenic aggregation.[28]

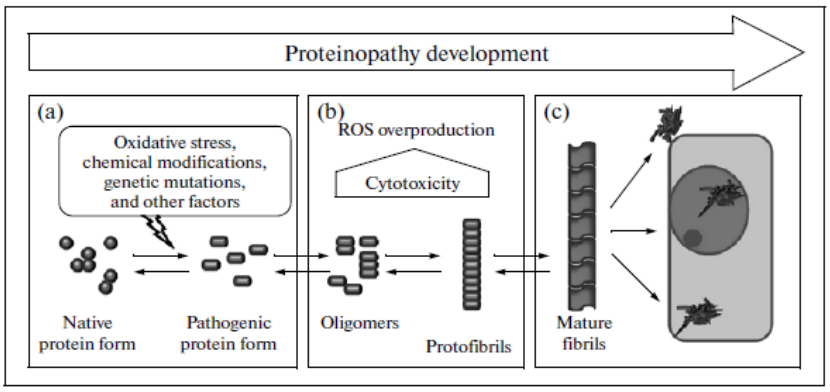

Fig. 1-1. Model of the formation of protein deposits in proteinopathies. (a) A potentially amyloidogenic protein is converted from a normal soluble form to a pathogenic aggregation prone form in response to various factors. (b) The pathogenic form gives rise to oligomers and other intermediates, which then produce protofibrils. (c) At the final stage of aggregation, mature fibrils assembled from protofibrils form protein

[27] D.M. Skovronsky, V. M. Lee, J.Q. Trojanowskl, "Neurodegenerative diseases: New concepts of pathogenesis and their therapeutic implications". *Annu. Rev.Pathol*., **2006**, 1, 151–170.
[28] R. Murphy, A. Tsai, "*Misbehaving Proteins: Protein (Mis)Folding, Aggregation, and Stability*", **2006**, Springer.

deposits in the nervous tissue; the deposits may occur both inside (intranuclear, cytoplasmic) and outside cells. ROS, reactive oxygen species.[adopted from ref. [29]]

Another known mechanism initiating pathogenic aggregation is based on structural changes in the protein as a result of its interaction with a molecule of the same protein in an aberrant conformation; this leads to the accumulation of pathogenic forms with an altered secondary structure and makes pathological aggregation more likely. This type of protein pathology (infectious proteins) is characteristic of prion diseases. However, data are accumulating supporting the idea that a similar mechanism may be involved in the pathogenesis of other NDDs. Moreover, the term "prionogenic proteins" came to be used for aggregation prone proteins because they share several structural characteristics with prion proteins.[[30]] Whichever etiological factors initiate aggregation of potentially pathogenic proteins, they trigger an irreversible process, which then proceeds via mechanisms surprisingly similar for different proteins and leads to proteinopathy and neurodegenerative changes. The intermediate aggregation products of almost all amyloidogenic proteins exert a pathological effect on membrane structures, affecting primarily mitochondria; they change the membrane permeability, suppress electron transport, and stimulate overproduction of reactive oxygen species.[[31]]

The fact that protein aggregation plays an important role in the onset of diseases with high social impact has stimulated many researchers to focus their work on these processes. The definition of the thermodynamic and kinetic

[[29]] T. A. Shelkovnikova, A. A. Kulikova, Ph. O. Tsvetkov, O. Peters, S. O. Bachurin, V. L. Buchman, N. N. Ninkina, "Proteinopathies, Neurodegenerative Disorders with Protein Aggregation Based Pathology ", *Molecular Biology ,* **2012***,* 46(3), 362–374.

[[30]] M. Cushman, B.S. Johnson, O.D. King, et al. "Prion like disorders: Blurring the divide between transmissibility and infectivity", *J. Cell Sci*., **2010**, 123, 1191 1201.

properties of the processes of aggregation and the characterization at the molecular level of the structures of the various species involved in the formation of amyloid fibrils may then suggest strategies to prevent or alleviate amyloidosis. [24]

[31] C. Behl, J.B. Davis, R. Lesley, D. Schubert, "Hydrogen peroxide mediates amyloid beta protein toxicity", *Cell*, **1994**, 77, 817–827.

2. ALZHEIMER'S DISEASE

Among NDDs, AD is one of the most serious health problems in the industrialized world. It is an insidious and progressive neurodegenerative disorder that accounts for the vast majority of age-related dementia and is characterized by a global cognitive decline and the accumulation of Aβ deposits and neurofibrillary tangles in the brain (**Fig. 2-1**).

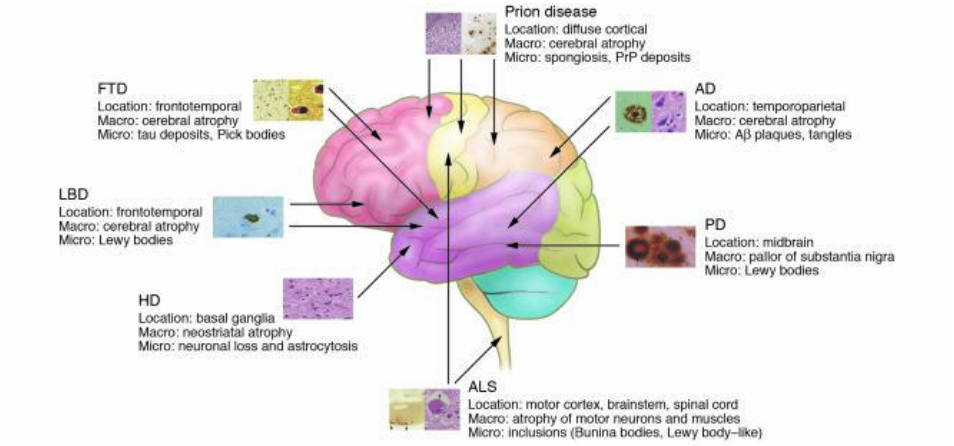

Fig. 2-1. Anathomic sites involved in microscopic and macroscopic changes typical of NDDs

The familial forms of AD are characterized by early onset: they represent only a small fraction (5%) of all the cases of AD and typically present onset ages younger than 65 years. The non-familial forms, also called sporadic forms, appear at age 65 years or older and typically represent the vast majority of all AD cases.[32] About a century ago, Alois Alzheimer first described in a dead patient the hallmarks of the neurodegenerative disease, which later acquired

[32] L. Bertram, R. E. Tanzi; "The genetic epidemiology of neurodegenerative disease", *J. Clin. Invest.,* **2005**, 115(6), 1449-1457.

his name: plaques and tangles.[33] Clinically, only a possible or probable diagnosis of AD is made, but the true diagnosis can be made only after the patient's death, revealing the presence of amyloid plaques, neurofibrillary aggregates and loss of neuronal cells. Plaques and aggregates can be found even in healthy people, very old, because the neurodegeneration of Alzheimer's usually precedes by decades the onset of clinical simptoms.[34,35] In a first step it is possible to refer to a "mild impairment of cognitive abilities" (MCI, mild cognitive impairment), with an intermediate situation between that of someone with Alzheimer's and that of the normal person, but this may also be the preliminary stage of other neurodegenerative disorders.[36,37] Clinical experience led to several international criteria for evaluating suspected cases of AD. Some of them consider only the presence of amyloid aggregates, while others consider both the amyloid plaques and the presence of tau filaments. [38] The diagnostic methods also involve the use of neuroimaging and biomarkers. Neuroimaging, for example, can be used to investigate brain atrophy using MRI (magnetic resonance imaging), or amyloid plaques with the help of PET (positron emission tomography), while increased levels of total and phosphorylated tau filaments are used as biomarkers in the analysis of cerebrospinal fluid.[34,39,40,41,42] Up until now there is no real therapy for AD, but

[33] L. Fratiglioni, D. De Ronchi, H. Aguero Torres, " Worldwide prevalence and incidence of dementia", *Drugs and Aging,* **1999***,* 15(5), 365-375.
[34] K. Blennow, M. J. De Leon, H. Zetterberg, "Alzheimer's disease", *Lancet,* **2006***,* 368, 387-403.
[35] M. Goedert, M.G. Spillantini, "A century of Alzheimer's disease", *Science,* **2006***,* 314; 777-781.
[36] M.S. Albert, D. Blacker, "Mild cognitive impairment and dementia", *Annual Reviews in Clinical Psychology*, **2006**, 2, 379-388.
[37] K. Palmer, A.K. Berger, R. Monastero, B. Winblad, L. Backman, L. Fratiglioni, "Predictors of progression from mild cognitive impairment to Alzheimer's disease"; *Neurology,* **2007***,* 68, 1596-1602.
[38] Braak H. and Braak E.(**1991**), "Neuropathological stageing of Alzheimer-related changes", *Acta Neuropathologica (Berlin),* 82:239-259.
[39] V. Jelic, A. Nordberg, "Early diagnosis of Alzheimer disease with positron emission tomography", *Alzheimer disease and associated disorders*, **2000**, 14 (Supplement 1):S109-S113.

clinical symptoms can be alleviated. Acetylcholinesterase inhibitors such as donepezil, rivastigmine and galantamine are approved for clinical use and have been shown to reduce behavioral symptoms, although not specifically directed at the disease that causes them. Epidemiological studies suggest other types of drugs that could be used as candidates against AD, such as anti-inflammatory drugs, drugs that lower cholesterol (such as statins), antioxidants (like vitamin E) and estrogen, but such information not always has been confirmed in clinical trials.[43]

2.1. AMYLOID PLAQUES AND NEUROFIBRILLAR AGGREGATES

Among the amyloidogenic diseases, AD is perhaps the best characterized. Specific mutations in the gene *app* are highly predictive for the disease, which appears in more than 95% of cases. Both in sporadic and in familial forms, whose phenotypes are indistinguishable, there is an abnormal processing of APP protein, resulting in an increased accumulation of the amyloidogenic peptides Aβ1-40 and Aβ1-42. Apparently, the increased synthesis of Aβ filaments accelerates the formation of protein aggregates, leading to early onset of the disease.

Although presenilins are homologous proteins with similar biological functions, mutations of the gene *ps2* are very rare, affecting only a few families in the world and until now, only six mutations of it have been described. In addition,

---

[40] P. Bailey, "Biological Markers in Alzheimer's disease", *Canadian Journal of Neurological Science,* **2007**, 34 (Supplement 1): S72-S76.

[41] M. Sjogren, N. Andreasen, L. Blennow," Advances in the detection of Alzheimer disease-use of cerebrospinal fluid markers", *Clinical Chimica Acta,* **2003,** 332, 1-10.

[42] M. Ward, "Biomarkers for Alzheimer's disease", *Expert Reviews in Molecular Diagnosis,* **2007,** 7(5), 635-646.

[43] Y-H. Suh, F. Checler, "Amyloid precursor protein, presenilins, and α-synuclein: molecular pathogenesis and pharmacological applications in Alzheimer's disease", *Pharmacological Reviews,* **2002,** 54(3), 469-525.

there is a marked difference in disease phenotype determined by mutations in the *ps1* and *ps2* genes: the first usually causes an early onset of the disease, while the second leads to a manifestation of the disease at variable age. Mutations in the *app* gene are grouped near and within the sites of cutting of α, β and ϒ secretases and alter the proteolysis of the membrane protein APP. Mutation analysis indicates that the age at which the disease occurs in families with *ps1* mutation is related to the location and the type of amino acid substitution.[44] In his report on the first case of Alzheimer's in 1907, Alois Alzheimer dscribed the two pathological lesions that became after the markers for the diagnosis of the disease: neuro-fibrillar aggregates and amyloid plaques (**Figure 2-1-1**).

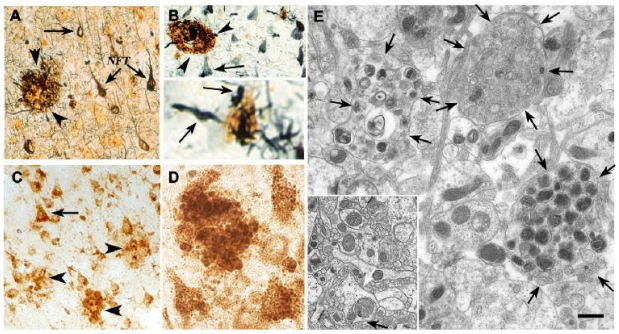

Figure 2-1-1. Alzheimer's disease. (A) The two hallmarks of AD: the β-amyloid plaques (arrowheads) and neurofibrillary aggregates (arrows) revealed by silver staining in the brain affected by AD. (B) Staining with antibodies against paired helical filament tau (arrows) and β amyloid (arrowheads) of neurites associated with amyloid deposits. (C,D) Antibodies against Cathepsin D decorate lysosomes in cell bodies of neurons and dystrophic neuritis associated with plaques (E) Dystrophic neuritis (arrows) are greatly enlarged compared with neuritis of a normal brain (electron microscopy). The

[44] G.Forloni, L. Terreni, S. Fogliarino, R. Invernizzi, A. Assini, G. Rubizzi, A. Negro, E. Calabrese, M. A. Volontà, C. Mariani, M. Franceschi, M. Tobaton, A. Bertoli, "Protein misfolding in Alzheimer's and Parkinson's disease: genetics and molecular mechanisms", *Neurobiology of Aging,* **2002,** 23, 957-976.

abnormal neuritis contain mostly autophagic vacuoles of various morphologies, which are rare in the normal brain.

The neurofibrillary aggregate is a real injury, located within the affected neurons. It was later discovered to be composed mainly by a form of tau protein associated with microtubules that is abnormally phosphorylated and aggregates generating paired helical filaments. A second lesion, called senile plaque, is made of small portions of material deposited extracellularly, between groups of axons and neuritis, many of which are quite swollen, or atrophic.

These extracellular deposits have been identified about fifty years later as a specific type of amyloid, the β-amyloid, consisting of fibrillar aggregates of the β-amyloid peptide (Aβ), derived from proteolysis of the precursor APP. The term Aβ includes a set of Aβ polipeptides of 39-43 aminoacid residues, whose biological functions are poorly understood. In its pathological oligomeric form, Aβ exerts a number of the cytotoxic actions that play a key role for the evolution of the neurodegenerative mechanism of AD. At ultrastructural level, the dystrophic neuritis (swollen) contain filaments of tau, but are much more abundantly filled with vacuolar structures, including dense bodies of lysosomes enriched in cathepsins. The proliferation of lysosomes in cell bodies of affected neurons reflects a synthesis of highly irregular components of the lysosomal system. In fact, a more detailed analysis shows that the vescicles that accumulate in dystrophic neuritis are not lysosomes, but are more properly autophagic vacuoles. These vacuoles represent intermediate stages of a process of macroautofagia, the process responsible for the lysosomal degradation of cytoplasmic constituents, including organelles.

2.2. BIOLOGY OF APP PROTEIN AND ORIGIN OF Aβ PEPTIDES

In 1984, as a first step towards the elucidation of the mechanism of formation of amyloid, Glenner and Wong discovered the N-terminal sequence of 24 residues isolated from the main component of cerebrovascular amyloid plaques. They named the molecule "beta protein" because of its β sheet structure. Three months later, they showed that the cerebrovascular amyloid of patients with Down syndrome was almost identical in sequence and hypothesized that a genetic defect on chromosome 21 could be an explanation for Alzheimer's disease. Using cDNA probes based on the amino acid sequence of the β protein, Kang cloned the gene coding for the precursor of the same (β APP) and localized it on chromosome 21 in humans. Concomitant cloning studies performed by other groups provided identical conclusions. After initial studies of Glenner and Wong, the aminoacidic sequence analysis of β-amyloid plaques suggested that the Aβ began mainly with a residue of aspartate and was between 39 and 43 residues long, showing a lack of uniformity in the N-terminal portion.[45] The APP protein is part of a conserved family of membrane proteins of type 1, which in mammals includes the APP-like proteins APLP1 and APLP2. Although its function remains uncertain, physiological roles have been proposed in the regulation of traffic through the cell, in neurotrophic signals, in cell adhesion and signaling. Once the APP has been synthesized, its glycosylated mature form is sent through the Golgi to the plasma membrane, where it is fairly quickly converted by one of the two following mechanisms (**Figure 2-1-2**): (1) an aspartyl protease on the cell surface, the tumor necrosis factor converting enzyme (TACE), or a disintegrin and metalloproteinase 10, also

referred to as α-secretase, may mediate the cutting of APP within its extracellular domain, generating a large soluble N-terminal fragment (α SAPP), which is released from the cell, and a C-terminal fragment (CTF) that remains associated with the membrane; (2) as an alternative the APP present on the cell surface is internalized into early endosomes, where the cut in a more distal site along the extracellular domain by a β-secretase (BACE, β-site APP cleaving enzyme) releases a soluble fragment of APP (β SAPP) and generates a C-terminal fragment of 99 residues (βCTF) associated with the membrane, which contains the entire Aβ peptide.

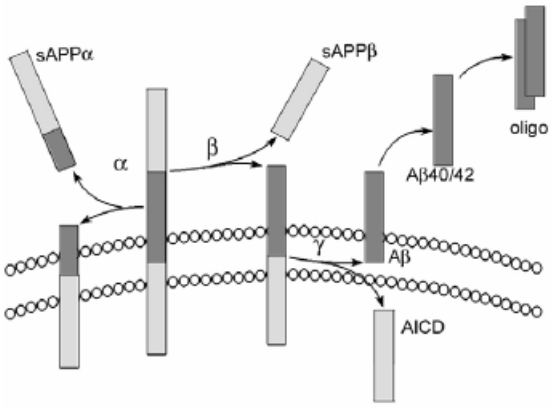

Figure 2-1-2. Functional domains of APP and the main sites of proteolytic cleavage (α, β, γ) by APP secretase. sAPP, soluble fragment of APP; AICD, APP intracellular domain.

An aspartyl protease, which has optimal activity at low pH, is localized mainly in endosomes, where the βCTF is generated, even if also the enzyme BACE is present in the trans Golgi network. The Aβ is generated by βCTF from an intramembranous cut in position ϒ, which mainly produces a peptide of 40 amino acids (Aβ1-40) and to a lesser extent a peptide of 42 aminoacids (Aβ1-

[45] D. B. Teplow, "Structural and kinetic features of amyloid β-protein fibrillogenesis", *Amyloid: Int. J. Exp.*

42). The cutting of APP in ϒ is mediated by the ϒ secretase complex, consisting of the proteins presenilins (PS), nicastrin, APH1 and PEN2. The components of the complex have been identified in many cellular compartments, including the plasma membrane, early endosomes, late endosomes, autophagic vacuoles and in lysosomes. The Aβ generated within cells is the suspected source of most of the Aβ deposited extracellularly and generating the fibrillar plaques. Before Aβ deposits extracellularly, the amount of soluble intracellular Aβ increases substantially in endosomal and lysosomal compartments, and it creates the plaques typical of the brain affected by Alzheimer's. The loss of cognitive abilities has been reported in models of AD in which intracellular Aβ levels are increased in the absence of plaque formation, supporting other evidence that Aβ is toxic intracellularly before being released. Once released, the extracellular Aβ, in soluble form or aggregated, is thought to interact pathologically with surface receptors, directly affecting the lipid bilayer of the membrane or acting in the endolisosomial sectors after reinternalisation. The degradation of Aβ *in vivo* is mediated by several proteases, whose overexpression or deletion, as expected, alters brain Aβ levels in mice. The best characterized proteases of this group are all zinc metallopeptidases: neprilysin, insulin degrading enzyme, and endothelin converting enzymes (ECE1 an ECE2).

Due to their intracellular localization and optimum of pH, it is unlikely that these proteases operate in highly acidic compartments such as late endosomes and autolisosoms. Although less characterized, also the protease catepsin B degrades Aβ peptides in lysosomes, especially Aβ1-42, and increases the

Clin. Invest., **1998**, 5, 121-142.

deposits of plaques in mice that express a mutated human APP, while an overexpression of the enzyme has an opposite effect. [46]

2.3.THE HYPOTHESIS OF AMYLOID CASCADE

Although there are strong evidences supporting the hypothesis that Aβ is responsible for AD, the soluble monomeric form of the peptide does not seem to show any direct neurotoxicity. The concentration of free monomeric Aβ is not directly related to severe memory impairment[47] while soluble oligomeric forms seem to show this correlation.[48,49] The discovery of soluble oligomers and the correlation between their presence and symptoms has led to speculation on AD amyloid cascade, which describes the causes of the disease at a molecular level.(**Figure 2-3-1**).[50]

[46] R. A. Nixon, "Autophagy, amyloidogenesis and Alzheimer disease"; *Journal of Cell Science,* 120, 4081-4091.
[47] S. Lesnè, M. T. Koh, L. Kotilinek, R. Kayed, C.G. Glabe, A. Yang, M. Gallagher, K. H. Ashe, "A specific amyloid β-protein assembly in the bain impairs memory", *Nature*, **2006**, 440 (7082), 352-357.
[48] D. M. Hartley, D. M. Walsh, C. P. Ye, T. Diehl, S. Vasquez, P. M. Vassilev, D. B. Teplow, D.J. Selkoe, "Protofibrillar intermediates of amyloid β-protein induce acute electrophysiological changes and progressive neurotoxicity in cortical neurons ", *J. Neurosci*, **1999,** 19(20), 8876-8884.
[49] W. L. Klein, G. A. Krafft, C. E. Finch, "Targeting small Aβ oligomers : the solution to an Alzheimer's disease conundrum?", *Trends Neurosci*., **2001**, 24(4), 219-224.
[50] J. Hardy, D. J. Selkoe, "The amyloid hypothesis of Alzheimer's disease: progress and problems on the road to therapeutics", *Science*, **2002,** 297, 5580, pp. 353-356.

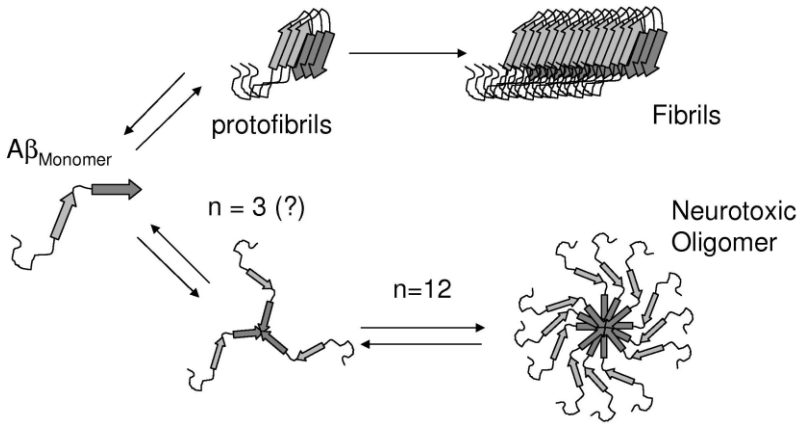

Figure 2-3-1. Two pathways for the aggregation of β-amyloid peptide. In the case of protofibrils formation and the subsequent assembly into fibrils the peptide is trapped into stable structures and is prevented to exert toxic effects. The neurotoxic effect of Aβ can be caused by a dodecameric assembly of the peptide.

Aβ peptides initially undergo a process of oligomerization and then further aggregation into fibrils and protofibrils. The oligomers are soluble and they are thought to play an important role in the pathogenic cascade of Aβ, making it toxic to neurons.[51,52,53] The oligomers share their topological characteristics with other forms of oligomeric peptides, suggesting that there is a common mechanism of cellular toxicity exhibited by these peptides.[54]

The oligomeric forms of Aβ fibrils may furtherly aggregate generating protofibrils and fibrils, but not necessary they give this further process of

[51] M. Bucciantini, E. Giannoni, F. Chiti, F. Baroni, L. Formigli, J. Zurdo, N. Taddei, G. Ramponi, C. M. Dobson, M. Stefani, "Inherent toxicity of aggregates implies a common mechanism for protein misfolding diseases", *Nature*, **2002,** 416, 6880, 507-511.

[52] Y. Gong, L. Chang, K. L. Viola, P. N. Lacor, M. P. Lambert, C. E. Finch, G. A. Krafft, W. L. Klein, () "Alzheimer's disease affected brain: presence of oligomeric Aβ-ligands (ADDLs) suggests a molecular basis for reversible memory loss", *Proc. Natl. Acad. Sci. U.S.A.*, **2003,** 100(18), 10417-10422.

[53] C. M. Dobson, "Protein chemistry. In the footsteps of alchemists", *Science*, **2004,** 304, (5675), 1259-1262.

[54] R. Kayed, E. Head, J. L. Thompson, T. M. McIntire, S. C. Milton, C. W. Cotman, C. G. Glabe, "Common structure of soluble amyloid oligomers implies common mechanisms of pathogenesis", *Science*, **2003,** 300(5618), 486-489.

aggregation. Then the oligomerization and fibrillation processes are considered two alternative routes in the metabolism of Aβ.[55,56,57] The formation of protofibrils and fibrils could be a protective event to lower the concentration of oligomers.[58] The mechanism by which the oligomers exert their toxicity is unclear, but one possibility is the production of reactive oxygen species, or a change in the function of the cell membrane and thus a disturb of calcium equilibrium levels or the dynamic properties of the membrane. However, another suggested mechanism is the alteration of metals equilibrium concentration.[59,60] The common feature of all these mechanisms is hypothesized to lead to the destruction of synapses and consequently to cell death.[61] It is possible that the oligomerization process exposes certain reactive residues of the peptide, and that the number of reactive residues increases after the aggregation into dodecamers. The kinetics of Aβ fibrillation include a lag phase in which the monomeric peptide is in rapid exchange with oligomeric species, and, after some time, a nucleus originates in the fibrillar

[55] G. Bitain, M. D. Kirkitadze, A. Lomakin, S. S. Vollers, G. B. Benedek, D. B. Teplow, "Amyloid β-protein assembly : Aβ40 and Aβ42 oligomerize through distinct pathways", *Proc. Natl. Acad. Sci. U.S.A.*, **2003**, 100(1), 330-335.

[56] S. Barghorn, V. Nimmrich, A. Striebinger, C. Krantz, P. Keller, B. Janson, M. Bahr, M. Schmidt, R. S. Bitner, J. Harlan, E. Barlow, U. Ebert, H. Hillen, "Globular amyloid β-peptide oligomer - a homogenous and stable neuropathological protein in Alzheimer's disease", *J. Neurochem.*, **2005**, 95(3), 834-847.

[57] Y. R. Chen, C. G. Glabe, "Distinct Early Folding and Aggregation Properties of Alzheimer Amyloid-β-Peptides Aβ40 and Aβ42: Stable Trimer Or Tetramer Formation by Aβ42", *J. Biol. Chem.*, **2006**, 281(34), 24414-24422.

[58] R. Carrotta, M. Manno, D. Bulone, V. Martorana, P. L. San Biagio, "Protofibril formation of amyloid β-protein at low pH via a non-cooperative elongation mechanism", *J Biol Chem*, 2005, 280(34), 30001-30008.

[59] A. I. Bush, C. L. Masters, R. E. Tanzi, "Copper, β-amyloid, and Alzheimer's disease: tapping a sensitive connection", *Proc. Natl. Acad. Sci.* U S A, 2003, 100(20), 11193-11194.

[60] D. M. Walsh, D. J. Selkoe (), "Deciphering the molecular basis of memory failure in Alzheimer's disease", *Neuron*, **2004,** 44(1), 181-193.

[61] F. Chiti, C. M. Dobson, "Protein misfolding, functional amyloid, and human disease", *Annu. Rev. Biochem.*, **2006,** 75, 333-366.

aggregates of peptides, which then promotes the aggregation of peptides into fibrils.[62]

Fibrillation of Aβ thus seems to be associated with a cascade of neuropatogenic events that determines the cognitive and behavioral decline characteristic of AD. The central role of Aβ fibrils in AD has stimulated the development of therapeutic approaches designed to prevent the formation of fibrils or disrupt existing ones. Understand what is the mechanism of Aβ aggregation is necessary to rationally develop effective therapeutic agents. Knowledge of the primary events of the aggregation would allow to block critical steps in the process of fibrillogenesis, in particular those that lead to the formation of toxic prefibrillar structures. Early studies of amyloid deposits have focused on the morphology of the fibrils and the primary structure of the Aβ peptide that they contained and on the formation of toxic prefibrillar structures. Recently two major areas of research have been opened: the study of conformational transitions associated with the assembly of monomers into fibrils and the identification and characterization of aggregation intermediates. [63]

2.4. Aβ MONOMERS AND OLIGOMERS STRUCTURE

Aβ1-40 and Aβ1-42 peptides present the following sequence:

NH_2-DEAFRHDSGY EVHHQKLVFF AEDVGSNKGA IIGLMVGGVV$_{40}$ IA$_{42}$-COOH

The sequence of Aβ1-40 is divided into two regions. Residues 1-28 make up a relatively hydrophilic domain with a high proportion of charged residues. In the amyloid precursor protein, this domain is extracellular. The carboxyl-terminal

[62] R. M. Murphy, "Peptide aggregation in neurodegenerative disease", *Annu.Rev. Biomed. Eng.*, **2002,** 4, 155-174.

[63] M. D. Kirkitadze, M. M. Condron , D. B. Teplow, "Identification and Characterization of Key Kinetic Intermediates in Amyloid β-protein Fibrillogenesis", *J. Mol.Biol.,* **2001**, 312, 1103-1119.

residues 28-40 represent a richly hydrophobic domain associated with the cell membrane in the amyloid precursor protein. According to a lot of different experimental evidences, Aβ1-40 and Aβ1-42 peptides mainly appear as a random coil in aqueous solution, but contain some secondary structure elements: a poly-proline II helix (PII) in the N-terminus, and two β-strands in the central part and in the C-terminus [[64]]. Monomers present a high tendency to aggregate and form Aβ oligomers, which eventually produce Aβ fibrils. In particular, the N-terminal domain exists as a soluble monomeric α-helical structure at pH 1-4 and pH greater than 7. Nevertheless, it rapidly precipitates and gives rise to an oligomeric β-sheet structure at pH values between 4 and 7. The observation that β-sheet formation by Aβ was promoted at low pH is of particular interest as the pH in AD brains has been found to be slightly lower than in normal brain, and this acidolysis may result in enhanced Aβ deposition. In the last few years, it has been shown that soluble oligomers might be pathologically more important than fibrillar amyloid deposits.[[65]] A specific mechanism for the toxicity of oligomeric assemblies was suggested by solution studies of isolated Aβ fragments. The great similarity between the Aβ1-42

[[64]] a) J. Danielsson, J. Jarvet, P. Damberg, A. Graslund, "The Alzheimer β-peptide shows temperature-dependent transitions between left-handed 3(1)-helix, β-strand and random coil secondary structures", *Febs J.,* **2005**, 272, 3938-3949; b) R. Riek, P. Guntert, H. Dobeli, B. Wipf, K. Wuthrich, "NMR studies in aqueous solution fail to identify significant conformational differences between the monomeric forms of two Alzheimer peptides with widely different plaque-competence, Aβ (1-40)(ox) and Aβ (1-42)(ox)", *Eur. J. Biochem.* **2001**, 268, 5930-5936.

[[65]] a) J. P. Cleary, D. M. Walsh, J. J. Hofmeister, G. M. Shankar, M. A. Kuskowski, D.J. Selkoe, K. H. Ashe, "Natural oligomers of the amyloid-protein specifically disrupt cognitive function", *Nat. Neurosci.,* **2005**, 8, 79-84; b) A. Demuro, E. Mina, R. Kayed, S. C. Milton, I. Parker, C. G. Glabe, "Calcium dysregulation and membrane disruption as a ubiquitous neurotoxic mechanism of soluble amyloid oligomers", *J. Biol. Chem.,* **2005**, 280, 17294-17300; c) R. Kayed, E. Head, J. L.Thompson, T. M. McIntire, S. C. Milton, C. W. Cotman, C.G. Glabe, "Common structure of soluble amyloid oligomers implies common mechanism of pathogenesis", *Science,* **2003**, 300, 486-489.

structure in apolar environments and that of a virus fusion peptide[66] suggests that membrane poration could be the key event for neurotoxicity. In fact, the α-helical peptide could induce formation of membrane channels, promoting the penetration of substances (such as metal ions) that can cause neuronal death.[67] The dynamics of monomeric Alzheimer Aβ1-40 in aqueous solution was studied by Danielsson et al. using nuclear magnetic resonance (NMR) experiments.[68] The persistence length of the Aβ1-40 monomer was found to decrease from eight to three residues when temperature was increased from 3 to 18°C. At 3°C the peptide shows structural propensities that correlate well with the suggested secondary structure regions of the peptide present in the fibrils, and with the α-helical structure in membrane-mimicking systems. They proposed a structural model for the monomeric soluble β-peptide with six different regions of secondary structure propensities. The peptide has two regions with β-strand propensity (residues 16-24 and 31-40), two regions with high PII-helix propensity (residues 1-4 and 11-15) and two unstructured regions with higher mobility (residues 5-10 and 25-30) that connect the structural elements. In particular, their relaxation results are in agreement with the model in which the C-terminus forms an antiparallel β-sheet with the central region. The central region has, mostly at low temperatures, a high fraction of PII, which is changed to a β-strand propensity when raising the temperature. The core of the central region (residues 18-20) has a high β-strand propensity at low temperatures. The mobile turn region (25-30) allows the C-terminus to

[66] O. Crescenzi, S. Tomaselli, R. Guerrini, S. Salvadori, A. M. D'Ursi, P. A. Temussi, D. Picone, "Solution structure of the Alzheimer Aβ-peptide (1-42) in an apolar microenvironment - Similarity with a virus fusion domain", *Eur. J. Biochem.,* **2002**, 269, 5642-5648.

[67] H. Lin, R. Bhatia, R. Lal, "Aβ protein forms ion channels: implications for Alzheimer's disease pathophysiology. *Faseb J.,* **2001**, 15, 2433-2444.

approach the β-strand, where side chains can be involved in hydrophobic interactions. A lot of experimental data show that the hydrophobic segment in the C-terminal domain of Aβ is largely responsible for Aβ peptide propensity to form β-sheet, while Aβ conformation is more dependent on the secondary structure adopted by the N-terminal domain. This was also supported by the fact that the single mutation of V18, an amino acid with the tendency to form β-sheets, to alanine, an amino acid forming α-helices, induced a great increase of the α-helical content of Aβ1-40 and dramatically diminished fibrillogenesis. In addition, the substitution of glutamine for glutamic acid at position 22 (the "Dutch" peptide) decreased the propensity of the Aβ *N*-terminal domain to adopt an α-helical structure, with a concomitant increase in amyloid formation. [69] As indicated by numerous *in vitro* and *in vivo* studies, Aβ1-40 and Aβ1-42 peptides have different aggregation and deposition properties. As a matter of facts, Aβ1-42 aggregation is much faster and its toxicity much higher. Aβ1-40 and Aβ1-42 thermal unfolding processes were investigated by parallel molecular dynamics (MD) simulations to explore the physical basis underlying the different dynamic behaviors of both Aβ peptides.[70] In Aβ1-40 peptide, due to the favorable spatial positions in R-helical conformations between residues 39-40 (VV) and 34-36 (LMV), these residues form an hydrophobic core in the C-terminus that certainly stabilizes the peptide. On the other hand, this hydrophobic core is destroyed in Aβ1-42, because the additional residues 41-42 (IA) form hydrophobic interactions with residues 39-40 (VV). This causes the

[68] J. Danielsson, A. Andersson, J. Jarvet, A. Graslund, "N-15 relaxation study of the Aβ-peptide: structural propensities and persistence length", *Magn. Reson. Chem.,* **2006**, 44, S114-S121.
[69] H. Sticht, P. Bayer, D. Willbold, S. Dames, C. Hilbich, K. Beyreuther, R. W. Frank, P. Rosch, "Structure of Amyloid beta Peptide of Alzheimer's Disease", *Eur. J. Biochem.,* **1995**, 233, 293-298.
[70] S. Liang, J. Hong-Fang, Z. Hong-Yu, "Why is the C-terminus of Aβ (1-42) more unfolded than that of Aβ (1-40)? clues from hydrophobic interaction", *J. Phys. Chem. B* **2008**, 112, 3164-3167.

disruption of the hydrophobic interactions between residues 39-40 (VV) and residues 34-36 (LMV). As a consequence, residues 34-36 (LMV) tend to close with 31-32 (II) to form a new hydrophobic core (**Fig. 2-4-1**).

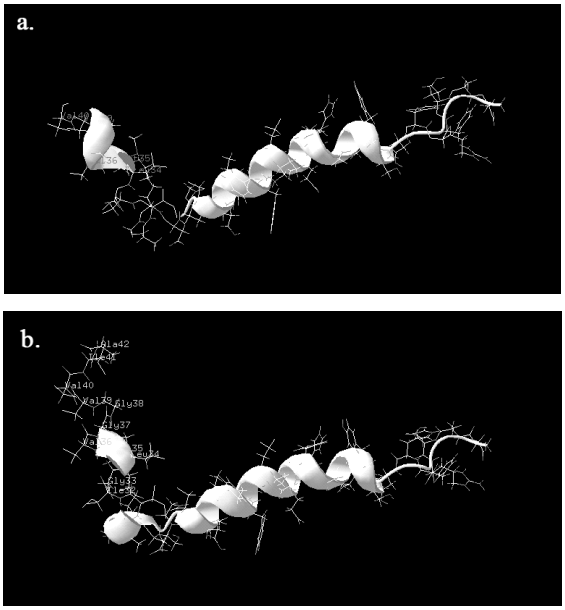

Fig. 2-4-1. Stereo views of the hydrophobic interactions in the C-terminus of Aβ1-40 (a) and Aβ1-42 (b) at 1.5 ns of the MD simulations. The residues involved in the hydrophobic interactions are shown in Corey-Pauling-Koltun spheres.

This finding provides some new clues to understand the different aggregation and deposition propensities of both peptides. As previously introduced, NMR investigations on small Aβ fragments[71] and Aβ1-40 Met35^{ox} suggest that in aqueous solution Aβ peptides can be described as random coils, with only a

[71] a) J. Jarvet, P. Damberg, K. Bodell, L. E. G. Eriksson, A. Graslund, "Reversible random coil to β-sheet transition and the early stage of aggregation of the Aβ (12-28) fragment from the Alzheimer peptide", *J. Am. Chem. Soc.,* **2000**, *122*, 4261-4268; b) J. P. Lee, E. R. Stimson, J. R. Ghilardi, P. W. Mantyh, Y. A. Lu, A. M. Felix, W. Llanos, A. Behbin, M. Cummings, M. Vancriekinge, et al. "1H NMR of Aβ peptide congeners in water solution - conformational changes correlate with plaque competence", *Biochemistry,* **1995**, 34, 5191-5200; c) S. Zhang, K. Iwata, M. J. Lachenmann, J. W. Peng, S. Li, E. R. Stimson, Y. Lu, A. M. Felix, J. E. Maggio, J.P. Lee, "The Alzheimer's peptide Aβ adopts a collapsed coil structure in water", *J. Struct. Biol.,* **2000**, 130, 130-141.

small population of local nonrandom structures. Nevertheless, a lot of studies suggest a critical role for *in vivo* conformational transitions between soluble α helical and β forms of the peptide. Unfortunately, direct observation of these conformational transitions is difficult, due to Aβ peptides poor tendency to dissolve in water. For this reason, detailed structural studies are normally performed in mixtures of water and organic solvents, particularly fluorinated alcohols, such as trifluoroethanol (TFE) or hexafluoroisopropanol (HFIP), and micellar solutions.[72,73] Aβ peptides do not aggregate when dissolved in these media and show a preferential α-helical conformation. Recently, it was demonstrated that, in addition to promoting α-helices, mixtures of water and TFE can induce β-sheet structures. In particular, in the concentration range between 10 and 32.5% of TFE (v/v), Aβ1-42 forms β-sheet structures, whereas in the concentration range 50-100% TFE CD spectra are typical of α-helices. Tommaselli and co-workers[74] exploited this property to characterize Aβ peptide conformational transitions from helical to β forms. By integrating NMR and CD experimental data with MD simulations, they demonstrated that the core sequence 25-35 plays a key-role in the α-to-β conformational transition. The β conformation can be stable in solutions that contain 90-99% water. Moreover, they found that α-to-β conformational transition is reversible, and

[72] H. Sticht, P. Bayer, D. Willbold, S. Dames, C. Hilbich, K. Beyreuther, R. W. Frank, P. Rosch, "Structure of Amyloid Aβ Peptide of Alzheimer's Disease", *Eur. J. Biochem.,* **1995**, *233*, 293-298.

[73] a) C. J. Barrow, M. G. Zagorski, "Solution structures of β peptide and its constituints fragments - relation to amyloid deposition", *Science,* **1991**, 253, 179-182; b) A. M. D'Ursi, M. R. Armenante, R. Guerrini, S. Salvadori, G. Sorrentino, D. Picone, "Solution structure of Aβ -peptide (25-35) in different media", *J. Med. Chem.,* **2004**, 47, 4231-4238; c) T. Kohno, K. Kobayashi, T. Maeda, K. Sato, A. Takashima, " Three-dimensional structures of the Aβ peptide (25-35) in membrane-mimicking environment", *Biochemistry,* **1996**, 35, 16094-16104.

[74] S. Tomaselli, V. Esposito, P. Vangone, N. A. J. van Nuland, A. Bonvin, R. Guerrini, T. Tancredi, P.A. Temussi, D. Picone, "The α-to-β conformational transition of Alzheimer's Aβ (1-42) peptide in aqueous media is reversible: A step by step conformational analysis suggests the location of β conformation seeding", *ChemBioChem,* **2006**, 7, 257-267.

that addition of appropriate amounts of HFIP turns the peptide conformation back from β to α; this reversion of β aggregates occurs slowly but unambiguously. Currently, attempts to identify regions of peptide that, induced by the surrounding medium, drive conformational transitions, represents a possible approach to understand the molecular basis of AD. In addition, the design of molecules able to interfere with the aggregation process can be rationalized starting from the structural characterization of a partially folded intermediate in the α-to-β transition and *vice versa*. This has great potential for possible therapeutic applications.

As previously introduced, Aβ oligomers are soluble and are suggested to play an important role in the pathogenic cascade of AD by being toxic to neurons. The toxic mechanism of the oligomers is thought to be either a direct or indirect mechanism, mediated through oxidative stress or by inducing inflammatory processes.[75] The structure of the oligomeric species discovered until now is not known in detail. Several aggregation states have been identified for amyloidogenic proteins before the formation of fibrils. As a matter of facts, the general term oligomers includes different kinds of assemblies such as dimers, trimers, protofibrils, ADDLs (Aβ-derived diffusible ligands) and annular or pore-like oligomers. Oligomers could also be classified into prefibrillar or fibrillar oligomers as they have different aggregation pathways. Aβ oligomers are most probably intermediates in amyloid fibrils formation. However they are not necessarily required to form fibrils.[76] Generally, Aβ1-40 generates a mixture of monomers, dimers, trimers and

[75] M. D. Kirkitadze, G. Bitan, D. B. Teplow, "Paradigm shifts in Alzheimer's disease and other neuro degenerative disorders: The emerging role of oligomeric assemblies", *J. Neurosci. Res.,* **2002**, 69, 567-577.

tetramers, whereas Aβ1-42 forms pentamers/hexamers, as well as dodecamers, octadecamers, and other large assemblies. Of these two peptides, only Aβ1-42 has been observed to form ADDLs.[77] Recently, a specific Aβ oligomer has been described. It is a dodecamer able to bind specifically the dendritic processes of the neuron and blocks the membrane potentiation.[78] This dodecamer impairs memory function in mice, the memory impairment being directly linked to the presence of dodecameric Aβ.[79] From the structural point of view, the oligomer appears to be as a micelle of Aβ-peptides with the hydrophobic C-terminus hidden in the micelle center and a critical micelle concentration of 17.6 μM.[80] The peptides in the oligomer appear to be mainly unstructured.[81] In 2005, Laurents *et al*. proposed a new different kind of Aβ aggregated forms, the so-called β-balls, detected at pH lower than 4.[82] According to their model, β-balls made by Aβ1-40 peptides have a spherical micelle structure with the 12 C-terminal amino acid residues hidden inside an hydrophobic micelle core and the rest of the peptide exposed to solvent. The peptide groups within the β-balls core are hydrogen-bonded forming β-sheet structures. In an extended conformation, these last 12 residues of Aβ1-40

---

[76] E. Cerf, R. Sarroukh, S. Tamamizu-Kato, L. Breydo, S. Derclaye, Y. F. Dufrene, V. Narayanaswami, E. Goormaghtigh, J. M. Ruysschaert, V. Raussens, "Antiparallel β -sheet: a signature structure of the oligomeric Aβ peptide", *Biochem. J.,* **2009**, 421, 415-423.

[77] L. Triguero, R. Singh, R. Prabhakar, "Comparative molecular dynamics studies of wild-type and oxidized forms of full-length Alzheimer Aβ peptides Aβ (1-40) and Aβ (1-42)", *J. Phys. Chem. B,* **2008**, 112, 7123-7131

[78] S. Barghorn, V. Nimmrich, A. Striebinger, C. Krantz, P. Keller, B. Janson, M. Bahr, M. Schmidt, R. S. Bitner, J. Harlan, et al., "Globular Aβ peptide(1-42) oligomer - a homogenous and stable neuropathological protein in Alzheimer's disease", *J. Neurochem.,* **2005**, 95, 834-847.

[79] S. Lesne, S.; M. T. Koh, L. Kotilinek, R. Kayed, C. G. Glabe, A. Yang, M. Gallagher, K. H. Ashe, "A specific Aβ protein assembly in the brain impairs memory", *Nature,* **2006**, 440, 352-357.

[80] R. Sabate, J. Estelrich, "Evidence of the existence of micelles in the fibrillogenesis of Aβ peptide", *J. Phys. Chem. B,* **2005**, 109, 11027-11032.

[81] F. Chiti, C. M. Dobson, "Protein misfolding, functional amyloid, and human disease", *Annu. Rev. Biochem.,* **2006**, 75, 333-366.

would be about 4.1 nm long, as detected by atomic force microscopy (8 nm). With the last 12 residues of Aβ1-40 modeled as a cylinder about 4.1 nm long with a radius of 0.25 nm, it can be estimated that about 350 Aβ1-40 C-terminal tails could fit into the micelle core. Other geometric forms, like elliptical or cylindrical micelles or bilayers, also permit the solvent exposure of a polar head group and the burial of a nonpolar tail. Both cylindrical micelles and bilayers can grow indefinitely on their ends or edges, respectively, whereas the number of monomers in spherical or elliptical micelles is limited geometrically. Then, the observation that the size distribution of β-balls is limited is more consistent with spherical or elliptical micelle geometries. β-balls have not been detected above pH 4. This model predicts that β-balls will be unstable above this pH since titration of the C-terminal carboxylate group (pK_a≈ 3.8) favors its solvent exposure and will break any hydrogen bonds that may form between the neutral carboxylic acid groups and disrupt the hydrophobic β-ball core. Previously, Yong *et al.*[*83*]suggested the existence of a spherocylindrical Aβ micelle forming at pH 1. Similarly to the β-ball, this oligomer could contain hidden C-terminal carboxylic acid groups and have a definite size range. This spherocylindrical micelle contains fewer monomers (30–50), and its dimensions suggest that the nonpolar residues, both the central and C-terminal hydrophobic segments, are buried within the micelle core. The higher ionic strength present at pH 1 could more effectively screen the charge-charge repulsions allowing K28 from different monomers to be positioned closer

[82] D. V. Laurents, P. M. Gorman, M. Guo, M. Rico, A. Chakrabartty, M. Bruix, "Alzheimer's Aβ 40 studied by NMR at low pH reveals that sodium 4,4-dimethyl-4-silapentane-1-sulfonate (DSS) binds and promotes β -ball oligomerization", *J. Biol. Chem.,* **2005**, 280, 3675-3685.

[83] W. Yong, A. Lomakin, M. D. Kirkitadze, D. B.Teplow, S. H.Chen, G. B. Benedek, "Structure determination of micelle-like intermediates in amyloid β protein fibril assembly by using small angle neutron scattering", *Proc. Natl. Acad. Sci. U. S. A.,* **2002**, 99, 150-154.

together and thus it accounts for its different geometry compared with β-balls. Other spherical Aβ peptide oligomers are present at endosomic or neutral pH prior to the formation of amyloid fibrils or protofibrils. Their C-terminal carboxylate groups are not buried but are charged and exposed, that is consistent with their smaller diameter. In contrast to the low pH Aβ oligomers, at neutral pH both positively and negatively charged groups are present and could be arranged to permit favorable electrostatic interactions in the oligomers.[84] The positioning of multiple positive charges on the exterior of the β-balls probably keeps them well separated in solution and prevents their evolution to fibrils. On the contrary, favorable electrostatic interactions in neutral pH spherical oligomers likely permit them to form progressively higher order aggregates.

2.5. Aβ FIBRILS QUATERNARY STRUCTURE

Due to their noncrystalline, insoluble nature, determination of the full molecular structures of amyloid fibrils requires specific experimental approaches.[85] In particular, full fibril structure determination requires experimental information at the primary, secondary, tertiary, and quaternary structural levels. Primary structure is defined as the amino acid sequence, while secondary describes segments with standard backbone conformations. While monomeric peptides present prevalently a random coil structure, for amyloid fibrils β-strands are the predominant secondary structural elements. The study

[84] L. O. Tjernberg, D. J. E. Callaway, A. Tjernberg, S. Hahne, C. Lilliehook, L. Terenius, J. Thyberg, C. Nordstedt, "A molecular model of Alzheimer Aβ peptide fibril formation", *J. Biol. Chem.,* **1999**, 274, 12619-12625.
[85] R. Tycko, "Progress towards a molecular-level structural understanding of amyloid fibrils", *Curr. Opin. Struct. Biol.,* **2004**, 14, 96-103.

of secondary structure in amyloid fibrils therefore consists on the identification of β-strand and non-β-strand segments (i.e., turns, loops, or bends). The secondary structure was investigated by hydrogen/deuterium (H/D) exchange [[86]], proline-scanning mutagenesis[[87]], infrared and Raman spectroscopies[[88]], electron paramagnetic resonance (EPR)[[89]], and solid-state NMR[[90]]. EPR and

[[86]] a) M. Hoshino, H. Katou, Y. Hagihara, K. Hasegawa, H. Naiki, Y. Goto, "Mapping the core of the β (2)-microglobulin amyloid fibril by H/D exchange", *Nat. Struct. Biol.,* **2002**, 9, 332-336; b) J. H. Ippel, A. Olofsson, J. Schleucher, E. Lundgren, S. S. Wijmenga, "Probing solvent accessibility of amyloid fibrils by solution NMR spectroscopy", *Proc. Natl. Acad. Sci. U. S. A.,* **2002**, 99, 8648-8653; c) I. Kheterpal, S. Zhou, K. D. Cook, R. Wetzel, "Aβ fibrils possess a core structure highly resistant to hydrogen exchange", *Proc. Natl. Acad. Sci. U. S. A.,* **2000**, 97, 13597-13601; d) K. Kuwata, T. Matumoto, H. Cheng, K. Nagayama, T. L. James, H. Roder, "NMR-detected hydrogen exchange and molecular dynamics simulations provide structural insight into fibril formation of prion protein fragment 106-126", *Proc. Natl. Acad. Sci. U. S. A.,* **2003**, 100, 14790-14795; e) A. Olofsson, A., J. H. Ippel, S. S. Wijmenga, S.S.; E. Lundgren, A. Ohman, "Probing solvent accessibility of transthyretin amyloid by solution NMR spectroscopy", *J. Biol. Chem.,* **2004**, 279, 5699-5707; f) S. S. S. Wang, S. A. Tobler, T.A. Good, E. J. Fernandez, "Hydrogen exchange-mass spectrometry analysis of Aβ peptide structure", *Biochemistry,* **2003**, 42, 9507-9514; g) N. A. Whittemore, R. Mishra, I. Kheterpal, A. D. Williams, R. Wetzel, E. H. Serpersu, "Hydrogen-deuterium (H/D) exchange mapping of Aβ(1-40) amyloid fibril secondary structure using nuclear magnetic resonance spectroscopy", *Biochemistry,* **2005**, 44, 4434-4441; h) K. I. Yamaguchi, H. Katou, M. Hoshino, K. Hasegawa, H. Naiki, Y. Goto, "Core and heterogeneity of β (2)-microglobulin amyloid fibrils as revealed by H/D exchange", *J. Mol. Biol.,* **2004**, 338, 559-571.

[[87]] A. D. Williams, E. Portelius, I. Kheterpal, J. T. Guo, K. D. Cook, Y. Xu, R. Wetzel, "Mapping Aβ fibril secondary structure using scanning proline mutagenesis", *J. Mol. Biol.,* **2004**, 335, 833-842.

[[88]] a) J. Dong, C. S. Atwood, V. E. Anderson, S. L. Siedlak, M. A. Smith, G. Perry, P. R. Carey, "Metal binding and oxidation of Aβ within isolated senile plaque cores: Raman microscopic evidence", *Biochemistry,* **2003**, 42, 2768-2773; b) P. E. Fraser, J. T. Nguyen, H. Inouye, W. K. Surewicz, D. J. Selkoe, M. B. Podlisny, D. A. Kirschner, "Fibril Formation by primate, rodent and dutch-hemorrahagic analogs of Alzheimer Aβ Protein", *Biochemistry,* **1992**, 31, 10716-10723.

[[89]] a) A. Der-Sarkissian, C. C. Jao, J. Chen, R. Langen, "Structural organization of □-synuclein fibrils studied by site-directed spin labeling", *J. Biol. Chem.,* **2003**, 278, 37530-37535; b) S. A. Jayasinghe, R. Langen, "Identifying structural features of fibrillar islet amyloid polypeptide using site-directed spin labeling", *J. Biol. Chem.,* **2004**, 279, 48420-48425; c) M. Torok, S. Milton, R. Kayed, P. Wu, T. McIntire, C. G. Glabe, R. Langen, "Structural and dynamic features of Alzheimer's Aβ peptide in amyloid fibrils studied by site-directed spin labeling", *J. Biol. Chem.,* **2002**, 277, 40810-40815.

[[90]] a) O. N. Antzutkin, J. J. Balbach, R. Tycko, "Site-specific identification of non-beta-strand conformations in Alzheimer's Aβ fibrils by solid-state NMR", *Biophys. J.,* **2003**, 84, 3326-3335; b) J. J. Balbach, Y. Ishii, O. N. Antzutkin, R. D. Leapman, N. W. Rizzo, F. Dyda, J. Reed, R. Tycko, "Amyloid fibril formation by Aβ (16-22), a seven-residue fragment of the Alzheimer's Aβ peptide, and structural characterization by solid state NMR", *Biochemistry,* **2000**, 39, 13748-13759; c) T. L. S. Benzinger, D. M. Gregory, T. S. Burkoth, H. Miller-Auer, D. G. Lynn, R. E. Botto, S. C. Meredith, "Two-dimensional structure of Aβ (10-35) fibrils", *Biochemistry,* **2000**, 39, 3491-3499; d) D. M. Gregory, T. L. S. Benzinger, T. S. Burkoth, H. Miller-Auer, D. G. Lynn, S. C. Meredith, R. E. Botto, "Dipolar recoupling NMR of biomolecular self-assemblies: determining inter- and intrastrand distances in fibrilized Alzheimer's Aβ peptide", *Solid State Nucl. Magn. Reson.,* **1998**, 13, 149-166; e) J. Heller, A. C. Kolbert, R. Larsen, M. Ernst, T. Bekker, M. Baldwin, S. B. Prusiner, A. Pines, D. E. Wemmer, "Solid-state NMR studies of the prion protein H1 fragment", *Protein Sci.,* **1996**, 5, 1655-1661; f) C. P. Jaroniec, C. E. MacPhee, N. S. Astrof, C. M. Dobson, R. G. Griffin, "Molecular conformation of a peptide fragment of

solid-state NMR measurements [91] were exploited also for the characterization of fibrils tertiary structure. X-ray diffraction[92]and solid-state NMR[93] were used to characterize quaternary structure, defined as the positions and orientations of β-sheets relative to one another.

Experimental determination of quaternary structure in amyloid fibrils has been quite difficult. The last models for amyloid fibrils structures support the idea that the core of an amyloid fibril contains two or more layers of β-sheets. The quaternary structure takes origin from a set of specific contacts involving amino acid side chains that project from adjacent β-sheets. In fibrils formed by relatively long peptides the adjacent β-sheets may be composed either by β-strands from the same peptide molecules or by β-strands from different molecules. This demonstrates that the side chain contacts from which quaternary structure takes origin can be either intramolecular or intermolecular. According to solid state NMR, hydrogen exchange and EPR data, in fibrils formed by the Aβ1-40 peptide residues 1-9 are structurally

---

transthyretin in an amyloid fibril", *Proc. Natl. Acad. Sci. U. S. A.,* **2002**, 99, 16748-16753; g) C. P. Jaroniec, C. E. MacPhee, V. S. Bajaj, M. T. McMahon, C. M. Dobson, R. G. Griffin, "High-resolution molecular structure of a peptide in an amyloid fibril determined by magic angle spinning NMR spectroscopy", *Proc. Natl. Acad. Sci. U. S. A,* **2004**, 101, 711-716; h) D. D. Laws, H. M. L. Bitter, K. Liu, H. L. Ball, K. Kaneko, H. Wille, F. E. Cohen, S. B. Prusiner, A. Pines, D. E. Wemmer, "Solid-state NMR studies of the secondary structure of a mutant prion protein fragment of 55 residues that induces neurodegeneration", *Proc. Natl. Acad. Sci. U. S. A.,* **2001**, 98, 11686-11690; i) A. T. Petkova, Y. Ishii, J. J. Balbach, O. N. Antzutkin, R. D. Leapman, F. Delaglio, R. Tycko, "A structural model for Alzheimer's Aβ fibrils based on experimental constraints from solid state NMR", *Proc. Natl. Acad. Sci. U. S. A.,* **2002**, 99, 16742-16747; j) A. T. Petkova, R. D. Leapman, Z. H. Guo, W. M. Yau, M. P. Mattson, R. Tycko, "Self-propagating, molecular-level polymorphism in Alzheimer's Aβ fibrils", *Science,* **2005**, 307, 262-265; k) C. Ritter, M. L. Maddelein, A. B. Siemer, T. Luhrs, M. Ernst, B. H. Meier, S. J. Saupe, R. Riek, "Correlation of structural elements and infectivity of the HET-s prion", *Nature,* **2005**, 435, 844-848.

[91] a) M. Margittai, R. Langen, "Template-assisted filament growth by parallel stacking of tau", *Proc. Natl. Acad. Sci. U. S. A.,* **2004**, 101, 10278-10283; b) A. A. Serag, C. Altenbach, M. Gingery, W. L. Hubbell, T. O. Yeates, "Arrangement of subunits and ordering of beta-strands in an amyloid sheet", *Nat. Struct. Biol.,* **2002**, 9, 734-739.

[92] a) E. D. Eanes, G. G. Glenner, "X-ray diffraction studies on amyloid filaments", *J. Histochem. Cytochem.,* **1968**, 16, 673-677; b) M. Sunde, C. C. F. Blake, "From the globular to the fibrous state: protein structure and structural conversion in amyloid formation", *Quarterly Reviews of Biophysics* **1998**, *31*, 1-39.

disordered, residues 10-22 and 30-40 form β-strands, and residues 23-29 form a bend or loop. The two β-strands form two separate in-register, parallel β-sheets, which can make contact with one another because of the intervening bend segment. Shivaprasad *et al*.[94] obtained the more recent information about Aβ1-40 quaternary contacts. They performed disulfide cross-linking experiments on Aβ1-40 double cysteine mutants. These data suggest a quaternary structure in which side chains of L17 and L34 are in proximity. As L17C/L34C, L17C/M35C, and L17C/V36C mutants were all able to form amyloid fibrils after oxidation in their monomeric states, they concluded that other quaternary structures for Aβ1-40 fibrils are also possible. At the same time, it has been demonstrated that Aβ1-40 modified with a lactam cross-link between residues D23 and K28 gives rise to amyloid fibrils significantly more rapidly than the wild-type peptide.[95] These experiments are in agreement with the observation by solid-state NMR of the presence of a salt bridge interaction between side chains of D23 and K28 in fibrils formed with gentle agitation, while this kind of salt bridge is absent in fibrils formed under purely quiescent conditions. This is an evidence of the polymorphism at molecular-level in Aβ1-40 fibrils. In 2006, Petkova and co-workers[96] obtained evidence of the fact that each layer of molecules consists of two β-sheet layers. Mass-per-length (MPL) measurements by scanning transmission electron microscopy showed that the basic structural unit in these fibrils contains two layers of Aβ1-40

[93] N. A. Oyler, R. Tycko, "Absolute structural constraints on amyloid fibrils from solid-state NMR spectroscopy of partially oriented samples", *J. Am. Chem. Soc.,* **2004**, 126, 4478-4479.
[94] S. Shivaprasad, R. Wetzel, "An intersheet packing interaction in Aβ fibrils mapped by disulfide cross-linking", *Biochemistry,* **2004**, 43, 15310-15317.
[95] K. L. Sciarretta, D. J. Gordon, A. T. Petkova, R. Tycko, S. C. Meredith, "A beta 40-Lactam(D23/K28) models a conformation highly favorable for nucleation of amyloid", *Biochemistry,* **2005**, 44, 6003-6014.
[96] A. T. Petkova, W. M. Yau, R. Tycko, "Experimental constraints on quaternary structure in Alzheimer's β -amyloid fibrils", *Biochemistry,* **2006**, 45, 498-512.

molecules in a cross-β motif. Specifically, the experimentally observed structural unit with minimum MPL, called " protofilament", is a four-layered β-sheet structure with both "internal" and "external" quaternary contacts. In particular, internal quaternary contacts exist between side chains of L17 and F19 and side chains of I32, L34, and V36, while external quaternary contacts involve the side chain of I31 and the peptide backbone at G37, and external quaternary contacts between the side chain of M35 and the peptide backbone at G33. These data support the *C*2*z* quaternary structure depicted in **Fig. 2-5-1**.

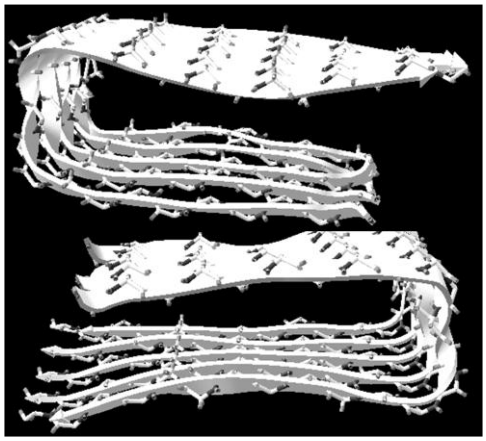

Fig. 2-5-1. Representation of candidate quaternary structure for Aβ1-40 fibrils with *C*2*z* symmetry

According to the model they proposed, side chains of L17, F19, I32, L34, and V36 create an hydrophobic cluster that apparently stabilizes the fold of a single molecular layer by internal quaternary contacts. Glycine residues 33, 37, and 38 create grooves into which the side chains of I31 and M35 fit at the interface between molecular layers, generating the external quaternary contacts. Oppositely, charged D23 and K28 side chains interact in an intermolecular fashion in the interior of a single molecular layer with STAG-(±2) stagger.

Besides, this model contains channels that are lined by side chains of F19, A21, D23, K28, A30, and I32 and that may contain “water wires”.

In addition, they demonstrated that the internal quaternary contacts in agitated and quiescent fibrils are different. In fact, Aβ1-40 fibrils grown under different conditions can have different dimensions, morphologies, MPL values, and NMR spectra, and therefore qualitatively different molecular structures.

2.6. COMPARISON BETWEEN OLIGOMERS AND FIBRILS STRUCTURE

Spherical Aβ intermediates were studied by S. Chimon *et al*.[97] in a recent work, in which they have verified if substantial structural transitions precede fibril formation in the amyloid misfolding of the full length Aβ. They studied the structural transition of Aβ1-40 in a 100 μM solution, in phosphate saline buffer at 4°C. They saw that monomeric Aβ1-40 peptides in random coil conformation self-assemble into aggregates without amyloid like β-sheet structure, then they generate toxic spherical intermediates predominated by well ordered β-sheet structures. These spherical intermediates have higher neurotoxicity than monomers or matured fibrils. These intermediates, analyzed by solid-state NMR, showed that they have well ordered structures: there is a structural disorder, for the first ten residues at the N-terminal region, while in the C-terminus the structural disorder is probably minimal. Comparing the structures of these intermediates with that of the fibrils, the dihedral angles and the suggested β-sheet regions were nearly identical between fibrils and

[97] S. Chimon, M. A. Shaibat, C. R. Jones, D. C. Calero, B. Aizezi, Y. Ishii, “Evidence of fibril-like β-sheet structures in a neurotoxic amyloid intermediate of Alzheimer's Aβ”, *Nature Structural & Molecular Biology,* **2007**, *14*, 1157-1164.

intermediates. The measurements of the interstrand distance suggest that both have in-register parallel β-sheet structure. In conclusion their hypothesis is that Aβ1-40 misfolds into an intermediate state that has well-defined fibrils like parallel β-sheet structures (secondary structure) but with only a metastable supramolecular packing (tertiary structure) before final fibrillization. The higher toxicity displayed by the intermediates may be attributed to the unique supramolecular structure that they assume in addition to the conformational changes of Aβ1-40. It was already known from previous studies carried out on Aβ oligomers that there is a dominance of β-sheet structure, but there was no distinction between parallel and antiparallel structures. Anyway, by using ATR-FTIR spectroscopy, it has been demonstrated recently that parallel and anti-parallel β-sheet structures can be distinguished based on the analysis of the Amide I (1700-1600 cm^{-1}) region. In antiparallel β-sheet structures the amide I region displays two typical components, while for parallel β-sheet structures the amide I region displays only the major component around 1630 cm^{-1}. FTIR spectra of Aβ1-42 in fibril forming conditions showed typical parallel β-sheet feature, characterized by a maximum of absorbance at 1630 cm^{-1} in the amide I region, while spectra of Aβ1-42 oligomers were significantly different, indicating that these entities adopt a different structure: the amide I region is characterized by the presence of the two characteristic components of antiparallel β-sheet structure, at 1630 and 1695 cm^{-1}. A quantitative analysis of the amide I region showed that random coil and/or helical structures represented 20-26 and 5-10% for oligomers and fibrils respectively, whereas β-sheet structures were the most abundant (48-57% and 75% respectively). So, even if fibrils and oligomers are rich in β-sheets, they do not adopt the same

conformation. The comparison of the overall shape of the Aβ1-42 spectra in the amide I and II range with the entire database by means of a cluster analysis based on Euclidian distance measurement, clearly indicated that Aβ fibrils spectra do not cluster with other protein spectra and that Aβ oligomers spectra are clustered with five antiparallel β-sheet proteins (avidin, concanavalin A, lentil lectin, xylanase). IR spectra of Aβ oligomers are very similar with bacterial outer membrane porins which are folded as β-barrels, with antiparallel β-sheet organization (**Fig. 2-6-1**). This β-barrel conformation is ideally suited to insert into a cellular membrane, spanning a lipid bilayer. Such an organization can potentially lead to permeabilization of cells, contributing to the toxicity associated with these species.[76]

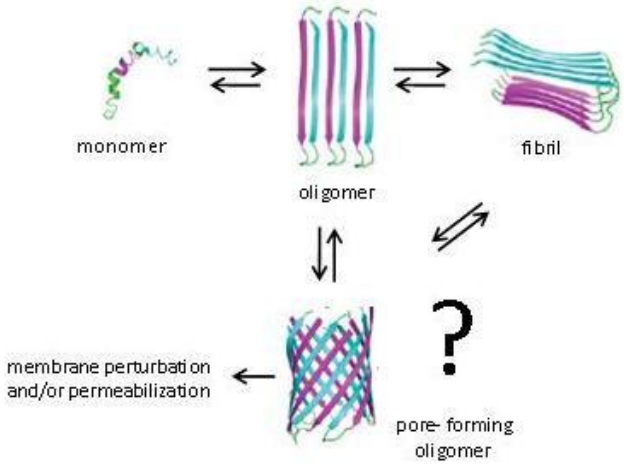

Fig. 2-6-1. A schematic representation of Aβ oligomers in a putative pore-forming conformation.

Liping Yu *et al*.[98] identified soluble forms of Aβ1-42 called preglobulomers and globulomers. Preglobulomers have a molecular weight of 16 kDa (about 4

[98] L. P. Yu, R. Edalji, J. E. Harlan, T. F. Holzman, A. P. Lopez, B. Labkovsky, H. Hillen, S. Barghorn, U. Ebert, P. L. Richardson, et al. "Structural characterization of a soluble Aβ peptide oligomer", *Biochemistry,* **2009**, 48, 1870-1877.

peptides/soluble aggregate), while Aβ1-42 globulomers have a molecular weight of 64 kDa (corresponding to 12-16 peptides/soluble aggregates). By NMR analysis the preglobulomers show characteristic chemical shifts of the backbone atoms, a pattern of protected amides, and NOE data which are all consistent with the presence of two β-strands from V18 to D23 and from K28 to V40. Residues V18-D23 form one strand of an intrachain antiparallel β-sheet connected by a β-hairpin to the other intrachain strand K28-G33, while L34-V40 forms an interchain in-register parallel β-sheet. So the model proposed is that of a dimer (**Fig. 2-6-2**).

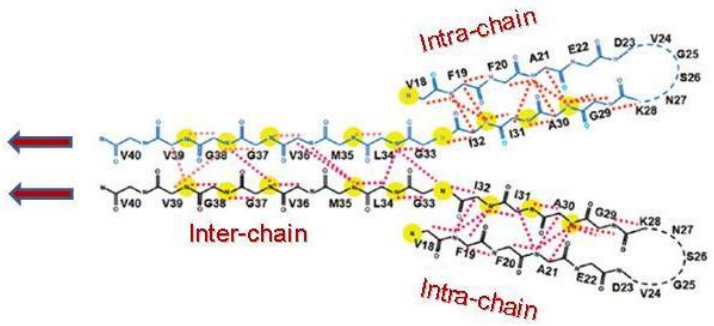

Fig. 2-6-2. Summary of NOE constraints obtained from the N-Met-Aβ1-42 samples. Dashed lines indicate observed NOEs. Circles indicate the backbone amides that exhibit slow exchange in the NH/ND exchange experiments. [99]

Globulomers, instead, were not suitable for structural studies, however amide exchange experiments gave a pattern consistent with the hypothesis that both pre-globulomers and globulomers adopt a similar secondary structure and that the Aβ1-42 globulomer is an oligomer of pre-globulomer units. The amide exchange data of the preglobulomer and globulomers were very different from the fibril forms. In fibril form the amides 11, 12, 15-22, 24, 25 and 28-30 are fully protected, while in the globulomer form only the last 11 residues of the

peptide are fully protected. Aβ fibrils are composed of two in-register interstrand parallel β-sheets connected by a bend between residues 25 and 30. Both the fibrils and the preglobulomers structures exhibit an interstrand parallel β-sheet for the C-terminal residues (34-42). However, in contrast to the fibril structures, the preglobulomers have an intrastrand antiparallel β-sheet connected by a β-hairpin between D23 and K28. Residues 10-16, which are parts of the first β-sheet in fibrils, are disordered in the pre-globulomer. Probably, a bend versus a turn between residues 22 and 30 is the trait that leads to fibrils versus soluble globulomers (**Fig. 2-6-3**).

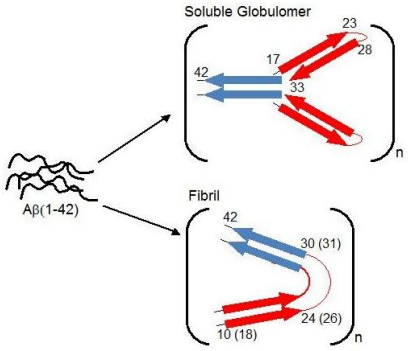

Fig. 2-6-3 Representation of the two stable forms of amyloid β-peptides. The form of soluble globulomer form and that of insoluble fibril. The parallel β-sheet which involves the hydrophobic C terminus of the peptide and common to both forms is highlighted in blue.

[99] L. M. Hou, H. Y. Shao, Y. B. Zhang, H. Li, N. K. Menon, E. B. Neuhaus, J. M. Brewer, I. J. L. Byeon, D. G. Ray, M. P. Vitek, et al., "Solution NMR studies of the Aβ (1-40) and Aβ (1-42) peptides establish that the met35 oxidation state affects the mechanism of amyloid formation", *J. Am. Chem. Soc.*, **2004**, 126, 1992-2005.

2.7. THERAPEUTIC APPROACHES BASED ON THE INHIBITION OF Aβ PEPTIDES AGGREGATION

The objectives for the treatment of patients suffering from AD are those of impeding, or at least to slow down, the loss of memory and cognitive functions, without inducing serious side effects. Furthermore, it aims at the development of drugs that affect multiple processes critical to the course of the disease, preventing damage to vital functions and the deterioration of the quality of life. The main approaches undertaken for the prevention of the aggregation and toxicity of Aβ are the following:

1) inhibition of aggregation using modified peptides and peptidomimetics derived from Aβ sequence;

2) use of antibodies directed against Aβ;

3) targeting of Aβ with peptides and proteins selected in vitro;

4) targeting of Aβ with small molecules.[100]

2.7.1. NATURAL PROTEIC LIGANDS INTERACTING WITH Aβ PEPTIDES

Although the mechanism of Aβ toxicity is not yet fully understood, many experiments have been conducted to determine the possible existence of natural proteins capable of binding to these peptides. Some of these natural ligands may represent a link between the accumulation of Aβ and their cellular toxicity. To detect *in vivo* protein-protein interactions of this type, the conventional system of the two hybrid is used, applied to Aβ peptides. Affinity for the Aβ is thus found by various molecules including catalase, cytochrome

[100] C. I. Stains, K. Mondal, I.Ghosh, "Molecules that Target beta-Amyloid"; *ChemMedChem,* ***2007,*** 2, 1674-1692.

oxidase, pyruvate dehydrogenase, transthyretin and casein kinase I and II.[101] For example, in the last case, the observation of an increased level of phosphorylation in Alzheimer's patients has led to the hypothesis that the Aβ is likely to disrupt in a direct manner the activity of certain kinases: in fact there was an increased concentration-dependent activity of casein kinase I and II, by monitoring the levels of phosphorylation of casein in dependence of the accumulation of Aβ.[102] Overexpression of a constitutively active form of casein kinase I has resulted in an increase of Aβ levels in the brain tissue cultures, and three different specific inhibitors of casein kinase I have determined a decrease in the levels of Aβ product. This approach has the potential for the identification of novel therapeutic agents for the treatment of AD, although it should still determine whether the observed effects are directly or indirectly mediated by Aβ in a physiological context.[103]

Transthyretin, a protein found in the cerebral fluid, has been discovered to bind the Aβ through a fractionation of a mixture of elements that resulted in a complex active against amyloid.[104] Subsequently, transgenic mice containing a mutation in the APP gene that predispose to the onset of AD, have shown an overexpression of transthyretin.[105] This overexpression correlates with a decrease in the progression of the symptoms of AD, that delay the onset of the disease. Several studies have suggested that the transthyretin decreases the rate of fibrils formation, decreasing their lateral association as well as their

[101] S.R. Hughes, S. Goyal, J.E. Sun, P. Gonzalez-DeWhitt, M.A. Fortes, N.G. Riedel, S.R. Sahasrabudhe, *Proc. Natl. Acad. Sci*. USA, **1996**, 93, 2065-2070.
[102] A. Chauhan, V.P.S. Chahuan, N. Murakami, H. Brockerhoff, H.M. Wisniewski, *Brain Res*., **1993**, 629, 47-52.
[103] M. Flajolet, G. He, M. Heiman, A. Lin, A.C. Nairn, P. Greengard, *Proc. Natl. Acad. Sci*. USA, **2007**, 104, 4159-4164.
[104] A. L. Schwarzman, L. Gregori, M. P. Vitek, S. Lyubski, W. J. Strittmatter, J. J. Enghilde, R. Bhasin, J. Silverman, K. H. Weisgraber, P. K. Coyle, M. G. Zagorski, J. Talafous, M. Eisenberg, A. M. Saunders, A. D. Roses, D. Goldgaber, *Proc. Natl. Acad. Sci*., USA, **1994**, 91, 8378-8372..

speed of elongation. The collected data indicate that, at concentrations of 2 μM of transthyretin and 140 pM of Aβ, transthyretin binds to fibrillar forms of Aβ and stops the formation of plaques. These data are particularly interesting, considering that transthyretin itself is directly involved in another protein misfolding disease.[106] It is clear, however, that there are many possible candidates among natural proteins that may interact with the Aβ, directly or indirectly, and modulate their activity.[100]

2.7.2. INHIBITION WITH MODIFIED PEPTIDES AND PEPTIDOMIMETICS

The intrinsic affinity of Aβ for itself suggested that Aβ–specific interactions could be the basis for the development of compounds binding to Aβ and preventing its polymerization. It has been claimed that fibrillogenesis can be inhibited by short synthetic peptides partially homologous to Aβ. Several elegant strategies have been used to design peptidic inhibitors of Aβ aggregation. Typically, fibril disrupting chemical elements are incorporated into Aβ derived peptides in the form of N– or C–terminal modifications, conformationally constrained amino acids, or modifications to the peptide backbone. These concepts have also been applied to D–amino acid variants of the parent Aβ sequence. Gazit *et al.*[107] analyzed a variety of short functional fragments from unrelated amyloid–forming proteins and observed a remarkable occurrence of aromatic residues. They speculated that aromatic residues raise the possibility that π–stacking may play an important role in the molecular recognition and self–assembly process that lead to amyloid

[105] T. D. Stein, J. A. Johnson, *J. Neurosci*., **2002**, 22, 7380 –7388
[106] S. M. Johnson, R. L. Wiseman, Y. Sekijima, N. S. Green, S. L. Adamski-Werner, J. W. Kelly, *Acc. Chem. Res*. **2005**, 38, 911 – 921.

formation. In Aβ the aromatic residues are the two phenylalanine residues in position 19 and 20. In particular, the short fragment of Aβ QKLVFF was shown to bind specifically to the full-length peptide.[108] Other studies have shown that not only QKLVFF, but also LVFFA and its derivatives[109] and LPFFD[110] are all potent inhibitors of amyloid formation. Another recent study demonstrated that the seven amino acid Aβ fragment, KLVFFAE, forms well–ordered amyloid fibrils.[111] These findings point to the pair of phenylalanine residues as the major structural element that mediates the binding of the QKLVFF peptide to the Aβ polypeptide. As the formation of amyloid fibrils is a process of molecular recognition and self–assembly, the high affinity and selectivity of the FF motif seems to provide the molecular recognition element needed for such process in the context of the full–length Aβ. Other examples of similar peptidic inhibitors, based on the LVFF sequence were proposed also by Cairo *et al*.,[112] Chalifour *et al*.[113] and by Austen and coworkers.[114] Chafekar and co-workers

---

[107] E. Gazit, "A possible role for π-stacking in the self-assembly of amyloid fibrils. *FASEB J.*, **2002**, *16*, 77-83.

[108] L. O. Tjernberg, J. Näslund, F. Lindqvist, J. Johansson, A. R. Karlström, J. Thyberg, L. Terenius, C. Nordstedt, "Arrest of β-Amyloid Fibril Formation by a Pentapeptide Ligand", *J. Biol. Chem.*, **1996**, *271*, 8545-8548.

[109] M. A. Findeis,G. M. Musso, C. C. Arico–Muendel, H. W. Benjamin,A. M. Hundal, J. J. Lee, J. Chin, M. Kelley, J. Wakefiel, N. J. Hayward, N.J.; S. M. Molineaux, "Modified-peptide inhibitors of amyloid beta-peptide polymerization", *Biochemistry*, **1999**, 38, 6791-6800.

[110] C. Soto, E. Sigurdsson, L. Morelli, R. Kumar, E. Castano, B. Frangione, "Beta-sheet breaker peptides inhibit fibrillogenesis in a rat brain model of amyloidosis: implications for Alzheimer's therapy", *Nat. Med.*, **1998**, *4*, 822-826.

[111] J. Balbach, A. Petkova, N. Oyler, O. Antzutkin, D. Gordon, S. Meredith, R. Tycko, "Amyloid fibril formation by A*β*16-22, a seven-residue fragment of the Alzheimer's *β*-amyloid peptide, and structural characterization by solid-state NMR", *Biochemistry,* **2000**, *39*, 13748-13759.

[112] C. C. Cairo, A. Strzelec, R. M. Murphy, L. L. Kiessling, "Affinity based inhibition of β-amyloid toxicity", *Biochem.*, **2002**, *41*, 8620- 8629.

[113] R. J. Chalifour, R. W. McLaughlin, L. Lavoie, C. Morisette, N. Tremblay, M. Boulè, P. Sarazin, D. Stéa, D. Lacombe, P. Tremblay, F. Gervais, "Stereoselective interactions of peptide inhibitors with the β-amyloid peptide", *J. Biol. Chem.*, **2003**, 278, 34874-34881.

[114] B. M. Austen, K. E. Paleologu, S. A. E. Ali, M. M. Qureshi, D. Allsop, O. M. A. El–Agnaf, "Designing peptide inhibitors for oligomerization and toxicity of Alzheimer's β -amyloid peptide", *Biochemistry*, **2008**, 47, 1984-1992.

[115] synthesized a first generation of KLVFF dendrimer and showed that the linkage of KLVFF to a dendrimeric scaffold potentiates its inhibitory effect on Aβ aggregation, and on the disassembly of pre-existing aggregates. A β-sheet breaker peptide iAβ5 (LPFFD) was proposed by Soto and coworkers,[110] and it displays the ability to inhibit in a dose dependent manner the aggregation of both Aβ1-40 and Aβ1-42, to disassemble preformed fibrils in vitro, and to prevent neuronal death induced by fibrils in cell culture. Etienne and coworkers [116] proposed α,α-disubstituted aminoacids (ααAA) in the hydrophobic core of Aβ (**fig. 2-7-2-1**); they used an alternating ααAA/L-aminoacid design to obtain a peptide that interacts with Aβ by hydrogen bonding as well as by side-chain interactions.

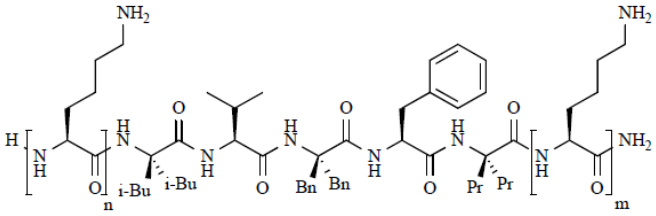

Fig. 2-7-2-1. Design of peptides with ααAAs as blockers of assembly; AMY–1: n=1, m=6; AMY–2: n=7, m=0.

Gordon *et al*.[117] and Hughes *et al*.[118] proposed N-methylated derivatives based on Aβ sequence (**Fig. 2-7-2-2**), able to prevent the aggregation of Aβ and

[115] S. M. Chafekar, H. Malda, M. Merkx,E. W. Meijer, D. Viertl, H. A. Lashuel, F. Baas, W. Scheper, " Branched KLVFF tetramers strongly potentiate inhibition of beta-amyloid aggregation", *ChemBioChem*, **2007**, 8, 1857-1864.

[116] M. Etienne, J. Aucoin, Y. Fu, R. McCarley, R. Hammer, "Stoichiometric inhibition of amyloid beta-protein aggregation with peptides containing alternating alpha, alpha-disubstituted amino acids", *J. Am. Chem. Soc.*, **2006**, *128*, 3522-3523.

[117] D. J. Gordon, K. L. Sciarretta, S. C. Meredith, "Inhibition of beta-amyloid 40 fibrillogenesis and disassembly of beta-amyloid(40) fibrils by short beta-amyloid congeners containing N-methyl aminoacids at alternate residues", *Biochemistry*, **2001**, 40, 8237-8245.

inhibiting the resulting toxicity of the peptide. N-methylation, in fact, is known to promote β-sheet formation by locking the residue into a β-conformation and has been shown to generate soluble monomeric β-sheet peptides.

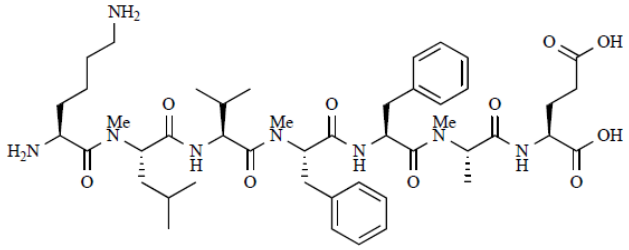

Fig. 2-7-2-2. Design of peptides containing N-methylated aminoacids.

2.7.3. TARGETING OF Aβ WITH PEPTIDES AND SELECTED PROTEINS

IN VITRO

Although antibodies are clearly the first choice for the targeting of proteins and peptides, the selection of peptides and proteins using phage display scaffolds proved to be an alternative route for targeting Aβ. In one of the more recent studies a library of 20 residue peptides has been used to select potential ligands of Aβ1-40 using phage display. In this way only two peptides were identified as capable of interacting with the amyloid deposits. The selected sequences have suggested a region rich in aromatic residues (W/F) X5-(W/F)X2(W/F), sometimes containing also proline residues, which probably have a turn shape.[119] The phage display has been used starting from the nucleus KLVFF to identify peptides capable of binding different Aβ species, that

[118] E. Hughes, R. M. Burke, A. J. Doig, "Inhibition of toxicity in the β-amyloid peptide fragment β-(25-35) using *N*-methylated derivatives", *J. Biol. Chem.*, **2000**, 275, 25109-25115.
[119] C. K. Kang, V. Jayasinha, P. T. Martin, "Identification of peptides that specifically bind Abeta1-40 amyloid in vitro and amyloid plaques in Alzheimer's disease brain using phage display", *Neurobiol. Dis*., **2003**, 14, 146 –156.

are generated during the pathway of aggregation. Surprisingly, peptides selected for binding to monomeric species had no effect on the speed of aggregation, while this effect was proper of ligands selected for the ability to interact with already aggregated species. A summary of the major peptides identified as Aβ ligands is shown in **Table 2**.[120]

Peptide	**Results of the screening**
DWGKGGRWRLWPGASGKTEA	Binding of A*β* in vitro (K_d = 60 nM)
PGRSPFTGKKLFNQEFSQDQ	Binding of amyloid deposits
D-QSHYRHISPAQV	Binding of A*β* in vitro (K_d = 400 nM)
FYLKVPSSLHHHH	Preferential binding to oligomeric forms
NYSKMIFSHHHH	Preferential binding to aggregated forms
GRDKLVFFHHHH	Preferential binding to monomeric forms
HNHKLVFFHHQH	Preferential binding to aggregate forms
MAQTFWLSIQGKTLYWQIRIYAID	Inhibition of fibrils formation

Table 2. Summary of the major peptides identified as Aβ ligands

2.7.4. ANTIBODIES AGAINST Aβ

Over the past 10 years, Aβ immunotherapy has emerged from preclinical studies in transgenic mouse models of AD to enter clinical trials in humans. At the moment, at least 13 different Aβ immunotherapies are in clinical trials worldwide (**Table 3** and **Table 4**).[121]

[120] B. P. Orner, L. Liu, R. M. Murphy, L. L. Kiessling, "Phage display affords peptides that modulate beta-amyloid aggregation", *J. Am. Chem. Soc*., **2006**, 128, 11882– 11889.
[121] C. A. Lemere, E. Masliah, E. "Can Alzheimer disease be prevented by amyloid-beta immunotherapy?", *Nature Reviews Neurology,* **2010**, *6*, 108-119.

Therapy	Sponsors	Antibody	Phase and number of trials	Estimated patient enrollement	Treatment duration	Primary outcome measures	Estimated completion date of final trial
Bapineuzumab (AAB-001)	Elan-Wyeth; Janssen	Anti-Aβ aminoterminal MAb	III; one trial	1.350	2.5 years	Safety and efficacy	July 2012
Bapineuzumab (AAB-001)	Elan-Wyeth; Janssen	Anti-Aβ aminoterminal MAb	III; five trials	4.650	18 months	Cognition and global function	April 2011
Solanezumab (LY2062430)	Eli Lilly	Anti-Aβ mid-region MAb	III; two trials	2.000	19 months	Cognition and global function	July 2012

Table 3: Examples of ongoing clinical trials of passive Aβ immunotherapies

Therapy	Sponsors	Vaccine	Phase and number of trials	Estimated patient enrollement	Treatment duration	Primary outcome measures	Estimated completion date of final trial
ACC001	Elan-Wyeth	Aβ aminoterminal conjugate	II; three trials	360	24 months	Safety, tolerability and treatment-related adverse effects	May 2012
V950	Merck	Aβ aminoterminal conjugate	I; one trial	124	48 months	Safety and tolerability	April 2014

Table 4. Examples of ongoing clinical trials of active Aβ immunotherapies

Several types of immunotheraphy for AD are under investigation. Presently there are three different approaches to generate antibodies directed against amyloid-β. The first strategy involves the active-immunization with full length Aβ, which contains 42 aminoacids. After injection, the peptide is taken up by antigen-presenting cells, and fragments of the peptide are presented to T cells. Subsequently, various B cells that can recognize epitopes on Aβ1-42 are engaged and proliferate. These eventually produce anti-Aβ antibodies. It is thought that these antibodies are key to effect the reduction in Aβ pathology that has been seen in a number of APP transgenic mouse models after Aβ1-42 immunization. The second type of active-immunization approach involves the administration of small fragments of Aβ conjugated to an unrelated carrier protein. This immunoconjugate approach is similar to the first strategy with the exception that the T cells are stimulated by the carrier protein rather than the Aβ fragment (which lacks T-cell epitopes). This approach also yields a strong antibody response to a region of the Aβ peptide. The third strategy, the passive immunization, is based on the administration of anti-Aβ antibodies directly. This approach does not require any type of immunological response from the host and, as such, has the potential to be useful in individuals that might not otherwise generate an immune response to Aβ administration.[122]

Recent developments have made it possible to use Aβ-immunotherapy, using site-directed antibodies not only for the treatment, but also to understand the kinetics of aggregation of Aβ peptides. Antibodies produced against Aβ1-42 have shown the ability to lower brain levels of amyloid plaques in mice. However, a clinical trial for the use of fibrils of Aβ1-42 for active immunization

[122] D. Schenk, "Amyloid-beta immunotherapy for Alzheimer's disease: the end of the beginning", *Nature Reviews*, **2002**, *3*, 824-828.

was discontinued when about 6% of patients developed meningoencephalitis, probably due to a potent immune response mediated by T cells.[123,124] To avoid the risk of autoimmune responses of this type and develop safer vaccines, the 1-15 N-terminal fragment of Aβ was then used, which was shown to be without side effects mediated by T cells in mice and man.[125,126]

Aβ antibodies are still emerging as useful chemical probes to define the passages with which the Aβ are assembled: antibodies able to bind the amyloid fibrils but not the soluble oligomeric forms of Aβ1-40 have been described.[127]

2.7.5. INHIBITION WITH NON-PEPTIDIC SMALL MOLECULES

Some non-peptidic small molecules are able not only to inhibit the formation and extension of β–amyloid fibrils (fAβ), but also to destabilize Aβ fibrils *in vitro*. These include naturally occurring or commercially available bioactive compounds, drugs, surfactants,[128] Cu/Zn chelators,[129] phenothiazines[130] and sulfonated dyes such as Congo red (CR) and its derivatives.[131] Among

[123] K. Birmingham, S. Frantz, "Set back to Alzheimer vaccine studies", *Nat. Med*., **2002**, 8, 199 –200.

[124] J. M. Orgogozo, S. Gilman, J. F. Dartigues, B. Laurent, M. Puel, L. C.Kirby, P. Jouanny, B. Dubois, L. Eisner, S. Flitman, B. F. Michel, M. Boada,A. Frank, C. Hock, Subacute meningoencephalitis in a subset of patients with AD after Abeta42 immunization, *Neurology,* **2003**, 61, 46–54.

[125] M. Lee, F. Bard, K. Johnson-Wood, C. Lee, K. Hu, S. G. Griffith, R. S.Black, D. Schenk, P. Seubert, "Abeta42 immunization in Alzheimer's disease generates Abeta N-terminal antibodies", *Ann. Neurol.,* **2005**, 58, 430–435.

[126] T. Town, J. Tan, N. Sansone, D. Obregon, T. Klein, M. Mullan, „Characterization of murine immunoglobulin G antibodies against human amyloid-beta1-42", *Neurosci. Lett*., **2001**, 307, 101 –104.

[127] M. Necula, R. Kayed, S. Milton, C. G. Glabe, "Small molecule inhibitors of aggregation indicate that amyloid beta oligomerization and fibrillization pathways are independent and distinct", *J. Biol. Chem*., **2007**, 282, 10311 –10324.

[128] R. Sabate, J. Estelrich, "Stimulatory and inhibitory effects of alkyl bromide surfactants on β-amyloid fibrillogenesis", *Langmuir*, **2005**, 21, 6944-6949.

[129] A. I. Bush, "Metal complexing agents as therapies for Alzheimer's disease", *Neurobiol. Aging*, **2002**, *23*, 1031-1038.

[130] S. Taniguchi, N. Suzuki, M. Masuda, S. Hisanaga, T. Iwatsubo, M. Goedert, M. Hasegawa, "Inhibition of heparin-induced Tau filament formation by phenothiazines, polyphenols, and porphyrins", *J. Biol. Chem.*, **2005**, 280, 7614-7623.

[131] S. J. Pollack, I. I. J. Sadler, "Sulfonated dyes attenuate the toxic effects of ?-amyloid in a structure-specific fashion", *Neurosci. Lett.*, **1995**, 197, 211-214.

them CR was the first small molecule reported to bind to amyloid in tissue sections, exhibiting the characteristic yellow–green birefringence under cross polarized light. Later thioflavin T (ThT) and thioflavin S (ThS) were also shown to stain amyloid deposits. These two dyes are the classical reagents to detect characteristic β–sheet mediated fibrillization. Many small molecules able to interact as Aβ ligands possess aromatic moieties that, according to the theory of Porat *et al*.,[132] can intercalate between grooves created by β-sheets in both the soluble oligomeric forms and as well as in the large fibrils. Among these molecules red wine and green tea related polyphenols[132,133] display a very high activity against amyloid fibrils and plaque formation. The wine–related polyphenols inhibit Aβ fibrils formation from Aβ(1–40) and Aβ (1–42) as well as destabilize preformed Aβ (1–40) and fAβ (1–42) fibrillar aggregates dose–dependently *in vitro*. Within this class of compounds tannic acid showed the best activity.

Another important Aβ-ligand is curcumin (diferulomethane) (**Figure 2-7-5-1**), a low molecular weight molecule with potent antioxidant and anti–inflammatory activities that has a favorable toxicity profile and is also under development as a potential cancer chemotherapeutic agent.

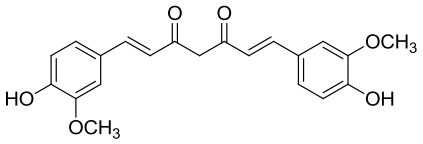

Figure 2-7-5-1. Curcumin structure

[132] Y. Porat, A. Abramowitz, E. Gazit, "Inhibition of amyloid fibril formation by polyphenols: structural similarity and aromatic interactions as a common inhibition mechanism", *Chem. Biol. Drug Des.,* **2006**, 67, 27-37.

[133] K. Ono, Y. Yoshiike, A. Takashima, K. Hasegawa, H. Naiki, M. Yamada, "Potent anti-amyloidogenic and fibril-destabilizing effects of polyphenols *in vitro*: implications for the prevention and therapeutics of Alzheimer's disease", *J. Neurochem.*, **2003**, *87*, 172-181.

Yang *et al.*[134] worked on Curcumin as Aβ aggregation inhibitor both *in vitro* and *in vivo*. They showed that under aggregating conditions *in vitro*, Curcumin inhibited the aggregation (IC_{50} = 0.8 μM) and disaggregated fibrillar Aβ40 (EC_{50} = 1 μM). *In vivo* studies showed that Curcumin injected peripherally into aged transgenic mice expressing AD pathology crossed the blood–brain barrier and bound Aβ plaques. When fed to aged transgenic mice with advanced amyloid accumulation, Curcumin labeled plaques and reduced amyloid levels and plaque burden. In 2007, Reinke *et al*. [135] studied the structure–activity relationships of amyloid β–aggregation inhibitors based on Curcumin. They studied the effect of three prominent features on inhibition of amyloid aggregation: the presence of two aromatic end groups, the substitution pattern of these aromatics, and the length and flexibility of the linker region. They found that modification of any one of the modules has profound effects on activity. In particular length and flexibility of the linker region are not independent variables and the optimal are rigid (less than two freely rotating carbons) and restricted between 8 and 16 Å. Interestingly, many of the best amyloid ligands fall within the observed optimal range. For example, Congo Red, Chrysamine G, Nordehydroguaiaretic Acid (NDGA) and rosmarinic acid all meet these requirements.

[134] F. Yang, G. P. Lim, A. N. Begum, O. J. Ubeda, M. R. Simmons, S. S. Ambegaokar, P. Chen, R. Kayed, C. G. Glabe, S. A. Frautschy, G. M. Cole, "Curcumin inhibits formation of amyloid β oligomers and fibrils, binds plaques, and reduces amyloid *in vivo", J. Biol. Chem.*, **2005**, 280, 5892-5901.

[135] A. A. Reinke, J. E. Gestwicki, "Structure–activity relationships of amyloid beta-aggregation inhibitors based on curcumin: influence of linker length and flexibility", *Chem. Biol. Drug Des.*, **2007**, 70, 206-215.

Rosmarinic acid (RA) (**Figure 2-7-5-2**) is another interesting inhibitor of Aβ aggregation, with IC_{50} of 0.29 and 1.1 μM for Aβ1-40 and Aβ1-42 respectively. [136,137]

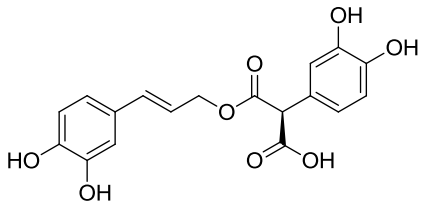

Figure 2-7-5-2. Rosmarinic acid structure.

It is a natural phenol antioxidant carboxylic acid present in many Lamiaceae herbs commonly used as culinary herbs such as rosemary, lemon balm, peppermint, oregano, sage and thyme. As reported by Iuvone *et al.*,[138] RA reduces a number of events caused by Aβ, among which reactive oxygen species formation, lipid peroxidation, DNA fragmentation, caspase-3 activation, and *tau* protein hyperphosphorylation. In addition, it inhibits phosphorylated p38 mitogen-activated protein kinase. These data support the neuroprotective effect of sage against Aβ peptide neurotoxicity, which supports and validates the traditional use of this spice in AD treatment.

Tetracycline (**Figure 2-7-5-3**) also is known for its ability to prevent Aβ peptides aggregation and to destabilize Aβ preformed fibrillar aggregates.[139]

---

[136] Y. Porat, A. Abramowitz, E. Gazit, "Inhibition of amyloid fibril formation by polyphenols: structural similarity and aromatic interactions as a common inhibition mechanism", *Chem. Biol. Drug Des.,* **2006**, 67, 27-37.

[137] K. Ono, K. Hasegawa, H. Naiki, M. Yamada, "Curcumin has potent anti-amyloidogenic effects for Alzheimer's β-amyloid fibrils *in vitro*", *J. Neurosci. Res.*, **2004**, *75*, 742-750.

[138] T. Iuvone, D. De Filippis, G. Esposito, A. D'Amico, A.A. Izzo, "The spice sage and its active ingredient rosmarinic acid protect PC12 cells from amyloid-beta peptide-induced neurotoxicity", *J. Pharmacology and Experimental Therapeutics*, **2006**, 317, 1143-1149.

[139] G. Forloni, L. Colombo, L. Girola, F. Tagliavini, M. Salmona "Anti-amyloidogenic activity of tetracyclines: studies in vitro", *FEBS Letters,* **2001**, 487, 404-407.

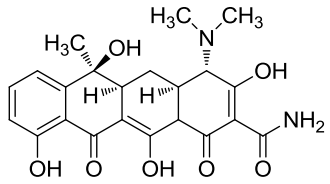

Figure 2-7-5-3. Tetracycline structure

Moreover a deep knowledge of its pharmacological and pharmacokinetic properties is already available, and the ability of some tetracycline derivatives to efficiently cross the blood brain barrier (BBB) makes it an interesting candidate for the development of drugs against AD.[140] Doxycicline, a tetracycline derivative, is already in a randomized double-blind phase II study for the evaluation of its efficacy in patients with Creutzfeldt-Jakob disease,[141] and a phase II clinical trial is also ongoing in patients suffering from transthyretin amyloidosis.[142]

[140] F. Tagliavini, G. Forloni, L. Colombo, G. Rossi, L. Girola, B. Canciani , N. Angeretti, L. Giampaolo, E. Peressini, T. Awan, L. De Gioia, E. Ragg, O. Bugiani and M.Salmona, "Tetracicline Affects Abnormal Properties of Synthetic PrP Peptides and PrP^{Sc} *in vitro", J.Mol.Biol.*, **2000**, 300, 1309-1322.
[141] *Europian Clinical Trials Database*; *Identifier*: *2006-001858-27.*
[142] *Clinical Trials.gov*; *Identifier*: *NCT01171859.*

3. NUCLEAR MAGNETIC RESONANCE (NMR) SPECTROSCOPY AS A TOOL FOR MOLECULAR RECOGNITION STUDIES

The search for new drugs has changed significantly in recent years with the introduction of genomics, high-throughput synthesis and biological screening. As a result of these developments it is necessary to find new methods of high-throughput screening to select the active compounds among a large number of compounds synthesized.

Different applications of NMR spectroscopy are nowadays used as screening techniques for the identification of lead structures, as well as for traditional purposes of drug design and examination of structure-activity relationships (SAR). NMR techniques in fact can be used directly as a rapid and reliable method for the characterization of mixtures of compounds for their ability to bind or not to a certain target. Furthermore the use of NMR techniques does not require any special knowledge of the functions of the proteins analyzed, and therefore it allows also the study of proteins for which no activity assay of biological type is available. In many steps of drugs development processes NMR can therefore shorten the time needed for the identification of appropriate candidate drugs and, starting from a known ligand, can drive in increasing the affinity through appropriate structural modifications.[143]

3.1. NMR SCREENING OF LIGANDS

The methods for ligands screening by NMR can be distinguished in:

1) techniques based on the observation of the ligand;

2) techniques based on the observation of the target;

[143] BioNMR in Drug Research, edited by Oliver Zerbe.

3) techniques based on the observation of the target – ligand complex.

They are also classified according to the NMR parameter changing as a result of the interaction. The parameters sensitive to the interaction are:

1) the chemical shifts;
2) NOE;
3) the relaxation time;
4) the translational diffusion coefficients.

Some of these parameters only indicate that there is binding, while others provide site-specific information about the groups involved in the binding. NMR can provide this site-specific information, essential in the early stages of the process of drug design, while the biological assays or other spectroscopic methods are not able to give it.

A limitation in the use of NMR as a tool for screening is the demand of large amount of compound to be analyzed: in one experiment the concentration of reasonable substance present in solution should be about 100 µM - 0.5 mM.

Other limitations arise from the low solubility of lead compounds still under developement.

The high concentrations required limit the number of compounds that can be tested simultaneously, as the total amount of ligands is normally limited by reasons of stability and solubility.

Among the NMR experiments used for compounds screening, those that identify changes in the target usually require an isotopic labeling of the target: for proteins, total ^{15}N labeling allows to identify very quickly changes that occur as a result of the binding and to identify the binding interface once that the correlation map ^{1}H-^{15}N has been assigned. Alternatively, a specific labeling of methyl groups with ^{13}C can be introduced, in order to increase sensitivity. Since

the amide groups are located in hydrophilic regions while the methyl groups are normally located in hydrophobic regions, the comparison of [^{15}N-^{1}H]-HSQC spectra and [^{13}C-^{1}H]-HSQC can provide interesting information.

Depending on the exchange kinetics between free ligand / protein and the complex, two different sets of signals (slow exchange) or a single set of signals representing the average situation (fast exchange) can be identified.

In the case of fast exchange, an experimental parameter A, as it could be for example the chemical shift or the scalar coupling or the relaxation time, is mediated by the **equation 1**:

$$A_{eff} = f_b A_b + (1-f_b)\, A_f$$

equation 1

in which f_b indicates the fraction of bound ligand. It depends on the dissociation constant K_D, which can be calculated by an equation that takes into account the total concentration of ligand and protein.

Assuming that concentrations of ligand necessary for one-dimensional experiments are of 1 mM (100 µM with the use of cryo-probes) and that NMR allows the determination of 10% of ligand bound, the upper limit of K_D that will determine appreciable differences in the spectra will be equal to the observed concentration of the molecule, and then in a typical ratio [substrate]: [protein] = 10:1, K_D values less than 100 mM will be identified, in the case of cryo-probes. However, K_D values of an order of magnitude lower than the concentration of the compound observed can not be discriminated for their effect on the spectra (for example with a cryo-probe a ligand 10 µM will cause the same spectral differences of a ligand 10 nM, if both are in rapid exchange).

Another class of experiments is based on the analysis of changes in the amplitude of ligand signals in the presence of the target, in one-dimensional

spectra. Assuming that the complex is in rapid exchange, the parameters observed for the ligand represent the weighted average of the free form and bound form. In general, in this type of experiments a reduction or an increase in the amplitude of some signals is observed. The magnitude of the observed effects depends on the molecular weight of the target.[143]

3.2. NMR EXPERIMENTS BASED ON CHEMICAL SHIFT PERTURBATION

The interaction of a ligand with the target can cause changes of chemical shift; for example, the formation of a hydrogen bond decreases the electron density of the atom acceptor, and then usually leads to a shift of the signal in the lower fields.

The interaction between a ligand and the target can then be followed by monitoring changes in chemical shift of both the ligand and the target, but for the screening of ligands even most sensitive methods can be used.

Because of signals overlap present in one-dimensional spectra of proteins, it is more convenient to monitor changes in chemical shift observing ^{15}N-^{1}H correlations in mixtures of one or more ligands with a ^{15}N labeled protein. If the assignment of the signals is feasible within a reasonable time, the binding sites can be easily identified: this is the method commonly used in the determination of structure-activity relationships (SAR). In these experiments, to exclude false positives, numerous preliminary tests are necessary to monitor any possible effects due to small changes in temperature, salt concentration and pH.[143]

3.3. NMR EXPERIMENTS BASED ON RELAXATION TIME CHANGES

Free compounds having low molecular weight are characterized by long relaxation times R1 = 1/T1 and R2 = 1/T2. Conversely compounds bound to a protein molecule of high molecular weight share the relaxation times of their receptor protein. Therefore, small molecules, once bound, exhibit high values of R1 and R2.

Then ligands can be identified in experiments based on the measurement of the relaxation times, with the two following steps:

1) acquisition of the experiment for the calculation of R1 or R2 on the compound alone;

2) acquisition of the same experiment on a sample containing the putative ligand in the presence of the receptor.

If there is interaction between the small molecule and the receptor, the values of T1 and T2 for the ligand decrease.[144]

3.4. NMR EXPERIMENTS BASED ON DIFFUSION

Changes in diffusion coefficients revealed by NMR can be used to test the interaction of a ligand with the target, or to evaluate the aggregation of the same molecule in solution. The experiments for the calculation of the diffusion coefficients are based on the fact that a decrease of the diffusion coefficient of the ligand can be observed, caused by the interaction of the ligand with the target. The diffusion coefficient is a peculiar property of the whole molecule, therefore all the signals of the ligand will be influenced in the same way. The hydrodynamic radius of a molecule can be calculated from the structure.

[144] H.Y. Carr, E.M. Purcell, "Effects of diffusion on free precession in nuclear magnetic resonance experiments", *Phys.Rev*., **1954**, 94, 630-638.

However, the calculation is very approximate because of uncertainties regarding the amplitude of the shell of hydration. The hydrodynamic radius can be roughly estimated with the use of the following empirical formula[143]:

$$r_H[nm]=MW[kDa]^{0.41}/1.55$$

equation 2

Using the Stokes-Einstein equation, the diffusion coefficient can be derived, defined as:

$$D= k_BT/f_T$$

equation 3

where k_B is the Boltzmann constant, T is the absolute temperature, f_T is the friction factor.

In the particular case of a spherical particle of hydrodynamic radius r_H in a solvent of viscosity η the friction factor is:

$$f_T = 6\pi\eta rH,$$

equation 4

therefore:

$$D = k_BT/6\pi\eta rH$$

equation 5

NMR information about the translational motions can be achieved through the use of gradient pulses, in PFG-NMR (Pulsed Field Gradient NMR) experiments. The idea is to increase an experimental variable that modulates the received signal and then transforms the data with respect to that variable producing a spectrum in this case related to the molecular translation.

Diffusion spectra can be obtained by increasing the area of the gradient pulse (q) and transforming the amplitudes of the NMR signals with respect to q^2. NMR experiments of this type are based on the fact that the diffusion coefficient can be calculated by signal areas or intensities, if the amplitude and duration of the gradient magnetic fields are known. The diffusion gradients can be applied either through the main magnetic field B_0, or through the radio frequency pulses B_1. PFG-NMR experiments with constant gradients in the z axis can be easily view thinking to layers of sample perpendicular to the z axis that are thin enough to be affected by a uniform magnetic field but thick enough to contain a large number of spins. Each layer is associated with a magnetization vector and these vectors are assigned to the positions of the layers in the *z* axis. The experiment starts with a radiofrequency pulse applied at 90° on the *x* axis, which rotates all carriers on *y* axis, creating a kind of magnetic stripe on the rotating coordinate system. The effect of the gradient g is therefore to twist the tape generating an helix, whose degree is inversely proportional to the gradient pulse. The effect of a constant gradient will therefore be the generation of a magnetization pattern with a cosine projection on the *yz* plane. The spread in the *z* direction will vanish this pattern more rapidly the smaller is the helix degree. Immediately after the 90 ° pulse, the signal generated along the *y* axis decays in amplitude: the decay is primarily determined by the loss of phase coherence of the nuclei due to inhomogeneities in the magnetic field. This decay becomes even more rapid in the presence of an applied gradient g. To be able to collect the signal, the magnetisation vector must be refocused, i.e. the helix must be disrupted with two coupled pulse gradients: the first encodes for nuclei position of the nuclei through phase angles position dependent, and therefore sensitizes the sample

to diffusion motions; the second gradient refocuses the magnetization vectors in the *yz* plane, generating an echo **(Fig. 3-4-1)**.

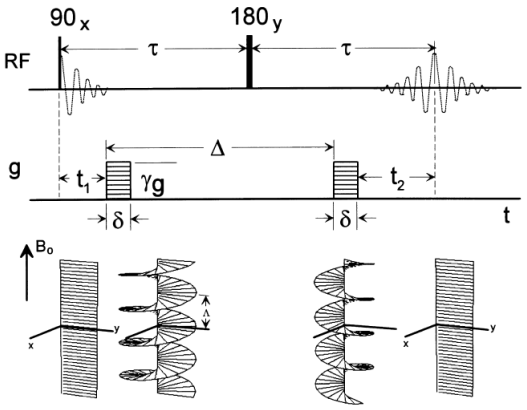

Fig. 3-4-1. Simple sequence of Carr-Purcell spin-echo: the tape of magnetization vectors generated by the 90 ° pulse on x-helix, produced by the first gradient pulse, can be observed. The effect of the 180 °pulse on *y* is applied to revert the effect of the preceding gradient pulse. (δ = diffusion gradient length; diffusion delay Δ; g = gradient strength).[[145]]

More complex sequences, containing two or three pulses at 90 °, with a fixed gradient, can generate up to five echoes; the first echo after the third pulse of radiofrequency is defined "stimulated echo" (STE). The second 90 ° pulse on *x* collects the magnetization by rotating only the *y* components in the directions *+ z* and *-z*. The *x* components remain transverse and may contribute to the primary and secondary echo. Then, after the collection period T, the third 90 ° pulse on *x* returns the z components on + y and-y directions, where the action of the second gradient pulse refocuses the magnetization vectors so that the signal STE appears at t = T+2τ. (**Fig. 3-4-2).** However, the magnetization vectors

[[145]]C.S. Johnson Jr., "Diffusion ordered nuclear magnetic resonance spectroscopy: principles and applications", *Progress in Nuclear Magnetic Resonance Spectroscopy*, **1999**, 34, 203-256.

are not coplanar at the time of the echo, and in fact their projection on the *xy* plane defines a circle tangential to the *xy* plane.[145]

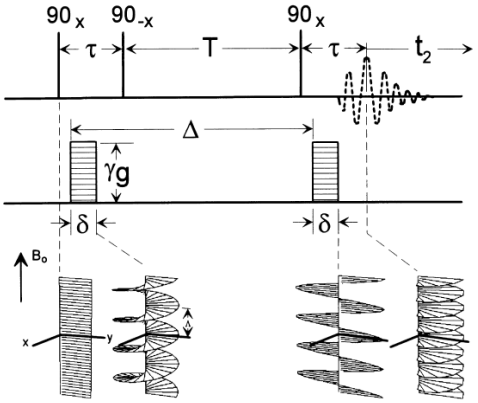

Figure 3-4-2. STE (Stimulated Echo) with gradient pulses (δ= diffusion gradient lenght ; Δ=diffusion delay; g=gradient strength).[145]

3.5. NOE (NUCLEAR OVERHAUSE EFFECT) BASED TECHNIQUES

A number of NMR techniques based on the NOE (Nuclear Overhause Effect) have been developed.[143]

The NOE effect is extremely useful in determining the 3D structure of molecules in solution, and is therefore a method of success, especially in structural analysis of proteins. When a ligand binds to the receptor protein, the NOE undergo a dramatic change leading to the observation of phenomena of Transferred NOEs (trNOEs). These changes represent the basis for a variety of experimental schemes designed to identify and characterize the binding activity.

The principles of the Transferred NOE were originally observed and described more than twenty years ago and have therefore found wide use in the determination of 3D structures of ligands associated with receptor proteins.

The observation of trNOEs is based on different correlation times of free and bound molecules. Molecules of low and medium molecular weight (Mw < 1000) have short correlation times τ_c and, as a consequence, these molecules exhibit generally positive NOEs, or equal to zero, depending on their molecular weight, their form and force fields. Large molecules, however, exhibit strongly negative NOEs. When a small molecule (ligand) is bound to a molecule of high molecular weight (the receptor protein) it behaves as part of a large molecule and adopts the corresponding NOE behavior, that is, it shows strongly negative NOEs, the so-called trNOEs. These trNOEs reflect the conformation of the bound ligand. The binding of a ligand to a receptor protein can then be detected easily by looking at the sign and the intensity of the observed NOEs. Furthermore, the discrimination between trNOEs that originate from the associated state and NOEs typical of the ligand in solution can be obtained based on the time required to obtain the maximum intensity, that for trNOEs is in the range of 50-100 ms, while for molecules not bound is four to ten times longer. Therefore, the maximum growth for trNOEs is observed at a mixing time (τ_{mix}) significantly shorter than for the isolated molecules present in solution.

In general inter- and intramolecular trNOEs can be observed; while intramolecular trNOEs are the key to define the bound conformations of the ligand, the intermolecular trNOEs occur between a ligand and a receptor protein, and therefore, in principle, allow to define the orientation of the ligands in the binding pockets.

One of the main drawbacks of this experiment is the possible presence of spin diffusion effects, which are typical for large molecules. In this case, the

magnetization transfer may be mediated also by other nuclei, also belonging to the receptor, as well as protons actually neighbors in space.

3.6. SATURATION TRANSFER DIFFERENCE (STD) NMR EXPERIMENTS

One of the experimental methods based on transferred NOE phenomena is STD (Saturation Transfer Difference). NMR spectroscopy based on the saturation transfer has been used for many years to characterize the binding in ligand-receptor complexes closely associated.

If a ligand shows two different signals due to an exchange between the free form and the associated one, it is possible that a transfer of saturation between the free and the bound state occurs. Then, irradiating for example signals of the free ligand, signals of the associated ligand can be identified. In addition to this, the saturation transfer method is used to analyze the kinetics of binding in the formation of protein-ligand complexes. The screening of multiple ligands simultaneously can be done using the technique of subtraction of spectra in homonuclear spectroscopy, in particular that of the proton. The STD spectrum is the result of the difference of two experiments: in a first experiment, called “on-resonance”, various protons of the receptor are selectively saturated through specific radio frequency pulses, applied in a spectral window that contains signals of the receptor but not of the ligand; in a second experiment, called “off-resonance”, the same pulse of radiofrequency is applied in a region devoid of signals of both the protein and the ligand. When a ligand is bound to the protein there will be a saturation transfer. The degree of saturation of the ligand in the on-resonance spectrum depends of course on the residence time

of the compound in the binding pocket of the protein; the dissociation of the ligand will transfer this saturation in solution, where the free ligand will give rise again to signals affected by intermolecular trNOE, and a decrease in intensity will be observed. In the case of the off-resonance spectrum, irradiation frequency is set to a value that is far from any signal of the ligand and the protein, for example 40 ppm. The result is a normal monodimensional spectrum of the mixture. The subtraction of the on-resonance spectrum from the off-resonance one generates a spectrum in which only the signals of the protons that have been weakened by the transfer of saturation are visible. Any molecule that does not present binding is thus canceled. The saturation of the protein and of the associated ligand is very fast, it takes about 100 ms. Therefore a fast dissociation of the ligand rapidly transfers the saturation in solution; if there is a large excess of ligand, a binding site can be used to saturate many molecules of ligand in a few seconds. Molecules in solution lose their signal after a normal T1/T2 relaxation, which takes about a few seconds for small molecules. Therefore, the proportion of saturated ligands in solution increases during the saturation time, and then the signals of bound molecules resulting from saturation of the protein is amplified. This results in the possibility of working with a relatively small amount of protein. Instead, if the binding is very tight and the dissociation rate is low, the saturation transfer toward the ligand molecules is not very efficient. This is what normally occurs for values of K_D below 1 nM. If the K_D values are greater than or equal to 100 nM, the rapid interchange between free form and bound form leads to an efficient transfer of saturation toward the molecules of ligand present in solution. It is clear that the intensity of the signals of the ligand that is observed is not proportional to the bond strength, but essentially depends on the speed

of exchange: the higher the speed of exchange and the greater the intensity of the STD signals. However, when the binding becomes very weak, the probability that the ligand interacts with the receptor becomes very low, and this is translated into weak STD signals.

The intensity of the STD signals also depends on the irradiation / saturation time and excess of ligand molecules used: the greater the amount of ligand used and the greater the time of irradiation applied, more intense will be the STD signal. In general, an irradiation time of 2 seconds and an excess of 100 times of the ligand, allows to obtain good results.[146]

The saturation of the ligand is greater for protons that are located more closely to the receptor. For those protons of the ligand that interact with protons of the protein through intermolecular NOE, a decrease in intensity in the on-resonance spectrum is observed, while no change of intensity in the off-resonance spectrum is detected. The subtraction of the on-resonance spectrum from the off-resonance generates a difference spectrum that shows only the signals of the protons that have been weakened by the transfer of saturation (**Fig. 3-6-1**). In this way the STD spectroscopy not only provides evidence of protein-ligand interaction, but also allows to obtain an epitope-mapping of the ligand, i.e. the identification of the regions of the ligand involved in the interaction with the receptor.[146]

[146] B. Meyer, T. Peters "NMR Spectroscopy Techniques for Screening and Identifying Ligand Binding to Protein Receptors", *Angew. Chem.Int*. Ed., **2003**,42(8), 864-890.

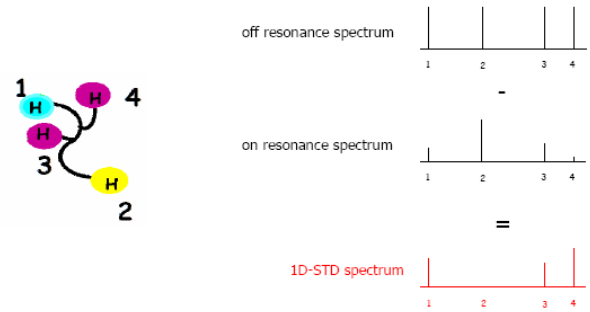

Fig. 3-6-1. STD spectrum is obtained subtracting the on resonance spectrum from the off resonance.

Objective and strategy

Alzheimer's Disease (AD) is the most common cause of dementia in Europe. Above age 65, the prevalence of the disease doubles every 5 years, reaching 5% above 85. Given the constant increase of the elderly population in Europe, more healthcare, social and economic resources will be required, with huge social and economic costs.

While there has been substantial progress in the scientific understanding of AD, in order to face a financially overwhelming public health problem, an unmet urgent need to identify effective therapies and early detection strategies remains.

The mechanisms underlying AD are not yet completely clear, but genetic, pathological and biochemical clues suggest that the progressive production and subsequent accumulation of β-amyloid (Aβ) peptides in the brain play a crucial role.

Many small molecules, both natural and synthetic compounds, have already been identified for their anti-amyloidogenic properties. They are commonly heteroaromatic polycyclic compounds such as flavons, thioflavins and polyphenols, but their mechanism of action as anti-amyloidogenic agents has not yet been clarified. Moreover these molecules are often poorly stable or soluble in physiological conditions, or they possess other pharmacologic activities that do not allow a correct therapeutic evaluation towards AD.

The aim of the work here described was the development of small molecules able to bind β-amyloid peptides, with better characteristics of solubility and stability, that could be useful for the therapy or the diagnosis of AD.

In this context, Nuclear Magnetic Resonance (NMR) Spectroscopy techniques have been used to analyze the interaction between some small molecules already known for their anti-amyloidogenic activity and Aβ peptides at

molecular level. The data obtained have been and will be exploited for the design and synthesis of new potential Aβ peptide ligands, useful as new therapeutic and diagnostic agents against AD.

Results and Discussion

Paper 1

Org. Biomol. Chem., ***2011***, *9, 463*

TETRACYCLINE PREVENTS Aβ OLIGOMERS TOXICITY THROUGH AN ATYPICAL SUPRAMOLECULAR INTERACTION

Cristina Airoldi,[a] Laura Colombo,[b] Claudia Manzoni,[b] Erika Sironi,[a] Antonino Natalello,[a] Silvia Maria Doglia,[a] Gianluigi Forloni,[b] Fabrizio Tagliavini,[c] Elena Del Favero,[d] Laura Cantù,[d] Francesco Nicotra[a] and Mario Salmona.[b]

[a] *Department of Biotechnology and Biosciences, University of Milano- Bicocca, P.zza della Scienza 2, 20126, Milan, Italy. E-mail: francesco.nicotra@unimib.it; Fax: +390264483565; Tel: +390264482152*
[b] *Department of Molecular Biochemistry and Pharmacology and Department of Neuroscience Mario Negri Institute for Pharmacological Research, Via La Masa 19, 20156, Milan, Italy*
[c] *Division of Neurology and Neuropathology, "Carlo Besta" National Neurological Institute, Via Celoria 11, 20133, Milan, Italy*
[d] *Department of Chemistry, Biochemistry and Biotechnologies for Medicine, University of Milano, LITA, V. F.lli Cervi, 93, 20090, Segrate, (MI), Italy*

Abstract

The antibiotic tetracycline was reported to possess an anti-amyloidogenic activity on a variety of amyloidogenic proteins both in *in vitro* and *in vivo* models. To unveil the mechanism of action of tetracycline on Aβ1–40 and Aβ1–42 at both molecular and supramolecular levels, we carried out a series of experiments using NMR spectroscopy, FTIR spectroscopy, dynamic laser light-scattering (DLS) and atomic force microscopy (AFM). Firstly we showed that the co-incubation of Aβ1–42 oligomers with tetracycline hinders the toxicity towards N2a cell lines in a dose-dependent manner. Therefore, the nature of the interaction between the drug and Aβ oligomers was investigated. To carry out NMR and FTIR studies we have prepared Aβ peptide solutions containing assemblies ranging from monomers to large oligomers. Saturation transfer difference (STD) NMR experiments have shown that tetracycline did not interact with monomers at variance with oligomers. Noteworthy, in this latter case we observed that this

interaction was very peculiar since the transfer of magnetization from Aβ oligomers to tetracycline involved all drug protons. In addition, intermolecular cross-peaks between tetracycline and Aβ were not observed in NOESY spectra, indicating the absence of a specific binding site and suggesting the occurrence of a supramolecular interaction. DLS and AFM studies supported this hypothesis since the co-dissolution of Aβ peptides and tetracycline triggered the immediate formation of new aggregates that improved the solubility of Aβ peptides, preventing in this way the progression of the amyloid cascade. Moreover, competitive NMR binding experiments showed for the first time that tetracycline competes with thioflavin T (ThT) in the binding to Aβ peptides. Our data shed light on a novel mechanism of anti-amyloidogenic activity displayed by tetracycline, governed by hydrophobic and charge multiparticle interactions.

Introduction

Alzheimer's disease (AD) is a neurodegenerative disorder that affects over 30 million individuals worldwide. Despite extensive research there is still no effective treatment; pharmacological intervention is limited to symptomatic therapy with cholinergic drugs and glutamatergic partial antagonists. As a result, AD has a severe impact on patients and their families' quality of life, and its economic burden is massive. A central pathological feature of AD is the accumulation of misfolded amyloid β (Aβ) peptides in the form of oligomers and amyloid fibrils in the brain.[1,2,3,4]

Aggregated Aβ species, particularly oligomeric assembly intermediates, are believed to trigger a cascade of events that lead to protein tau hyperphosphorylation, misfolding and assembly into abnormal filaments with the formation of neurofibrillary tangles and disruption of the neuronal cytoskeleton, widespread synaptic loss and neurodegeneration.[5] A substantial effort has been made in the last 20 years to develop AD therapies. The considerable efforts in the design of Aβ targeting molecules

[1] J. Hardy and D. Allsop, *Trends Pharmacol. Sci.*, **1991**, 12, 383–388.
[2] C. J. Pike, D. Burdick, A. J. Walencewicz, C. G. Glabe and C. W. Cotman, *J Neurosi*, **1993**, **13**, 1676–1687.
[3] D. J. Selkoe, *Ann. N. Y. Acad. Sci.*, **2000**, 924, 17–25.
[4] K. Ono and M. Yamada, *J. Neurochem.*, **2006**, 97, 105–115.

have been useful, providing several classes of compounds with different modes of activity, but the drugs selected for clinical trials have given unsatisfactory results or caused adverse events, and there is still an urgent need for safe and effective molecules for AD treatment. Based on structural analogies with Congo red, tetrapyrroles and acridine derivatives, we hypothesized that tetracyclines might interact with the disease-related isoform of prion protein (PrP^{Sc}) and misfolded Aβ peptides. We have shown that tetracyclines promote PrP^{Sc} and Aβ degradation by proteases, inhibit the aggregation of amyloidogenic peptides PrP106–126 and PrP82–146 and of Aβ and destabilize aggregates. The anti-amyloidogenic effect of tetracyclines has also been confirmed with other amyloidogenic proteins, such as transthyretin,W7FW14F apomyoglobin, amylin, huntingtin, a2-macroglobulin, a-synuclein, poly(A) binding protein nuclear 1[6] in *in vitro* and *in vivo* models. Tetracyclines include several congeners. They have relatively low toxicity and some of them, such as doxycycline and minocycline, efficiently cross the blood brain barrier. Tetracyclines have an amphiphilic character, due to their extended hydrophobic core formed of aromatic moieties, with a large number of hydrophilic substituents. Derived from a common hydronaphthacene nucleus containing four fused rings, these compounds have various substitutions at positions 5, 6 and 7 and five asymmetric centers: C-4, C-4a, C-5a, C-6 and C-12a. **Scheme 1** reports the structure of tetracycline.

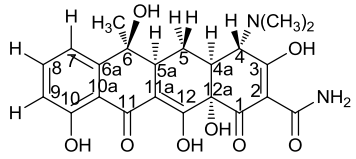

Scheme 1. Tetracycline structure; numbering of hydrogens and carbons.

Multiple functional groups with acidic-base properties contribute to their high solubility in polar organic solvents and water, which is enhanced at low pH. Most of them have

[5] I. Cardoso, G. Merlini and M. J. Saraiva, *FASEB J.*, **2003**, 17, 803–809.
[6] G. Forloni, M. Salmona, G. Marcon and F. Tagliavini, *Infectious disorders: drug targets*, 2009, **9**, 23–30.

an isoelectric point between 4 and 6 due to their amphoteric character. In the hydrochloride form, tetracyclines had four potentially dissociable proton centers, namely C1-C3 tricarbonyl methane, O-10 andO-12 ketophenolic hydroxyl groups and C-4 dimethylammonium group. However, the formation of intra- and inter-molecular hydrogen bonds and the conformational change due to the dielectric constant of the medium interfere in the deprotonation scheme. Tetracyclines undergo complex formation with a variety of metal cations (such as Ca^{2+}, Mg^{2+}, Cu^{2+}, Co^{2+} and Ni^{2+}) and they are transported in plasma as a calcium complex. Based on the *in vitro* and preclinical *in vivo* data, a randomized double-blind phase II study for the evaluation of the efficacy of doxycycline in patients with Creutzfeldt-Jakob disease has been approved and funded by the Italian Agency for Drugs (*European Clinical Trials Database*; *Identifier*: *2006-001858-27*). Moreover, a phase II clinical trial is also ongoing in patients suffering from transthyretin amyloidosis (*ClinicalTrials.gov*; *Identifier*: *NCT01171859*). These observations prompted us to focus more in detail on Aβ and study whether these drugs antagonize the cytotoxic effects of the oligomeric forms of Aβ, and explore in detail their anti-fibrillogenic mode of action at the molecular level. In this paper we show that tetracycline, when co-dissolved with Aβ, forms immediately supramolecular complexes, preventing the formation of fibrillar aggregates and the progression of the amyloid cascade. We hypothesize that this mechanism of action may be extended to other amyloidogenic proteins as well.

Results and discussion

In vitro toxicity assay

The toxicity of Aβ1–42 on N2a cells was studied in the concentration range of 5–500 nM. Pre-incubation of Aβ1–42 with tetracycline for 70 h at molar ratios of 1 : 4 or 1 : 8 significantly reduced peptide toxicity after 24 h of exposure (**Fig. 1a**).

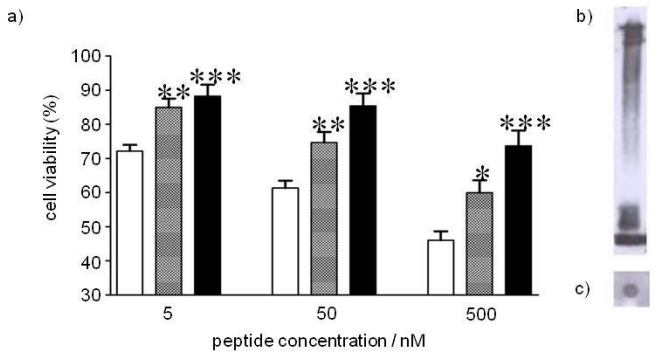

Fig. 1. *In vitro* Aβ toxicity assay. a) Viability of N2a cells after 24 h of exposure to 5–500 nM Aβ1–42. White bars, Aβ1–42 alone; grey bars, Aβ1–42 - tetracycline at a 1 : 4 molar ratio; black bars, Aβ1–42 – tetracycline at a 1 : 8 molar ratio. Error bars are the SEMof 4 replicates. *** p<0.0001; ** p < 0.001; * p < 0.01 *vs.* Aβ1–42 alone by one way ANOVA followed by the Dunnett post-hoc test. b) Western Blot and c) Dot Blot analysis of freshly dissolved Aβ1–42 performed using 6E10 and A11 antibodies, respectively.

Western Blot and Dot Blot analysis confirmed the presence of oligomers in the fresh peptide solution (**Fig. 1b** and **c**). To elucidate the mechanism of action of tetracycline protection against neurotoxicity we investigated its interaction with Aβ1–40 and Aβ1–42 by NMR spectroscopy, AFM, FTIR and DLS.

NMR and FTIR characterization of Aβ peptides in solution

^{1}H-NMR line width broadening monitoring and PFG-NMR diffusion measurements[7,8] were carried out at 5, 25 or 37 ◦C with both peptides in the concentration range of 50–500 μM. The analysis of the experiments showed that they were mostly in oligomeric forms in PBS, pH 7.4. Conversely, when Aβ1–40 was dissolved in PBS, pH 12, at 5 ◦C, or in DMSO [9] at 37 ◦C, it acquired an unordered monomeric structure, as deduced from ^{1}H-NMR line width narrowing (compared to spectra at pH 7.4) and FTIR analysis, as described below (**Fig. 3**). ^{1}H-NMR spectra acquired on the sameAβ1–40 or Aβ1–42 samples dissolved in PBS at pH 7.4 or pH 12, 5 ◦C are reported in Fig. 2. For both

[7] E. Ilyina, V. Roongta, H. Pan, C. Woodward and K. H. Mayo, *Biochemistry*, 1997, **36**, 3383–3388
[8] J. Danielsson, J. Jarvet, P. Damberg and A. Graslund, *Magn. Reson. Chem.*, 2002, **40**, S89–S97
[9] W. B. Stine Jr., K. N. Dahlgren, G. A. Krafft and M. J. LaDu, *J. Biol. Chem.*, **2003**, 278, 11612 11622.

peptides, S/N ratios were higher and ^{1}H-NMR signals sharper in the spectrum recorded at pH 12, also in agreement with the measurements of relaxation times, which showed higher T1 and selective T1 values under these experimental conditions (**ESI†, S1 – Tables 1S and 2S**). NMR diffusion measurements allowed a further characterization of Aβ peptide oligomers at pH 7.4. Calibration curves correlating molecular weights with diffusion coefficients (logD *vs.* logMW) were used to estimate D values for Aβ peptide monomers and small oligomers at 5, 25 or 37 ◦C.[10] Protein size standards employed were bradykinin (1090 Da), bovine insulin (5734 Da, not used for the calibration curve at 37 ◦C),[11] ubiquitin (8500 Da), cytochrome C (13 000 Da), lysozyme (14 700 Da). Expected and observed D values for Aβ1–40 at different temperatures (5, 25 or 37 ◦C) at pH 7.4 are reported in **Table 1**; DOSY spectra are depicted in **ESI†, S1 – Figure 1S**. The measured coefficients at 5 and 25 ◦C, pH 7.4 were consistent with the presence of a mixture of monomers and small oligomers, with *D* values being lower than expected for the monomer (-11.8% and -15.2% respectively).

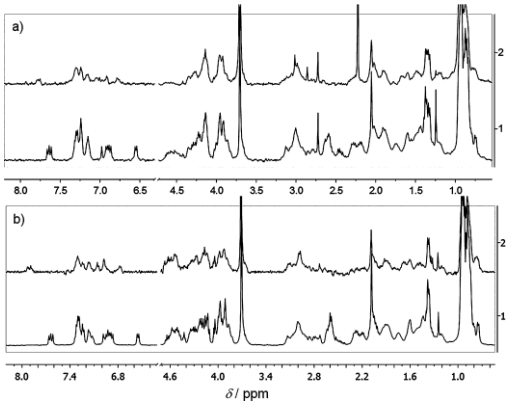

Fig. 2. a) ^{1}H-NMR spectra of 0.5 mM Aβ1–40 acquired in PBS, pH 12 (1) or at pH 7.4 (2, enhanced 2x), 5 ◦C, number of scans (NS) = 128. b) ^{1}H-NMR spectra of 0.25 mM Aβ1–42 acquired in PBS, pH 12 (1) or at pH 7.4 (2, enhanced 6x), 5 ◦C, NS = 512.

[10] P. Groves, M. O. Rasmussen, M. D. Molero, E. Samain, F. J. Canada, H. Driguez and J. Jimenez-Barbero, *Glycobiology*, **2004**, 14, 451–456.
[11] Insulin is a dimer at 37 ◦C; M. Lin and C. K. Larive, *Anal. Biochem.*, **1995**, 229, 214–220.

pH	T (°C)	expected diff. coeff. for the monomer	observed diffusion coefficient[a]	Δ
7.4	5	$0.845*10^{-10}$ m^2/s	$0.745*10^{-10}$ m^2/s	- 11.8%
7.4	25	$1.626*10^{-10}$ m^2/s	$1.378*10^{-10}$ m^2/s	- 15.2%
7.4	37	$2.841*10^{-10}$ m^2/s	$1.862*10^{-10}$ m^2/s	- 34.5%

[a] uncertainty less than 1%

Table 1. Aβ1–40 diffusion coefficients in solution at 5, 25 or 37 ◦C, pH7.4

The diffusion coefficient at 37 ◦C was 65.5% of that estimated for the monomer, as expected as a consequence of the temperature-dependence of Aβ peptide aggregation. In particular, due to the short T2 values of large aggregates, it is realistic to assume that they do not significantly contribute to the high-resolution NMR spectrum (it is indeed a NMR-silent species) and that the major contributions to the observed decrease of the resonance intensity in the diffusion experiment depends on the formed monomeric, dimeric and trimeric peptides. In the case of Aβ1–42, due to the low intensity of ^1H peptide signals, an uncertainty greater than 6.0% was obtained for experiments carried out at pH 7.4, even when the spectra were acquired with a high number of scans (512) (**Fig. 2b**). Longer acquisition times were not possible due to peptide aggregation and precipitation. For this reason, data on Aβ1–42 were considered unreliable and are not reported here. FTIR spectroscopy indicated that both Aβ peptides formed oligomers with major β-sheet intermolecular interactions in PBS, pH 7.4 (**Fig. 3**). The FTIR spectrum of Aβ peptides in D_2O PBS buffer, pH 7.4, displayed two bands at ~1,622 and ~1,686 cm^{-1} for Aβ1–40 and at ~1,625 and ~1,686 cm^{-1} for Aβ1–42. These bands are the specific signature of intermolecular β-sheet interactions in oligomers,[12,13] but they could be also due to β-hairpin structures.[14] Recently, it has been demonstrated that the infrared response of Aβ1–42[13] and of Aβ1–40[12] oligomers in the Amide I region

[12] G. Habicht, C. Haupt, R. P. Friedrich, P. Horstchansky, C. Sachse, J. Meinhardt, K. Wieligmann, G. P. Gellerman, M. Brodhun, J. Gotz, K. J. Halbhuber, C. Rocken, U. Horn and M. Fandrich, *Proc. Natl. Acad. Sci. U. S. A.*, **2007**, 104, 19232–19237.
[13] E. Cerf, R. Sarroukh, S. Tamamizu-Kato, L. Breydo, S. Derclaye, Y. Dufrene, V. Narayanaswami, E. Goormaghtigh, J.M. Ruysschaert and V. Raussens, *Biochem. J.*, **2009**, 421, 415–523.
[14] J. L. Arrondo, F. J. Blanco, L. Serrano and F. M. Goni, *FEBS Lett.*, **1996**, 384, 35–37.

consists of two intermolecular β-sheet bands, whereas fibrils lead only to the lowest wavenumber band,[13] as already observed for a prion peptide.[15] The FTIR spectrum of both peptides showed an additional broad band around 1,642 cm^{-1} (more intense in the case of Aβ1–40) that can be assigned to the peptide unordered structure.[16] This last result may suggest that Aβ1–40 oligomers are present at lower extent compared with Aβ1–42, in agreement with its higher aggregation propensity. On the contrary, the spectra of Aβ1–40 in PBS, pH 12 and in deuterated DMSO (data not shown) displayed, respectively, only an absorption band at ~1,640 cm^{-1} and ~1,666 cm^{-1} that can be assigned to the peptide unordered structure in D_2O[16] and in DMSO.[17] We can therefore conclude that, under these conditions, the peptide is in a monomeric form and does not aggregate into oligomers with intermolecular β-sheet structures. Thus, NMR and FTIR findings consistently demonstrated that the Aβ peptides form oligomers at pH 7.4; this result is further supported by the AFM data reported below. In addition, these data support a higher level of oligomerization for Aβ1–42 *vs.* Aβ1–40. On the other hand, when dissolved in PBS, pH 12, or in DMSO, Aβ1–40 was found to be in unordered monomeric form. In light of these results, we decided to use these different experimental conditions to generate samples representative of the different aggregation states of Aβ peptides.

[15] A. Natalello, V. V. Prokorov, F. Tagliavini, M. Morbin, G. Forloni, M. Beeg, C. Manzoni, L. Colombo, M. Gobbi, M. Salmona and S. M. Doglia, *J. Mol. Biol.*, **2008**, 381, 1349–1361.
[16] J. L. Arrondo and F. M. Go˜ ni, *Prog. Biophys. Mol. Biol.*, **1999**, 72, 367–405.
[17] M. Jackson and H. H. Mantsch, *Biochim. Biophys. Acta.*, **1991**, 1078, 231–235.

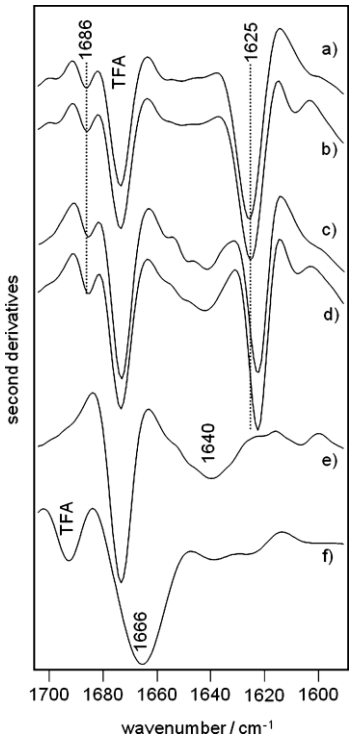

Fig. 3. Second derivative FTIR absorption spectra of Aβ1–42 and Aβ1–40 in presence or absence of tetracycline. Spectra of Aβ1–42 in D_2O PBS buffer, pH 7.4 in absence (a) and in presence (b) of tetracycline at a 1:4 molar ratio. Spectra of Aβ1–40 in D_2O PBS, pH 7.4 in absence (c) and in presence (d) of tetracycline at a 1:2 molar ratio. Spectra of Aβ1–40 in D_2O PBS, pH 12 (e) and in deuterated DMSO (f), both in presence of tetracycline at a 1:2 molar ratio. The 1,673 cm^{-1} peak in D_2O buffers (a–e) and the 1,692 cm^{-1} peak in DMSO (f) are respectively due to the infrared response of residual TFA.

Binding of tetracycline to Aβ oligomers

Different NMR experimental approaches were used to evaluate the interaction of Aβ peptides with tetracycline. Saturation transfer difference (STD) NMR experiments[18,19,20,21] in PBS, pH 7.4, provided clear evidence of tetracycline binding to

[18] B. Meyer and T. Peters, *Angew. Chem., Int. Ed.*, **2003**, 42, 864.
[19] M. Mayer and T. L. James, *J. Am. Chem. Soc.*, **2002**, 124, 13376–13377.
[20] S. Di Micco, C.Bassarello, G.Bifulco, R.Riccio and L. Gomez-Paloma, *Angew. Chem., Int. Ed.*, **2006**, 45, 224–228.

the Aβ1–40 and Aβ1–42 oligomers. STD spectra at peptide: tetracycline molar ratios from 1:2 to 1:30 were acquired employing different saturation times and temperatures (**Fig. 4 and ESI†, S2**). In all cases, after selective irradiation of the peptide resonances, tetracycline signals appeared in the STD spectra indicating the existence of magnetization transfer from the oligomers to the drug. A detailed ligand-epitope mapping was not possible because each tetracycline proton showed the corresponding STD signal. Additional evidence for tetracycline binding to Aβ oligomers was obtained by measuring its diffusion coefficient at different peptide:drug molar ratios by PFG-NMR. Calibration curves correlating molecular weight with diffusion coefficient (logD *vs.* logMW) were used to estimate *D* values for tetracycline monomers at 5, 25 or 37 ◦C.[10] Molecular size standards employed were glucose (180 Da), lactose (342 Da), raffinose (504 Da), bradykinin (1040 Da). Expected and observed *D* values for tetracycline in absence or in presence of Aβ peptides at 5 ◦C, pH 7.4 or pH 12, are reported in **Table 2**. Tetracycline diffusion coefficients decreased significantly at increasing peptide:drug molar ratios, as expected for its interaction with a large molecular weight species.[22,23] Conversely, when Aβ1–40 was dissolved in PBS, pH 12, at 5 ◦C, or in DMSO at 37 ◦C, acquiring an unordered monomeric structure, the tetracycline diffusion coefficient measured on tetracycline peptide mixtures was unchanged, indicating the absence of drug peptide interactions (**Table 2**),[24] and STD spectra showed only Aβ1–40 signals (**ESI†, S2**).

[21] F. Souard, E. Munoz, P. Penalver, C. Badia, R. Del Villar-Guerra, J. Luis Asensio, J. Jimenez-Barbero and C. Vicent, *Chem. Eur. J.*, **2008**, 14, 2435–2442.
[22] L. Mengfen, M. J. Shapiro and J. R.Wareing, *J. Am. Chem. Soc.*, **1997**, 119, 5249–5250.
[23] L. H. Lucas and C. K. Larive, *Concepts Magn. Reson.*, **2004**, 20A,24–41.
[24] We tried the deconvolution of DOSY spectra.We used the DOSYtoolbox by M. Nillson, and G.Morris. Results of our analysis are reported in ESI S3†.

Aβ sequence	pH	peptide:tetracycline ratio	diffusion coefficient[a]
	7.4	tetracycline alone	$2.059*10^{-10}$ m^2/s
1-40	7.4	1:2	$1.620*10^{-10}$ m^2/s
1-42	7.4	1:2	$1.589*10^{-10}$ m^2/s
1-42	7.4	1:4	$1.691*10^{-10}$ m^2/s
1-42	7.4	1:8	$1.762*10^{-10}$ m^2/s
	12	tetracycline alone	$2.021*10^{-10}$ m^2/s
1-40	12	1:2	$1.959*10^{-10}$ m^2/s

[a] uncertainty less than 1%

Table 2 Tetracycline diffusion coefficients in absence or presence of Aβ peptides at 5◦C, pH 7.4 or pH 12.

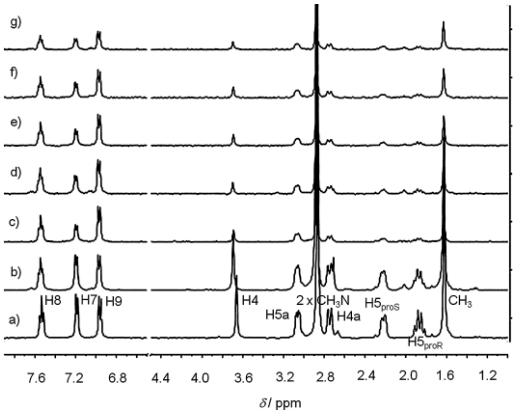

Fig. 4. a) ^{1}H-NMR spectra of tetracycline, NS = 32. b) Aβ1–42-tetracycline mixture, at a 1:30 molar ratio, NS = 32. c–g), STD spectra of the mixture recorded at different peptide saturation times (c, 5 s; d, 3 s; e, 2 s; f, 1.2 s; g, 0.5 s). NS = 896, on-resonance frequency = -1.0 ppm, off-resonance frequency = 40 ppm. Spectra b–g were recorded on the same sample; all samples were dissolved in PBS, pH 7.4, at 25 ℃.

To detect Nuclear Overhauser Effect (NOE) contacts between tetracycline protons and peptide residues, 2D-NOESY spectra of the peptide-drug mixtures were acquired with mixing times ranging from 0.1 s to 0.65 s. These experiments permitted to confirm the existence of tetracycline intermolecular interactions with both Aβ1–40 and Aβ1–42 as deduced by the observed drug cross-peak change of sign (trNOE) (**Fig. 5a, b; ESI†, S4**). For isolated tetracycline, the NOE cross peaks were positive, *i.e.* their signs were

opposite with respect to the diagonal peaks as expected for a small molecule with a short correlation time. However, a change of sign occurred in the presence of Aβ1–40 or Aβ1–42 indicating an increase in the correlation time, supporting the existence of interaction with the peptides.[18,**25**] Nevertheless, the fine details of the interaction at atomic resolution could not be deduced, since no intermolecular cross-peaks between tetracycline and Aβ peptides were identified, and no significant changes in the peptide chemical shifts were observed after titration with the drug (**ESI†, S5**). On the other hand, tetracycline cross-peaks maintained their positive signs in NOESY spectra recorded at pH 12 or in DMSO in the presence of Aβ1–40 (**Fig. 5c–f**), confirming the absence of binding to Aβ1–40 monomers under these experimental conditions. As Aβ monomers are the species mostly represented in Aβ1–40 and Aβ1–42 ^{1}H-NMR spectra, the absence of changes in the peptide chemical shifts and of intermolecular cross-peaks between tetracycline and Aβ peptides could also be due to the lack of interaction between tetracycline and Aβ monomers. We also verified the influence of tetracycline on the structural properties of Aβ peptides by FTIR and circular dichroism (CD; reported in **ESI†, S6**). In our experimental conditions, the coincubation with tetracycline did not modify the secondary structure of the peptides. In fact, both peptides in PBS, pH 7.4, showed the infrared response characteristic of oligomers. In contrast, Aβ1–40 in PBS at pH 12, as well as in DMSO, was found to be in unordered monomeric form (**Fig. 3**). Considering that tetracycline is known to prevent the aggregation of a variety of amyloidogenic proteins and peptides, the finding that the drug does not bind a specific Aβ peptide epitope raises the question of the drug mechanism of action at molecular level. We therefore analyzed tetracycline-Aβ peptide interactions by DLS and AFM.

[25] D. Neuhaus,M. P.Williamson, *The kinetics of the NOE in The Nuclear Overhauser Effect in Structural and Conformational Analysis*, VCH Publishers Inc., New York, **1986**, pp. 103–140.

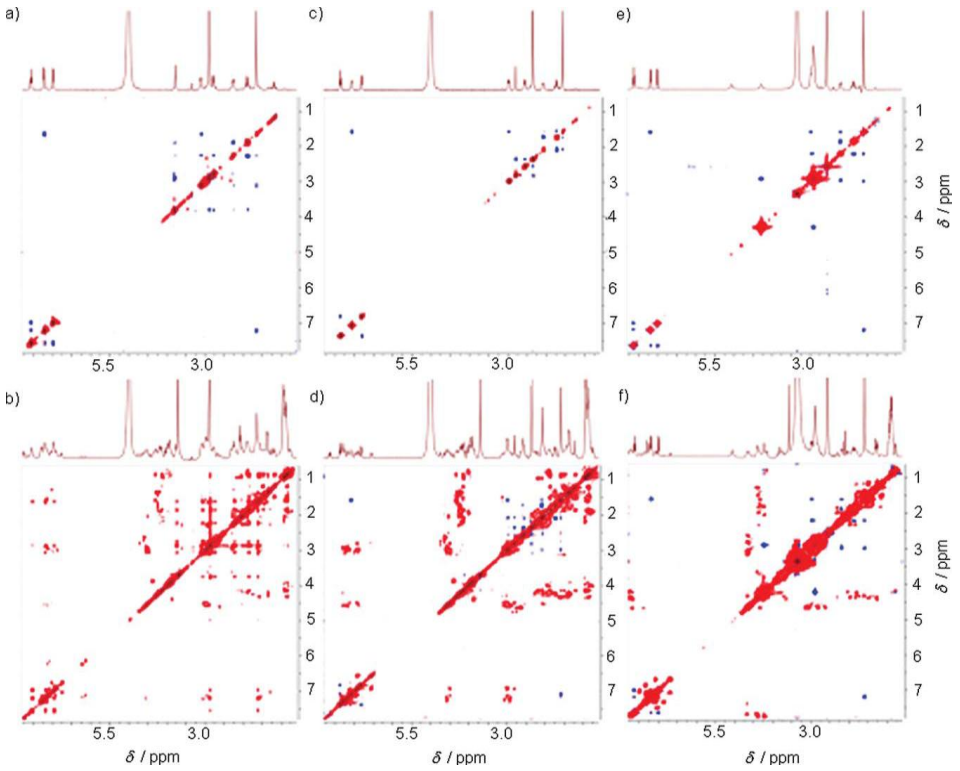

Fig. 5 2D-NOESY spectra of tetracycline in the absence (a, mix 650 ms, c, mix 650 ms, e, mix 500 ms) or presence (b, mix 300 ms; d, mix 300 ms; f, mix 500ms) of Aβ1–40. Peptide:drug at a 1:2 molar ratio. Samples were dissolved in PBS, pH 7.4 (**A** and **B**), or pH 12 (**C** and **D**) at 5 ◦C, or in DMSO (**E** and **F**) at 37 ◦C.

DLS and AFM analysis of supramolecular complexes

These two techniques were employed aiming the structural characterization of the complexes at the supramolecular level. They are complementary for what concerns the accessible timescales of the aggregation process. In particular, DLS has been shown to be sensitive to the first stages of complex formation. Samples of Aβ1–40 alone, or mixed with tetracycline at a 1 : 8 molar ratio, were analyzed immediately after preparation to observe the initial assembly of the peptide and to minimize the presence of preformed seeds. The weight-average hydrodynamic diameter D_H of the particles present into the two samples is reported in **Fig. 6a**. As previously

described,[26] the size of the oligomeric assemblies of Aβ1–40, dissolved in PBS, pH 7.4, increases slowly with time, reaching a value D_{Hfin} after 24 h, (open symbols in Fig. 6a). The analysis of this early-stage kinetics fits with a growth curve described by the equation $D_H(t) = D_{Hfin}$ [1-exp(-t/τ)] that has a characteristic time τ = 4 h, indicative of a nearly seeds-free sample. The addition of tetracycline to freshly dissolved Aβ1–40 immediately triggered the formation of much larger aggregates (full symbols in Fig. 6a). Noteworthly, such larger aggregates are very stable and do not show any later-stage evolution. Light scattering measurements performed at longer intervals of time (48 h) showed that the Aβ1–40 sample underwent an extensive aggregation process, at variance with the sample co-incubated with tetracycline that maintained the same state of aggregation. AFM studies were carried out to clarify the nature of the assemblies formed by co-incubation of Aβ peptides and tetracycline. Immediately after co-dissolution of Aβ1–42 and tetracycline, clustered material was visible in the form of dispersed aggregates with bigger weight than the regularly distributed background of oligomers (peptide alone, mean and confidence interval, 1.56 nm, 1.23–1.90 nm *vs.* peptide-tetracycline 2.94 nm, 2.54–3.34 nm, $p < 0.0001$ according to t-test). After 120 h, bigger shaped clusters were observed (peptide alone 3.42 nm, 2.76–4.09 nm *vs.* peptide tetracycline 16.96 nm, 13.99–19.92 nm, $p < 0.0001$). The same trend, although at lesser extent, was observed for Aβ1–40 after 120 h of incubation (peptide alone 0.38 nm, 0.33–0.44 nm *vs.* peptide-tetracycline 1.66 nm, 1.38–1.95 nm, $p < 0.0001$) (**Fig. 6b; ESI†, S7**)

[26] G. Di Fede,M. Catania,M.Morbin,G.Rossi, S. Suardi,G. Mazzoleni, M. Merlin, A. R. Giovagnoli, S. Prioni, A. Erbetta, C. Falcone, M. Gobbi, L. Colombo, A. Bastone, M. Beeg, C. Manzoni, B. Francescucci, A. Spagnoli, L. Cantù, E. Del Favero, E. Levy, M. Salmona and F. Tagliavini, *Science*, **2009**, 323, 1473–1477.

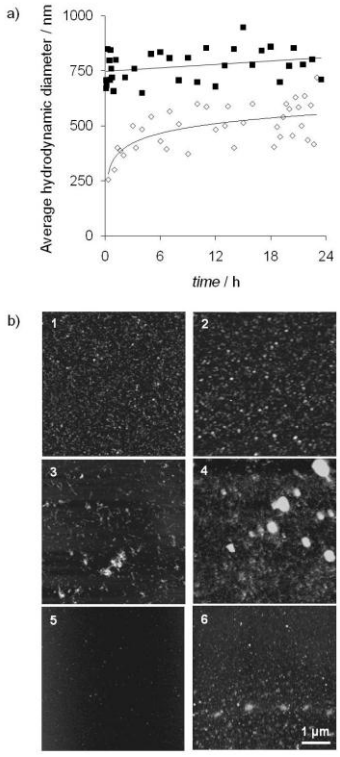

Fig. 6 a) Short-time-evolution of the weight-average hydrodynamic diameter of Aβ1–40 aggregates in aqueous solution determined by dynamic laser light scattering in the presence (full symbols) or in the absence (open symbols) of tetracycline at peptide:drug 1:8 molar ratio. b) Atomic force microscopy images of freshly dissolved Aβ1–42 in the absence (1) or presence of tetracycline (2) at a 1 : 4 molar ratio; and after 120 h of incubation at 5 ◦C in the absence (3) or presence of tetracycline (4); Aβ1–40 after 120 h of incubation in the absence (5) or presence of tetracycline (6).

Tetracycline competes with thioflavin T for binding to Aβ

Tetracycline competes with Thioflavin T (ThT) for binding to Aβ peptides. ThT (**Scheme 2**) is a benzothiazole dye that exhibits enhanced fluorescence upon binding to amyloid fibrils *ex vivo* and *in vitro*.[27]

[27] R. Khurana, C. Coleman, C. Ionescu-Zanetti, S. A. Carter, V. Krishna, R. K. Graver, R. Roy and S. Singh, *J. Struct. Biol.*, **2005**, 151, 229–238.

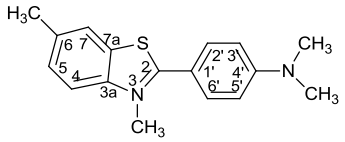

Scheme 2. Thioflavin T structure; numbering of hydrogens and carbons

Recently, it has been found that ThT can also bind Aβ oligomers.[[28]] This molecule is usually employed to monitor the aggregation process of Aβ peptides and quantify the formation of amyloid fibrils in the absence or presence of anti-amyloidogenic compounds. In experiments aimed at evaluating tetracycline efficacy in hindering Aβ fibrillogenesis, we observed that the drug competes with ThT in binding to peptides. Under our experimental conditions, tetracycline interfered with ThT fluorescence suggesting the presence of a direct interaction or a competitive binding to Aβ oligomers, as it was recently reported by Hudson *et al.* for polyphenols.[[29]] To clarify this point, we performed competitive binding experiments by NMR. Firstly, we determined the feasibility of STD-NMR studies to detect ThT binding to Aβ1–40 and Aβ1–42 oligomers, which was proven to be successful. Then, competitive titration STD experiments were performed. In particular, different concentrations of tetracycline were mixed with a solution containing Aβ1–40 or Aβ1–42 (80 μM, PBS, pH 7.4, 25 ◦C) and ThT, to obtain ThT:tetracycline molar ratios of 1:0, 1:0.25, 1:0.5 and 1:1. For each molar ratio, a STD spectrum was acquired and the fractional STD effect on the ThT protons was determined. The alternative protocol was also performed, by mixing solutions of Aβ peptides and tetracycline with different concentrations of ThT. It was observed that, in both cases, the addition of the second ligand to the mixture reduced the STD effect of the first ligand pre-incubated with peptides. The residual fractional STD effect of ThT was higher than that of tetracycline, as an indication of its higher affinity for oligomers (**Table 3**).

[[28]] I. Maezawa, H. S. Hong, R. Liu, C. Y. Wu, R. H. Cheng, M. P. Kung, H. F. Kung, K. S. Lam, S. Oddo and F. M. La Ferla, *L. W. J. Neurochem.*, **2008**, 104, 457–468.

tetracycline : ThT ratio	tetracycline H8 fractional STD effects[a]	ThT H7 fractional STD effects [a]
0:1	-	1.00
0.25:1	-	0.95
0.5:1	-	0.92
1:1	0.18	0.82
1:0.5	0.64	-
1:0.25	0.76	-
1:0	1.00	-

[a] Fractional STD effects were calculated as $(I_0\text{-}I)/I_0$, where $(I_0\text{-}I)$ is the peak intensity in the STD spectrum and I_0 is the peak intensity in the off-resonance spectrum. The largest STD effect ($I_{0\ STD}$) was set to 1 and relative intensities (I_{STD}) were determined.

Table 3. Decrease of the fractional STD effect of H8 tetracycline and H7 ThT protons as a function of different compound molar ratios.

The better interaction for ThT results were also confirmed by tr-NOESY experiments acquired on Aβ1–40 or Aβ1– 42 :ThT : tetracycline mixture (**ESI†, S8**). Indeed, the tr-NOESY spectra showed all tetracycline cross peaks with negative sign only when the tetracycline:ThT molar ratio was 1:0.5. For higher molar ratios of ThT the tetracycline cross peaks turned to be positive indicating that ThT was able to displace the interaction of the antibiotic with the oligomers. This competitive features were not due to a major change in the structure of the oligomers, since FTIR experiments permitted to verify that the major structural features of the two peptides were non altered by the presence of ThT (**ESI†, S9**). The ability of tetracycline to prevent ThT binding to Aβ1–40 and Aβ1–42 oligomers, even if at higher concentrations, further supports tetracycline capability to bind Aβ peptides.

Experimental

Peptide synthesis and purification

Aβ1–40, and Aβ1–42 were prepared by solid-phase peptide synthesis on a 433A synthesizer (Applied Biosystems) using Fmoc-protected L-amino acid derivatives, NOVASYN-TGA resin on a 0.1 mM scale.[[26]] Peptides were cleaved from the resin as previously described and purified by reverse phase HPLC on a semi-preparative C4

[29] S. A. Hudson, H. Ecroyd, T. W. Kee and J. A. Carver, *FEBS J.*, **2009**, 276, 5960–5972.

column (Waters) using water–acetonitrile gradient elution.[30] Peptide identity was confirmed by MALDITOF analysis (model Reflex III, Bruker). Peptide purity was always above 95%.

Preparation of peptide batch solutions

Aβ1–40 was treated as previously described[31] to obtain reproducible, disaggregated preparations containing only monomers and small oligomers. For Aβ1–42 experiments a batch was selected that contained pre-amyloidogenic seeds highly toxic to N2a cells. Immediately before use, lyophilized Aβ1–40 and Aβ1–42 were dissolved in 10 mM NaOH in 9 : 1 H_2O:D_2O or D_2O at variable concentrations, then diluted 1:1 with 10 mM phosphate buffer saline, pH 7.4 containing 150 mM NaCl (PBS). The pH of each sample was verified with a Microelectrode (Mettler Toledo) for 5 mm NMR tubes and adjusted with NaOD or DCl. For samples dissolved in D_2O, all pH values were corrected for isotope effects. To avoid bacterial contamination NaN_3 0.01% w/v was added to samples in 9:1 H2O:D2O. In the experiments carried out up to 120 h, samples were kept at 5 ◦C to minimize Aβ peptide aggregation and tetracycline oxidation and precipitation.

In vitro toxicity assay

Aβ1–42 was dissolved in 10 mM NaOH and mixed with tetracycline solution in PBS to obtain peptide:drug molar ratios of 1:4 or 1:8. Solutions were then incubated under static conditions at 37 ◦C for 70 h. Aliquots of peptide were also incubated in PBS in the absence of tetracycline. Peptide solutions were serially diluted in Dulbecco's MEM (DMEM) immediately before cell treatment. N2a cells were harvested in DMEM supplemented with 10% fetal calf serum (FCS). For toxicity assays, cells were trypsinized and 100 ml of 5 x 10^4 cell/ml suspension in DMEM with 1% FCS were plated (96 multiwell plates, Iwaki). Four h after plating, 10 ml aliquots of different Aβ1–42

[30] M. Salmona, M. Morbin, T. Massignan, L. Colombo, G. Mazzoleni, R. Capobianco, L. Diomede, F. Thaler, L. Mollica, G. Musco, J. J. Kourie, O. Bugiani,D. Sharma, H. Inouye,D. A. Kirschner,G. Forloni and F. Tagliavini, *J. Biol. Chem.*, **2003**, 278, 48146–4815.
[31] C. Manzoni, L. Colombo, M. Messa, A. Cagnotto, L. Cant`u and E. Del Favero, *Amyloid*, **2009**, 16, 71–80.

solutions were added to the cell medium; cell impairment was evaluated after 24 h incubation using the MTT reduction assay (Sigma-Aldrich).

SDS-PAGE and DOT BLOT assay

Peptide solutions were diluted 1:1 with loading buffer containing 12% (w/v) SDS (sodium dodecyl sulfate) and 100 mM dithiothreitol in 0.5 M Tris-HCl buffer, pH 6.8, and immediately denatured at 100 ◦C for 5 min. Samples were analyzed by electrophoresis on 1. 5mm thick 12.5% polyacrylamide gels (SDS-PAGE) followed by Western Blot analysis with anti-Aβ primary antibody 6E10 (Signet Laboratories) and anti-mouse peroxidase-conjugated secondary antibody (DAKO). Antibody binding was detected by chemoluminescence (ECL detection system,GEHealthcare). For Dot Blot assays, 4 mg aliquots of Aβ1–42 were spotted on nitrocellulose membranes (0.2 mm filter paper, Whatman); after air drying the membranes were blocked overnight in 10 mM Tris-HCl, pH 7.4, 100 mM NaCl, 0.1% Tween-20 (TBST) supplemented with 5% non-fat milk. Membranes were washed in TBST and incubated sequentially with A11 anti-oligomer antibody[32] (Biosource) and anti-rabbit peroxidase-conjugated secondary antibody (Sigma). Antibody binding was detected by chemoluminescence.

NMR spectroscopy

NMR experiments were recorded on a Varian 400-MHzMercury or a Bruker 600-MHz Advance equipped with a Bruker CryoProbe. Both spectrometers were equipped with a *z*-axis gradient coil. Tetracycline was dissolved in PBS, pH 7.4 or 12, or in d_6-DMSO (methyl sulfoxide), and then added to the peptide solution. Basic sequences were employed for 2D-TOCSY, 2D-NOESY, diffusion and STD experiments. ^{1}H spectra were acquired with 128, 160, 256 or 512 transients and 2 s recycle delay. 2D-TOCSY spectra were recorded with 16 or 32 transients, 256 t1 increments, 1 s recycle delay, a mixing time between 60 and 120 ms, and with a spin-lock pulse of nearly 7000 Hz. 2D-NOESY spectra were recorded with 64, 72, 80 or 96 transients and 256 t1 increments, a recycle

[32] R. Kayed, E. Head, J. L. Thompson, T. M. McIntire, S. C. Milton, C. W. Cotman and C. G. Glabe, *Science*, **2003**, 300, 486–489.

delay variable between 1 and 2.5 s, and a mixing time between 100 and 800 ms. The spectral width was varied between 4504 and 6006 Hz. Peptide spin systems were initially identified using the 2D-TOCSY spectra. Intra-residue and sequential interresidue connectivities were then assigned using the 2D-NOESY spectra. For STD, a train of Gaussian-shaped pulses each of 50 ms was employed to saturate selectively the protein envelope; the total saturation time of the protein envelope was varied between 5 s and 0.5 s. For experiments in H_2O solvent, the WATERGATE or the excitation sculpting solvent suppression was employed. Diffusion experiments were performed employing an array of 20 or 30 spectra for each experiment (128, 256 or 512 transients each, with a 1 or 2 s recycle delay) varying the gradient strength from 3.33 to 19.4 G/cm^2. The lengths of and delays between the gradient pulses were optimized depending on the experimental conditions and ranged between 0.002 and 0.005 s and 0.2–0.7 s, respectively. Data fitting and diffusion coefficients determination were performed with the software *Dosytoolbox*.[33]

Dynamic laser light scattering (DLS)

DLS measurements were performed on a custom apparatus[34] using a diode laser (l = 532 nm) and a digital correlator (Brookhaven Instruments Co). Samples (c = 0.65 mg ml-1) were kept at controlled temperature (T = 37 ◦C). The scattered intensity correlation functions were analysed with the cumulant analysis method[35] giving the weight average hydrodynamic diameter of the particles in solution.

Atomic force microscopy (AFM)

For AFM analysis peptide samples were diluted to 5 mM with 10 mM HCl and 60 ml aliquots were immediately spotted onto a freshly cleaved Muscovite mica disk and incubated for 0.5 min.The disk was then washed with H_2O and dried under a gentle nitrogen stream. Samples were mounted onto a Multimode AFM with a NanoScope V

[33] http: // personalpages .manchester . ac . uk / staff /mathias . nilsson /software.htm
[34] P. Lago, L. Rovati, L. Cant`u and M. Corti, *Rev. Sci. Instrum.*, 1993, **64**, 1797–1802.
[35] D. E. Koppel, *J. Chem. Phys.*, 1972, **57**, 4814–4820.

system (Veeco/Digital Instruments) operating in Tapping Mode using standard phosphorus-doped silicon probes (*T*: 3.5–4.5 mm, *L*: 115–135 mm, *W*: 30–40 mm, *f* 0: 311–364 kHz, *K*: 20–80 N m-1) (Veeco).

FTIR spectroscopy

FTIR spectra were measured in transmission on the same samples examined by NMR spectroscopy. Twenty ml of the peptide D_2O solutions were placed between 2 BaF_2 windows separated by a 100 mm Teflon spacer. FTIR spectra were recorded using a FTS40A spectrometer (Bio-Rad, Digilab Division, Cambridge, MA) equipped with a nitrogen-cooled mercury–cadmium– tellurium (MCT) detector under the following conditions: 2 cm^{-1} spectral resolution, 1000 scan co-addition, 25 kHz scan speed, and triangular apodization. Peptide spectra were obtained after subtraction of the buffer spectrum from that of the peptide solution. Second-derivatives of the absorption spectra[[36]] were performed to resolve the secondary structure and aggregate components that overlap into the broad and structure less Amide I band in the measured spectrum. This mathematical procedure permitted the identification of the different components that give rise to negative bands in the derivative spectrum, and whose minima correspond to the component peaks in the measured spectrum. For this analysis the Savitsky–Golay (5 points) procedure was employed after binomial smoothing of the absorption spectra (11 points).

Circular Dichroism (CD)

Spectra were recorded by the JASCO J-815 spectropolarimeter (JASCO corporation, Tokyo, Japan) under the following conditions: scanning speed 10 nm min^{-1}, band width 1 nm, 5 accumulations per sample, and 0.1 cm path length cuvette.

Theoretical basis of PFG-NMR diffusion measurements

Pulse field gradient (PFG) NMR diffusion measurements allow molecular size estimation through the measurement of diffusion coefficients.[[37]] The diffusion coefficient is

[[36]] H. Susi and D. M. Byler, *Methods Enzymol.*, **1986**, 130, 290–311.
[[37]] P. Stilbs, *Anal. Chem.*, **1981**, 53, 2135–2137.

inversely proportional to the hydrodynamic radius of the particle as described by the Stokes–Einstein equation:

$$D_T = k_B T / 6\pi\eta R'$$

where D is the diffusion constant, k_B is the Boltzmann constant, T is temperature, η is viscosity and R' the hydrodynamic radius. The hydrodynamic radius is scaled with a power law of the mass. Differences in peptide aggregation state, or the addition of peptide or tetracycline to the sample, affected the viscosity of the solution and thereby the measured diffusion coefficient. This was accounted for by measuring the HDO diffusion and then correcting the measured values according to the following equation:[38]

$$D_{corrected} = D_{HDO,\,neat} / D_{HDO,measured} * D_{observed}$$

In our case, HDO_{neat} values for PBS buffer used for peptide dissolution were determined at 5, 25 and 37 ◦C. When two substances, a ligand and a receptor, interact, there is a change both in their mass and in most cases, shape. When the ligand is in fast exchange between the bound and the free states on the timescale of the diffusion experiment, the measured diffusion coefficient is the weighted mean value of the free and bound states.

$$D_{observed} = (1 - p_{complex}) D_{free} + p_{complex} D_{complex}$$

When the equilibrium between the ligand free state and the ligand bound state is fast on the translational diffusion time scale (ms), it leads to an averaged observed diffusion coefficient, higher than that expected for the complex, but lower than that expected for the free ligand. This makes the diffusion coefficient a sensitive observable parameter when measuring ligand-receptor interactions.

Conclusions

The present study was prompted by the observation that tetracycline can reduce the *in vitro* toxicity of oligomeric Aβ1–42 in a dose-dependent manner. This is a particularly important finding since oligomers are considered the neurotoxic species which play a pivotal role on the onset and progression of AD. NMR and FTIR studies have unveiled the capacity of tetracycline to interact with Aβ peptides in a non-conventional manner, as shown by the absence of a specific epitope in the drug and the absence of a well defined binding site on the Aβ peptides. Noteworthy, NMR data showed for the first time that tetracycline competes with ThT in the binding to Aβ peptides. DLS and AFM also indicated that supramolecular complexes are immediately formed when Aβ peptides are co-dissolved with tetracycline, preventing the formation of aggregates. Incubation of both Aβ peptides with tetracycline led to the formation of colloidal particles that specifically sequester oligomers, preventing in this way the progression of the amyloid cascade. We can hypothesize that the internal structure of aggregates formed by Aβ peptides with tetracycline is disordered and non-homogeneous, governed by hydrophobic and charge multiparticle interactions. The formation of supramolecular aggregates that improve the solubility of Aβ peptides is in good agreement with a recent report on the mechanism of action of small anti-amyloidogenic molecules.[39] However, in contrast to the molecules studied by those authors, tetracycline does not spontaneously form colloidal aggregates in aqueous solution. Our observations shed light on the anti-fibrillogenic activity of tetracycline with both Aβ and other amyloidogenic proteins. These data may be useful for the development of novel tetracycline analogues devoid of antibiotic activity for the treatment of brain and peripheral amyloidosis. In addition, the experimental protocol here described can be applied to the screening of new potential Aβ ligands showing

[38] J. Danielsson, J. Jarvet, P. Damberg and A. Graslund, *Biochemistry*, **2004**, 43, 6261–6269.
[39] B. Y. Feng, B. H. Toyama, H.Wille, D.W. Colby, S. R. Collins, B. C. H. May, S. B. Prusiner, J. Weissman and B. K. Shoichet, *Nature Chemical Biology*, **2008**, 4, 197–199.

anti-amyloidogenic properties and to the characterization of their mechanism of action at molecular level.

Acknowledgements

The research leading to these results has received funding from the European Community's Seventh Framework Programme (FP7/2007-2013) under grant agreement n° 212043. We acknowledge the Italian Ministry of Health (533F/Q/1), Cariplo Foundation (Project NOBEL-GUARD), Banca Intesa SanPaolo, and PRIN (PROT.2007T7MSAJ) for financial support and Flamma (Italy) for the kind gift of Fmoc amino acids.

Supplementary information

S1 – NMR Characterization of Aβ1-40 and Aβ1-42 assemblie.

Figure 2 (main text) shows ^{1}H-NMR spectra acquired on the same samples of Aβ1-40 or Aβ1-42 in PBS at pH 7.4 or pH 12, 5°C. For both peptides, S/N ratios were higher and ^{1}H-NMR signals sharper in the spectrum recorded at pH 12, in agreement with higher relaxation times (**Table 1S and 2S**). In addition, several differences in proton resonances were seen. These findings are consistent with the diffusion coefficients reported in Table 1 (main text) and demonstrate oligomerization of Aβ peptides at pH 7.4. In addition, they support a higher level of oligomerization for Aβ1-42 versus Aβ1-40.

Table 1S. T1 values of His residues for Aβ1-40 and Aβ1-42 peptide in solution at 5°C, pH 7.4 or pH 12.

Aβ sequence	pH	T1 value[a]
1-40	7.4	1.964 s
1-40	12	3.178 s
1-42	7.4	1.717 s
1-42	12	2.733 s

[a] T1 values were calculated as exponential decay of the average integral of His6, His13 and His 14.

Table 2S. Selective T1 values of some aromatic signals for Aβ1-40 and Aβ1-42 peptide in solution at 5°C, pH 7.4 or pH 12.

Aβ sequence	pH	signal	selT1 value[a]
1-40	7.4	His (2H)	0.680 s
		His (4H)	0.569 s
		Tyr (3H, 5H)	0.469 s
1-40	12	His (2H)	1.734 s
		His (4H)	1.385 s
		Tyr (3H, 5H)	1.143 s
1-42	7.4	His (4H)	0.296 s
		His (4H)	0.307 s
		Tyr (3H, 5H)	0.249 s
1-42	12	His (4H)	1.042 s
		His (4H)	0.866 s
		Tyr (3H, 5H)	0.896 s

[a] Selective T1 values were calculated as exponential decay of isolated signal from the aromatic region of Aβ peptide ^{1}H spectra

Figure 1S reports DOSY spectra obtained for peptide Aβ1-40, pH 7.4, at 5, 25 or 37°C.

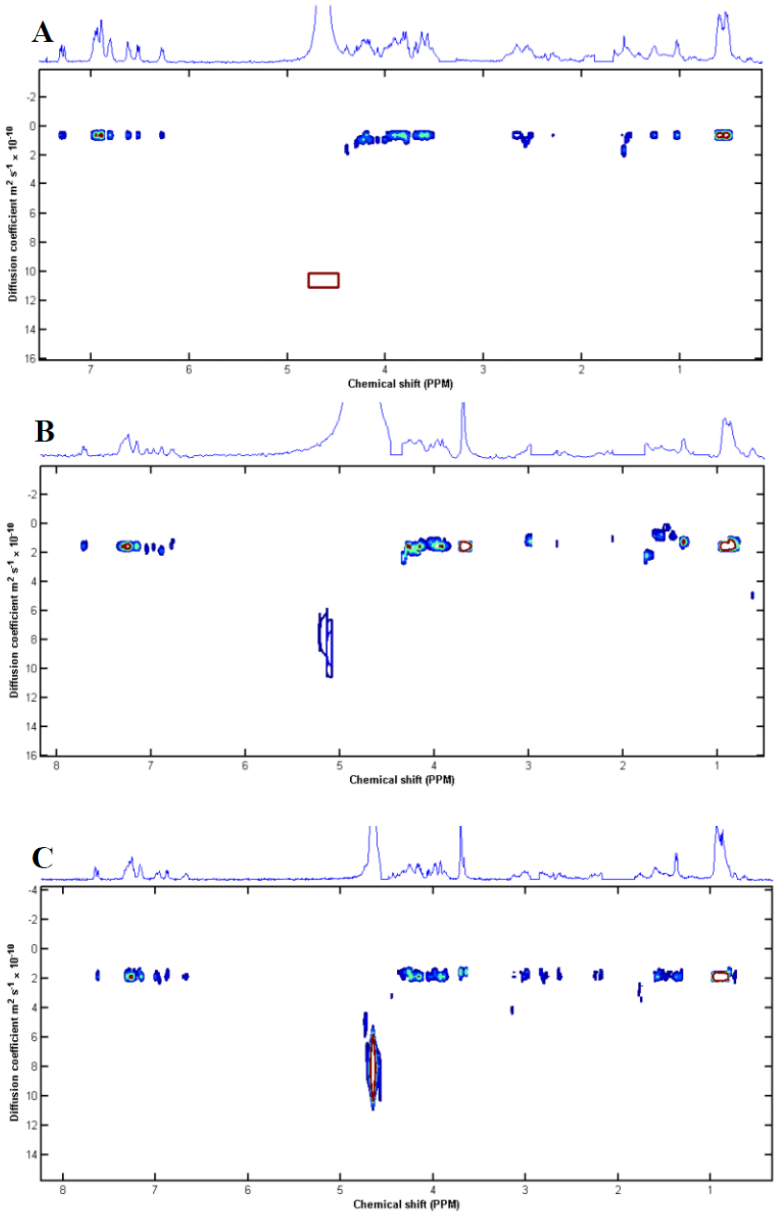

Figure 1S. 2D-DOSY spectra of Aβ1-40, 0.5 mM, at 5 (**A**), 25 (**B**) or 37°C (**C**), pH = 7.

S2 - Aβ1-40 and Aβ1-42 STD-NMR

STD-NMR experiments of Aβ peptide-tetracycline mixtures were carried out for both peptides at different temperatures, at several peptide:drug molar ratios, and with different frequencies for the protein envelope saturation pulse. Peptides dissolved in PBS, pH 7.4, provided clear evidence of tetracycline binding. The first example is shown in Figure 4 (main text); further experiments are illustrated in **Figure 2S-6S**.

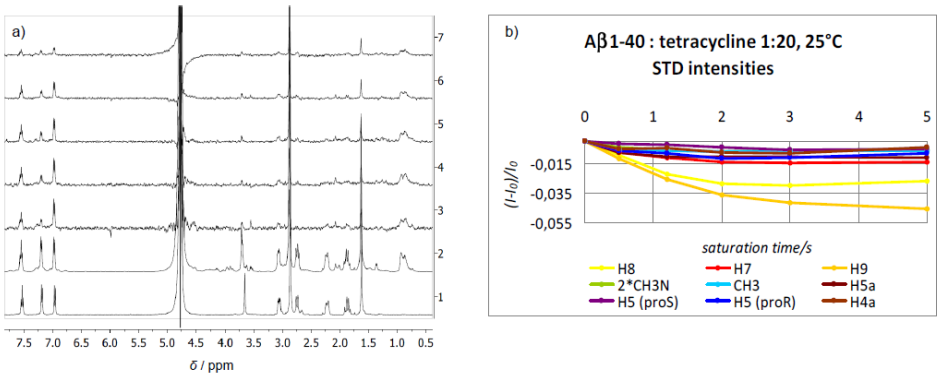

Figure 2S. a) ^{1}H NMR spectra of tetracycline, NS=32 (1), Aβ1-40-tetracycline mixture, at 1:20 molar ratio, NS=128 (2), STD spectra of the mixture recorded with different peptide saturation times (3, 5 s; 4, 3 s; 5, 2 s; 6, 1.2 s; 7, 0.5 s; enhanced 3x), NS=1792, on-resonance frequency= -1.0 ppm, off-resonance frequency=40 ppm. Spectra 2-7 were recorded on the same sample; all samples were dissolved in PBS, pH 7.4, 25°C. b) Fractional STD effects for each tetracycline proton, calculated by $(I-I_0)/I_0$, where $(I-I_0)$ is the peak intensity in the STD spectrum and I_0 is the peak intensity of an unsaturated reference spectrum.

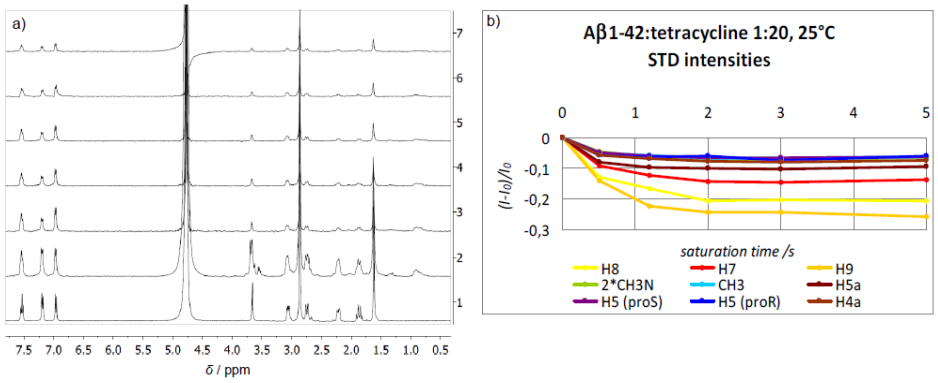

Figure 3S. a) ^{1}H NMR spectra of tetracycline, NS=32 (1), Aβ1-42-tetracycline mixture, at 1:20 molar ratio, NS=128 (2), STD spectra of the mixture recorded with different peptide saturation times (3, 5 s; 4, 3 s; 5, 2 s; 6, 1.2 s; 7, 0.5 s; enhanced 3x), NS=1792, on-resonance frequency= -1.0 ppm, off-resonance frequency=40 ppm. Spectra 2-7 were recorded on the same sample; all samples were dissolved in PBS, pH 7.4, 25°C. b) Fractional STD effects for each tetracycline proton, calculated by $(I-I_0)/I_0$, where $(I-I_0)$ is the peak intensity in the STD spectrum and I_0 is the peak intensity of an unsaturated reference spectrum.

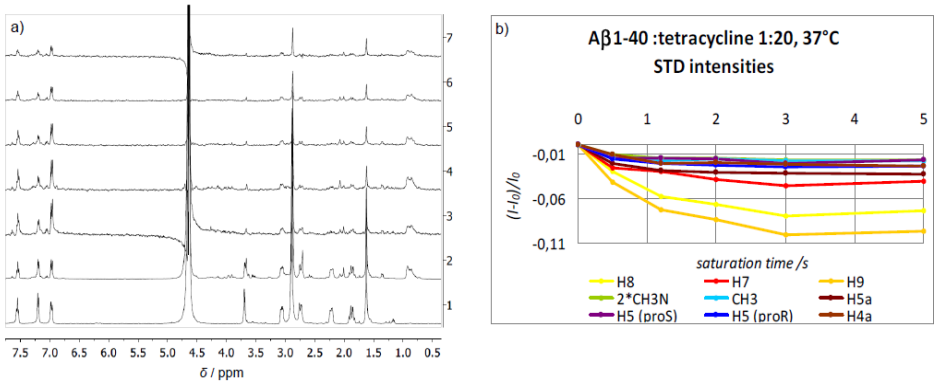

Figure 4S. a) ^{1}H NMR spectra of tetracycline, NS=32 (1), Aβ1-40-tetracycline mixture, at 1:20 molar ratio, NS=128 (2), STD spectra of the mixture recorded with different peptide saturation times (3, 5 s; 4, 3 s; 5, 2 s; 6, 1.2 s; 7, 0.5 s; enhanced 3x), NS=1792, on-resonance frequency= -1.0 ppm , off-resonance frequency=40 ppm. Spectra 2-7 were recorded on the same sample; all samples were dissolved in PBS, pH 7.4, 37°C. b) Fractional STD effects for each tetracycline proton, calculated by $(I-I_0)/I_0$, where $(I-I_0)$ is the peak intensity in the STD spectrum and I_0 is the peak intensity of an unsaturated reference spectrum.

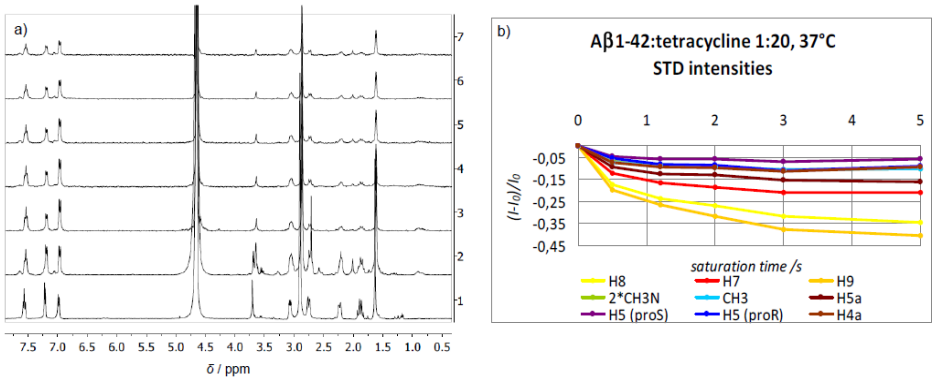

Figure 5S. a) ^{1}H NMR spectra of tetracycline, NS=32 (1), Aβ1-42-tetracycline mixture, at 1:20 molar ratio, NS=128 (2), STD spectra of the mixture recorded with different peptide saturation times (3, 5 s; 4, 3 s; 5, 2 s; 6, 1.2 s; 7, 0.5 s; enhanced 3x), NS=1792, on-resonance frequency= -1.0 ppm, off-resonance frequency=40 ppm. Spectra 2-7 were recorded on the same sample; all samples were dissolved in PBS, pH 7.4, 37°C. b) Fractional STD effects for each tetracycline proton, calculated by $(I-I_0)/I_0$, where $(I-I_0)$ is the peak intensity in the STD spectrum and I_0 is the peak intensity of an unsaturated reference spectrum.

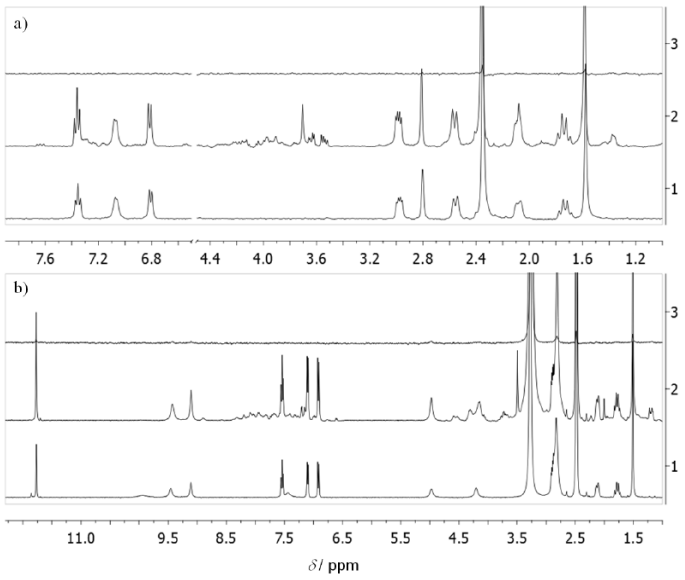

Figure 6S. a) ^{1}H NMR spectra of tetracycline, NS=32 (1), Aβ1-40-tetracycline mixture, at a 1:2 molar ratio, NS=128 (2), and STD spectrum of the mixture recorded with saturation times=2 s, NS=512 (3), in PBS, pH 12, 5°C. b) ^{1}H NMR spectra of tetracycline NS=32, (1), Aβ1-40- tetracycline mixture, at a 1:2 molar ratio, NS=128 (2) and STD spectrum of the mixture recorded with

saturation times=2s, NS=512 (3) in DMSO, 25°C, on-resonance frequency= -1.0 ppm, off-resonance frequency=40 ppm.

S3 – Diffusion data deconvolution

The analysis of diffusion experiments acquired on a sample containing Aβ1-40 and tetracycline (1:2 molar ratio) and performed with SCORE, DECRA and MCR are reported in the following figures (**7S-18S**). HDO signal region was excluded to avoid complications associated with its spectral overlap with peptide and tetracycline resonances. As expected, the best results were obtained with SCORE. It was possible to separate Aβ1-40 and tetracycline spectra (and diffusion coefficients, reproducing values obtained with DOSY analysis) by increasing the number of components imposed for the deconvolution; in fact, the best fitting with results produced by DOSY were obtained by SCORE for 5 components. Nevertheless, two of the additional components identified showed diffusion coefficients higher than those calculated for tetracycline and Aβ1-40, and they clearly could not represent the oligomer diffusion coefficient, while one component presented a negative diffusion coefficient associated with an exponential increase of signal intensities vs the gradient amplitude, and the corresponding spectrum is mostly dominated by noise. We can conclude that this kind of analysis was not effective for the separation of diffusion coefficients of monomers and oligomers. [[40]] The following figures (**7S-10S**) report the deconvolution of diffusion data performed by SCORE for 2, 3, 4 or 5 components.

[[40]] a) M. Nillson and G. Morris, Magn. Reson. Chem. 2006, **44**, 655–660;b) M. Nillson and G. Morris, Anal. Chem. 2008**, 80**, 3777–3782; c) M. Nillson and G. Morris, Journal of Magnetic Resonance 2009, **200**, 296–302.

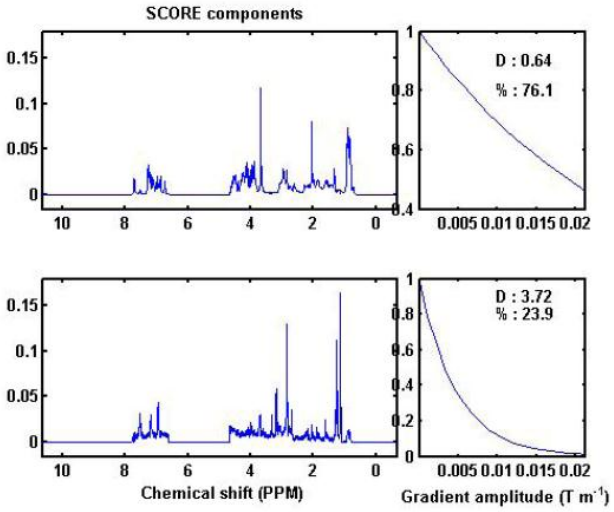

Figure 7S. Deconvolution of diffusion data performed by SCORE for 2 components (sample: Aβ1-40:tetracycline 0.5mM:1mM, pH 7.4, 5°C).

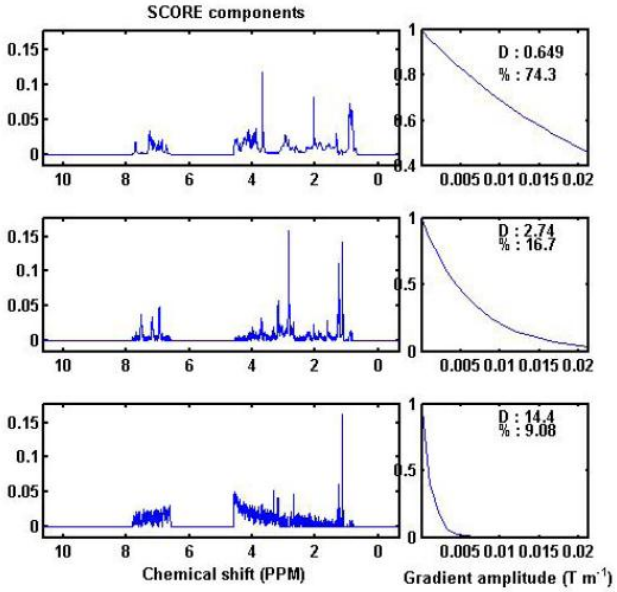

Figure 8S. Deconvolution of diffusion data performed by SCORE for 3 components (sample: Aβ1-40:tetracycline 0.5mM:1mM, pH 7.4, 5°C).

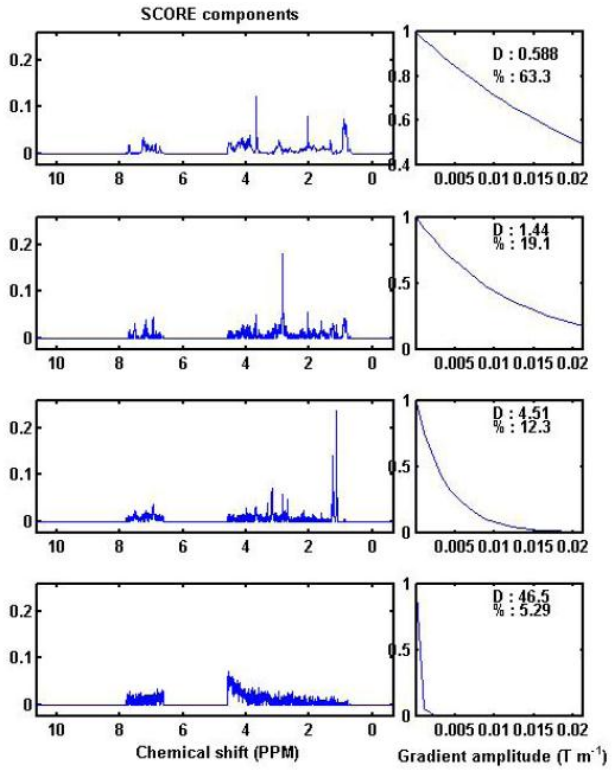

Figure 9S. Deconvolution of diffusion data performed by SCORE for 4 components (sample: Aβ1-40:tetracycline 0.5mM:1mM, pH 7.4, 5°C).

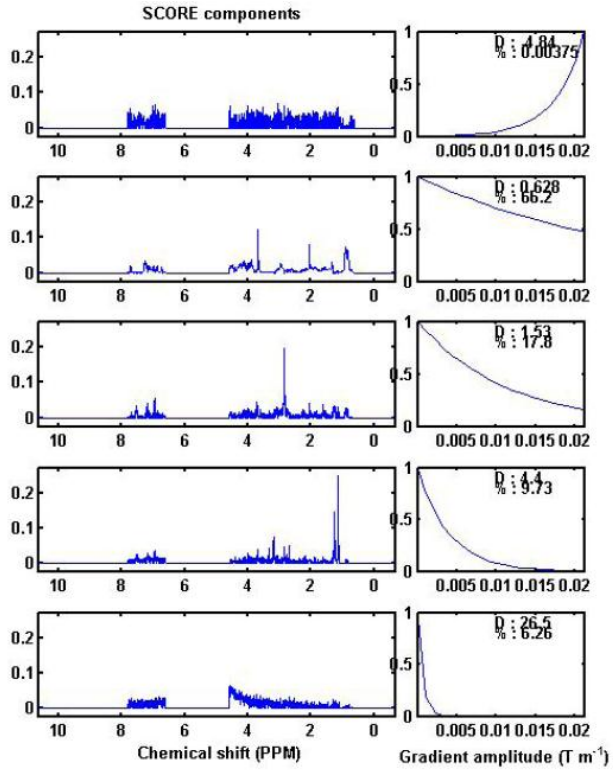

Figure 10S. Deconvolution of diffusion data performed by SCORE for 5 components (sample: Aβ1-40:tetracycline 0.5mM:1mM, pH 7.4, 5°C).

The following figures (**11S-14S**) report the deconvolution of diffusion data performed by DECRA for 2, 3, 4 or 5 components.

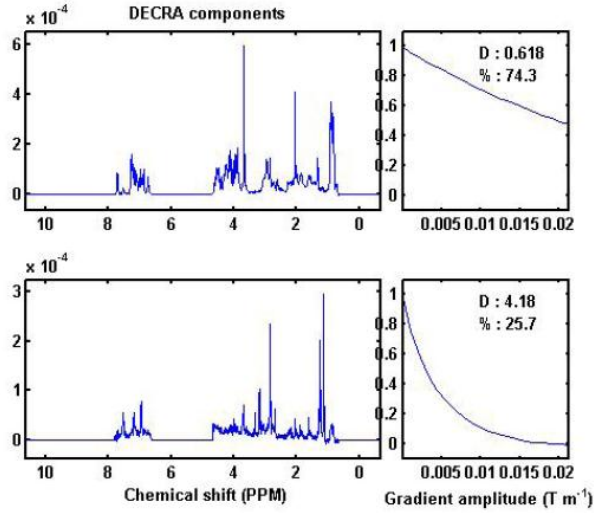

Figure 11S. Deconvolution of diffusion data performed by DECRA for 2 components (sample: Aβ1-40:tetracycline 0.5mM:1mM, pH 7.4, 5°C).

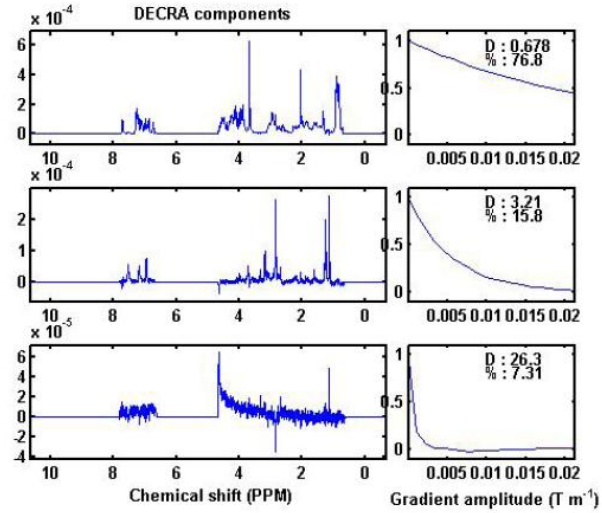

Figure 12S. Deconvolution of diffusion data performed by DECRA for 3 components (sample: Aβ1-40:tetracycline 0.5mM:1mM, pH 7.4, 5°C).

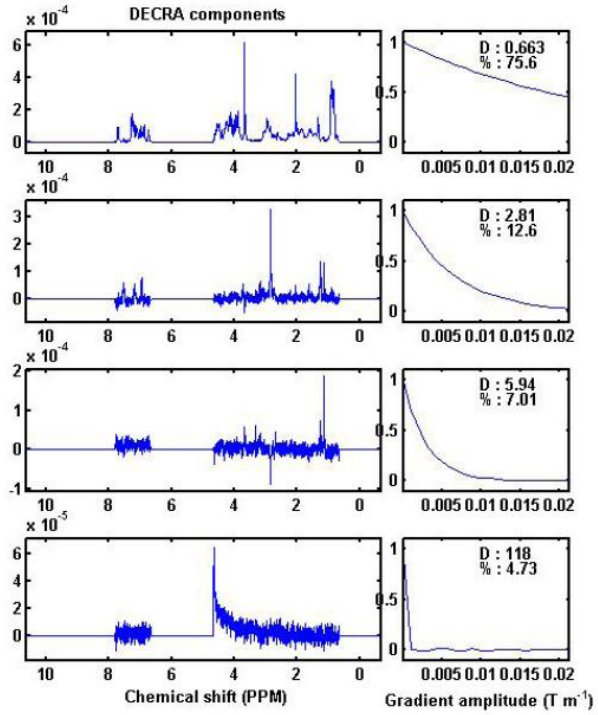

Figure 13S. Deconvolution of diffusion data performed by DECRA for 4 components (sample: Aβ1-40:tetracycline 0.5mM:1mM, pH 7.4, 5°C).

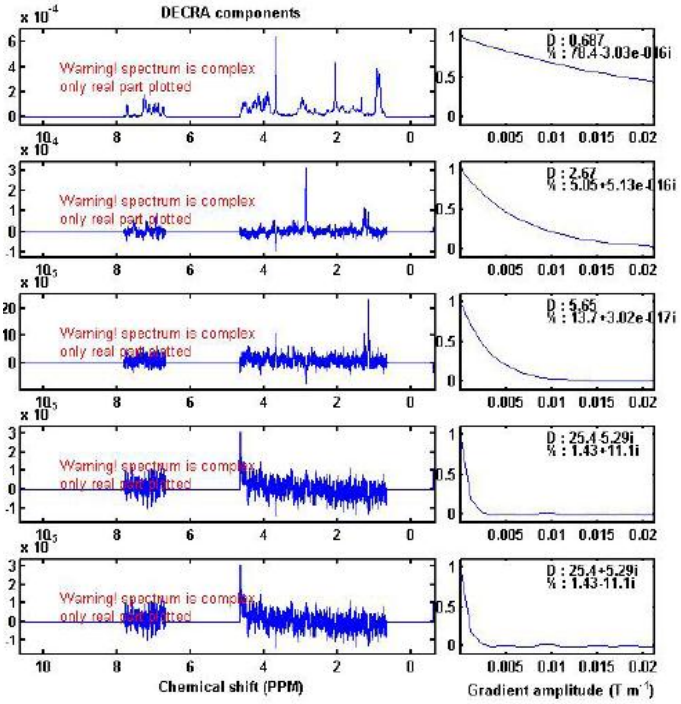

Figure 14S. Deconvolution of diffusion data performed by DECRA for 5 components (sample: Aβ1-40:tetracycline 0.5mM:1mM, pH 7.4, 5°C).

The following figures (**15S-18S**) report the deconvolution of diffusion data performed by MCR for 2, 3, 4 or 5 components.

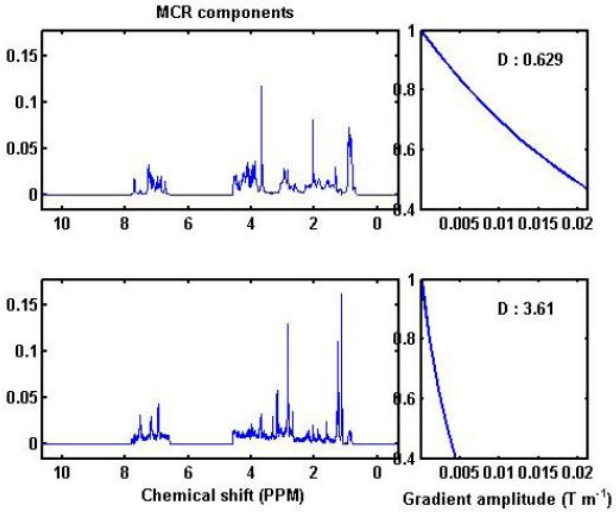

Figure 15S. Deconvolution of diffusion data performed by MCR for 2 components (sample: Aβ1-40:tetracycline 0.5mM:1mM, pH 7.4, 5°C).

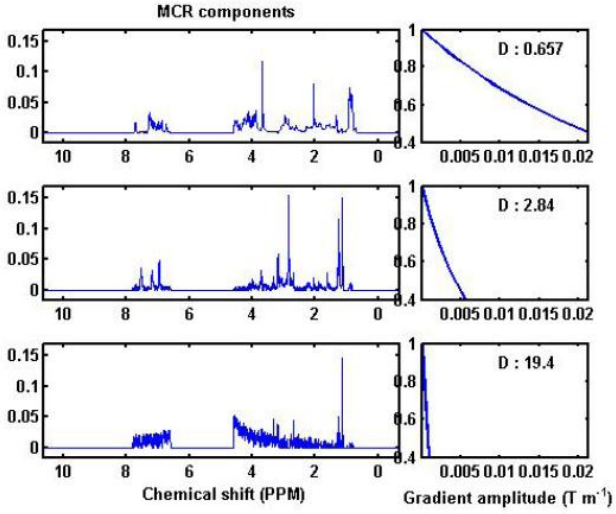

Figure 16S. Deconvolution of diffusion data performed by MCR for 3 components (sample: Aβ1-40:tetracycline 0.5mM:1mM, pH 7.4, 5°C).

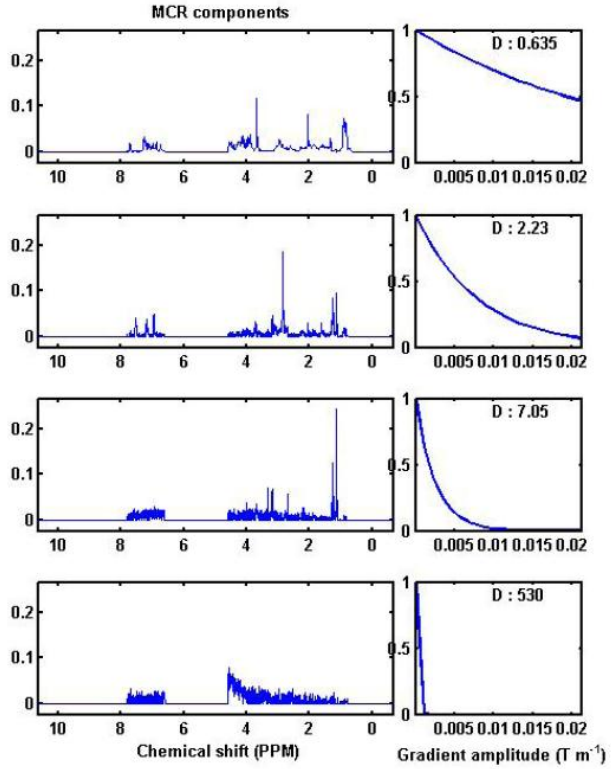

Figure 17S. Deconvolution of diffusion data performed by MCR for 4 components (sample: Aβ1-40:tetracycline 0.5mM:1mM, pH 7.4, 5°C).

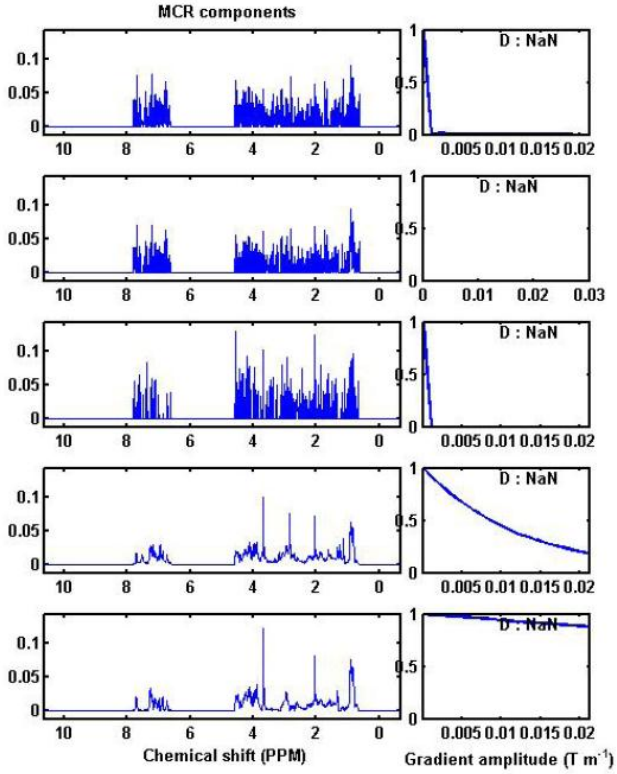

Figure 18S. Deconvolution of diffusion data performed by MCR for 5 components (sample: Aβ1-40:tetracycline 0.5mM:1mM, pH 7.4, 5°C).

S4 - Aβ1-42 trNOESY

TrNOESY spectra confirmed tetracycline interaction with both Aβ1-40 and Aβ1-42, as deduced by drug cross-peak change of sign (trNOE). **Figure 19S-b** shows the trNOESY spectrum of Aβ1-42:tetracycline at a 1:4 molar ratio.

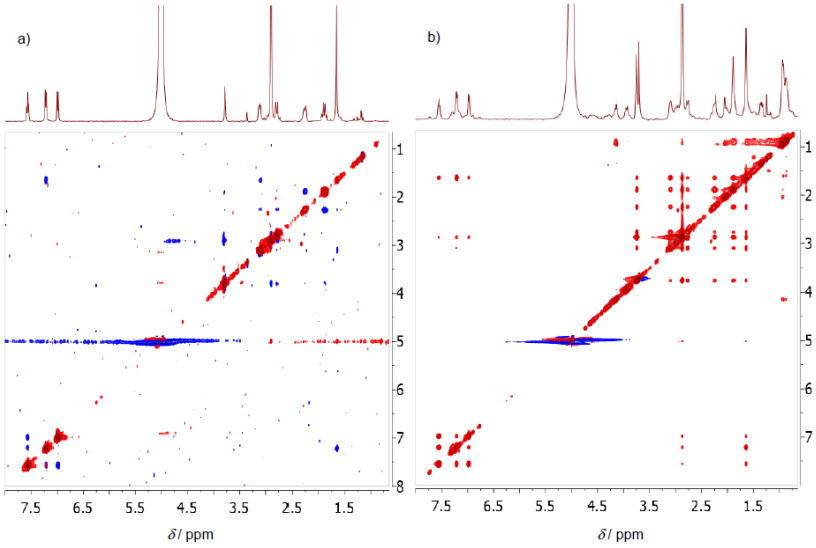

Figure 19S. a) 2D-NOESY spectrum of tetracycline, mix 650 ms; b) 2D-NOESY spectrum of Aβ1-42: tetracycline, at a 1:4 molar ratio, mix 300 ms. Samples were dissolved in PBS, pH 7.4, 5°C.

S5 - Aβ1-40 and Aβ1-42 titration with tetracycline

^{1}H titration experiments of Aβ1-40 and Aβ1-42 (**Figure 20S**) were performed to study the chemical shift changes induced in the presence of tetracycline. No significant changes in peptide chemical shifts were observed after tetracycline addition (up to a 1:8 molar ratio). Only a negligible downfield shift of about 0.02 ppm was observed for 2H protons of the three His residues (His6, His13, His14). These data were confirmed by analysis of the corresponding 2D-TOCSY spectra (data not shown).

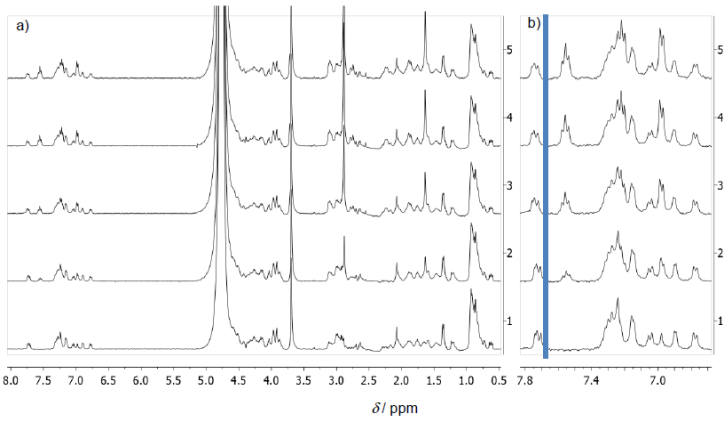

Figure 20S. a) ^{1}H NMR spectra of Aβ1-42 (0.25mM) (1), Aβ1-42-tetracycline mixture, at a 1:1 molar ratio (2), Aβ1-42-tetracycline mixture, at a 1:2 molar ratio (3), Aβ1-42-tetracycline mixture, at a 1:3 molar ratio (4), Aβ1-42-tetracycline mixture, at a 1:4 molar ratio (5). b) Expansion of the 7.9-6.8 ppm region of the spectra reported in (a). NS=128, PBS, pH 7.4, 25°C.

S6 – CD spectra of Aβ1-42 in the presence of Tetracycline

The effect of tetracycline on the secondary structures of Aβ1-42 was studied also by CD in the far-UV region. CD spectra of Aβ1-42 in the absence and in the presence of tetracycline are almost super imposable and indicate a β-sheet secondary structures,[41] in agreement with the FTIR results.

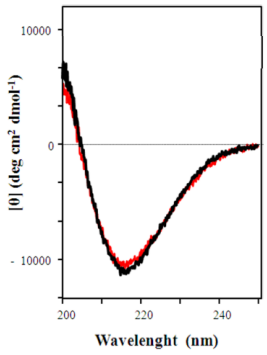

Figure 21S. CD spectra of Aβ1-42 (25 µM concentration) in the absence (black) and in the presence of 50 µM tetracycline (red). The samples were prepared at 0.25 mM peptide

[41] S. M. Kelly, T. J. Jess, N. C. Price, BBA, 2005, **1751**, 119-139.

concentration – plus 0.5 mM tetracycline when required- as reported for the other analyses in the paper and diluted of a factor 10 to perform CD measurements.

S7 – Atomic Force Microscopy. Analysis of aggregate height formed following co-dissolution of Aβ peptides with tetracycline.

The aggregate height was determined with a Research NanoScope 7.20 (Veeco) software after analysis of 50 independent spots in three different areas of 5 μm^2 (**Figure 22S**). Statistical analysis (**Tables 3S-5S**) was carried out by t-test. Aβ1-42, time 0, mean and confidence interval, peptide alone 1.56 nm, 1.23-1.90 nm *vs* peptide-tetracycline 2.94 nm, 2.54-3.34 nm, $p<0.0001$. Aβ1-42; time 120 h, peptide alone 3.42 nm, 2.76-4.09 nm *vs* peptide-tetracycline 16.96 nm, 13.99-19.92 nm, $p<0.0001$. Aβ1-40; time 120 h, peptide alone 0.38 nm, 0.33-0.44 nm *vs* peptide-tetracycline 1.66 nm, 1.38-1.95 nm, $p<0.0001$.

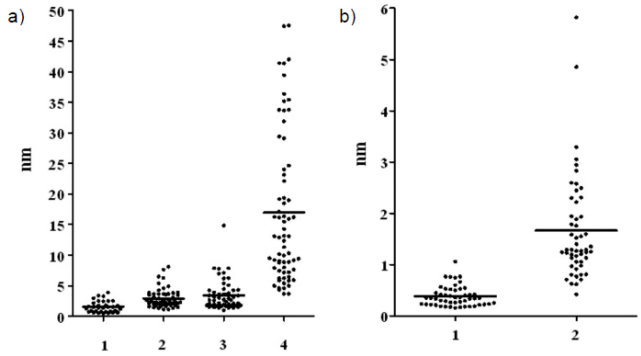

Figure 22S. Scattered plot of aggregate height distribution. Panel a. (1) Aβ1-42 time zero, (2) Aβ1-42-tetracycline, time zero; (3) Aβ1-42, time 120 h, (4) Aβ1-42-tetracycline, time 120 h. Panel b. (1) Aβ1-40 time 120 h, (2) Aβ1-40-tetracycline, time 120 h.

	Parameter	A Value
		Y
1	Table Analyzed	Data 1
2	Column A	1-42 0hrs
3	vs	vs
4	Column B	1-42 0hrs tetra
5		
6	Unpaired t test	
7	P value	P<0.0001
8	P value summary	***
9	Are means signif. different? (F	Yes
10	One- or two-tailed P value?	Two-tailed
11	t, df	t=4.724 df=88
12		
13	How big is the difference?	
14	Mean ± SEM of column A	1.564 ± 0.1629 N=50
15	Mean ± SEM of column B	2.940 ± 0.2002 N=57
16	Difference between means	-1.376 ± 0.2912
17	95% confidence interval	-1.956 to -0.7961
18	R squared	0.2023
19		
20	F test to compare variances	
21	F,DFn, Dfd	2.609, 56, 32
22	P value	0.0045
23	P value summary	**
24	Are variances significantly diff	Yes

Table 3S. Statistical analysis (t test) of scattered Aβ1-42 vs Aβ1-42-tetracycline, time zero

	Parameter	A Value
		Y
1	Table Analyzed	Data 1
2	Column A	1-42 120hrs
3	vs	vs
4	Column B	1-42 120hrs tetra
5		
6	Unpaired t test	
7	P value	P<0.0001
8	P value summary	***
9	Are means signif. different? (P < 0.05)	Yes
10	One- or two-tailed P value?	Two-tailed
11	t, df	t=7.993 df=120
12		
13	How big is the difference?	
14	Mean ± SEM of column A	3.424 ± 0.3320 N=54
15	Mean ± SEM of column B	16.96 ± 1.484 N=68
16	Difference between means	-13.53 ± 1.693
17	95% confidence interval	-16.88 to -10.18
18	R squared	0.3475
19		
20	F test to compare variances	
21	F,DFn, Dfd	25.16, 67, 53
22	P value	P<0.0001
23	P value summary	***
24	Are variances significantly different?	Yes

Table 4S. Statistical analysis (t test) of scattered Aβ1-42 vs Aβ1-42-tetracycline, time 120 hours.

	Parameter	A Value Y
1	Table Analyzed	Data 1
2	Column A	1-40 120hrs
3	vs	vs
4	Column B	1-40 120hrs tetra
5		
6	Unpaired t test	
7	P value	P<0.0001
8	P value summary	***
9	Are means signif. different? (P < 0.05)	Yes
10	One- or two-tailed P value?	Two-tailed
11	t, df	t=8.714 df=100
12		
13	How big is the difference?	
14	Mean ± SEM of column A	0.3839 ± 0.02781 N=50
15	Mean ± SEM of column B	1.664 ± 0.1416 N=52
16	Difference between means	-1.280 ± 0.1470
17	95% confidence interval	-1.572 to -0.9885
18	R squared	0.4316
19		
20	F test to compare variances	
21	F,DFn, Dfd	26.94, 51, 49
22	P value	P<0.0001
23	P value summary	***
24	Are variances significantly different?	Yes

Table 5S. Statistical analysis (t test) of scattered Aβ1-40 vs Aβ1-40-tetracycline, time 120 hours.

S8 – Tetracycline - Thioflavin T competitive binding studies

trNOESY spectra confirmed tetracycline and ThT binding to Aβ1-40 and Aβ1-42, as deduced by compound cross-peak change of sign (trNOE) (**Figure 23S**).

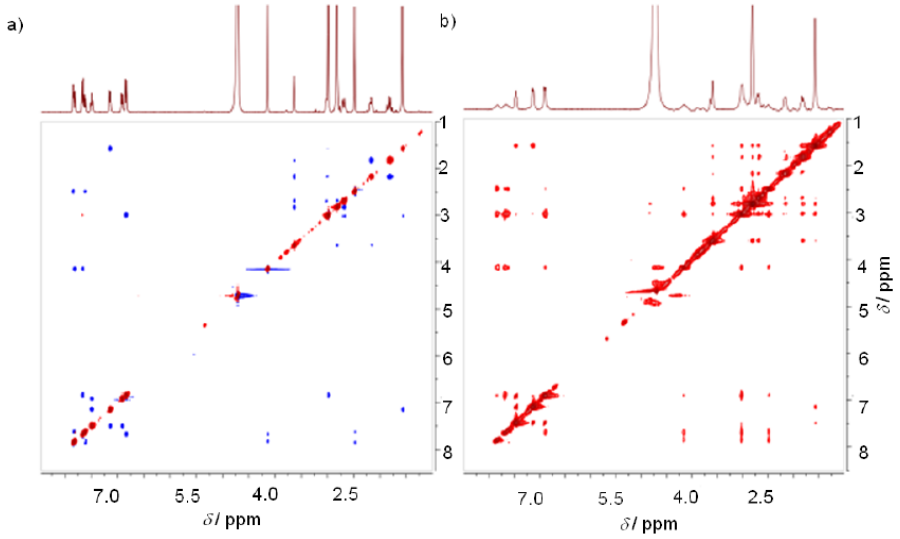

Figure 23S. NOESY spectrum of tetracycline:ThT mixture, at a 1:1 molar ratio, mix 800 ms (a), trNOESY of Aβ1-42:tetracycline:ThT mixture, at tetracycline:ThT 2:1 molar ratio, mix 250 ms b). Peptide:tetracycline at a 1:15 molar ratio. Samples were dissolved in PBS, pH 7.4 25°C.

S9 – FTIR spectra of Aβ peptides in presence of thioflavin T

The effect of ThT on the structural properties of Aβ1-40 and Aβ1-42 was examined by their infrared absorption in the Amide I region. The second derivative spectra of the peptides are reported in **Figure 24S** in presence and absence of ThT. The spectra are dominated by the two intermolecular β-sheet bands, which are signature of Aβ peptide oligomers (see Results and Discussion in the main text). In addition the spectra display a band around 1,605 cm^{-1} due to a ThT absorption, reported in the bottom of the figure. It can be seen that ThT does not induce appreciable differences in the intermolecular β-sheet bands of the two peptides, similarly to what observed for tetracycline. Moreover, the FTIR response of ThT around 1605 cm^{-1} is very similar in the absence and in the presence of Aβ oligomers, displaying only a minor downshift. It seems that this band is not very sensitive to the ThT interaction.

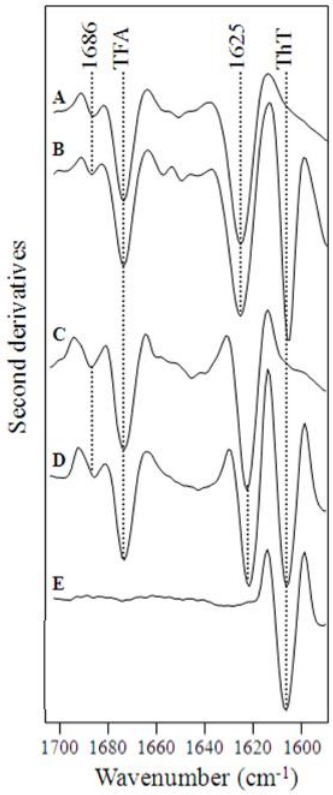

Figure 24S. FTIR second derivative spectra of Aβ peptides in presence of ThT. Spectra of Aβ1-42 (in D_2O PBS buffer, pH 7.4) in the absence (A) and in the presence (B) of ThT at a 1:4 molar ratio. Spectra of Aβ1-40 (in D_2O PBS, pH 7.4) in the absence (C) and in the presence (D) of ThT at a 1:4 molar ratio. The spectrum of free ThT in the same buffer is also reported

PAPER 2

*Journal of Biotechnology, **2011**, 56(4), 317–324.*

CURCUMIN DERIVATIVES AS NEW LIGANDS OF AB PEPTIDES

Cristina Airoldi[a], Cristiano Zona[a], Erika Sironi[a], Laura Colombo[b], Massimo Messa[b], Dario Aurilia[a] , Maria Gregori[c], Massimo Masserini[c], Mario Salmona[b], Francesco Nicotra[a], Barbara La Ferla[a]

[a]*Department of Biotechnology and Biosciences, University of Milano – Bicocca, Piazza della Scienza 2, 20126 Milano, Italy*
[b]*Department of Molecular Biochemistry and Pharmacology, Mario Negri Institute for Pharmacological Research, Via La Masa 19, 20156 Milan, Italy*
[c]*Department of Experimental Medicine, University of Milano – Bicocca, via Cadore 48, 20052 Monza, MB, Italy*

Abstract

Curcumin derivatives with high chemical stability, improved solubility and carrying a functionalized appendage for the linkage to other entities, have been synthesized in a straightforward manner. All compounds retained curcumin ability to bind Aβ peptide oligomers without inducing their aggregation. Moreover all curcumin derivatives were able to stain very efficiently Aβ deposits.

Introduction

Alzheimer's disease (AD) is the most common cause of dementia among neurodegenerative diseases in the elderly population.[1,2,3,4,5] The mechanisms

[1] Brookmeyer, R., Gray, S., Kawas, C., **1998**. Projections of Alzheimer's disease in the United States and the public health impact of delaying disease onset. American Journal of Public Health 88, 1337–1342.
[2] Brookmeyer, R., Corrada, M.M., Curriero, F.C., Kawas, C., **2002**. Survival following a diagnosis of Alzheimer disease. Archives of Neurology, 59, 1764–1767.
[3] Masters, C.L., Cappai, R., Barnham, K.J., Villemagne, V.L., **2006**. Molecular mechanisms for Alzheimer's disease: implications for neuroimaging and therapeutics. Journal of Neurochemistry 97, 1700–1725.
[4] Selkoe, D.J., **2001**. Clearing the brain's amyloid cobwebs. Neuron 32, 177–180.

underlying AD are not yet completely clear but genetic, pathological and biochemical clues suggest that the progressive production and subsequent accumulation of the β-amyloid peptides (Aβ) play a central role. Under abnormal conditions, the accumulation of Aβ progressively forms oligomeric, multimeric and fibrillar aggregates, triggering neurodegeneration. The aggregation and accumulation of Aβ culminates with the formation of extracellular plaques, one of the morphological hallmarks of the disease, detectable only postmortem in AD brains. Based on the conformation/oligomerization hypothesis, molecules able to stabilize the soluble Aβ conformation, to destabilize the altered amyloidogenic conformer, and to prevent the required conformational transition could be effective inhibitors of amyloid plaque formation and very potent drug candidates for AD treatment[6,7,8,9]. Among them is Curcumin (1,1-diferuloylmethane), a natural low molecular weight molecule with a wide variety of biological effects.[10,11,12] Curcumin is an active principle of the perennial herb Curcuma longa (commonly known as turmeric) which is used in the Indian traditional diet and as herbal medicine.[13,14] In 2001 Lim et al.[15] reported that Curcumin was able to block

[5] Sisodia, S.S., St George-Hyslop, P.H., **2002**. Gamma-secretase, notch, A beta and Alzheimer's disease: where do the presenilins fit in? Nature Reviews Neuroscience 3, 281–290.
[6] Bush, A.I., **2002**. Metal complexing agents as therapies for Alzheimer's disease. Neurobiology of Aging 23, 1031–1038.
[7] Pollack, S.J., Sadler, I.I.J., Hawtin, S.R., Tailor, V.J., Shearman, M.S., **1995**. Sulfonated dyes attenuate the toxic effects of β-amyloid in a structure-specific fashion. Neuroscience Letters 197, 211–214.
[8] Sabate, R., Estelrich, J., **2005**. Stimulatory and inhibitory effects of alkyl bromide surfactants on β-amyloid fibrillogenesis. Langmuir 21, 6944–6949.
[9] Taniguchi, S., Suzuki, N., Masuda, M., Hisanaga, S., Iwatsubo, T., Goedert, M., Hasegawa, M., **2005**. Inhibition of heparin-induced tau filament formation by phenothiazines, polyphenols, and porphyrins. Journal of Biological Chemistry 280, 7614–7623.
[10] Goel, A., Kunnumakkara, A.B., Aggarwal, B.B., **2008**. Curcumin as "Curecumin": from kitchen to clinic. Biochemical Pharmacology 75, 787–809.
[11] Thomas, T., Nadackal, T.G., Thomas, K., **2001**. Aspirin and non-steroidal antiinflammatory drugs inhibit amyloid-β aggregation. Neuroreport 12, 3263–3267.
[12] Zhao, B.L., Li, X.J., He, R.G., Cheng, S.J., Xin, W.J., **1989**. Scavenging effect of extracts of green tea and natural antioxidants on active oxygen radicals. Cell Biophysics 14, 175–185.
[13] Kelloff, G.J., Crowell, J.A., Hawk, E.T., Steele, V.E., Lubet, R.A., Boone, C.W., Covey, J.M., Doody, L.A., Omenn, G.S., Greenwald, P., Hong, W.K., Parkinson, D.R., Bagheri, D., Baxter, G.T., Blunden, M., Doeltz, M.K., Eisenhauer, K.M., Johnson, K., Knapp, G.G., Longfellow, D.G., Malone, W.F., Nayfield, S.G., Seifried, H.E., Swall, L.M., Sigman, C.C., **1996**. Strategy and planning for chemopreventive drug development: Clinical Development Plans II. Journal of Cellular Biochemistry, 54–71.

Alzheimer's disease pathogenesis at multiple sites of the inflammation cascade, but the direct effects of Curcumin on the formation and destabilization of Aβ fibrills remain unclear. Reinke and Gestwicki[16] studied the structure–activity relationships (SAR) of Aβ-aggregation inhibitors based on Curcumin, pointing out the predominant features affecting inhibition of amyloid aggregation: the coplanarity of the two aromatic rings and the distance between them (from 8 to 16 A˚). Accordingly, modifications that do not influence these parameters could improve Curcumin activity against Aβ toxicity. Narlawar et al.[17] replaced the 1,3-dicarbonyl moiety with isosteric heterocycles to minimize the metal chelation properties of Curcumin and to lock its conformation into an enol-type arrangement, important for its Aβ-binding capability.[18]

This modification provided active compounds at low micromolar concentrations. Based on these information, we synthesized a new series of compounds (**2-6 – Fig. 1**) replacing the 1,3-dicarbonyl moiety with differently functionalized isosteric pyrazole rings, in order to guarantee the coplanarity and to improve solubility and stability in physiological conditions. As a matter of fact, the main limitations in the use of natural Curcumin as drug are its total lack of solubility in physiological conditions and its high

[14] Lim, G.P., Chu, T., Yang, F.S., Beech, W., Frautschy, S.A., Cole, G.M., **2001**. The curry spice curcumin reduces oxidative damage and amyloid pathology in an Alzheimer transgenic mouse. Journal of Neuroscience 21, 8370–8377.

[15] Lim, G.P., Chu, T., Yang, F.S., Beech, W., Frautschy, S.A., Cole, G.M., (2001) The curry spice curcumin reduces oxidative damage and amyloid pathology in an Alzheimer transgenic mouse. Journal of Neuroscience 21, 8370-8377.

[16] Reinke, A.A., Gestwicki, J.E., **2007**. Structure–activity relationships of amyloid β- aggregation inhibitors based on curcumin: influence of linker length and flexibility. Chemical Biology and Drug Design 70, 206–215.

[17] Narlawar, R., Pickhardt, M., Leuchtenberger, S., Baumann, K., Krause, S., Dyrks, T., Weggen, S., Mandelkow, E., Schmidt, B., **2008**. Curcumin-derived pyrazoles and isoxazoles: Swiss army knives or blunt tools' for Alzheimer's disease? Chemmedchem, 3, 165–172.

[18] Yanagisawa, D., Shirai, N., Amatsubo, T., Taguchi, H., Hirao, K., Urushitani, M., Morikawa, S., Inubushi, T., Kato, M., Kato, F., Morino, K., Kimura, H., Nakano, I., Yoshida, C., Okada, T., Sano, M., Wada, Y., Wada, K., Yamamoto, A., Tooyama, I., **2010**. Relationship between the tautomeric structures of Curcumin derivatives and their Aβ -binding activities in the context of therapies for Alzheimer's disease. Biomaterials 31, 4179–4185.

instability.[19,20,21] These compounds were tested for their ability to interact with Aβ peptide oligomers and to stain amyloid deposits in Tg CRND8 mice.

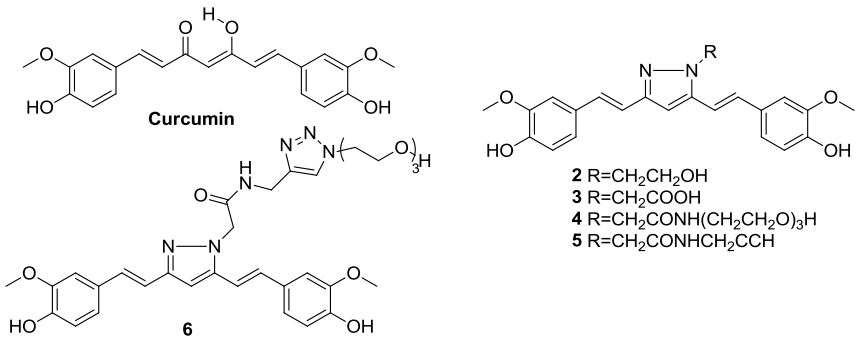

Fig. 1. Schematic representation of synthesised and tested Curcumin derivatives.

2. Materials and methods

2.1. Molecular mechanics (MM) and molecular dynamics (MD) calculations

Molecular mechanics and dynamics studies were conducted with MacroModel 9.8.207[22] as implemented in version 9.1.207 of the Maestro suite[23], using MM3* force field[24]. The starting coordinates for dynamics calculations were those obtained after energy minimization of the structures followed by conformational search. In particular, a systematic variation of the torsional degrees of freedom of the molecules

[19] Bernabe-Pineda, M., Ramirez-Silva, M.T., Romero-Romo, M., Gonzadlez-Vergara, E., Rojas-Hernandez, A., **2004**. Determination of acidity constants of curcumin in aqueous solution and apparent rate constant of its decomposition. Spectrochimica Acta Part A—Molecular and Biomolecular Spectroscopy 60, 1091–1097.
[20] Tonnesen, H.H., Karlsen, J., **1985**. Studies on Curcumin and curcuminoids. 6. Kinetics of curcumin degradation in aqueous-solution. Zeitschrift Fur Lebensmittel- Untersuchung Und-Forschung 180, 402–404
[21] Wang, Y.J., Pan, M.H., Cheng, A.L., Lin, L.I., Ho, Y.S., Hsieh, C.Y., Lin, J.K., **1997**. Stability of Curcumin in buffer solutions and characterization of its degradation products. Journal of Pharmaceutical and Biomedical Analysis 15, 1867–1876.
[22] MacroModel, **2008**, 9.6 ed. Schrodinger, LLC, New York.
[23] Maestro, **2010**, 9.1 ed. Schrodinger, LLC, New York.
[24] Allinger, N.L., Yuh, Y.H., Lii, J.H., **1989**. Molecular mechanics – the MM3 force-field for hydrocarbons. 1. Journal of the American Chemical Society 111, 8551–8566.

permitted different starting structures to be constructed that were further minimized to provide the corresponding local minima. For each compound the conformer with the lowest energy was considered. Simulations were carried out over 5 ns at 310 K with a 0.25 fs time step and a 20 ps equilibration step; 100 structures were sampled and minimized for further analysis. The continuum GB/SA solvent model[25] was employed and the general PRCG (Polak–Ribiere Conjugate Gradient) method for energy minimization was used. An extended cut-off was applied and the SHAKE procedure for bonds was not selected.

2.2. Synthetic procedures

2.2.1. General comments

All commercial chemicals were purchased from Sigma–Aldrich. All chemicals were used without further purification, while all required anhydrous solvents were dried with molecular sieves, for at least 24 h prior to use. Rhodamine B alcohol was synthesized as described elsewhere. Thin layer chromatography (TLC) was performed on silica gel 60 F254 plates (Merck) with detection using UV light when possible, or by charring with a solution of $(NH_4)_6Mo_7O_{24}$ (21 g), $Ce(SO_4)_2$ (1 g), concentrated H_2SO_4 (31 mL) in water (500 mL) or with an ethanol solution of ninhydrin or with Dragendorff' spray reagent[26]. Flash column chromatography was performed on silica gel 230–400 mesh (Merck). ^{1}H and ^{13}C NMR spectra were recorded at 25 ◦C unless otherwise stated, with a Varian Mercury 400 MHz instrument. Chemical shift assignments, reported in ppm, are referenced to the corresponding solvent peaks. MS were recorded on a QTRAP system with ESI source while HRMS were registered on a QSTAR elite system with a nanospray ion source.

[25] Still, W.C., Tempczyk, A., Hawley, R.C., Hendrickson, T., **1990**. Semianalutical treatment of solvation for molecular mechanics and dynamics. Journal of the American Chemical Society 112, 6127–6129.
[26] Thoma, K., Rombach, R., Ullmann, E., **1964**. Thin-layer chromatographic differentiation of homologous polyethileneglycols. Scientia Pharmaceutica 32, 216–224.

2.2.2. Typical reaction conditions

(E) Ethyl 2-[3,5-bis(4-hydroxy-3-methoxystyryl)-1H-pyrazol-1-yl]acetate (1): to a solution of Curcumin (1.00 g, 2.7 mmol, 1 equiv.) in Toluene dry (28 mL) ethyl 2-hydrazinylacetate hydrochloride (0.84 g, 5.4 mmol, 2 equiv.), triethylamine (0.75 mL, 5.4 mmol, 2 equiv.) and TFA (0.1 mL, 1.3 mmol, 0.5 equiv.) were added and the reaction was held at reflux for 2.5 h. The reaction mixture was then cooled to room temperature, diluted with CH_2Cl_2 and washed with HCl 5%(aq) twice. The organic phase was dried with Na_2SO_4 and evaporated in vacuum to afford the crude product which was further purified by flash column chromatography (CH_2Cl_2/isopropanol = 8/2) to afford the desired product as yellow solid (1.06 g, 87%). ^{1}H NMR (400 MHz, DMSO d_6) δ ppm 7.22–6.70 (m, 11H, CH Ar and conjugated double bond), 5.16 (s, 2H CH_2CO), 4.13 (q, J = 7.05 Hz, 2H, OCH_2CH_3), 3.82–3.77 (m, 6H, OCH_3), 1.19 (t, J = 7.12 Hz, 3H, OCH_2CH_3). ^{13}C NMR (100 MHz, DMSO d_6) δ 168.32 (CO), 150.02, 147.86, 147.27, 146.68, 143.35 (5 CqAr), 132.25, 129.79 (2 CHAr), 128.49, 128.06 (2 CqAr), 120.81, 120.01, 117.75, 115.57, 111.66, 110.24, 109.58, 98.63 (8 CHAr and conjugated double bond), 61.11 (CH_2), 55.76, 55.59 (2 CH_3), 50.30 (CH_2), 14.09 (CH_3). MS (ESI) calcd. for [M+H]+ 451.48; found [M+H]+ 451.60.

(E,E)4,4'-*{*[1-(2-Hydroxyethyl)-1H-pyrazole-3,5-diyl]bis(ethene-2,1-diyl)*}*bis(2-methoxy-phenol) (2): to a solution of **1** (0.605 g, 1.34 mmol, 1 equiv.) in THF dry (20 mL) at 0 ◦C, a 1 M solution of $LiAlH_4$ in THF (5.4 mL, 5.4 mmol, 4 equiv.) was added dropwise. The temperature was raised to r.t. and the reaction was monitored by TLC. After the disappearance of the starting material the reaction mixture was cooled to 0 ◦C and the following solutions were added in the order indicated: H_2O (0.21 mL), NaOH (aq) 4 M (0.26 mL), H_2O (0.65 mL), Na_2SO_4 (1.52 g). The reaction mixture was then filtrated and the solvent was evaporated in vacuum. The crude product was further purified by flash column chromatography (CH_2Cl_2/EtOH=8/2) to afford the final product as a bright yellow amorphous powder (0.38 g, 70%). The ^{1}H NMR and ^{13}C NMR agree with the

characterization reported by Narlawar et al.[27] ^{1}H NMR (400 MHz, $CDCl_3$) δ ppm 7.08–6.62 (m, 11H, CH Ar and conjugated double bond), 4.28 (t, J = 6.0 Hz, 2H NCH_2CH_2OH), 3.98–3.91 (m, 6H, OCH_3), 3.65 (t, J = 6.0 Hz, 2H NCH_2CH_2OH). ^{13}C NMR (100 MHz, $CDCl_3$) δ ppm 150.013, 147.79, 147.31, 146.65, 143.53 (5 CqAr), 132.19, 129.76 (2 CHAr), 128.52, 128.13 (2 CqAr), 120.75, 120.22, 117.43, 115.72, 111.50, 110.32, 109.43, 98.72 (8 CHAr and conjugated double bond), 62.32 (CH_2), 56.43, 56.22 (2 CH_3), 51.30 (CH_2). MS (ESI) calcd. For [M+H]+ 409.48; found [M+H]+ 409.30.

(E) 2-[3,5-bis(4-Hydroxy-3-methoxystyryl)-1H-pyrazol-1-yl]acetic acid (3): compound **1** (3.00 g, 6.66 mmol, 1 equiv.) was dissolved in a methanolic solution of KOH 1.8 M (70 mL). The solution was left under magnetic stirring at r.t. over night. The solvent was evaporated in vacuum and purified by flash column chromatography (eluent AcOEt/MeOH gradient from 9/1 to 7/3) to afford the final product (2.81 g, quant.). ^{1}H NMR (400 MHz, CD3OD) δ ppm 7.23–6.72 (m, 11H, CH Ar and conjugated double bond), 4.93 (s, 2H, CH_2CO), 3.85–3.79 (m, 6H, OCH_3). ^{13}C NMR (100 MHz, DMSO) δ ppm 170.17 (CO), 147.85, 147.16, 146.58, 142.80 (4 CqAr), 131.54, 129.13 (2 CHAr), 128.62, 128.17 (2 CqAr), 120.61, 119.87, 118.08, 115.58, 112.31, 110.08, 109.53, 98.38 (8 CHAr and conjugated double bond), 55.74, 55.58 (2 CH_3), 51.58 (CH_2). MS (ESI) calcd. for [M+H]+ 423.43; found [M+H]+ 423.4.

(E)2-[3,5-bis(4-Hydroxy-3-methoxystyryl)-1H-pyrazol-1-yl]-N-(prop-2-yn-1yl) aceta mide (4): HOBt (17 mg, 0.12 mmol, 1.2 equiv.) and TBTU (39 mg, 0.12 mmol, 1.2 equiv.) were added to a solution of the compound **3** (42 mg, 0.1 mmol, 1 equiv.) in DMF dry (1 mL). The reaction mixture was left in the dark, at r.t., under magnetic stirring for 15 min. Propargylamine (13 µL, 0.2 mmol, 2 equiv.) and triethylamine (7 µL, 0.5 mmol, 5 equiv.) were added and the reaction was left in the dark, at r.t., under magnetic stirring overnight. Then the solvent was evaporated in vacuum, the crude product was diluted with CH_2Cl_2 and washed three times with water. The organic phase was dried with

[27] Narlawar, R., Pickhardt, M., Leuchtenberger, S., Baumann, K., Krause, S., Dyrks, T., Weggen, S., Mandelkow, E., Schmidt, B., **2008**. Curcumin-derived pyrazoles and isoxazoles: Swiss army knives or blunt

Na_2SO_4 and concentrated to afford the crude product which was further purified by flash column chromatography (eluent petroleum ether/AcOEt gradient from 3/7 to 0/10) to afford the desired product as a powder (31 mg, 68%). ^{1}H NMR (400 MHz, CD_3OD) δ ppm 7.38–6.73 (m, 11H, CH Ar and conjugated double bond), 5.12 (s, 2H CH_2CO), 4.04 (s, 2H, CH_2NH), 3.96–3.83 (m, 6H, OCH_3), 2.63 (s, 1H, CH). ^{13}C (100 MHz, CDCl3) δ ppm 169.31 (CO) 152.55, 149.33, 148.03, 145.63 (4Cq Ar), 135.08, 132.22 (2 CHAr), 130.75, 130.13 (2 CqAr), 122.07, 121.40, 118.27, 116.46, 112.40, 111.08, 110.70, 100.52 (8 CHAr and conjugated double bond), 80.27 (Cq), 72.42 (CH), 56.64, 56.55 (2 CH_3), 52.66 (CH_2), 29.71 (CH_2). MS (ESI) calcd. for [M+H]+ 456.49; found [M+H]+ 460.4.

(E) 2-[3,5-bis(4-Hydroxy-3-methoxystyryl)-1H-pyrazol-1-yl]-N-*{*2-[2-(2-hydroxyethoxy) ethoxy]ethyl*}* acetamide (5): HOBt (40 mg, 0.29 mmol, 1.2 equiv.) and TBTU (91 mg, 0.29 mmol, 1.2 equiv.) were added to a solution of compound **3** (100 mg, 0.24 mmol, 1 equiv.) in DMF dry (1.0 mL). The reaction mixture was left in the dark, at r.t., under magnetic stirring for 15 min. 2-(2-(2- Aminoethoxy)ethoxy)ethanol **9** (71 mg, 0.47 mmol, 2 equiv.) and triethylamine (0.2 mL, 1.44 mmol, 6 equiv.) were dissolved in DMF dry (0.5 mL) and the solution was added to the reaction, which was then left in the dark, at r.t., under magnetic stirring over night. The solvent was evaporated in vacuum and the crude product was purified by flash column chromatography (eluent petroleum ether/AcOEt gradient from 1/4 to AcOEt/EtOH 9/1) to afford the desired product (48 mg, 37%). ^{1}H NMR (600 MHz, D_2O) δ ppm 7.27–7.07 (m, 6H CH Ar and conjugated double bond), 6.96–6.90 (m, 3H CH Ar and conjugated double bond), 6.85–6.78 (m, 2H CH Ar and conjugated double bond), 3.93–3.87 (m, 6H, OCH_3), 3.61–3.58 (m, 2H, CH_2CH_2OH), 3.57–3.53 (m, 2H, OCH_2CH_2OH), 3.52–3.49 (m, 2H, OCH_2CH_2N), 3.46–3.40 (m, 6H, CH_2O, OCH_2CH_2N). ^{13}C NMR (100 MHz, MeOD) δ 169.70 (CO), 149.22, 148.52, 147.88, 145.58, 142.70 (5 CqAr), 134.99, 132.18 (2 CHAr), 130.53, 129.97 (2 CqAr), 121.99, 121.32, 118.07, 116.34, 112.22, 110.73, 110.28, 100.26 (8 CHAr and conjugated

tools' for Alzheimer's disease? Chemmedchem 3, 165–172.

double bond), 73.44, 71.31, 71.20, 70.47, 70.37 (5 CH_2), 56.45, 56.35 (2 CH_3), 52.62, 40.39 (2 CH_2). MS (ESI) calcd. for [M+H]+ 554.60; found [M+H]+ 554.70.

(E) 2- [3,5 – bis (4-Hydroxy-3-methoxystyryl)-^{1}H-pyrazol-1-yl]-N-*{*[1- (2 - (2 -(2 -ydroxy ethoxy) ethoxy)ethyl)-1H-1,2,3-triazol- 4-yl]methyl*}*acetamide (6): $CuSO_4 \cdot 5H_2O$ (57 mg, 0.23 mmol, 1.2 equiv.) was dissolved in water (2 mL) and sodium ascorbate (57 mg, 0.29 mmol, 1.5 equiv.) was added. The reaction was stirred until the formation of an orange suspension. This freshly prepared catalyst was added to a solution of compound **4** (86 mg, 0.2 mmol, 1 equiv.) and 2-[2-(2 azidoethoxy)ethoxy] ethanol **8**[[28]](252 mg, 0.9 mmol, 1.2 equiv.) in THF (12 mL), stirring at r.t. until the formation of a light blue precipitate, which was removed by filtration. The crude product was purified by flash column chromatography (eluent gradient from AcOEt to AcOEt/MeOH 9/1) to afford the desired product (103 mg, 72%). ^{1}H NMR (400 MHz, CD_3OD) δ ppm 7.83 (s, 1H, H triazole), 7.16–6.72 (m, 11H CH Ar and conjugated double bond), 4.97 (s, 2H, CH_2CO), 4.47 (s, 2H, $NHCH_2$), 4.38 (t, J = 4.99 Hz, 2H, NCH_2CH_2O), 3.91–3.86 (m, 6H, OCH_3), 3.75 (t, J = 4.93, 2H, NCH_2CH_2O), 3.64–3.57 (m, 2H, OCH_2CH_2OH), 3.55–3.49 (m, 4H, OCH_2CH_2OH, OCH_2CH_2O), 3.48–3.43 (m, 2H, CH_2O). ^{13}C NMR (100 MHz, MeOD) δ 169.65 (CO), 152.46, 149.30, 149.23, 147.98, 145.81, 145.55 (6 CqAr), 134.92, 132.19 (2 CHAr), 130.59, 129.96 (2 CqAr), 125.11, 122.03, 121.35, 118.14, 116.36, 112.28, 110.71, 110.35, 100.33 (9 CHAr and conjugated double bond), 73.62, 71.39, 71.34, 70.22, 62.20 (5 CH_2), 56.49, 56.39 (2 CH_3), 51.28, 35.78 (2 CH_2). MS (ESI) calcd. For [M+H]+ 635.28; found [M+H]+ 635.5.

2-[2-(2-Aminoethoxy) ethoxy]ethanol: 2-[2-(2- azidoethoxy)ethoxy]ethanol (200 mg, 1.14 mmol, 1 equiv.) was dissolved in methanol and Pd Lindlar on charcoal was added to the solution. The black suspension was stirred under hydrogen atmosphere over night at r.t. The resulting mixture was filtered through a nylon membrane filter 0.45 µm to obtain the analytically pure 2-[2-(2 aminoethoxy) ethoxy]ethanol in a quantitative

[[28]] Schneekloth, A.R., Pucheault, M., Tae, H.S., Crews, C.M., **2008**. Targeted intracellular protein degradation induced by a small molecule: en route to chemical proteomics. Bioorganic & Medicinal Chemistry Letters 18, 5904–5908

yield. The ^{1}H NMR and ^{13}C NMR agree with the characterization reported by Sato et al.[29]

2.3. Peptide synthesis and purification

Aβ1–40, and Aβ1–42 were prepared by solid-phase peptide synthesis on a 433A synthesizer (Applied Biosystems) using Fmoc protected L-amino acid derivatives, NOVASYN-TGA resin on a 0.1 mM scale.[30] Peptides were cleaved from the resin as previously described[31] and purified by reverse phase HPLC on a semi-preparative C4 column (Waters) using water:acetonitrile gradient elution. Peptide identity was confirmed by MALDI-TOF analysis (model Reflex III, Bruker). Peptide purity was always above 95%.

2.4. NMR spectroscopy binding studies

NMR experiments were recorded on a Bruker 600-MHz Advance equipped with a Bruker CryoProbe and a z-axis gradient coil and on a Varian 400-MHz Mercury. A batch of Aβ1–42 was selected that contained pre-amyloidogenic seeds highly toxic to N2a cells. Immediately before use, lyophilized Aβ1–42 was dissolved in 10 mM NaOD in D_2O at a concentration of 160 μM, then diluted 1:1 with 10 mM phosphate buffer saline, pH 7.4 containing 100 mM NaCl (PBS) and one of the tested compounds. Compounds **2**–**6** were dissolved in 10 mM NaOD in D_2O and then diluited in PBS, pH 7.4, sonicated for 1 h and added to the peptide solution. The pH of each sample was verified with a Microelectrode (Mettler Toledo) for 5 mm NMR tubes and adjusted with NaOD or DCl.

---

[29] Sato, H., Hayashi, E., Yamada, N., Yatagai, M., Takahara, Y., **2001**. Further studies on the site-specific protein modification by microbial transglutaminase. Bioconjugate Chemistry 12, 701–710.

[30] Di Fede, G., Catania, M., Morbin, M., Rossi, G., Suardi, S., Mazzoleni, G., Merlin, M., Giovagnoli, A.R., Prioni, S., Erbetta, A., Falcone, C., Gobbi, M., Colombo, L., Bastone, A., Beeg, M., Manzoni, C., Francescucci, B., Spagnoli, A., Cantu, L., Del Favero, E., Levy, E., Salmona, M., Tagliavini, F., **2009**. A recessive mutation in the APP gene with dominant-negative effect on amyloidogenesis. Science 323, 1473–1477

[31] Salmona, M., Morbin, M., Massignan, T., Colombo, L., Mazzoleni, G., Capobianco, R., Diomede, L., Thaler, F., Mollica, L., Musco, G., Kourie, J.J., Bugiani, O., Sharma, D., Inouye, H., Kirschner, D.A., Forloni, G., Tagliavini, F., **2003**. Structural properties of Gerstmann–Straussler–Scheinker disease amyloid protein. Journal of Biological Chemistry 278, 48146–48153.

All pH values were corrected for isotope effect. Basic sequences were employed for 2D-TOCSY, 2D-NOESY and STD experiments. For STD, a train of Gaussian-shaped pulses each of 50 ms was employed to saturate selectively the protein envelope; the total saturation time of the protein envelope was adjusted by the number of shaped pulses and was varied between 3 s and 0.3 s.

2.5. Sections staining

Brains from Tg CRND8 mice encoding a double mutant form of amyloid precursor protein 695 (KM670/671NL+V717F) under the control of the PrP gene promoter[32] were dissected and immediately frozen at −80 ◦C until use. To investigate the binding of the compounds to amyloid plaques, cryostatic 20 µm sections obtained from fresh tissue and mounted on gelatin coated microscope slides were covered with a solution of EtOH:water 50:50 (v/v) containing the different test compounds. After 30 min of incubation the sections were washed two times with PBS 10 mM. Thereafter, the sections were incubated sequentially in EtOH 70%, EtOH 96% and xylene before the application of the coverslip. Samples were observed with an Olympus BX51 microscope with filter UV(Ex 330–385 nm/Em >420) and FITC (Ex 450–480 nm/Em >515); pictures were obtained with an Olympus Camedia C-5060 Digital Compact Camera in wide field and fluorescent observation. Thioflavin T staining (6 µM) was used as reference compound.[33]

[32] Chishti, M.A., Yang, D.S., Janus, C., Phinney, A.L., Horne, P., Pearson, J., Strome, R., Zuker, N., Loukides, J., French, J., Turner, S., Lozza, G., Grilli, M., Kunicki, S., Morissette, C., Paquette, J., Gervais, F., Bergeron, C., Fraser, P.E., Carlson, G.A., St George-Hyslop, P., Westaway, D., **2001**. Early-onset amyloid deposition and cognitive deficits in transgenic mice expressing a double mutant form of amyloid precursor protein 695. Journal of Biological Chemistry 276, 21562–21570.

[33] Giaccone, G., Morbin, M., Moda, F., Botta, M., Mazzoleni, G., Uggetti, A., Catania, M., Moro, M.L., Redaelli, V., Spagnoli, A., Rossi, R.S., Salmona, M., Di Fede, G., Tagliavini, F., **2010**. Neuropathology of the recessive A673V APP mutation: Alzheimer disease with distinctive features. Acta Neuropathologica 120, 803–812.

3. Results

3.1. Molecular mechanics (MM) and molecular dynamics (MD) calculations

The major aim of the molecular mechanics and dynamics calculations was to provide 3D models suitable to support the coplanarity of the two aromatic rings in compounds **2**–**6**. To this purpose, we calculated the more stable conformation for Curcumin keto form, Curcumin enol form and compound **3**, as representative of our small library of Curcumin derivatives, by MM and MD simulations. Calculations were performed by using MM3* force field, as implemented in the MacroModel program (Maestro Suite). After a first run of minimization, a conformational search was performed for each molecule. The conformation with the lowest energy was selected, minimized and submitted to MD simulation. 100 structures were sampled and further minimized. **Fig. 2** reports the conformation with lowest energy found for the three compounds.

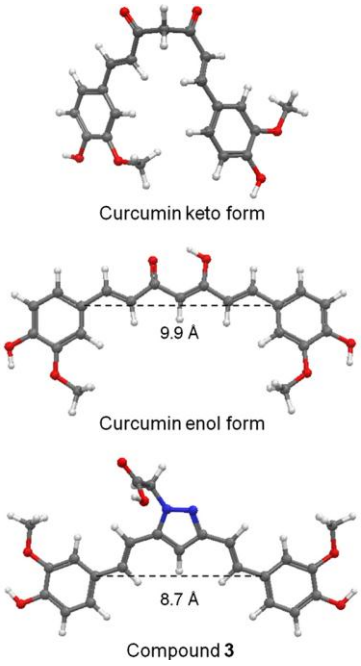

Fig. 2. Structures obtained for Curcumin keto form, Curcumin enol form and compound **3** by MM and MD simulations. For each compound, the conformation with the lowest energy is depicted.

For Curcumin enol form and compound **3** the distances between the two aromatic ring are reported.

Results obtained are in agreement with what expected. In contrast to the Curcumin keto form, compound **3** presents a conformation very similar to that showed by the Curcumin enol form, with the aromatic rings lying on the same plane. The distance between the two aromatic entities is less in this molecule if compared with the Curcumin enol form, 8.7 ˚A and 9.9 ˚A respectively. Nevertheless, its value fits within the range calculated by Reinke and Gestwicki[34] according to which this distance has to be more than 8 ˚A but less than 16 ˚A to allow an effective interaction with Aβ peptides. Hence, computational data confirmed the possibility of substituting Curcumin keto-enol moiety with a pyrazole ring, ensuring that this modification does not influence structural features fundamental for Curcumin derivative binding to Aβ peptides.

3.2. Synthesis

In order to generate the small library of Curcumin derivatives in a straightforward manner we first synthesised pyrazole derivative **1** which was converted to all other derivatives (**Fig.3**). Treatment of Curcumin with ethyl 2-hydrazinylacetate hydrochloride in refluxing toluene afforded compound **1** in good yield (87%). Reduction of **1** with $LiAlH_4$ afforded product **2** in a 70% yield. Carboxylic acid **3** was obtained, in a quantitative yield, from compound **1** by basic hydrolysis of the ethyl ester. Derivatives **4** and **5** were obtained from **3** through the coupling respectively with propargyl amine and 2-[2-(2-aminoethoxy)ethoxy]ethanol in the presence of the coupling agents hydroxybenzotriazole (HOBt) and O-(benzotriazol-1-yl)- N,N,N',N'- tetramethyluronium tetrafluoroborate (TBTU) in 68% and 37% yield. Finally, Cu(I) catalysed chemoselective

[34] Reinke, A.A., Gestwicki, J.E., **2007**. Structure–activity relationships of amyloid β- aggregation inhibitors based on curcumin: influence of linker length and flexibility. Chemical Biology and Drug Design 70, 206–215.

reaction of alkyne **4** with 2-[2-(2-azidoethoxy)ethoxy]ethanol, afforded final compound **6** in 72% yield.

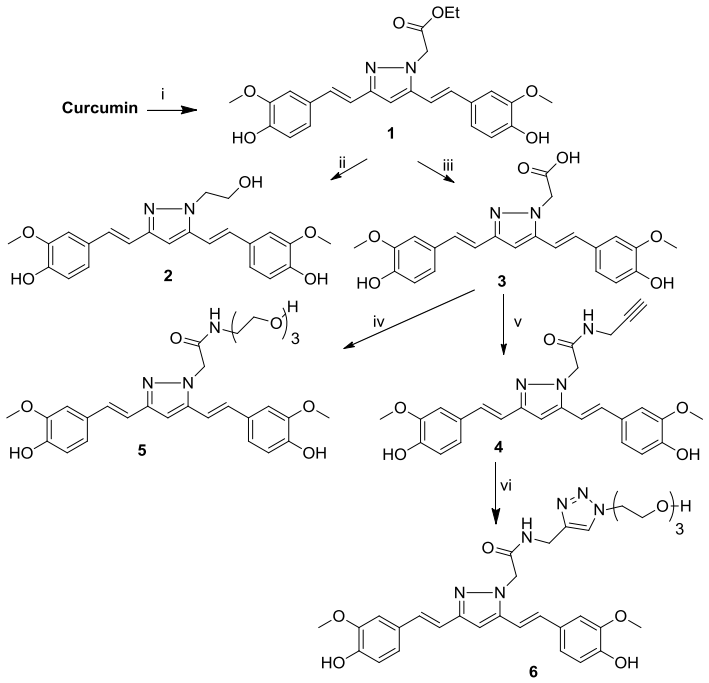

Fig. 3. Reagents and conditions: (i) ethyl 2-hydrazinylacetate hydrochloride, TEA, TFA, reflux, 2.5 h, 87%; (ii) THF, $LiAlH_4$, 0 ◦C →R.T., 70%; (iii) KOH, MeOH, r.t., 12 h, quant.; (iv) HOBt, TBTU, DMF, r.t., 15 min, then 2-(2-(2-aminoethoxy)ethoxy) ethanol, TEA, R.T., 12 h, 37%; (v) HOBt, TBTU, DMF, r.t., 15 min, then propargylamine, TEA, r.t., 12 h, 68%; (vi) $CuSO_4 \cdot 5H_2O$, sodium ascorbate, 1.5, water/THF, 2-(2-(2 azidoethoxy) ethoxy) ethanol, r.t. 72%.

3.3. Compound solubility in water

As previously reported,[[35]] Curcumin is completely insoluble in water at neutral pH. The chemical functionalizations introduced in our molecules improved significantly their solubility, that, in particular, was tested in PBS, pH 7.4, 25 ◦C. Values obtained are

[[35]] Kaewnopparat, N., Kaewnopparat, S., Jangwang, A., Maneenaun, D., Chuchome, T., Panichayapakaranant, P., **2009**. Increased solubility, dissolution and physicochemical studies of Curcumin-polyvinylpyrrolidone K-30 solid dispersions. World Academy of Science, Engineering and Technology 55, 229–234.

reported in **Table 1**. In these conditions, compounds **2–6** result perfectly soluble in the millimolar range of concentration.

Compound	Solubility (mg/ml)	Solubility (mM)
Curcumin	Insoluble[35]	Insoluble[35]
2	1.5	3.5
3	3.0	7.0
4	0.5	1.0
5	0.5	1.0
6	0.9	1.7

Table 1. Solubility of Curcumin and compounds **2–6** in PBS, pH 7.4, 25 ◦C.

3.4. NMR binding studies

Compounds **2–6** were tested for their ability to bind Aβ1–42 peptide by exploiting saturation transfer difference (STD) NMR and tr-NOESY experiments. STD has been extensively used as a comprehensive and efficient method to investigate protein and peptide–ligand interactions.[36,37,38] Very recently, we employed STD-NMR experiments in order to characterize tetracycline and thioflavin T interaction with Aβ1–40 and Aβ1–42 peptides.[39] The same methodology has been applied here in order to check the effect of Curcumin derivatives chemical functionalization on Aβ1–42 oligomer recognition and binding processes. As a matter of fact, aggregated Aβ species, in particular the oligomeric assembly intermediates, are believed to trigger a cascade of events that leads to the formation of neurofibrillary tangles and disruption of the

[36] Berteau, O., Sandstrom, C., Bielicki, J., Anson, D.S., Kenne, L., **2003**. Glycosidase–substrate interactions analysis by STD-NMR spectroscopy: study of alpha-l-fucosidase. Journal of the American Chemical Society 125, 15296–15297.
[37] Biet, T., Peters, T., **2001**. Molecular recognition of UDP-Gal by beta-1,4- galactosyltransferase T1. Angewandte Chemie – International Edition 40, 4189–4192.
[38] Meyer, B., Peters, T., **2003**. NMR spectroscopy techniques for screening and identifying ligand binding to protein receptors. Angewandte Chemie – International Edition 42, 864–890.
[39] Airoldi, C., Colombo, L., Manzoni, C., Sironi, E., Natalello, A., Doglia, S.M., Forloni, G., Tagliavini, F., Del Favero, E., Cantu, L., Nicotra, F., Salmona, M., **2011**. Tetracycline prevents Aβ oligomer toxicity through an atypical supramolecular interaction. Organic & Biomolecular Chemistry 9, 463–472.

neuronal cytoskeleton, widespread synaptic loss and neurodegeneration.[40] The binding studies were performed on mixtures containing a batch of Aβ1–42 enriched in oligomers and compounds **2**–**5** or **6** at the final concentration of 80 μM and 0.5 mM respectively. Our data demonstrated that all molecules retain Curcumin ability to bind peptide oligomers. In all cases, after selective irradiation of the peptide resonances at −1.0 ppm, some compound signals appeared in the STD spectra, indicating the existence of magnetization transfer from the oligomers to the drug. STD spectra recorded on a Aβ1–42 – compound **3** mixture at six different saturation times of the peptide envelope are reported in **Fig. 4** as an example.

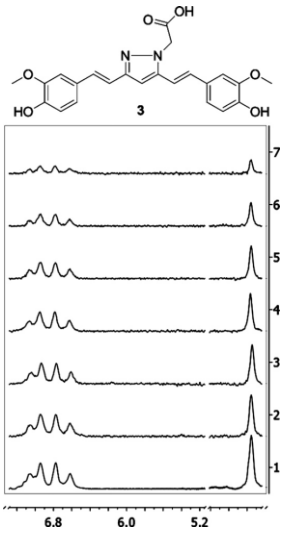

Fig. 4. (1) ^{1}H-NMR spectrum of Aβ1–42 – compound **3** mixture, at a 1:7 molar ratio, NS = 64. (2–7) STD spectra of the mixture recorded at different peptide saturation times (2, 3 s; 3, 2 s; 4, 1.5 s; 5, 1 s; 6, 0.6 s; 7, 0.3 s). NS = 128, on-resonance frequency = −1.0 ppm, off-resonance frequency = 40 ppm. All spectra were recorded on the same sample; sample was dissolved in PBS, pH 7.4, at 37 ◦C.

A detailed ligand-epitope mapping revealed that the “Curcumin moiety”, constituted by the aromatic system (the two rings and the conjugates double-bonds), is always

[40] Cardoso, I., Merlini, G., Saraiva, M.J., **2003**. 4-iodo-4-Deoxydoxorubicin and tetracyclines disrupt transthyretin amyloid fibrils in vitro producing noncytotoxic species: screening for TTR fibril disrupters. Faseb Journal 17, 803–809.

implicated in the binding. On the other hand, the different chains present on the pyrazole ring do not contribute to the interaction, being the corresponding signals absent in STD spectra. An additional evidence of Curcumin derivative binding to Aβ oligomers was obtained by tr-NOESY experiments (**Fig.5**). The change in Curcumin derivative cross-peak sign, from positive (blue color), in the absence of Aβ peptides, to negative (red color) in presence of Aβ peptides, reflects a change in our compound correlation time, due to the binding to a bigger entity,[41] represented by Aβ oligomers.

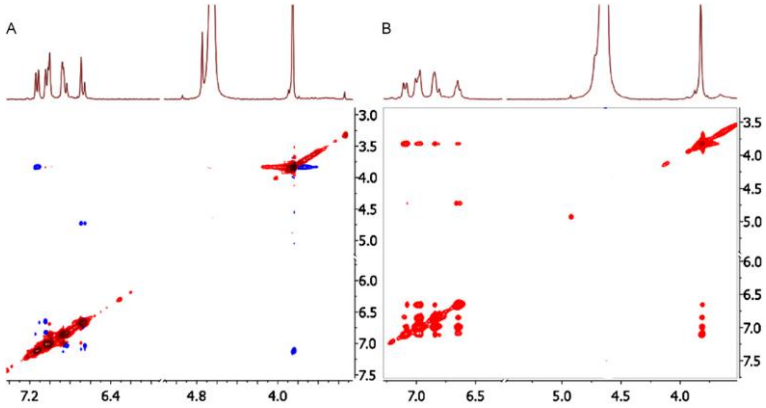

Fig. 5. 2DNOESY spectra of compound **3** in the absence (A, mixing time 600 ms) or presence (B, mixing time 200 ms) of Aβ1–42. Peptide:drug at 1:12.5 molar ratio. Samples were dissolved in PBS, pH 7.4 at 37 ◦C.

3.5. Staining of amyloid deposits in Tg CRND8 mice

The ability of the synthesized compounds to bind amyloid deposits was tested in brain sections from Tg CRND8 mice. These animals carry a human APP with double mutations and accumulate Aβ deposits in brain parenchyma and at cerebrovascular level. Cryostatic sections of 20 µm were obtained from fresh tissue, mounted on gelatin coated microscope slides and used for a staining assay. Solutions of EtOH:water 50:50 (v/v) of test compounds were layered on tissue sections (the concentrations used were

[41] Meyer, B., Peters, T., **2003**. NMR spectroscopy techniques for screening and identifying ligand binding to protein receptors. Angewandte Chemie - International Edition 42, 864–890.

different depending on the ability of compound to label amyloidogenic deposits). Fluorescent sections were viewed using fluoromicroscope equipped with UV and FITC filters. Thioflavin T (ThT) at 3 µM was used as a reference. All test compounds were able to label amyloid plaques and vascular walls at a concentration of 6 µM, but **6** and **4** were used at final concentration of 12 and 18 µM, respectively, to obtain signals comparable to Thioflavin T staining. These results suggested that tested compounds are able to recognize the β-pleated sheet structure of amyloid fibrils similarly to ThT and without being involved in aspecific binding to tissue preparations (**Fig. 6**).

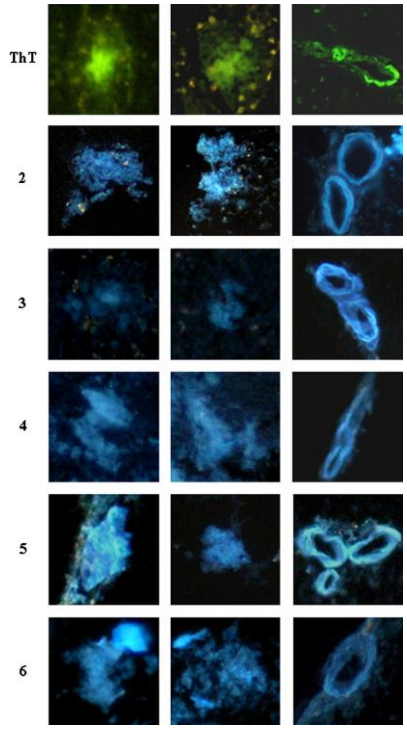

Fig. 6. Staining of amyloid deposits in brain sections of Tg CRND8 mice: plaques and vascular walls stained with ThT, 2, 3, 4, 5 and 6. Fluorescent sections were viewed using fluorescence microscopy FITC for ThT and UV for Curcumin-derived compounds.

4. Discussion

Curcumin derivatives were synthesized in order to avoid the disadvantages of Curcumin itself, in particular those regarding its solubility and its stability in aqueous media. All compounds present an improved solubility, showing a solubility higher than 1 mM in PBS, pH 7.4, that is significant, being Curcumin completely insoluble in water. This property is very important for drug administration, bioavailability and also assimilation. The second enhanced property of our synthetic derivatives consists in their very high chemical stability in all organic and water media, as demonstrated by NMR studies. The formation of the pyrazole moiety, as cited previously, locks the keto-enol tautomerism in an enol-type arrangement, important for its Aβ-binding capability,[42] and, at the same time, removes the chemically labile β-diketone moiety. NMR experiments carried out some hours after compound dissolution in PBS, pH 7.4, and incubation at 37 ◦C, afforded spectra identical to those recorded immediately after their dissolution (**Supplementary information – Fig. S1**). In contrast, Curcumin is described to undergo degradation few minutes after dissolution in PBS buffer; in particular, when Curcumin is incubated in 0.1 M PBS and serum-free medium, pH 7.2 at 37 ◦C, about 90% decomposed within 30 min.[43] We also demonstrated the ability of our compounds to interact with Aβ peptides. As previously reported, the blocked Curcumin enol-tautomer is implicated in Curcumin interaction with Aβ1–40 and Aβ1–42 oligomers[42]. We confirmed by MM and MD calculations that the introduction of a pyrazole ring allows our molecules to assume a conformation analogue to that showed by the Curcumin enol form, in which the aromatic rings are coplanar. Compounds **2**–**6** capability of binding Aβ peptide oligomers were demonstrated definitely by STD and tr-NOESY NMR

[42] Yanagisawa, D., Shirai, N., Amatsubo, T., Taguchi, H., Hirao, K., Urushitani, M., Morikawa, S., Inubushi, T., Kato, M., Kato, F., Morino, K., Kimura, H., Nakano, I., Yoshida, C., Okada, T., Sano, M., Wada, Y., Wada, K., Yamamoto, A., Tooyama, I., **2010**. Relationship between the tautomeric structures of Curcumin derivatives and their A β-binding activities in the context of therapies for Alzheimer's disease. Biomaterials 31, 4179–4185.

[43] Wang, Y.J., Pan, M.H., Cheng, A.L., Lin, L.I., Ho, Y.S., Hsieh, C.Y., Lin, J.K., **1997**. Stability of Curcumin in buffer solutions and characterization of its degradation products. Journal of Pharmaceutical and Biomedical Analysis 15, 1867–1876.

experiments. Moreover, working on samples of amyloid deposits in brain sections of Tg CRND8 mice, compounds ability to stain the Aβ plaque[44] in *ex vivo* models with high specificity and selectivity was also demonstrated. Since it is known that some compounds[45] with the ability to recognize Aβ peptides are also able to trigger their aggregation, we carried out experiments in order to verify that our compounds did not present the last feature. To achieve this task, congo red (CR) binding assay and AFM structural characterization of Aβ peptide in presence and absence of the synthesized compounds were performed. All these experiments indicated that none of the tested compounds induce peptide aggregation and that, indeed, some of them give a modest inhibition of Aβ fibril formation (**Supplementary information-Fig. S2 and S3**). This feature is relevant for the use of these Curcumin derivatives as potential AD diagnostic tools. In conclusion, the favorable physical–chemical properties of these compounds and the presence of a chemically functionalized appendage on the pyrazole moiety that allows their linkage to other entities, along with their ability to interact with Aβ peptides–oligomers and plaques suggest that these compounds could be very promising candidates for possible future applications both in the therapy and in the diagnosis of Aβ related disease.

Acknowledgments

The research leading to these results has received funding from the European Community's Seventh Framework Programme (FP7/2007–2013) under Grant Agreement No. 212043. We acknowledge the Italian Ministry of Health 25 (533F/Q/1), Cariplo Foundation (Project NOBEL-GUARD), Banca IntesaSanPaolo, and PRIN (PROT.

[44] Koronyo-Hamaoui, M., Koronyo, Y., Ljubimov, A.V., Miller, C.A., Ko, M.K., Black, K.L., Schwartz, M., Farkas, D.L., **2011**. Identification of amyloid plaques in retinas from Alzheimer's patients and noninvasive in vivo optical imaging of retinal plaques in a mouse model. NeuroImage 54, S204S217.

[45] Re, F., Airoldi, C., Zona, C., Masserini, M., La Ferla, B., Quattrocchi, N., Nicotra, F., **2010**. β-amyloid aggregation inhibitors: small molecules as candidate drugs for therapy of Alzheimer's disease. Current Medicinal Chemistry 17, 2990–3006.

2007T7MSAJ) for financial support and Flamma (Italy) for the kind gift of Fmoc-amino acids.

Supplementary Data

Curcumin derivative chemical stability

Curcumin derivative chemical stability was verified by ^{1}H-NMR spectroscopy. **Figure 1** reports ^{1}H-NMR spectra of compound **3** acquired immediately after dissolution in PBS (1), pH 7.4 and after 14 h (2). The two spectra are identical.

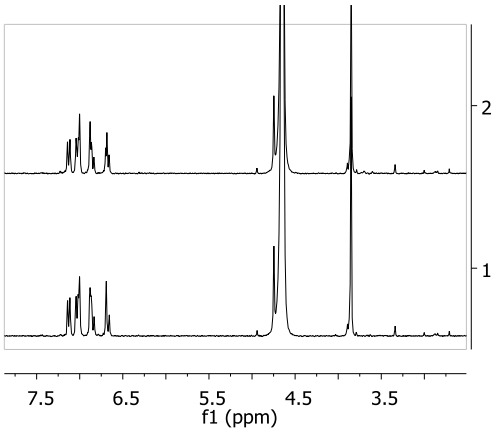

Fig. 1. NMR spectra of a 1 mm solution of compound **3** dissolved in PBS, pH 7.4, 37°C, immediately after dissolution (1) and after 14h (2).

Effect of curcumin derivatives on Aβ (1-42) aggregation

Congo Red (CR) binding assay

Aβ (1-42) was de-seeded as reported previously.[46] Curcumin derivatives (1 mM) were solubilized in NaOH 10 mM and then diluted to 10 µM in PBS at pH 7.4. Aβ (1-42) 20 µM was incubated with or without the different curcumin derivatives (40 µM) in PBS at pH 7.4 at 37°C for a period of 5 days in dark. At the end of incubation β-sheet formation

in each sample was determined by Congo Red dye (CR) binding. For this purpose, CR was dissolved in PBS to a concentration of 120 µM, passed through a 0.22 µm filter and then mixed with the incubated samples to give a final concentration of 6 µM CR. Solutions were vortexed and incubated at 25°C for 15 min. Absorbance spectra were recorded for samples and for CR alone preparations, using a Jasco V-530 spectrophotometer in a 1 cm path length cuvette. Corrections were made for the Absorbance of buffer and compounds not incubated with Aβ.

Aggregated Aβ was quantified using the equation 1:

$$[\text{A}\beta \text{ fibrils}] = ({}^{541}\text{A}/4780) - ({}^{403}\text{A}/6830) - ({}^{403}\text{A}_{CR}/8620) \qquad (1)$$

where ${}^{541}\text{A}$, ${}^{403}\text{A}$ and ${}^{403}\text{A}_{CR}$ are the absorbances of the sample and Congo Red at the wavelength of 541 nm and 403 nm, respectively.[47] From these data, relative fibril content were calculated as the ratio of sample fibril concentration to pure Aβ (1-42) fibril concentration. For each sample, at least three replicates were measured.

Results and Discussion

Even if the compounds (**2, 3, 4, 5, 6**) were developed in order to bind Aβ (1-42), it is significant to evaluate an eventual capability of interfering with the peptide aggregation process. For this purpose the effect of curcumin derivatives on amyloid fibril formation was evaluated using CR binding assay. CR was used instead of the most common Thioflavin T (ThT) assay, since it has recently been reported that ThT fluorescence is biased using curcumin and its derivative, while CR assay is not affected.[48] The results are reported in **Fig. 2**. The Absorbance of CR added to Aβ incubated alone for 5 days strongly increases and the spectrum displays a characteristic

---

[46] Manzoni, C., Colombo, L., Messa, M., Cagnotto, A., Cantu, L., Del Favero, E., Salmona, M., (2009) Overcoming synthetic A beta peptide aging: a new approach to an age-old problem. Amyloid-Journal of Protein Folding Disorders 16, 71-80.

[47] Klunk, W.E., Jacob, R.F., Mason, R.P., (**1999**) Quantifying amyloid beta-peptide (A beta) aggregation using the Congo red A beta (CR-A beta) spectrophotometric assay. Analytical Biochemistry 266, 66-76.

[48] Hudson, S.A., Ecroyd, H., Kee, T.W., Carver, J.A., (**2009**) The thioflavin T fluorescence assay for amyloid fibril detection can be biased by the presence of exogenous compounds. Febs Journal 276, 5960-5972.

red shift with respect to CR alone, consequent to the formation of fibrils. In the presence of any of the synthesized compounds the absorbance increase, caused by the aggregation process, is attenuated, suggesting their ability to partially prevent fibrils formation. In particular, compounds **3** and **6** showed the strongest effect, reducing the amount of aggregated Aβ (1-42) after 5 days of about 41% and 34%, respectively.

The assessment that none of the synthesized compounds induce aggregation is relevant for the potential use of these curcumin derivatives in diagnosis. Moreover, the ability of compounds **3** and **6** to reduce amyloid fibril formation increases the interest on these compounds, not only as diagnostic tools, but also as therapeutic agents.

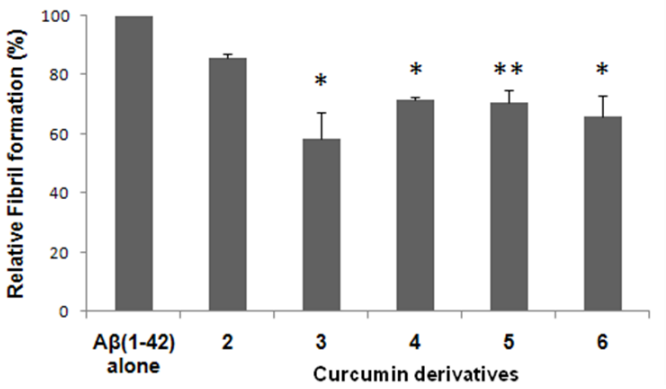

Fig. 2. Relative fibril formation of Aβ (1-42) after 5 days of incubation at 37°C with or without various curcumin derivatives, as estimated from Congo Red binding. Values were calculated as the ratio of sample fibril concentration to pure Aβ (1-42) fibril concentration. The graph represents the mean ± standard deviation of at least three independent experiments. (n= 3, * $p< 0.05$, ** $p< 0.01$ compared to Aβ (1-42) in buffer).

Structural characterization of Aβ peptide in presence and absence of synthesized compounds by Atomic Force Microscopy (AFM)

Methods

Aβ peptide solutions were prepared as follows: Aβ peptides were dissolved to the final concentration of 110μM by adding half of the final volume of freshly prepared 10 mM NaOH. The sample was vigorously mixed and then an equal volume of Tris-HCl 200

mM, pH 7.4 was added. The samples were incubated for 5 days at 37 °C in the presence or in the absence of a twofold concentration of the test compounds.

For AFM analysis peptide samples were diluted to the final concentration of 5 µM with 10 mM HCl. Sixty µl of sample were immediately spotted onto a freshly cleaved muscovite mica disk (Veeco/Digital Instruments, Mannheim, Germany) and incubated for 5 minutes. The disk was then washed with copious amounts of milliQ water and dried under a gentle nitrogen stream. Samples were mounted onto a Multimode AFM with a NanoScope V system (Veeco/Digital Instruments, Mannheim, Germany) operating in Tapping Mode using standard phosphorus-doped silicon probes (Veeco, Mannheim, Germany).[49]

Results

The interaction of test compounds with Aβ1-42 was analyzed by Atomic Force Microscopy (AFM). The presence of test compounds during the incubation caused some morphological changes, altered the aggregation process inducing structural modifications. Aβ1-42 appeared folded, enriched in oligomers, proto-fibrils and fibrils (**Figure 3A**). Curcumin-derived compounds decreased the presence of aggregates, increasing the percentage of amorphous material and forming tight agglomerates (**Figures 3B-F**).

[49] Albani, D., Polito, L., Batelli, S., De Mauro, S., Fracasso, C., Martelli, G., Colombo, L., Manzoni, C., Salmona, M., Caccia, S., Negro, A., Forloni, G., (**2009**) The SIRT1 activator resveratrol protects SK-N-BE cells from oxidative stress and against toxicity caused by alpha-synuclein or amyloid-beta (1-42) peptide. Journal of Neurochemistry 110, 1445-1456.

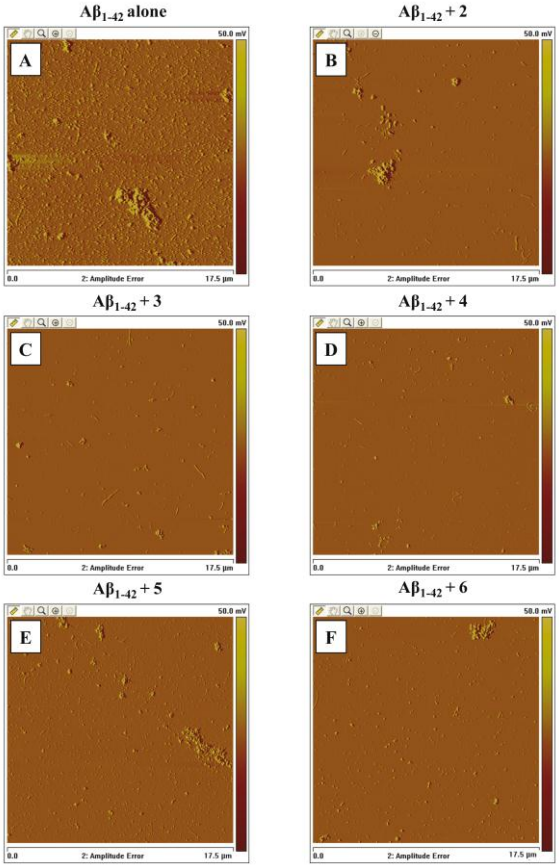

Fig. 3. Tapping mode AFM images (Amplitude Data) of $A\beta_{1-42}$: Morphology of aggregates A) $A\beta_{1-42}$ alone B–F) $A\beta_{1-42}$ co-incubate with curcumin-derived compound (1:2 molar ratio = Aβ:curcumin derivatives).

PAPER 3

Chem. Commun., ***2011***, *47, 10266–10268*

CIS-GLYCO-FUSED BENZOPYRAN COMPOUNDS AS NEW AMYLOID BETA PEPTIDE LIGANDS

Cristina Airoldi,[a] Francisco Cardona,[ab] Erika Sironi,[a] Laura Colombo,[c] Mario Salmona,[c] Artur Silva,[b] Francesco Nicotra[a] and Barbara La Ferla*[a]

[a] Dept. of Biotechnology and Biosciences, University of Milano-Bicocca, P.zza della Scienza 2, 20126, Milan, [b] Dept. of Chemistry, University of Aveiro, Campus Universitario de Santiago, 3810-193 Aveiro, Portugal, [c] Dept. of Molecular Biochemistry and Pharmacology Mario Negri Institute for Pharmacological Research, via La Masa 19, 20156, Milan, Italy.

Abstract

A small library of glyco-fused benzopyran compounds has been synthesised. Their interaction features with Aβ peptides have been characterised by using STD-NMR and trNOESY experiments. The conformational analysis of the compounds has also been carried out through molecular mechanics (MM) and molecular dynamics (MD) simulations.

Alzheimer's disease (AD) is the most common cause of dementia among neurodegenerative diseases in the elderly population.[1,2,3,4,5] A central pathological feature of AD is the accumulation of misfolded amyloid-β (Aβ) peptides in the form of oligomers and amyloid fibrils and plaques in the brain. Molecules able to stabilize the soluble Aβ conformation, to destabilize the altered amyloidogenic conformer, and to prevent the required conformational transition could be effective inhibitors of amyloid

[1] R. Brookmeyer, S. Gray and C. Kawas, Am. J. Public Health, **1998**, 88, 1337–1342.
[2] R. Brookmeyer, M. M. Corrada, F. C. Curriero and C. Kawas, Arch. Neurol., **2002**, 59, 1764–1767.
[3] C. L. Masters, R. Cappai, K. J. Barnham and V. L. Villemagne, J. Neurochem., **2006**, 97, 1700–1725.
[4] D. J. Selkoe, Neuron, **2001**, 32, 177–180.
[5] S. S. Sisodia and P. H. St George-Hyslop, Nat. Rev. Neurosci., **2002**, 3, 281–290.

plaque formation and very potent drug candidates for AD treatment.[6,7,8] Many natural and synthetic compounds able to interact as Aβ ligands have been identified. Among them, we have paid attention to a set of small molecules in which aromatic moieties seem to play a key role.[9] Unfortunately, many of these compounds lack solubility, chemical stability and/or show pharmacological activities not directly correlated to AD. Therefore, the correct therapeutic evaluation of these molecules towards AD cannot be performed in a straightforward manner. In this context, and in order to overcome these chemical-based limitations, we have designed a pool of potential Aβ-ligands which display a glyco-fused benzopyran structure (**Scheme 1**), therefore maintaining the required aromatic moiety, while generating chemically stable and water soluble compounds.

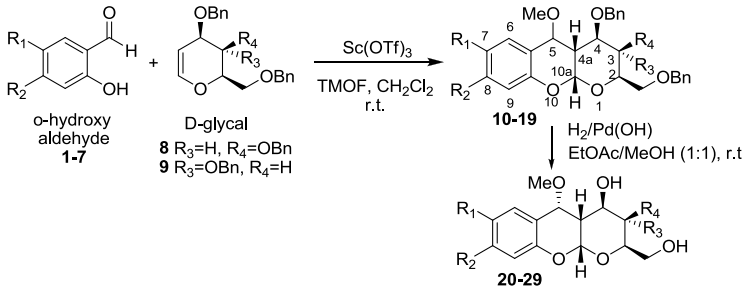

Scheme 1

Moreover, the glycidic entity assures further possible derivatizations, such as conjugation to other molecular entities (nanoparticles, polymeric supports, etc.), which may be employed as useful features for diagnostic and therapeutic purposes. Notably glycomimetics inserted in these kinds of carbohydrate–aromatic hybrids have recently gained great interest.[10,11] The employed synthetic strategy exploits the reaction

[6] A. I. Bush, Neurobiol. Aging, **2002**, 23, 1031–1038.
[7] R. Sabate and J. Estelrich, Langmuir, **2005**, 21, 6944–6949.
[8] S. Taniguchi, N. Suzuki, M. Masuda, S. Hisanaga, T. Iwatsubo, M. Goedert and M. Hasegawa, J. Biol. Chem., **2005**, 280, 7614–7623.
[9] F. Re, C. Airoldi, C. Zona, M. Masserini, B. La Ferla, N. Quattrocchi and F. Nicotra, Curr. Med. Chem., **2010**, 17, 2990–3006.
[10] D. C. Koester, A. Holkenbrink and D. B. Werz, Synthesis, **2010**, 19, 3217–3242.
[11] M. Leibeling, D. C. Koester, M. Pawliczek, S. C. Schild and D. B. Werz, Nat. Chem. Biol., **2010**, 6, 199–201.

between o-hydroxybenzaldehydes and glycals using a catalytic amount of scandium triflate in the presence of trimethyl orthoformate (TMOF), as described by Yadav *et al*.[12] In order to verify the influence of the various parts of the molecule on the interaction with the Aβ peptide, we generated a small library of glyco-fused benzopyran compounds, using differently substituted O-hydroxybenzaldehydes and employing both glucal (**8**) and galactal (**9**). In all cases, we obtained cis-fused pyrano[3,2-b]benzopyrans (21–91% yield), but in contrast to previous reports,[12] the reaction afforded a variable ratio of separable mixtures of two diastereoisomers at C5 (**Table 1**); the major isomer was then deprotected to afford the final compounds **20–29**.

O-hydroxy benzaldehyde	D-glycal	Protected products	C5 R/S (yield%)	Deprotected compounds C5 R (yield%)
1 R_1,R_2= H,H	**8**	**10**R_1,R_2,R_3,R_4= H,H,H,OBn	92/8 (59%)	**20**R_1,R_2,R_3,R_4= H,H,H,OH (97%)
2 R_1,R_2= NO_2,H	**8**	**11** R_1,R_2,R_3,R_4= NO_2,H,H,OBn	100/0 (40%)	**21**R_1,R_2,R_3,R_4= NH_2,H,H,OH (94%)
3 R_1,R_2= OBn,H	**8**	**12** R_1,R_2,R_3,R_4= OBn,H,H,OBn	100/0 (35%)	**22** R_1,R_2,R_3,R_4= OH,H,H,OH (100%)
4 R_1,R_2= OMe,H	**8**	**13** R_1,R_2,R_3,R_4= OMe,H,H,OBn	85/15 (73%)	**23** R_1,R_2,R_3,R_4= OMe,H,H,OH (96%)
5 R_1,R_2= CH_3,H	**8**	**14** R_1,R_2,R_3,R_4= CH_3,H,H,OBn	95/5 (91%)	**24** R_1,R_2,R_3,R_4= CH_3,H,H,OH (95%)
6 R_1,R_2= H, OMe	**8**	**15** R_1,R_2,R_3,R_4= H,OMe,H,OBn	53/47 (64%)	**25** R_1,R_2,R_3,R_4= H,OMe,H,OH (97%)
7 R_1,R_2= H,CH_3	**8**	**16** R_1,R_2,R_3,R_4= H,CH_3,H,OBn	100/0 (45%)	**26** R_1,R_2,R_3,R_4= H,CH_3,H,OH (97%)
5	**9**	**17** R_1,R_2,R_3,R_4= CH_3,H,OBn,H	100/0 (66%)	**27** R_1,R_2,R_3,R_4= CH_3,H,OH,H (98%)
6	**9**	**18** R_1,R_2,R_3,R_4= H,OMe,OBn,H	100/0 (37%)	**28** R_1,R_2,R_3,R_4= H,OMe,OH,H (97%)
7	**9**	**19** R_1,R_2,R_3,R_4= H, CH_3, OBn,H	100/0 (21%)	**29** R_1,R_2,R_3,R_4= H, CH_3, OH,H (98%)

Table 1 cis-Fused glyco benzopyrans

[12] J. S. Yadav, B. V. S. Reddy, L. Chandraiah, B. Jagannadh, S. K. Kumar and A. C. Kunwar, Tetrahedron Lett., **2002**, 43, 527–4530.

From the molecular recognition perspective, very recently, we have employed Saturation Transfer Difference (STD) NMR experiments[13,14,15,16,17,18,19,20,21,22] to characterize the interaction of Aβ1–42 peptide with tetracycline, thioflavin T[23] and curcumin derivatives.[24] Thus, the same methodology has been applied herein to check the effect of glyco-fused benzopyran derivatives on the Aβ1–42 oligomer recognition process. In particular, the interaction studies with the amyloid peptide Aβ1–42 were carried out using the debenzylated compounds **20–29**, and STD-NMR and trNOESY experiments. STD-NMR experiments were performed using ligand:peptide 20:1 mixtures dissolved in deuterated PBS, pH 7.4, 25°C. Each mixture was analyzed irradiating the sample at -1.0 ppm to achieve the selective saturation of some aliphatic resonances of Aβ oligomers. The presence of NMR signals of the test molecule in the STD spectra is a non-ambiguous demonstration of the existence of interaction. Conversely, the absence of NMR resonances in the STD spectra indicates that the employed molecule is not an Aβ ligand. In all cases, several NMR resonances of **20–29** appeared in the corresponding STD spectra recorded in the presence of Aβ oligomers

[13] M. Mayer and B. Meyer, Angew. Chem., Int. Ed., **1999**, 38, 1784–1788.
[14] B. Meyer and T. Peters, Angew. Chem., Int. Ed., **2003**, 42, 864–890.
[15] C. Airoldi, A. Palmioli, A. D'Urzo, S. Colombo, M. Vanoni, E. Martegani and F. Peri, ChemBioChem, **2007**, 8, 1376–1379.
[16] A. Palmioli, E. Sacco, C. Airoldi, F. Di Nicolantonio, A. D'Urzo, S. Shirasawa, T. Sasazuki, A. Di Domizio, L. De Gioia, E. Martegani, A. Bardelli, F. Peri and M. Vanoni, Biochem. Biophys. Res. Commun., **2009**, 386, 593–597.
[17] R. Caraballo, H. Dong, J. P. Ribeiro, J. Jime´nez-Barbero and O. Ramstro¨ m, Angew. Chem., Int. Ed., **2010**, 49, 589–593.
[18] C. Airoldi, S. Sommaruga, S. Merlo, P. Sperandeo, L. Cipolla, A. Polissi and F. Nicotra, Chem.–Eur. J., **2010**, 16, 1897–1902.
[19] T. Haselhorst, T. Fiebig, J. C. Dyason, F. E. Fleming, H. Blanchard, B. S. Coulson and M. von Itzstein, Angew. Chem., Int. Ed., **2011**, 50, 1055–1058.
[20] C. Airoldi, S. Sommaruga, S. Merlo, P. Sperandeo, L. Cipolla, A. Polissi and F. Nicotra, ChemBioChem, **2011**, 12, 719–727.
[21] Y. Yuan, D. W. Bleile, X. Wen, D. A. R. Sanders, K. Itoh, H.-w. Liu and B. M. Pinto, J. Am. Chem. Soc., **2008**, 130, 3157–3168.
[22] M. D. Dıaz, M. Palomino-Schatzlein, F. Corzana, C. Andreu, R. J. Carbajo, M. del Olmo, A. Canales-Mayordomo, A. Pineda- Lucena, G. Asensio and J. Jimenez-Barbero, ChemBioChem, **2010**, 11, 2424–2432.
[23] C. Airoldi, L. Colombo, C. Manzoni, E. Sironi, A. Natalello, S. M. Doglia, G. Forloni, F. Tagliavini, E. Del Favero, L. Cantu, F. Nicotra and M. Salmona, Org. Biomol. Chem., **2011**, 9, 463–472.
[24] C. Airoldi, C. Zona, E. Sironi, L. Colombo, M. Messa, D. Aurilia, M. Gregori, M. Masserini, M. Salmona, F. Nicotra and B. La Ferla, J. Biotechnol., **2011**, 56(4), 317–324.

(**Fig. 1C** and **D** and **Fig. S1 (ESIz)**), thus showing their ability to recognize and bind Aβ1-42, with the notable exception of compound **21**, whose signals are absent (**Fig. 1B**).

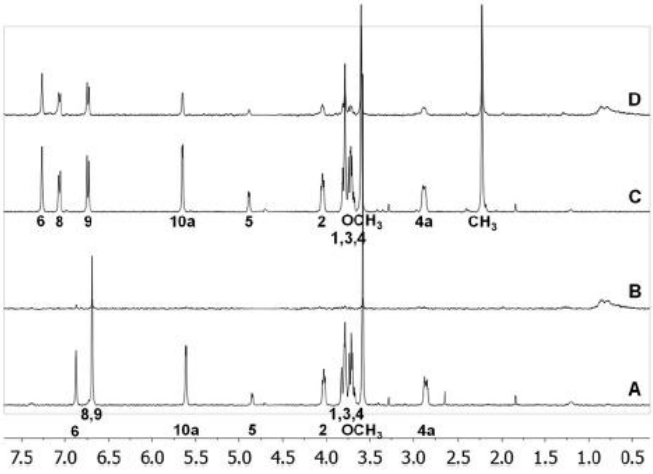

Fig. 1 Comparison between STD experiments acquired in the presence of compounds **21** and **24**. ^{1}H NMR (A and C) and 1D-STD NMR (B and D) spectra recorded on Aβ:ligand mixtures dissolved in deuterated PBS at 25 °C and containing Aβ1–42 (80 μM) and a test molecule (1.6 mM) (A and B, compound **21**; C and D, compound **24**). ^{1}H spectra were acquired with 64 scans, 1D-STD spectra with 512 scans and 2 s of saturation time.

Additional trNOESY experiments acquired on the same ligand:peptide mixtures supported these results. The change in the sign of the cross-peaks of the test molecule, from positive (blue color), in the absence of Aβ1–42 peptide, to negative (red color), in the presence of Aβ1–42 peptide, reflects an increase of its effective rotational motion correlation time, and supports its binding to a large molecular entity,[14] here represented by the Aβ oligomers. In agreement with the STD results, all trNOESY spectra of **20–29** acquired in the presence of Aβ1–42 showed the key change, from positive to negative, of the corresponding cross-peak signs, except for compound **21**. In this case, the NOE-cross peaks remained positive, indicating that this molecule does not bind to Aβ1–42 in a significant manner (**Fig. S2, ESIz**).

Since the STD intensity is proportional to the ligand binding affinity for the molecular target,[13,14] we exploited competitive STD experiments to rank the affinity[25] of compounds **20**, **22–29** for the peptide. Due to extensive resonance overlapping, the acquisition of competitive STD spectra on a unique mixture containing all the molecules was not feasible. Hence, we performed three different competitive experiments of the different molecules in the presence of Aβ1–42 oligomers. Separate experiments for mixtures containing the D-galactose derivatives (**20–26**), the D-glucose analogues (**27–29**), or ''the best ligands'' identified from the two previous screenings (**24** and **29**) were performed. In the first and second competitive experiments, we measured the STD effect on H6, and in the third experiment on H10a (see **Scheme 1**). For each molecule, the fractional STD effect was calculated as $(I - I_0)/I_0$, where I is the intensity of the monitored signal in the STD spectrum and I_0 is the intensity of the same signal in a reference spectrum. Compounds **24** and **29** showed the same affinity for Aβ1–42, as their H10a signals presented equal intensities. Hence, to compare the data obtained in the different competitive experiments, the fractional STD effects of **24** and **29** were set equal to 1 and, therefore, the relative intensities for the other molecules were calculated. The results are summarized in **Fig. 2**. Thus, **24**, **26**, **27** and **29**, whose aromatic rings are substituted with a methyl group, are the ligands with the highest affinities for Aβ oligomers, followed by **23**, **25** and **28**, which present a O-methyl group as a substituent, and by **20**, with no aromatic substituent. These molecules display fractional STD effects higher than 70%. Finally, **22**, with a hydroxyl group at position 7, has the lowest affinity.

[25] J. P. Ribeiro, S. Andre´ , F. J. Canada, H.-J. Gabius, A. P. Butera, R. J. Alves and J. Jimenez-Barbero, ChemMedChem, **2010**, 5, 415–419.

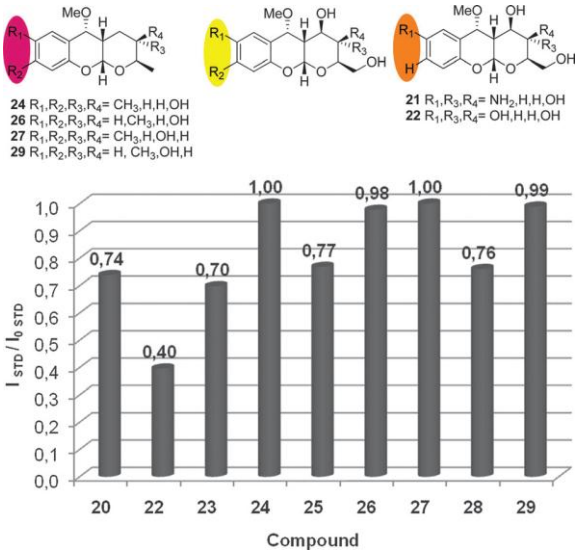

Fig. 2 (A) Highlight of the polar/apolar substituents on the aromatic ring: violet colour apolar, orange colour polar and yellow colour in between. (B) Fractional STD effects calculated for compounds **20, 22, 23, 24, 25, 26, 27, 28** and **29**. These values are proportional to compound affinity for Aβ1–42 oligomers.

These data, together with the absence of binding of **21** (with an amine substituent) to Aβ oligomers, clearly indicate that the lower the polarity of the substituents on the aromatic ring, the greater the compound affinity for Aβ1–42. Moreover, the position of substituents on the aromatic ring (position 7 or 8), as well as the nature of the saccharide entity are not relevant, as supported by the evidence that compounds **24**, **26**, **27** and **29** showed equal binding affinity, and the same applies for compounds **23**, **25** and **28**. These findings are in full agreement with the STD-based epitope-mapping, recorded with five different saturation times (0.5, 1.2, 2.0, 3.0, 5.0 s) (**Fig. S3, ESIz**). According to the STD relative intensities, the region of the ligand mainly involved in the interaction with Aβ (the binding epitope) is the aromatic ring, while protons of the saccharide portion showed the least intense STD signals. These evidences explain why the stereochemistry of sugar carbons does not influence the binding affinity, while the polarity of the aromatic substituents, as previously stated, plays a crucial role in the

interaction. The conformational analysis of these molecules, carried out using molecular mechanics (MM) and molecular dynamics (MD) simulations, fully supported the NMR results. Calculations were performed by usingMM3*[26,27] force field, as implemented in the MacroModel[28] program (Maestro Suite). The differences in affinity for Aβ1–42 peptide are due to the nature of the substituent on the aromatic ring and are not a consequence of conformational differences. In fact, according to the modeling data, compounds **20–29** present the same conformation. The 30 conformations with the lowest energy found for compounds **20–29** are reported in **Fig. S4 and Fig. S5 (ESIz)**.The values of the key proton–proton distances and dihedral angles monitored during the MD are reported in the **ESIz (Fig. S6–S16)**.

A new class of small molecules Aβ peptide ligands, with a glyco-fused benzopyran structure, has been developed. As expected, the aromatic moiety is mainly involved in the interaction with the peptides. Those compounds with apolar substituents attached to the aromatic ring showed the highest interaction. The glyco-fused moiety surely confers solubility in physiological conditions and is not much involved in the interaction; this finding could allow further useful functionalizations for therapeutic and diagnostic purposes. Finally, the conformational analysis showed a common conformation for all compounds, thus supporting the importance of the aromatic substituents revealed by NMR studies.

Acknowledgements

The research leading to these results has received funding from the European Community's Seventh Framework Programme (FP7/2007-2013) under grant agreement n°. 212043 and from Regione Lombardia, Fondo per la promozione di accordi istituzionali, Progetto n°. 4779 ''Network Enabled Drug Design (NEDD)''. We acknowledge the Italian Ministry of Health (533F/Q/1), Cariplo Foundation (Project

[26] N. L. Allinger, Y. H. Yuh and J. H. Lii, J. Am. Chem. Soc., **1989**, 111, 8551–8566.
[27] M. Martın-Pastor, J. F. Espinosa, J. L. Asensio and J. Jimenez- Barbero, Carbohydr. Res., **1997**, 298, 15–49.

NOBELGUARD), Banca Intesa SanPaolo and PRIN (PROT.2007T7MSAJ) for financial support, and Flamma (Italy) for the kind gift of Fmoc amino acids. Francisco Cardona kindly acknowledges Fundacao para a Ciencia e Tecnologia (FCT, Portugal) for the PhD grant (SFRH/44888/2008).

The tricyclic derivatives object of this paper have been **patented** as β-amyloid peptide ligands in an Italian patent intitled "Nuovi composti triciclici glicofusi, procedimento per la loro produzione e loro impiego quali ligandi dei peptidi β amiloidi (Aβ)" (ref. RM2011A000264).

Further unpublished results

The antibiotic activity of tricyclic derivatives **20**, **21**, **22**, **23**, **24** and **27** was evaluated against some Gram positive and Gram negative bacterial strains. Minimal inhibitory concentrations (MIC) were determined following standard protocols for testing susceptibility to antibiotic agents.[29] The bacterial strains used were: *Pseudomonas aeruginosa* PAO1 (Gram negative), *Escherichia coli* K12 wild type strain MG1655 (Gram negative), the permeable *E. coli* mutant strain AS19[30] (Gram negative), *Staphylococcus aureus* (Gram positive) ans *Staphylococcus epidermidis* (Gram positive). The procedure for a broth microdilution test was followed. Briefly, 96-well microtiter plates were prepared with compound concentration ranging from 500 to 0,5 μM in triplicates. The assayed strains were grown in Mueller-Hinton broth (MHB) and inoculus corresponding to OD_{600} of 0.05 were added to each well. The microtiter plates were incubated for 18-20 h at 37°C and the MIC of each compound determined. MIC was defined as the lowest concentration inhibiting bacterial growth.

All the tricyclic compounds tested did not display antibiotic activity, as reported in **Table 2**.

---

[28] MacroModel, MacroModel 9.6, Schrodinger, LLC, New York, **2008**.
[29] I. Wiegand, K. Hilpert, R. E. Hancock, Nat. Protoc., **2008**, 3, 163.

	MIC (μM)						
Strain	**Tetracycline**	**20**	**21**	**22**	**23**	**24**	**27**
***E. coli* MG1655**	31.3	>500	>500	>500	>500	>500	>500
***E. coli* AS19**	1	>500	>500	>500	>500	>500	>500
***P. aeruginosa* PA01**	250	>500	>500	>500	>500	>500	>500
S. aureus	7.8	>500	>500	>500	>500	>500	>500
S. epidermidis	7.8	>500	>500	>500	>500	>500	>500

Table 2. Minimal inhibitory concentration for tetracycline and for compounds **20**, **21**, **22**, **23**, **24** and **27**.

Supporting Information

Synthesis

General Remarks

All solvents were dried with molecular sieves for at least 24 h prior to use. Thin layer chromatography (TLC) was performed on silica gel 60 F254 plates (Merck) with detection using UV light when possible, or by charring with a solution of concd. H_2SO_4/EtOH/H_2O (5:45:45) or a solution of $(NH_4)_6Mo_7O_{24}$ (21 g), $Ce(SO_4)_2$ (1 g), concd. H_2SO_4 (31 mL) in water (500 mL). Flash column chromatography was performed on silica gel 230-400 mesh (Merck). ^{1}H and ^{13}C NMR spectra were recorded at 25 °C unless otherwise stated, with a Varian Mercury 400 MHz instrument. Chemical shift assignments, reported in ppm, are referenced to the corresponding solvent peaks. HRMS were recorded on a QSTAR elite LC/MS/MS system with a nanospray ion source. Optical rotations were measured at room temperature using an Atago Polax-2L polarimeter and are reported in units of 10^{-1} deg·cm2·g^{-1}.

[30] M. Sekiguchi, S. Iida, Proc. Natl. Acad. Sci. USA, **1967**, 58, 2315-2320.

General synthetic strategy for the synthesis of protected compounds **10**-**19**: (J. S. Yadav, B. V. S. Reddy, L. Chandraiah, B. Jagannadh, S. Kiran Kumar and Ajit C. Kunwar *Tetrahedron Letters*, 2002, 43, 4527).

A mixture containing the appropriate O-hydroxybenzaldehyde (**1**-**7**) (2.5 equiv.), trimethylorthoformiate (2.5 equiv.) and scandium triflate (3% mol) in CH_2Cl_2 is stirred at r.t. for 20 min. The mixture is then cooled at 0°C and the appropriate tri-*O*-benzyl glycal (**8**-**9**) is added. The reaction is then left stirring at r.t. for 30 min. The reaction is then diluted with CH_2Cl_2, washed with water, dried over Na_2SO_4, filtrated and the solvent is removed under reduced pressure. The crude is purified by flash chromatography (eluent Toluene/AcOEt 9.75/0.25) to afford pure compounds **10-19.**

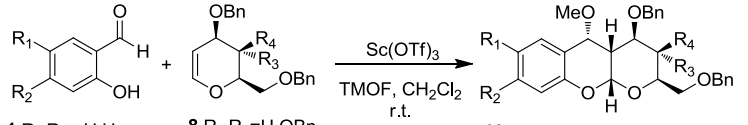

1 R_1,R_2= H,H
2 R_1,R_2= NO_2,H
3 R_1,R_2= OBn,H
4 R_1,R_2= OMe,H
5 R_1,R_2= CH_3,H
6 R_1,R_2= H, OMe
7 R_1,R_2= H,CH_3

8 R_3,R_4=H,OBn
9 R_3,R_4=OBn, H

10 R_1,R_2,R_3,R_4= H,H,H,OBn
11 R_1,R_2,R_3,R_4= NO_2,H,H,OBn
12 R_1,R_2,R_3,R_4= OBn,H,H,OBn
13 R_1,R_2,R_3,R_4= OMe,H,H,OBn
14 R_1,R_2,R_3,R_4= CH_3,H,H,OBn
15 R_1,R_2,R_3,R_4= H,OMe,H,OBn
16 R_1,R_2,R_3,R_4= H,CH_3,H,OBn
17 R_1,R_2,R_3,R_4= CH_3,H,OBn,H
18 R_1,R_2,R_3,R_4= H,OMe,OBn,H
19 R_1,R_2,R_3,R_4= H, CH_3, OBn,H

(2R,3R,4R,4aS,5R/S,10aR)-3,4-bis(benzyloxy)-2-benzyloxymethyl-5-methoxy-2,3,4, 4a, 5,10a-hexa hydropyrano[2,3-b]chromene (10): yield 59%, C5 R/S 92/8.

(5R)

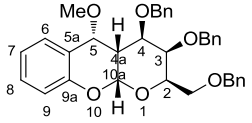

^{1}H NMR (400 MHz, $CDCl_3$) δ 7.55 (d, *J* = 7.6 Hz, 1H, H6), 7.37 – 7.22 (m, 15H, Ar), 7.23 – 7.15 (m, 1H, H8), 6.99 (t, *J* = 7.5 Hz, 1H, H7), 6.83 (d, *J* = 8.1 Hz, 1H, H9), 5.66 (d, *J* = 2.9 Hz, 1H, H10a), 4.96 (d, *J* = 11.4 Hz, 1H, OC*H*$_2$Ph), 4.77 (d, *J* = 4.3 Hz, 1H, H5), 4.62 – 4.31 (m, 5H, OCH_2Ph), 4.18 (t, *J* = 6.4 Hz, 1H, H2), 3.79 (s, 1H, H3), 3.68 – 3.63 (m, 1H, H4), 3.63 – 3.59 (m, 2H, CH_2O), 3.58 (s, 3H, OMe), 3.36 – 3.26 (m, 1H, H4a); ^{13}C NMR (101

MHz, $CDCl_3$) δ 152.27, 139.03, 138.89, 138.15, 129.12, 128.62, 128.44, 128.41, 128.38, 128.13, 128.01, 127.95, 127.77, 127.55, 126.26, 122.43, 121.38, 115.59, 97.74, 76.22, 75.62, 75.16, 73.97, 73.71, 72.78, 71.71, 69.13, 57.10, 34.72. $[\alpha]_D^{20}$= +5,3 (c=1, $CHCl_3$). MS: m/z calcd for $[M + Na]^+$ = 575.2, $[M + K]^+$ = 591.2; found $[M + Na]^+$ = 575.3, $[M + K]^+$ = 591.3.

(5S)

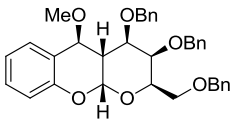

^{1}H NMR (400 MHz, $CDCl_3$) δ 7.39 – 7.24 (m, 13H, Ar), 7.24 – 7.20 (m, 1H, H6), 7.18 (dd, *J* = 7.0, 2.2 Hz, 2H, Ar), 7.07 (d, *J* = 7.4 Hz, 1H, H8), 6.88 (m, 2H, H7, H9), 5.71 (d, *J* = 3.2 Hz, 1H, H10a), 4.92 (d, *J* = 11.5 Hz, 1H, OCH_2Ph), 4.54 (ddd, *J* = 34.5, 23.4, 11.7 Hz, 5H, OCH_2Ph), 4.40 (d, *J* = 2.1 Hz, 1H, H5), 4.20 (M, 1H, H2), 3.98 (s, 1H, H3), 3.72 – 3.64 (m, 2H, CH_2O), 3.37 (s, 3H, OMe), 3.32 (dd, *J* = 11.8, 2.4 Hz, 1H, H4), 3.06 – 2.98 (m, 1H, H4a). ^{13}C NMR (101 MHz, $CDCl_3$) δ 153.89, 138.79, 138.09, 137.76, 131.20, 130.35, 128.67, 128.64, 128.50, 128.25, 128.21, 128.03, 128.01, 127.85, 127.83, 120.81, 118.54, 116.96, 95.00, 75.17, 74.79, 74.77, 73.79, 71.62, 71.53, 71.52, 68.94, 56.38, 37.70, 29.93. $[\alpha]_D^{20}$= +8,7 (c=1, $CHCl_3$). MS: m/z calcd for $[M + Na]^+$ = 575.2, $[M + K]^+$ = 591.2; found $[M + Na]^+$ = 575.3, $[M + K]^+$ = 591.3.

(2R,3R,4R,4aR,5R,10aR)-3,4-bis(benzyloxy)-2-benzyloxymethyl-5-methoxy-7-nitro-2, 3, 4, 4a, 5,10a-hexahydropyrano[2,3-b]chromene (11): yield 40%, C5 R/S 100/0

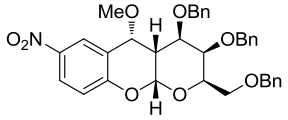

^{1}H NMR (400 MHz, $CDCl_3$) δ 8.44 – 8.41 (m, 1H, H6), 8.08 (dd, *J* = 9.0, 2.8 Hz, 1H, H8), 7.43 – 7.17 (m, 15H, Ar), 6.87 (d, *J* = 9.0 Hz, 1H, H9), 5.73 (d, *J* = 2.9 Hz, 1H, H10a), 4.96 (d, *J* = 11.3 Hz, 1H, OCH_2Ph), 4.73 (t, *J* = 7.4 Hz, 1H, H5), 4.64 – 4.36 (m, 5H, OCH_2Ph),

4.11 (t, *J* = 6.4 Hz, 1H, H2), 3.86 (s, 1H, H3), 3.64 (dd, *J* = 9.2, 5.8 Hz, 2H, CH_2O), 3.59 (d, *J* = 7.4 Hz, 3H, OMe), 3.50 (dd, *J* = 11.1, 2.5 Hz, 1H, H4), 3.41 – 3.32 (m, 1H, H4a). ^{13}C NMR (101 MHz, $CDCl_3$) δ 157.58, 142.33, 138.72, 138.01, 137.95, 128.68, 128.53, 128.42, 128.39, 128.23, 128.18, 128.08, 127.94, 127.81, 125.33, 123.31, 123.21, 116.20, 98.87, 75.28, 75.23, 74.68, 73.83, 73.02, 72.39, 72.13, 68.95, 57.10, 33.96.$[\alpha]_D^{20}$= -4,5 (c=1, $CHCl_3$). MS: m/z calcd for $[M + H]^+$ = 598.2, $[M + Na]^+$ = 620.2, $[M + K]^+$ = 636.2; found $[M + H]^+$ = 598.3, $[M + Na]^+$ = 620.4, $[M + K]^+$ = 636.4.

(2R,3R,4R,4aR,5R,10aR)-3,4,7-tris(benzyloxy)-2-benzyloxymethyl-5-methoxy-2,3,4, 4a, 5,10a-hexahydropyrano[2,3-b]chromene (12): yield 35%, C5 R/S 100/0

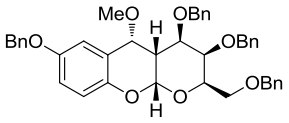

^1H NMR (400 MHz, $CDCl_3$) δ 7.52 – 7.25 (m, 20H, Ar), 7.23 (d, *J* = 2.2 Hz, 1H, H6), 6.86 (dd, *J* = 8.8, 3.0 Hz, 1H, H8), 6.81 – 6.74 (m, 1H, H9), 5.64 (d, *J* = 2.9 Hz, 1H, H10a), 5.10 – 4.95 (m, 3H, OCH_2Ph), 4.76 (d, *J* = 4.4 Hz, 1H, H5), 4.64-4.34 (m, 5H, OCH_2Ph), 4.20 (t, *J* = 6.5 Hz, 1H, H2), 3.83 (s, 1H, H3), 3.67 (dd, *J* = 11.1, 2.6 Hz, 1H, H4), 3.65 – 3.61 (m, 2H, CH_2O), 3.58 (s, 3H, OMe), 3.36 – 3.25 (m, 1H, H4a). ^{13}C NMR (101 MHz, $CDCl_3$) δ 149.98, 139.05, 138.93, 138.16, 130.59, 129.64, 128.61, 128.43, 128.40, 128.36, 128.13, 127.97, 127.94, 127.75, 127.52, 126.52, 121.97, 115.37, 97.62, 76.33, 75.66, 75.16, 73.93, 73.71, 72.69, 71.65, 69.15, 57.11, 34.78, 20.99. $[\alpha]_D^{20}$= -5,5 (c=1, $CHCl_3$); MS: m/z calcd for $[M + Na]^+$ = 681.3, $[M + K]^+$ = 697.3; found $[M + Na]^+$ = 681.5, $[M + K]^+$ = 697.4.

(2R,3R,4R,4aR,5R/S,10aR)-3,4-bis(benzyloxy)-2-benzyloxymethyl-5,7-dimethoxy-2,3, 4, 4a, 5,10a-hexahydropyrano[2,3-b]chromene (13): yield 73%, C5 R/S 85/15

(5R)

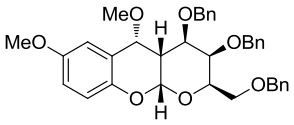

^{1}H NMR (400 MHz, $CDCl_3$) δ 7.37 – 7.21 (m, 15H, Ar), 7.11 (d, *J* = 0.9 Hz, 1H, H6), 6.76 (d, 2H,H8 and H9), 5.61 (d, *J* = 2.9 Hz, 1H, H10a), 4.96 (d, *J* = 11.4 Hz, 1H, OCH_2Ph), 4.74 (d, *J* = 4.4 Hz, 1H, H5), 4.60-4.36 (m, 5H, OCH_2Ph), 4.18 (t, *J* = 6.4 Hz, 1H, H2), 3.80 (s, 4H, ArOMe and H3), 3.66 (dd, *J* = 11.1, 2.6 Hz, 1H, H4), 3.61 (dt, *J* = 7.0, 3.4 Hz, 2H, CH_2O), 3.57 (s, 3H, OMe), 3.33 – 3.24 (m, 1H, H4a). ^{13}C NMR (101 MHz, $CDCl_3$) δ 154.39, 146.10, 139.05, 138.92, 138.16, 128.62, 128.44, 128.41, 128.38, 128.14, 127.97, 127.95, 127.76, 127.54, 123.12, 116.33, 115.18, 110.81, 97.61, 76.27, 75.76, 75.16, 73.92, 73.72, 72.77, 71.65, 69.14, 57.07, 56.06, 34.72. $[\alpha]_D^{20}$= +7,1 (c=1, $CHCl_3$); MS: m/z calcd for $[M + K]^+$ = 621.2; found $[M + K]^+$ = 621.5.

(5S)

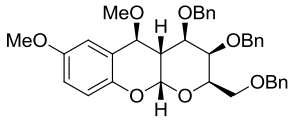

^{1}H NMR (400 MHz, $CDCl_3$) δ 7.39 – 7.15 (m, 15H, Ar), 6.84 – 6.76 (m, 2H, H8 and H9), 6.58 (s, 1H, H6), 5.64 (d, *J* = 3.1 Hz, 1H, H10a), 4.91 (d, *J* = 11.5 Hz, 1H, OCH_2Ph), 4.66 – 4.40 (m, 5H, OCH_2Ph), 4.35 (d, *J* = 2.0 Hz, 1H, H5), 4.26 – 4.17 (m, 1H, H2), 4.00 (s, 1H, H3), 3.76 (s, 3H, ArOMe), 3.70 – 3.63 (m, 2H, CH_2O), 3.40 (s, 3H, OMe), 3.34 (dd, *J* = 11.8, 2.3 Hz, 1H, H4), 3.03 – 2.94 (m, 1H, H4a). ^{13}C NMR (101 MHz, $CDCl_3$) δ 153.63, 147.66, 138.79, 138.10, 137.74, 128.63, 128.50, 128.46, 128.42, 128.25, 128.21, 128.03, 128.03, 127.97, 127.89, 127.83, 127.72, 127.50, 119.01, 117.67, 116.63, 115.27, 99.18, 94.88, 74.97, 74.80, 73.79, 71.60, 71.49, 71.42, 70.65, 70.02, 69.88, 68.96, 56.57, 55.96, 37.60. $[\alpha]_D^{20}$= +6,6 (c=1, $CHCl_3$); MS: m/z calcd for $[M + K]^+$ = 621.2; found $[M + K]^+$ = 621.6.

(2R,3R,4R,4aR,5R/S,10aR)-3,4-bis(benzyloxy)-2-benzyloxymethyl-5-methoxy-7-methyl -2, 3, 4,4a,5,10a-hexahydropyrano[2,3-b]chromene (14): yield 91%, C5 R/S 95/5

(5R)

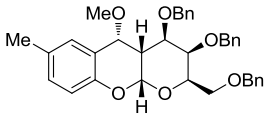

^{1}H NMR (400 MHz, $CDCl_3$) δ 7.33 (d, *J* = 7.1 Hz, 1H, H6), 7.31 – 7.21 (m, 15H, Ar), 6.99 (d, *J* = 7.3 Hz, 1H, H8), 6.72 (d, *J* = 8.2 Hz, 1H, H9), 5.61 (d, *J* = 2.9 Hz, 1H, H10a), 4.96 (d, *J* = 11.4 Hz, 1H, OCH_2Ph), 4.74 (d, *J* = 4.5 Hz, 1H, H5), 4.62 – 4.33 (m, 5H, OCH_2Ph), 4.18 (t, *J* = 6.4 Hz, 1H, H2), 3.80 (s, 1H, H3), 3.66 (dd, *J* = 11.2, 2.6 Hz, 1H, H4), 3.61 (dd, *J* = 6.3, 4.1 Hz, 2H, CH_2O), 3.57 (s, 3H,OMe), 3.33 – 3.23 (m, 1H, H4a), 2.31 (s, 3H, Me). ^{13}C NMR (101 MHz, $CDCl_3$) δ 149.98, 139.05, 138.93, 138.16, 130.59, 129.64, 128.61, 128.43, 128.40, 128.36, 128.13, 127.97, 127.75, 127.52, 126.52, 121.97, 115.37, 97.63, 76.92, 76.33, 75.66, 75.16, 73.93, 73.71, 72.69, 71.65, 69.15, 57.1, 34.78, 20.99. $[\alpha]_D^{20}$= -5,2 (c=1, $CHCl_3$); MS: m/z calcd for $[M + H]^+$ = 567.3, $[M + Na]^+$ = 589.3, $[M + K]^+$ = 605.2; found $[M + H]^+$ = 567.6, $[M + Na]^+$ = 589.5, $[M + K]^+$ = 605.6.

(5S)

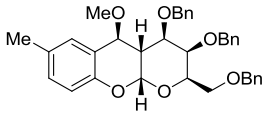

^{1}H NMR (400 MHz, $CDCl_3$) δ 7.40 – 7.13 (m, 15H, Ar), 7.01 (dd, *J* = 8.3, 1.7 Hz, 1H, H8), 6.82 (s, 1H, H6), 6.75 (d, *J* = 8.3 Hz, 1H, H9), 5.66 (d, *J* = 3.2 Hz, 1H, H10a), 4.92 (d, *J* = 11.5 Hz, 1H, OCH_2Ph), 4.65 – 4.42 (m, 5H, OCH_2Ph), 4.37 – 4.30 (d, *J* = 2.0 Hz 1H, H5), 4.26 – 4.17 (m, 1H, H2), 3.98 (s, 1H, H3), 3.72 – 3.63 (m, 2H, CH_2O), 3.38 (s, 3H, ArOMe), 3.36 – 3.29 (dd, *J* = 2.38, 11.78 Hz, 1H, H4), 3.06 – 2.93 (m, 1H, H4a), 2.26 (s, 3H, Me). ^{13}C NMR (101 MHz, $CDCl_3$) δ 151.53, 138.81, 138.10, 137.77, 131.35, 131.03, 129.91, 128.64, 128.60, 128.54, 128.49, 128.26, 128.21, 128.01, 127.93, 127.82, 118.18, 116.64, 94.89, 75.00, 74.84, 74.80, 73.79, 71.55, 71.47, 71.35, 68.96, 56.42, 37.60, 29.93, 20.77. $[\alpha]_D^{20}$= -2,1 (c=1, $CHCl_3$); MS: m/z calcd for $[M + H]^+$ = 567.3, $[M + Na]^+$ = 589.3, $[M + K]^+$ = 605.2; found $[M + H]^+$ = 567.6, $[M + Na]^+$ = 589.5, $[M + K]^+$ = 605.6.

(2R,3R,4R,4aR,5R/S,10aR)-3,4-bis(benzyloxy)-2-benzyloxymethyl-5,8-dimethoxy-2,3, 4, 4a, 5, 10a-hexahydropyrano[2,3-b]chromene (15): yield 64%, C5 R/S 53/47
(5R)

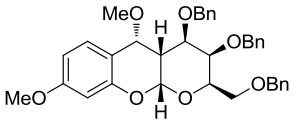

^{1}H NMR (400 MHz, $CDCl_3$) δ 7.42 (d, *J* = 8.6 Hz, 1H, H6), 7.37 – 7.21 (m, 15H, Ar),6.56 (dd, *J* = 8.5, 2.4 Hz, 1H, H7), 6.39 (d, *J* = 2.4 Hz, 1H, H8), 5.62 (d, *J* = 2.8 Hz, 1H, H10a), 4.96 (d, *J* = 11.4 Hz, 1H, OCH_2Ph), 4.71 (d, *J* = 4.4 Hz, 1H, H5), 4.60-4.35 (m, 5H, OCH_2Ph), 4.19 (t, *J* = 6.4 Hz, 1H, H2), 3.80 (s, 1H, H3), 3.78 (s, 3H, ArOMe), 3.66 (dd, *J* = 11.1, 2.4 Hz, 1H, H4), 3.60 (t, *J* = 6.3 Hz, 2H, CH_2O), 3.55 (s, 3H, OMe), 3.31 – 3.24 (m, 1H, H4a). ^{13}C NMR (101 MHz, $CDCl_3$) δ 160.56, 153.13, 139.03, 138.97, 138.15, 128.61, 128.43, 128.40, 128.12, 127.96, 127.75, 127.52, 127.14, 114.73, 107.86, 100.74, 97.96, 76.04, 75.67, 75.16, 74.05, 73.72, 72.86, 71.82, 69.18, 56.99, 55.55, 34.91, 29.92. $[\alpha]_D^{20}$= -2,2 (c=1, $CHCl_3$); MS: m/z calcd for $[M + Na]^+$ = 605.3, $[M + K]^+$ = 621.2; found $[M + Na]^+$ = 605.6, $[M + K]^+$ = 621.5.

(5S)

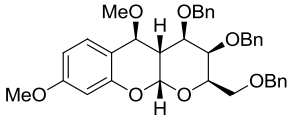

^{1}H NMR (400 MHz, $CDCl_3$) δ 7.39 – 7.16 (m, 15H, Ar), 6.97 (d, *J* = 8.4 Hz, 1H, H6), 6.47 (dd, *J* = 8.3, 2.5 Hz, 1H, H7), 6.43 (d, *J* = 2.3 Hz, 1H, H8), 5.71 (d, *J* = 3.2 Hz, 1H, H10a), 4.97 – 4.87 (d, *J* = 11.4 Hz, 1H, OCH_2Ph), 4.65 – 4.43 (m, 5H, OCH_2Ph), 4.37 (d, *J* = 2.1 Hz, 1H, H5), 4.19 (d, *J* = 5.5 Hz, 1H, H2), 3.98 (s, 1H, H3), 3.77 (s, 3H, ArOMe), 3.70 – 3.63 (m, 2H,CH_2O), 3.35 (s, 3H, OMe), 3.32 (d, *J* = 2.4 Hz, 1H, H4), 3.00 (m, 1H, H4a). ^{13}C NMR (101 MHz, $CDCl_3$) δ 161.44, 155.01, 138.80, 138.10, 137.84, 131.97, 128.67, 128.65, 128.50, 128.25, 128.20, 128.03, 128.02, 127.84, 111.11, 108.00, 101.38, 95.17, 75.34, 74.78, 74.35, 73.79, 71.70, 71.60, 71.57, 69.00, 56.13, 55.54, 37.84, 29.93. $[\alpha]_D^{20}$= -4,6

(c=1, $CHCl_3$). MS: m/z calcd for $[M + Na]^+$ = 605.3, $[M + K]^+$ = 621.2; found $[M + Na]^+$ = 605.7, $[M + K]^+$ = 621.6.

(2R,3R,4R,4aR,5R,10aR)-3,4-bis(benzyloxy)-2-benzyloxymethyl-5-methoxy-8-methyl-2, 3, 4, 4a, 5, 10a-hexahydropyrano[2,3-b]chromene (16): yield 45%, C5 R/S 100/0

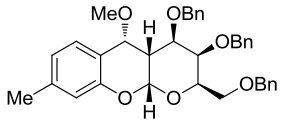

^{1}H NMR (400 MHz, $CDCl_3$) δ 7.42 (d, *J* = 7.8 Hz, 1H, H6), 7.37 – 7.20 (m, 15H, Ar), 6.81 (d, *J* = 7.8 Hz, 1H, H7), 6.66 (s, 1H, H9), 5.63 (d, *J* = 2.8 Hz, 1H, H10a), 4.97 (d, *J* = 11.4 Hz, 1H, OCH_2Ph), 4.74 (d, *J* = 4.2 Hz, 1H, H5), 4.62 – 4.34 (m, 5H, OCH_2Ph), 4.19 (t, *J* = 6.3 Hz, 1H, H2), 3.81 (s, 1H, H3), 3.66 (dd, *J* = 11.1, 2.6 Hz, 1H, H4), 3.62 (dd, *J* = 6.2, 4.6 Hz, 2H, CH_2O), 3.56 (s, 3H, OMe), 3.34 – 3.21 (m, 1H, H4a), 2.31 (s, 3H, Me). ^{13}C NMR (101 MHz, $CDCl_3$) δ 152.11, 139.20, 139.07, 139.00, 138.19, 128.61, 128.44, 128.41, 128.37, 128.12, 127.97, 127.94, 127.75, 127.51, 126.10, 122.28, 119.48, 116.04, 97.74, 76.22, 75.74, 75.16, 74.03, 73.70, 72.84, 71.69, 69.16, 57.06, 34.89, 21.41. $[\alpha]_D^{20}$= -6,2 (c=1, $CHCl_3$). MS: m/z calcd for $[M + K]^+$ = 605.2; found [$[M + K]^+$ = 605.2.

(2R,3S,4R,4aR,5R,10aR)-3,4-bis(benzyloxy)-2-benzyloxymethyl-5-methoxy-7-methyl-2, 3, 4, 4a, 5, 10a-hexahydropyrano[2,3-b]chromene (17): yield 66%, C5 R/S 100/0

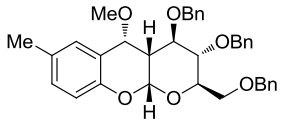

^{1}H NMR (400 MHz, $CDCl_3$) δ 7.43 – 7.18 (m, 14H, Ar and H6), 7.09 (dd, *J* = 6.7, 2.7 Hz, 2H, Ar), 6.99 (d, *J* = 6.3 Hz, 1H, H8), 6.72 (d, *J* = 8.2 Hz, 1H, H9), 5.60 (d, *J* = 3.0 Hz, 1H, H10a), 4.82 (d, *J* = 10.7 Hz, 1H, OCH_2Ph), 4.74 (d, *J* = 4.4 Hz, 1H, H5), 4.71 – 4.44 (m, 5H, OCH_2Ph), 4.07 (d, *J* = 9.9 Hz, 1H, H2), 3.86 – 3.79 (m, 2H, CH_2O), 3.74 (dd, *J* = 10.8, 1.9 Hz, 1H, H3), 3.72 – 3.65 (m, 1H, H4), 3.55 (s, 3H, OMe), 2.83 (ddd, *J* = 10.5, 4.4, 3.2 Hz,

1H, H4a), 2.30 (s, 3H, Me). ^{13}C NMR (101 MHz, $CDCl_3$) δ 149.83, 139.14, 138.40, 138.19, 130.78, 129.78, 128.61, 128.58, 128.44, 128.17, 128.01, 127.91, 127.89, 127.55, 126.48, 121.83, 115.50, 97.17, 78.56, 78.54, 76.43, 75.60, 74.92, 73.77, 72.55, 68.67, 57.39, 40.09, 20.98. $[\alpha]_D^{20}$= +3,7 (c=1, $CHCl_3$). MS: m/z calcd for $[M + Na]^+$ = 589.3, $[M + K]^+$ = 605.2; found $[M + Na]^+$ = 589.4, $[M + K]^+$ = 605.3.

(2R,3S,4R,4aR,5R,10aR)-3,4-bis(benzyloxy)-2-benzyloxymethyl-5,8-dimethoxy-2,3,4, 4a,5,10a-hexahydropyrano[2,3-b]chromene (18): yield 37%, C5 R/S 100/0

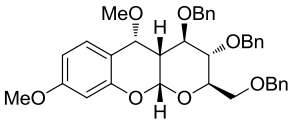

^{1}H NMR (400 MHz, $CDCl_3$) δ 7.43 (d, *J* = 8.6 Hz, 1H, H6), 7.38 – 7.19 (m, 10H, Ar), 7.15 – 7.05 (m, 2H, Ar), 6.56 (dd, *J* = 8.5, 2.3 Hz, 1H, H7), 6.40 (t, *J* = 5.9 Hz, 1H, H9), 5.61 (d, *J* = 2.8 Hz, 1H, H10a), 4.83 (d, *J* = 10.6 Hz, 1H, H4a), 4.72 (d, *J* = 4.4 Hz, 1H, OCH_2Ph), 4.70-4.44 (m, 5H, OCH_2Ph), 4.08 (d, *J* = 10.0 Hz, 1H, H2), 3.88 – 3.73 (m, 3H, H3 and CH_2O), 3.79 (s, 3H, OMe), 3.73 – 3.65 (m, 1H, H4), 3.52 (s, 3H, OMe), 2.89 – 2.75 (m, 1H, H4a). ^{13}C NMR (101 MHz, $CDCl_3$) δ 160.66, 152.96, 139.13, 138.37, 138.18, 128.62, 128.60, 128.44, 128.18, 128.15, 128.02, 127.93, 127.91, 127.56, 127.12, 114.56, 108.09, 100.84, 97.50, 78.51, 78.45, 76.18, 75.63, 74.97, 73.78, 72.70, 68.67, 57.29, 55.57, 40.20. $[\alpha]_D^{20}$= +11,6 (c=1, $CHCl_3$). MS: m/z calcd for $[M + Na]^+$ = 605.3, $[M + K]^+$ = 621.2; found $[M + Na]^+$ = 605.6, $[M + K]^+$ = 621.4.

(2R,3S,4R,4aR,5R,10aR)-3,4-bis(benzyloxy)-2-benzyloxymethyl-5-methoxy-8-methyl-2, 3,4,4a,5,10a-hexahydropyrano[2,3-b]chromene (19): yield 21%, C5 R/S 100/0

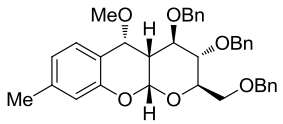

^{1}H NMR (400 MHz, $CDCl_3$) δ 7.41 (d, *J* = 7.9 Hz, 1H, H6), 7.39 – 7.18 (m, 13H, Ar), 7.14 – 7.03 (m, 2H, Ar), 6.80 (d, *J* = 7.7 Hz, 1H, H7), 6.65 (s, 1H, H9), 5.62 (d, *J* = 2.7 Hz, 1H, H10a), 4.82 (d, *J* = 10.6 Hz, 1H, OCH_2Ph), 4.74 (d, *J* = 3.8 Hz, 1H, H5), 4.72 – 4.39 (m, 5H, OCH_2Ph), 4.07 (d, *J* = 10.0 Hz, 1H, H2), 3.89 – 3.72 (m, 3H, H3 and CH_2O), 3.68 (t, *J* = 9.7 Hz, 1H, H4), 3.53 (s, 3H, OMe), 2.87 – 2.78 (m, 1H, H4a), 2.30 (s, 3H, Me). ^{13}C NMR (101 MHz, $CDCl_3$) δ 151.94, 139.37, 139.14, 138.39, 138.20, 128.62, 128.59, 128.44, 128.17, 128.02, 127.92, 127.90, 127.55, 126.05, 122.43, 119.33, 116.17, 97.28, 78.52, 76.93, 76.34, 75.61, 74.96, 73.77, 72.58, 68.68, 57.33, 40.17, 21.38. $[\alpha]_D^{20}$= +8,3 (c=1, $CHCl_3$). MS: m/z calcd for $[M + Na]^+$ = 589.3, $[M + K]^+$ = 605.2; found $[M + Na]^+$ = 589.5, $[M + K]^+$ = 605.2.

General synthetic strategy for the deprotection of compounds **10**-**19** (C7 R only) to afford compounds **20**-**29**. To a 6 mM solution of the protected compound in AcOEt/MeOH 1:1, previously degassed, $Pd(OH)_2$ 5% mol is added and the reaction mixture is stirred under H_2 atmosphere for 45min.-1.5 h. Then the catalist is removed by filtration and the solvent evaporated under reduced pressure to afford pure compounds **20-29.**

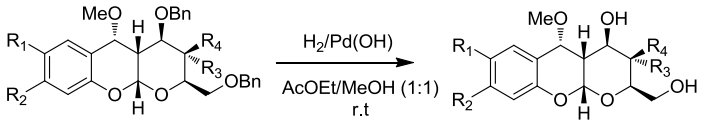

10 R_1,R_2,R_3,R_4= H,H,H,OBn
11 R_1,R_2,R_3,R_4= NO_2,H,H,OBn
12 R_1,R_2,R_3,R_4= OBn,H,H,OBn
13 R_1,R_2,R_3,R_4= OMe,H,H,OBn
14 R_1,R_2,R_3,R_4= CH_3,H,H,OBn
15 R_1,R_2,R_3,R_4= H,OMe,H,OBn
16R_1,R_2,R_3,R_4= H,CH_3,H,OBn
17 R_1,R_2,R_3,R_4= CH_3,H,OBn,H
18 R_1,R_2,R_3,R_4= H,OMe,OBn,H
19 R_1,R_2,R_3,R_4= H, CH_3, OBn,H

20 R_1,R_2,R_3,R_4= H,H,H,OH
21 R_1,R_2,R_3,R_4= NH_2,H,H,OH
22 R_1,R_2,R_3,R_4= OH,H,H,OH
23 R_1,R_2,R_3,R_4= OMe,H,H,OH
24 R_1,R_2,R_3,R_4= CH_3,H,H,OH
25 R_1,R_2,R_3,R_4= H, OMe,H,OH
26 R_1,R_2,R_3,R_4= H,CH_3,H,OH
27 R_1,R_2,R_3,R_4= CH_3,H,OH,H
28 R_1,R_2,R_3,R_4= H, OMe,OH,H
29 R_1,R_2,R_3,R_4= H,CH_3,OH,H

(2R,3R,4R,4aS,5R,10aR)-2-hydroxymethyl-5-methoxy-2,3,4,4a,5,10a hexahydropyrano [2,3-b]chromene-3,4-diol (20): yield 97%

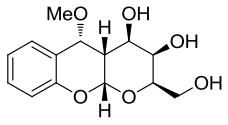

^{1}H NMR (400 MHz, CD_3OD) δ 7.45 (d, *J* = 7.7 Hz, 1H, H6), 7.18 (t, *J* = 7.7 Hz, 1H, H8), 6.94 (dd, *J* = 17.4, 9.9 Hz, 1H, H7), 6.78 (d, *J* = 8.2 Hz, 1H, H9), 5.62 (d, *J* = 3.1 Hz, 1H, H10a), 4.91 (d, *J* = 2.4 Hz, 1H, H5), 3.99 (t, *J* = 6.0 Hz, 1H, H2), 3.81 (s, 2H, H3 and H4), 3.80 – 3.74 (m, 2H, CH_2O), 3.69 (s, 3H, OMe), 3.00 – 2.92 (m, 1H, H4a). ^{13}C NMR (101 MHz, CD_3OD) δ 156.35, 132.98, 130.04, 125.32, 124.83, 119.22, 100.69, 81.51, 76.68, 71.54, 71.23, 65.57, 61.65, 38.46. $[\alpha]_D^{20}$= -7,6 (c=1, $CHCl_3$); MS: m/z calcd for $[M + Na]^+$ = 305.1, $[M + K]^+$ = 321.1; found $[M + Na]^+$ = 305.3, $[M + K]^+$ = 321.2.

(2R, 3R, 4R, 4aS, 5R, 10aR) -7- amino- 2-hydroxymethyl -5 -methoxy-2,3,4,4a,5,10a hexa hydro pyrano [2,3-b]chromene-3,4-diol (21): yield 94%

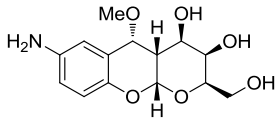

^{1}H NMR (400 MHz, CD_3OD) δ 6.89 (s, 1H, H6), 6.65-6.55 (m, 2H, H8 and H9), 5.52 (d, *J* = 3.0 Hz, 1H, H10a), 4.83 (d, *J* = 4.9 Hz, 1H, H5), 3.98 (t, *J* = 5.8 Hz, 1H, H2), 3.87 – 3.78 (m, 2H, H3 and H4), 3.79 – 3.73 (m, 1H, CH_2O), 3.67 (s, 3H, OMe), 2.96 – 2.85 (m, 1H, H4a). ^{13}C NMR (101 MHz, CD_3OD) δ 149.10, 144.77, 125.69, 121.06, 119.69, 118.60, 117.30, 114.55, 100.39, 81.79, 80.99, 76.53, 71.56, 71.43, 65.59, 61.71, 38.72. $[\alpha]_D^{20}$= +13,3 (c=1, $CHCl_3$). MS: m/z calcd for $[M + H]^+$ = 298.1 $[M + Na]^+$ = 320.1, $[M + K]^+$ = 336.1; found $[M + H]^+$ = 298.3, $[M + Na]^+$ = 320.3, $[M + K]^+$ = 336.3.

(2R,3R,4R,4aS,5R,10aR)-2-hydroxymethyl-5-methoxy-2,3,4,4a,5,10a hexahydropyrano [2,3-b]chromene-3,4,7-triol (22): yield 100%

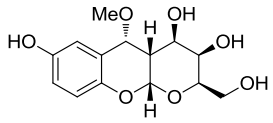

^{1}H NMR (400 MHz, CD_3OD) δ 6.88 (s, 1H, H6), 6.62 (s, 2H, H8 and H9), 5.54 (d, *J* = 2.8 Hz, 1H, H10a), 4.84 (d, *J* = 4.8 Hz, 1H, H5), 3.98 (t, *J* = 5.9 Hz, 1H, H2), 3.84 (d, *J* = 2.7 Hz, 1H, H4), 3.81 (s, 1H, H3), 3.76 (dd, *J* = 5.8, 2.3 Hz, 2H, CH_2O), 3.68 (s, 3H, OMe), 2.98 – 2.84 (m, 1H, H4a). ^{13}C NMR (101 MHz, CD_3OD) δ 155.33, 149.19, 125.97, 119.88, 119.77, 116.18, 116.06, 100.47, 81.66, 76.55, 71.57, 71.35, 65.59, 61.67, 38.61. $[\alpha]_D^{20}$= +11,1 (c=1, $CHCl_3$); MS: m/z calcd for $[M + Na]^+$ = 321.1; found $[M + Na]^+$ = 321.2.

(2R, 3R, 4R, 4aS, 5R, 10aR)-2-hydroxymethyl- 5,7-dimethoxy-2,3,4,4a,5,10a hexa hydro pyrano [2,3-b]chromene-3,4-diol (23): yield 96%

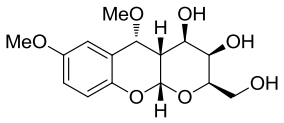

^{1}H NMR (400 MHz, CD_3OD) δ 7.00 (d, *J* = 2.1 Hz, 1H, H6), 6.77 (dd, *J* = 8.9, 2.3 Hz, 1H, H8), 6.71 (d, *J* = 8.8 Hz, 1H, H9), 5.57 (d, *J* = 3.0 Hz, 1H, H10a), 4.87 (s, 1H, H5), 3.98 (t, *J* = 6.0 Hz, 1H, H2), 3.83 – 3.79 (m, 2H, H3 and H4), 3.76 (dd, *J* = 6.1, 3.0 Hz, 2H, CH_2O), 3.74 (s, 3H, OMe), 3.68 (s, 3H, OMe), 2.98 - 2.89 (m, 1H, H4a). ^{13}C NMR (101 MHz, CD_3OD) δ 158.33, 150.09, 125.97, 119.98, 118.90, 114.61, 100.59, 81.54, 76.60, 71.60, 71.26, 65.57, 61.52, 58.83, 38.47. $[\alpha]_D^{20}$= +8,9 (c=1, $CHCl_3$); MS: m/z calcd for $[M + Na]^+$ = 335.1; found $[M + Na]^+$ = 335.3.

(2R, 3R, 4R, 4aS, 5R, 10aR) -2-hydroxymethyl-5-methoxy-7-methyl-2, 3, 4, 4a, 5, 10a-hexahydropyrano[2,3-b]chromene-3,4-diol (24): yield 95%

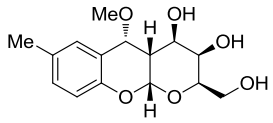

^{1}H NMR (400 MHz, CD_3OD) δ 7.24 (s, 1H, H6), 6.98 (d, *J* = 8.2 Hz, 1H, H8), 6.66 (d, *J* = 8.3 Hz, 1H, H9), 5.57 (d, *J* = 3.0 Hz, 1H, H10a), 3.98 (t, *J* = 6.0 Hz, 1H, H2), 3.83 – 3.78 (m, 2H, H3 and H4), 3.77 (dd, *J* = 6.0, 2.9 Hz, 2H, CH_2O), 3.68 (s, 3H, OMe), 2.96 – 2.89 (m, 1H, H4a), 2.26 (s, 3H, Me). ^{13}C NMR (101 MHz, CD_3OD) δ 150.14, 130.22, 129.54, 126.29, 120.97, 115.09, 96.65, 77.67, 72.66, 67.62, 67.37, 61.64, 57.73, 34.59, 19.57. $[\alpha]_D^{20}$= +13,3 (c=1, $CHCl_3$); MS: m/z calcd for $[M + Na]^+$ = 319.1, $[M + K]^+$ = 335.1; found $[M + Na]^+$ = 319.4, $[M + K]^+$ = 335.4.

(2R,3R,4R,4aS,5R,10Ar)- 2-hydroxymethyl- 5,8-dimethoxy-2,3,4,4a,5,10a-hexahydro pyrano[2,3-b]chromene-3,4-diol (25): yield 97%

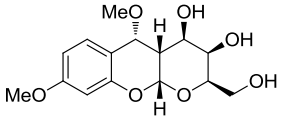

^{1}H NMR (400 MHz, CD_3OD) δ 7.32 (d, *J* = 8.6 Hz, 1H, H6), 6.54 (dd, *J* = 8.6, 2.4 Hz, 1H, H7), 6.35 (d, *J* = 2.4 Hz, 1H, H9), 5.58 (d, *J* = 3.0 Hz, 1H, H10a), 4.84 (d, *J* = 4.9 Hz, 1H, H5), 4.00 (t, *J* = 6.0 Hz, 1H, H2), 3.86 – 3.79 (m, 2H, H3 and H4), 3.77 (dd, *J* = 6.0, 3.3 Hz, 2H, CH_2O), 3.74 (s, 3H, OMe), 3.67 (s, 3H, OMe), 2.96-2.86 (m, 1H, H4a). ^{13}C NMR (101 MHz, CD_3OD) δ 160.95, 153.28, 126.97, 113.53, 107.31, 100.40, 96.94, 77.53, 72.80, 67.62, 67.29, 61.64, 57.61, 54.54, 34.63. $[\alpha]_D^{20}$= -7,6 (c=1, $CHCl_3$); MS: m/z calcd for $[M + Na]^+$ = 335.1, $[M + K]^+$ = 351.1; found $[M + Na]^+$ = 335.4, $[M + K]^+$ = 351.3.

(2R,3R,4R,4aS,5R,10aR)- 2-hydroxymethyl- 5-methoxy-8-methyl-2,3,4,4a,5,10a-hexa hydropyrano[2,3-b]chromene-3,4-diol (26): yield 97%

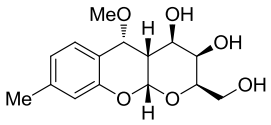

^{1}H NMR (400 MHz, CD_3OD) δ 7.29 (d,*J* = 7.8 Hz, 1H, H6), 6.76 (d, *J* = 7.8 Hz, 1H, H7), 6.60 (s, 1H, H9), 5.57 (d, *J* = 3.0 Hz, 1H, H10a), 4.85 (d, *J* = 4.7 Hz, 1H, H5), 3.98 (t, *J* = 5.9 Hz, 1H, H3), 3.83 – 3.73 (m, 4H, CH_2O, H2, H4), 3.67 (s, 3H, OMe), 2.96 – 2.85 (m, 1H, H4a), 2.25 (s, 3H, Me).

^{13}C NMR (101 MHz, CD_3OD) δ 156.14, 143.22, 133.19, 129.62, 125.66, 122.29, 119.72, 100.65, 81.54, 76.64, 71.24, 65.63, 61.61, 38.51, 23.91. $[\alpha]_D^{20}$= +8,3 (c=1, $CHCl_3$); MS: m/z calcd for $[M + Na]^+$ = 319.1; found $[M + Na]^+$ = 319.3.

(2R,3S,4R,4aS,5R,10aR)- 2-(hydroxymethyl)- 5-methoxy-7-methyl-2,3,4,4a,5,10a-hexa hydropyrano[2,3-b]chromene-3,4-diol (27): yield 98%

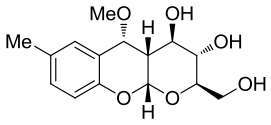

^{1}H NMR (400 MHz, CD_3OD) δ 7.12 (s, 1H, H6), 6.85 (d, *J* = 8.3 Hz, 1H, H8), 6.54 (d, *J* = 8.3 Hz, 1H, H9), 5.38 (d, *J* = 2.9 Hz, 1H, H10a), 3.75 – 3.59 (m, 3H, CH_2O and H2), 3.53 (s, 4H, H3 and OMe), 3.34 (t, *J* = 8.9 Hz, 1H, H4), 2.50 – 2.40 (m, 1H, H4a), 2.13 (s, 3H, Me). ^{13}C NMR (101 MHz, CD_3OD) δ 150.01, 130.29, 129.54, 126.43, 121.13, 115.15, 96.39, 77.56, 73.82, 70.37, 70.10, 61.29, 57.52, 40.03, 19.56. $[\alpha]_D^{20}$= +13,3 (c=1, $CHCl_3$); MS: m/z calcd for $[M + K]^+$ = 335.1; found $[M + K]^+$ = 335.3.

(2R,3S,4R,4aS,5R,10aR)- 2-hydroxymethyl- 5,8-dimethoxy-2,3,4,4a,5,10a-hexahydro pyrano[2,3-b]chromene-3,4-diol (28): yield 97%

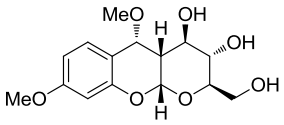

^{1}H NMR (400 MHz, CD_3OD) δ 7.33 (d, *J* = 8.6 Hz, 1H, H6), 6.54 (dd, *J* = 8.6, 2.4 Hz, 1H, H7), 6.36 (d, *J* = 2.4 Hz, 1H, H9), 5.51 (t, *J* = 6.6 Hz, 1H, H10a), 4.83 (d, *J* = 4.8 Hz, 1H, H5), 3.87 – 3.66 (m, 6H, CH_2O and H4 and OMe), 3.66 (d, *J* = 6.3 Hz, 3H, OMe), 3.48 (t, *J* = 9.2 Hz, 1H, H3), 2.57 (ddd, *J* = 10.3, 4.9, 3.1 Hz, 1H, H4a). ^{13}C NMR (101 MHz, CD_3OD) δ 160.95, 153.13, 127.12, 113.68, 107.43, 100.38, 96.66, 77.40, 73.93, 70.26, 70.02, 61.24, 57.39, 54.54, 40.05. $[\alpha]_D^{20}$= +11,6 (c=1, $CHCl_3$); MS: m/z calcd for $[M + Na]^+$ = 335.1, $[M + K]^+$ = 351.1; found $[M + Na]^+$ = 335.5, $[M + K]^+$ = 351.5.

(2R,3S,4R,4aS,5R,10aR)- 2-hydroxymethyl- 5-methoxy- 8-methyl-2,3,4,4a,5,10a-hexa hydropyrano[2,3-b]chromene-3,4-diol (29): yield 98%

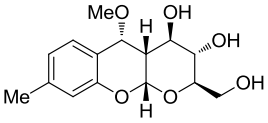

^{1}H NMR (400 MHz, CD_3OD) δ 7.31 (d, *J* = 7.8 Hz, 1H, H6), 6.78 (d, *J* = 7.7 Hz, 1H, H7), 6.62 (s, 1H, H9), 5.52 (d, *J* = 2.9 Hz, 1H, H10a), 4.85 (d, *J* = 4.7 Hz, 1H, H5), 3.85 (dd, *J* = 13.7, 4.5 Hz, 1H, C*H*$_2$O), 3.76 (q, *J* = 4.2 Hz, 2H, C*H*$_2$O and H2), 3.68 – 3.62 (m, 4H, H4 and OMe), 3.48 (t, *J* = 9.0 Hz, 1H, H3), 2.58 (ddd, *J* = 10.4, 4.9, 3.1 Hz, 1H, H4a), 2.27 (s, 3H, Me). ^{13}C NMR (101 MHz, CD_3OD) δ 152.07, 139.31, 126.11, 121.84, 118.54, 115.68, 96.45, 77.50, 73.84, 70.30, 70.04, 61.25, 57.47, 40.04, 19.99. $[\alpha]_D^{20}$= -7,8 (c=1, $CHCl_3$); MS: m/z calcd for $[M + Na]^+$ = 319.1, $[M + K]^+$ = 335.1; found $[M + Na]^+$ = 319.4, $[M + K]^+$ = 335.3.

Peptide synthesis and purification

Procedure

Aβ1-42 was prepared by solid-phase peptide synthesis on a 433A synthesizer (Applied Biosystems) using Fmoc-protected L-amino acid derivatives, NOVASYN-TGA resin on a 0.1 mM scale.[31] Peptide was cleaved from the resin as previously described[32] and purified by reverse phase HPLC on a semi-preparative C4 column (Waters) using water:acetonitrile gradient elution. Peptide identity was confirmed by MALDI-TOF analysis (model Reflex III, Bruker). Peptide purity was always above 95%.

NMR spectroscopy binding studies

Material and Methods

NMR experiments were recorded on a Varian 400-MHz Mercury. A batch of Aβ1-42 was selected that contained pre-amyloidogenic seeds highly toxic to N2a cells. Immediately before use, lyophilized Aβ1-42 was dissolved in 10 mM NaOD in D_2O at a concentration of 160μM, then diluted 1:1 with 10 mM phosphate buffer saline, pH 7.4 containing 100 mM NaCl (PBS) and one of the tested compounds. Compounds **2**, **3**, **4**, **5** and **6** were dissolved in 10 mM NaOD in D_2O and then diluited in PBS, pH 7.4, sonicated for 1 h and added to the peptide solution. The pH of each sample was verified with a Microelectrode (Mettler Toledo) for 5 mm NMR tubes and adjusted with NaOD or DCl. All pH values were corrected for isotope effect. Basic sequences were employed for 2D-TOCSY, 2D-NOESY and STD experiments. For STD, a train of Gaussian-shaped pulses each of 50 ms was employed to saturate selectively the protein envelope; the total saturation time of the protein envelope was adjusted by the number of shaped pulses and was varied between 3 s and 0.3 s.

---

[31] G. Di Fede,M. Catania,M.Morbin,G.Rossi, S. Suardi,G. Mazzoleni, M. Merlin, A. R. Giovagnoli, S. Prioni, A. Erbetta, C. Falcone, M. Gobbi, L. Colombo, A. Bastone, M. Beeg, C. Manzoni, B. Francescucci, A. Spagnoli, L. Cantù, E. Del Favero, E. Levy, M. Salmona and F. Tagliavini, *Science*, **2009**, 323, 1473–1477.

[32] M. Salmona, M. Morbin, T. Massignan, L. Colombo, G. Mazzoleni, R. Capobianco, L. Diomede, F. Thaler, L. Mollica, G. Musco, J. J. Kourie, O. Bugiani,D. Sharma, H. Inouye,D. A. Kirschner,G. Forloni and F. Tagliavini, *J. Biol. Chem.*, **2003**, 278, 48146–4815.

Supporting Figures

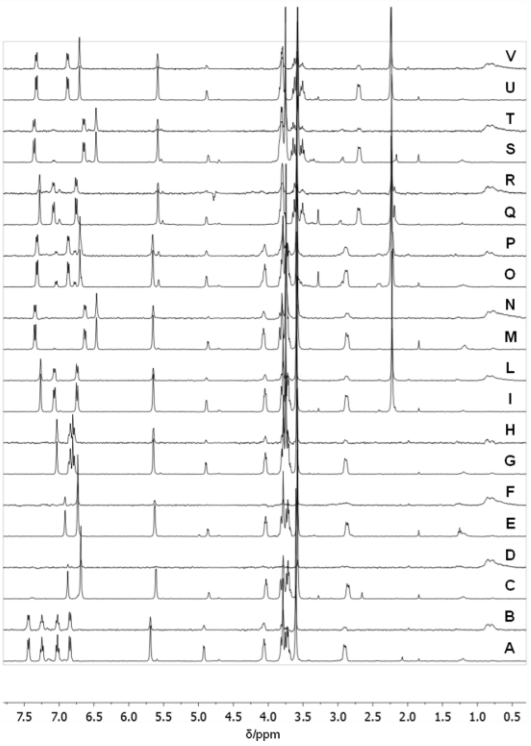

Figure 1S. ^{1}H spectra (**A**, **C**, **E**, **G**, **I**, **M**, **O**, **Q**, **S** and **U**) and 1D-STD spectra (**B**, **D**, **F**, **H**, **L**, **N**, **P**, **R**, **T** and **V**) of mixtures dissolved in deuterated PBS at 25°C containing Aβ1-42 (80 uM) and a test molecule (1.6 mM) (**A** and **B**, compound **13**; **C** and **D**, compound **14**; **E** and **F**, compound **15**; **G** and **H**, compound **16**; **I** and **L** compound **17**; **M** and **N**, compound **18**; **O** and P, compound **19**; **Q** and **R**, compound **20**; **S** and **T**, compound **21** e **U** and **V**, compound **22**). ^{1}H spectra were acquired with 64 scans, 1D-STD spectra with 512 scans and 2 s of saturation time.

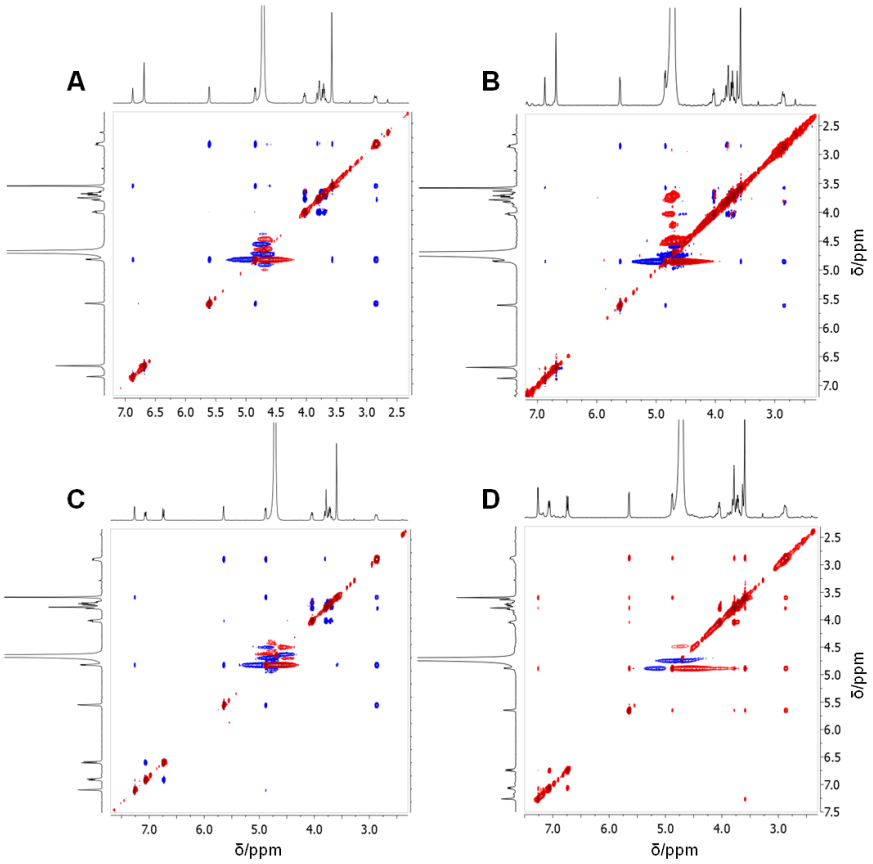

Figure 2S. 2D-NOESY spectra of compounds **21** (**A**) e **24** (**C**) dissolved in deuterated PBS, pH 7.5, 25°C, mixing time 0.9 s. trNOESY of mixture containing Aβ1-42 (80 uM) and compound **21** (**B**) or compound **24** (**D**) dissolved in deuterated PBS, pH 7.5, 25°C, mixing time 0.3 s. Positive cross-peak are blue, negative ones red.

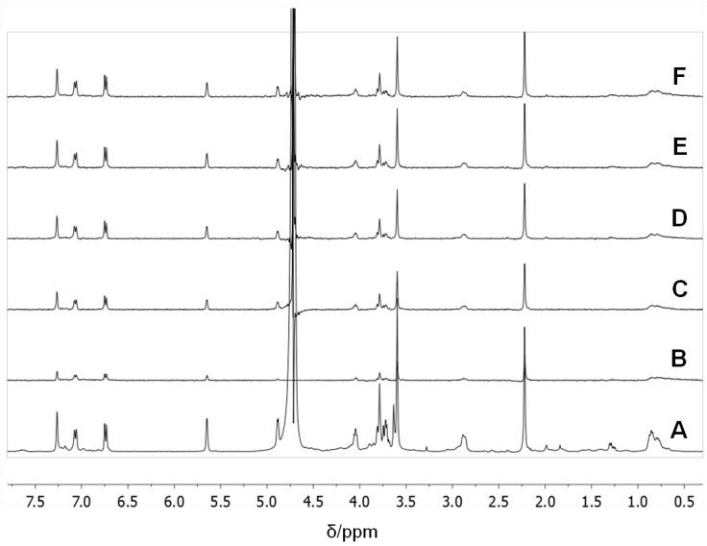

Figure 3S. **A)** ^{1}H NMR spectrum of the mixture containing Aβ1-42 (80 uM) and compound **24** (1.6 mM) in PBS, pH=7.5, 25°C; **B**-**F)** STD-NMR spectra of the same mixture acquired with different saturation times. (**B**, 0.5 s; **C**, 1,2 s; **D**, 2,0 s; **E** 3,0 s; **F**, 5,0 s).

Molecular Mechanics (MM) and Molecular Dynamics (MD) calculations

Material and Methods

Molecular mechanics and dynamics studies were conducted with MacroModel 9.8.207 [33] as implemented in version 9.1.207 of the Maestro suite,[34] using MM3* force field.[35] The starting coordinates for dynamics calculations were those obtained after energy minimization of the structures, followed by conformational search. In particular, a systematic variation of the torsional degrees of freedom of the molecules permitted different starting structures to be constructed that were further minimized to provide the corresponding local minima. For each compound the conformer with the lowest energy was considered. Simulations were carried out over 5 ns at 298 K with a 0.25 fs

[33] MacroModel, (2008), 9.6 ed. Schrödinger, LLC, New York.
[34] Maestro, (2010), 9.1 ed. Schrödinger, LLC, New York

time step and a 20 ps equilibration step; 100 structures were sampled and minimized for further analysis. The continuum GB/SA solvent model[36] was employed and the general PRCG (Polak–Ribiere Conjugate Gradient) method for energy minimization was used. An extended cut-off was applied and the SHAKE procedure for bonds was not selected. The values of the key proton-proton distances H2-H3, H2-H4, H3-H4, H4a-H10a, H4a-H5 and H5-H10a as well as the values of the dihedral angle H2-C2-C3-H3, H3-C3-C4-H4, H4a-C4a-C10a-H10a and H4a-C4a-C5-H5 were monitored during the MD and are reported in supporting information. All compounds showed the same values of H2-H4, H4a-H5, H4a-H10a, and H5-H10a distances (Fig. 3), and of the dihedral angles H4a-C4a-C10a-H10a (average value θ= 62°) and H4a-C4a-C5-H5 (average value θ= -53°), which are the diagnostic parameters to identify molecule conformation. On the other hand, on the basis of the distances H2-H3 and H3-H4 (Fig. 5S) and the dihedral angles H2-C2-C3-H3 and H3-C3-C4-H4, molecules **20**-**29** could be clustered into two groups (**20-26**, with average $\theta_{H2\text{-}C2\text{-}C3\text{-}H3}$= -60°, $\theta_{H3\text{-}C3\text{-}C4\text{-}H4}$= 60° and **27-29,** with average $\theta_{H2\text{-}C2\text{-}C3\text{-}H3}$= -180°, average $\theta_{H3\text{-}C3\text{-}C4\text{-}H4}$=180°), depending on C3 stereochemistry (**Fig.s 6S-15S**).

[35] Allinger, N.L., Yuh, Y.H., Lii, J.H., (1989) Molecular mechanics - the MM3 force-field for hydrocarbons .1. Journal of the American Chemical Society 111, 8551-8566.
[36] Still, W.C., Tempczyk, A., Hawley, R.C., Hendrickson, T., (1990) Semianalitical treatment of solvation for molecular mechanics and dynamics. Journal of the American Chemical Society 112, 6127-6129.

Supporting Figures

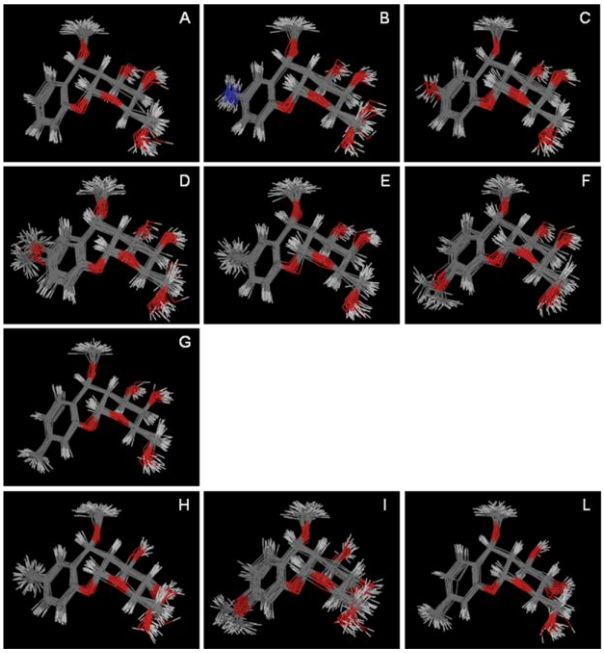

Figure 4S. Superimposition of the 30 structures with the lowest energy calculated through MD simulations in water, 298K; **A**, compound **20**; **B**, compound **21**; **C**, compound **22**; **D**, compound **23**; **E**, compound **24**; **F**, compound **25**; **G**, compound **26**; **H**, compound **27**; **I**, compound **28**; **L**, compound **29**.

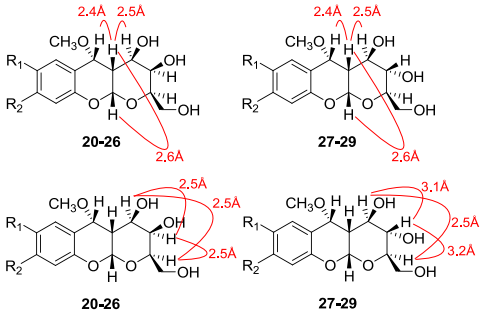

Fig. 5S. Average values for H2-H3, H2-H4, H3-H4, H4a-H10a and H5-H10a interproton distances. Concerning H2-H3 and H3-H4, compounds **20**-**29** can be clustered into two groups (bottom).

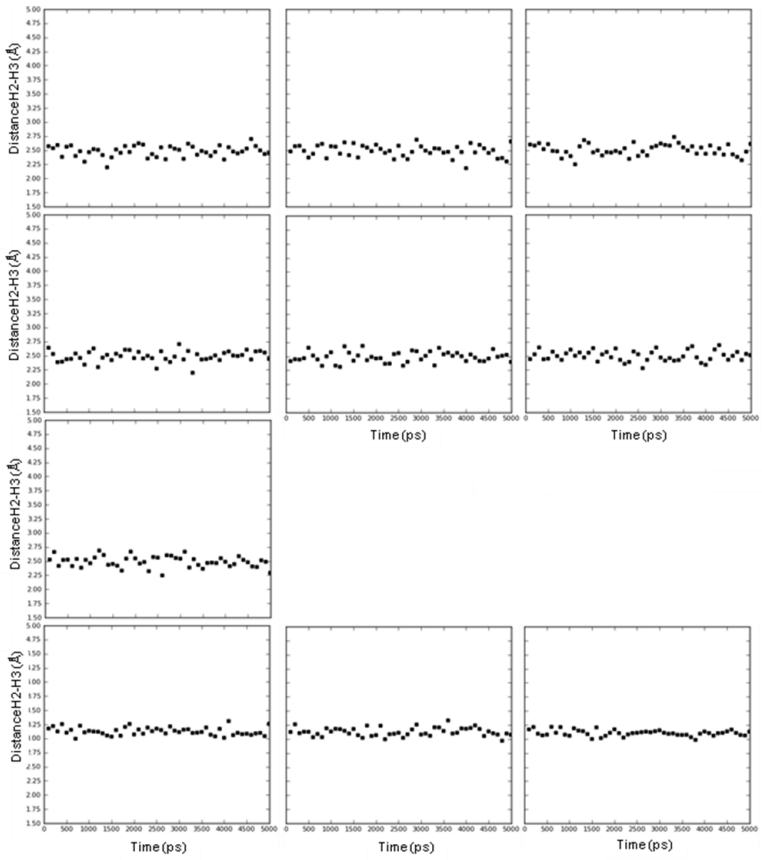

Figure 6S. H2-H3 distance (Å). **A**, compound **20**; **B**, compound **21**; **C**, compound **22**; **D**, compound **23**; **E**, compound **24**; **F**, compound **25**; **G**, compound **26**; **H**, compound **27**; **I**, compound **28**; **L**, compound **29**.

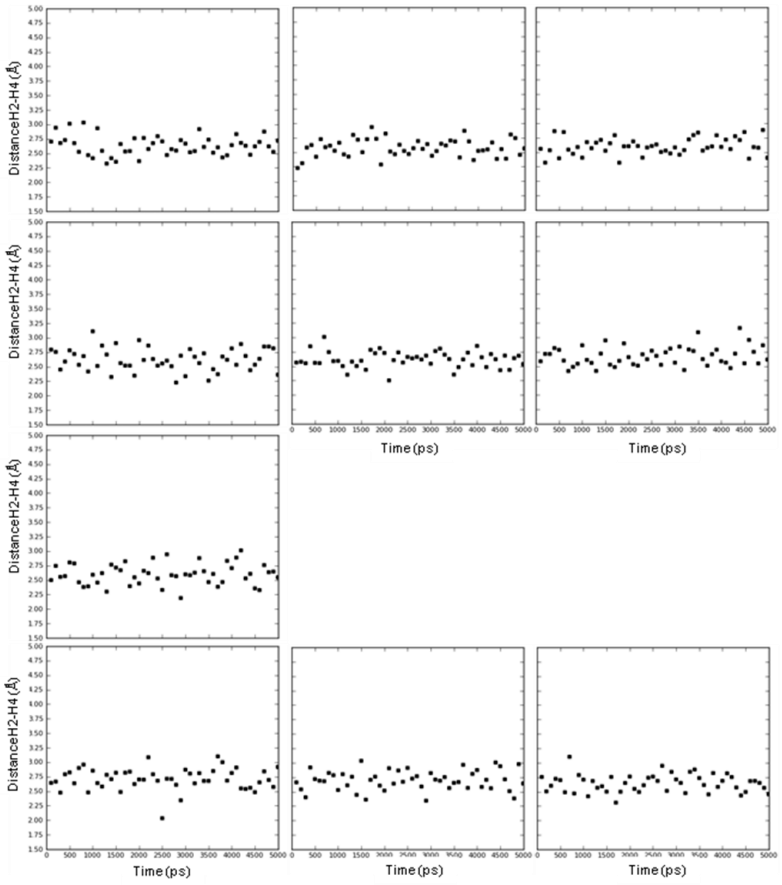

Figure 7S. H2-H4 distance (Å). **A**, compound **20**; **B**, compound **21**; **C**, compound **22**; **D**, compound **23**; **E**, compound **24**; **F**, compound **25**; **G**, compound **26**; **H**, compound **27**; **I**, compound **28**; **L**, compound **29**.

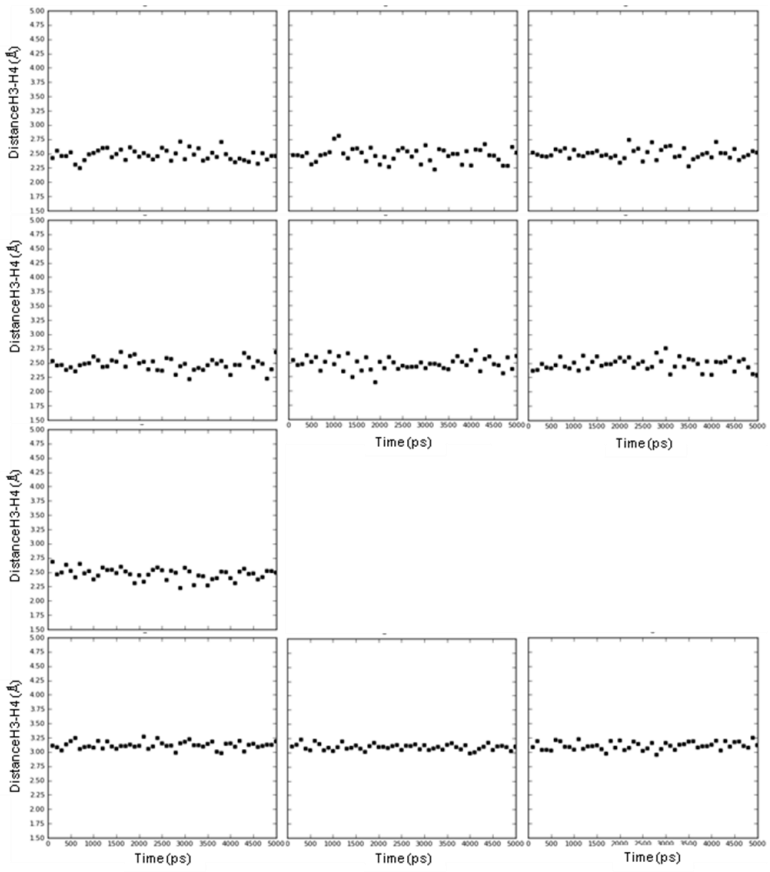

Figura 8S. H3-H4 distance (Å). **A**, compound **20**; **B**, compound **21**; **C**, compound **22**; **D**, compound **23**; **E**, compound **24**; **F**, compound **25**; **G**, compound **26**; **H**, compound **27**; **I**, compound **28**; **L**, compound **29**.

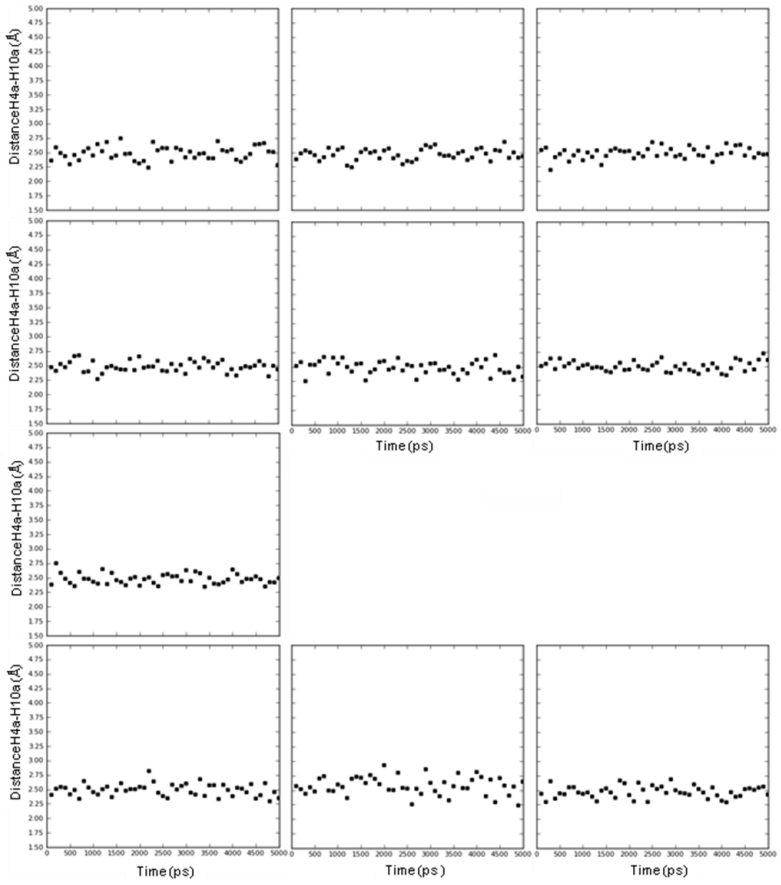

Figure 9S. H4a-H10a distance (Å). **A**, compound **20**; **B**, compound **21**; **C**, compound **22**; **D**, compound **23**; **E**, compound **24**; **F**, compound **25**; **G**, compound **26**; **H**, compound **27**; **I**, compound **28**; **L**, compound **29**.

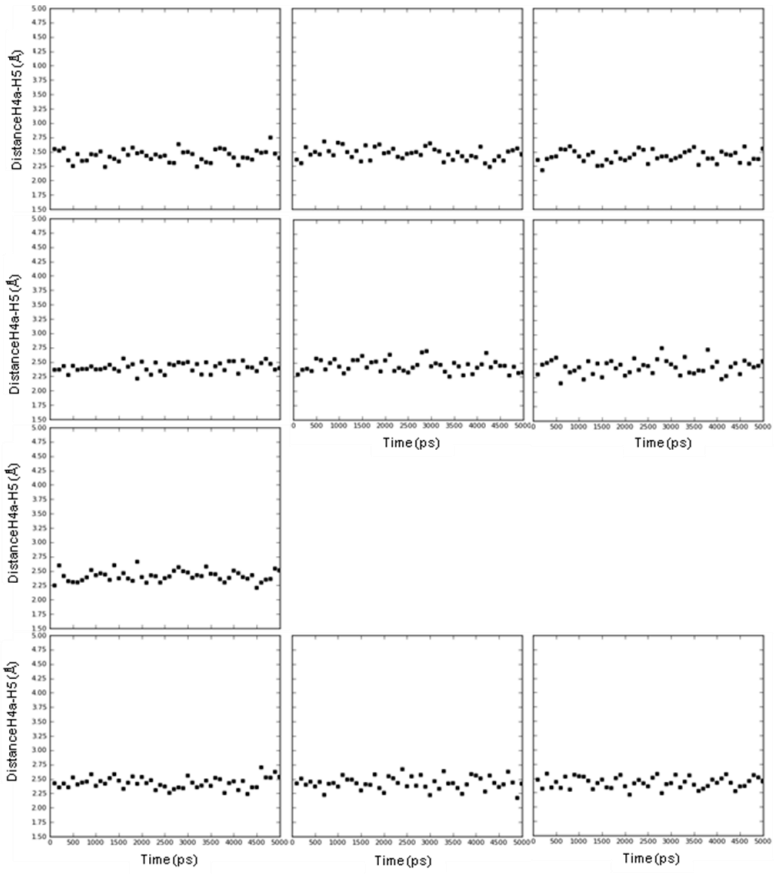

Figure 10S. H4a-H5 distance (Å). **A**, compound **20**; **B**, compound **21**; **C**, compound **22**; **D**, compound **23**; **E**, compound **24**; **F**, compound **25**; **G**, compound **26**; **H**, compound **27**; **I**, compound **28**; **L**, compound **29**.

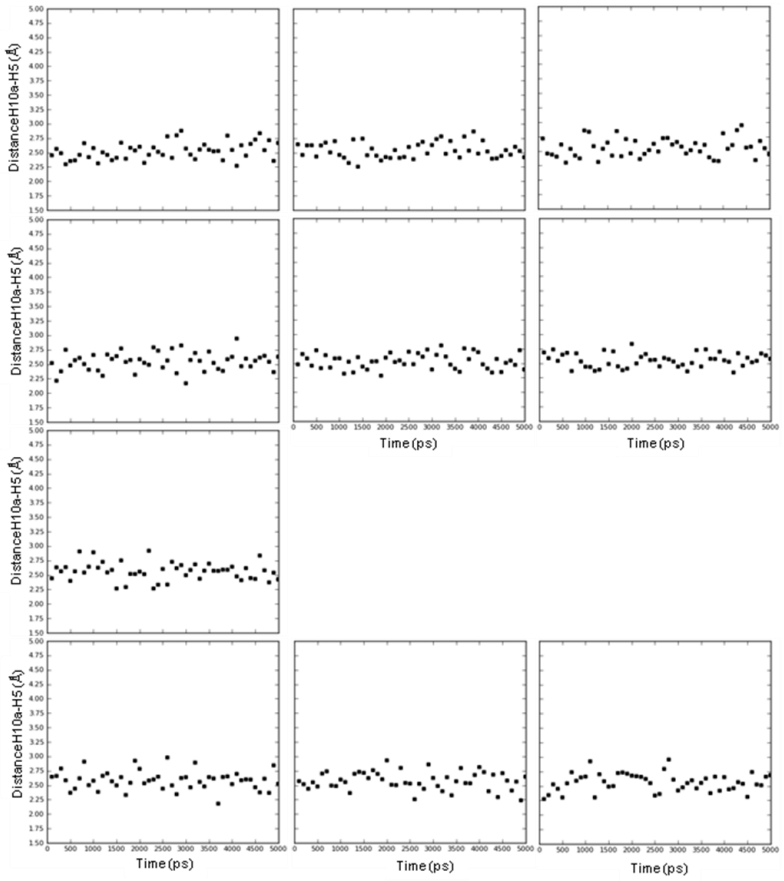

Figure 11S. H10a-H5 distance (Å). **A**, compound **20**; **B**, compound **21**; **C**, compound **22**; **D**, compound **23**; **E**, compound **24**; **F**, compound **25**; **G**, compound **26**; **H**, compound **27**; **I**, compound **28**; **L**, compound **29**.

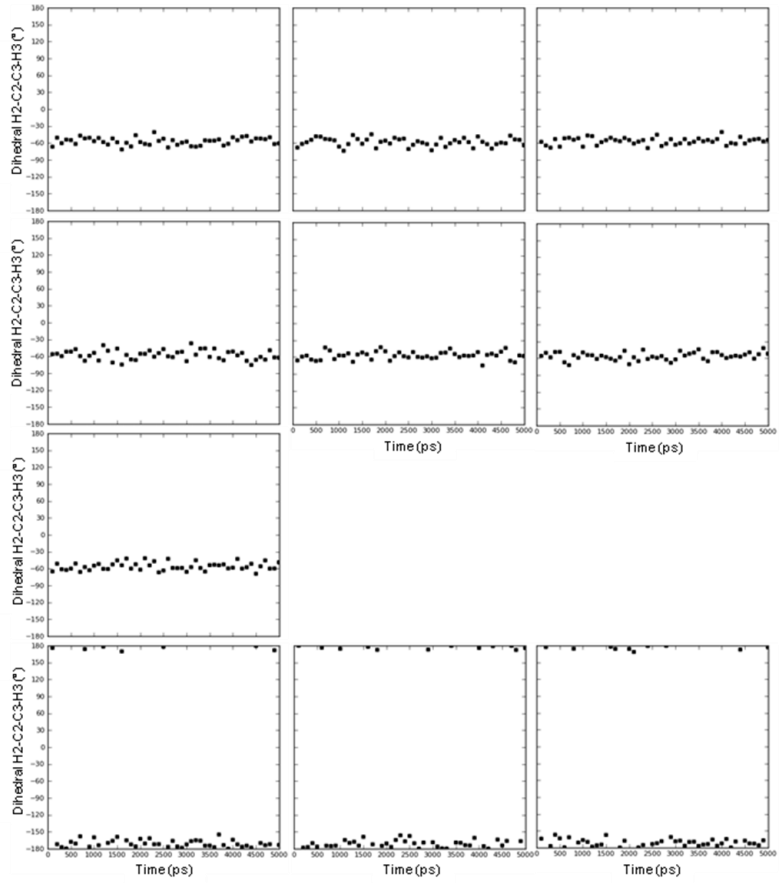

Figure 12S. H2-C2-C3-H3 dihedral angle (°). **A**, compound **20**; **B**, compound **21**; **C**, compound **22**; **D**, compound **23**; **E**, compound **24**; **F**, compound **25**; **G**, compound **26**; **H**, compound **27**; **I**, compound **28**; **L**, compound **29**.

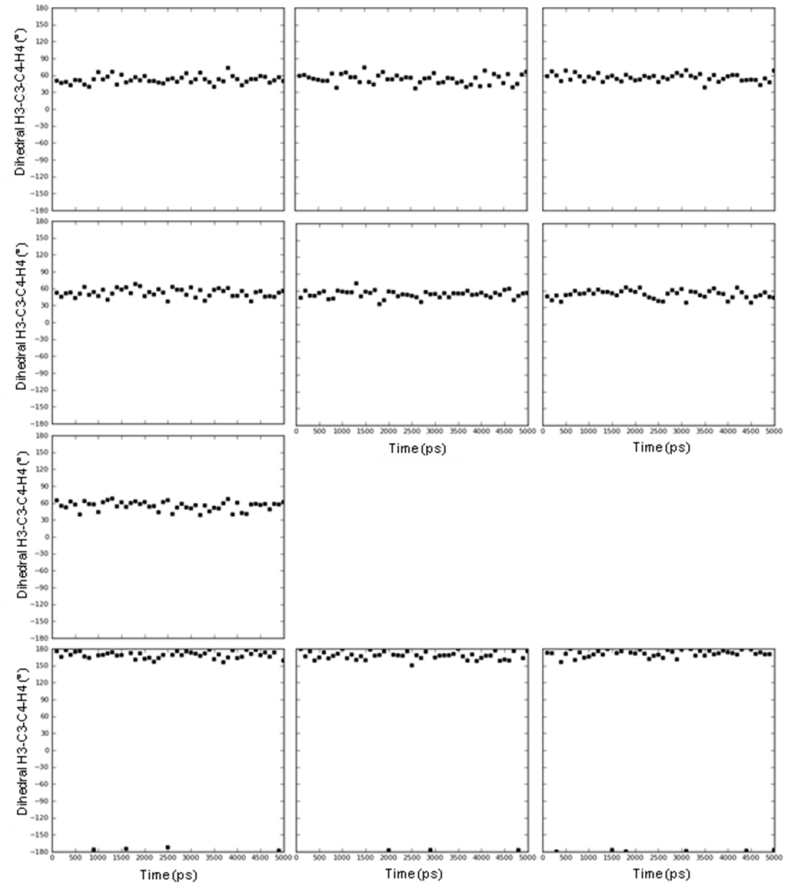

Figure 13S. H3-C3-C4-H4 dihedral angle (°). **A**, compound **20**; **B**, compound **21**; **C**, compound **22**; **D**, compound **23**; **E**, compound **24**; **F**, compound **25**; **G**, compound **26**; **H**, compound **27**; **I**, compound **28**; **L**, compound **29**.

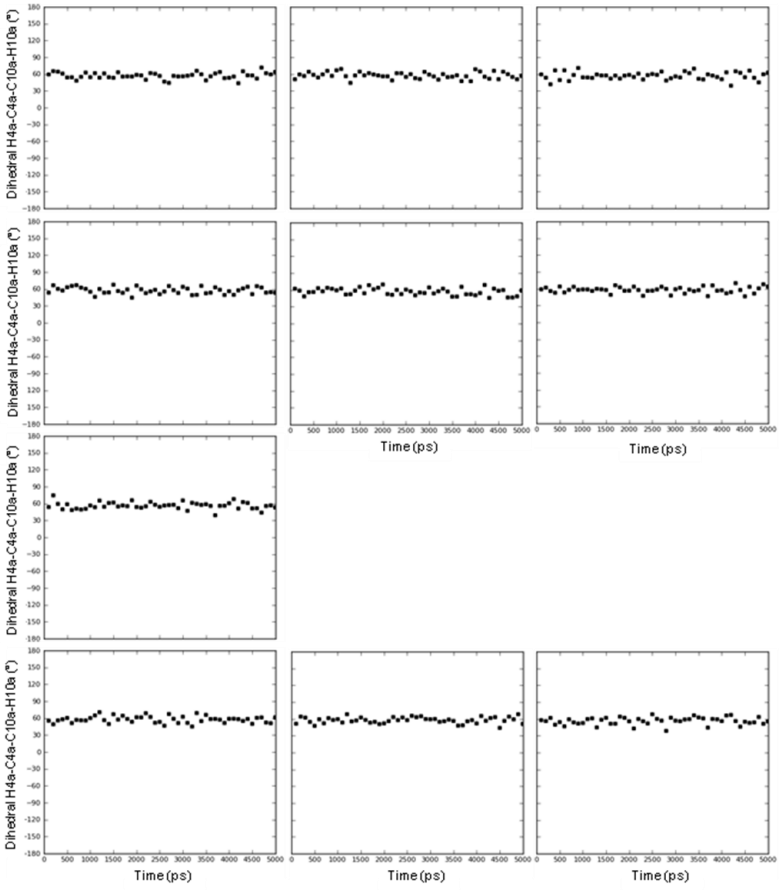

Figure 14S. H4a-C4a-C10a-H10a dihedral angle (°). **A**, compound **20**; **B**, compound **21**; **C**, compound **22**; **D**, compound **23**; **E**, compound **24**; **F**, compound **25**; **G**, compound **26**; **H**, compound **27**; **I**, compound **28**; **L**, compound **29**.

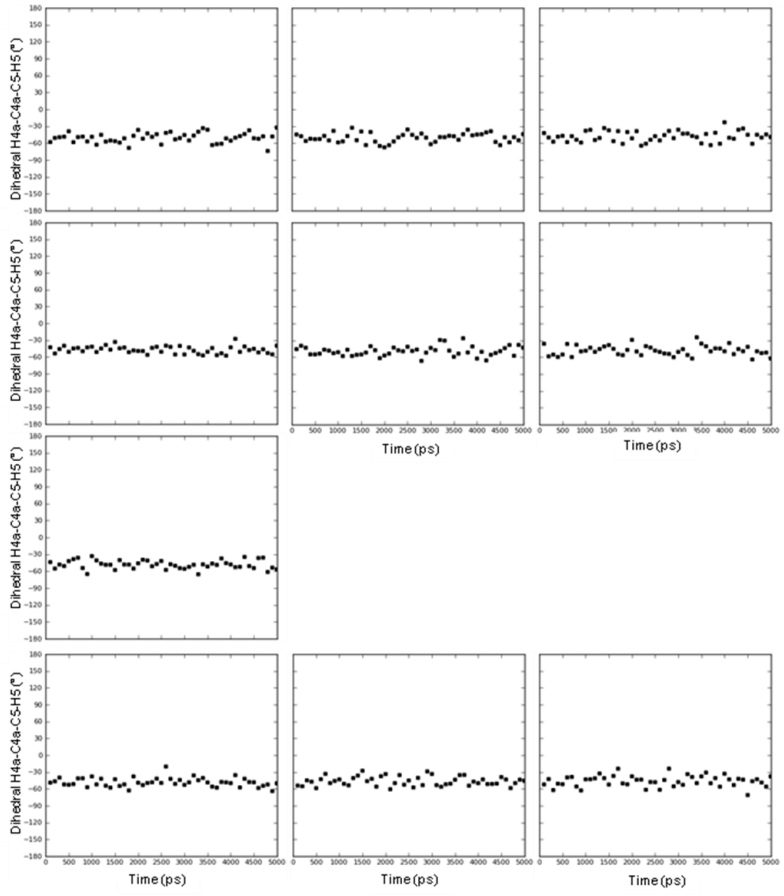

Figure 15S. H4a-C4a-C5-H5 dihedral angle (°).**A**, compound **20**; **B**, compound **21**; **C**, compound **22**; **D**, compound **23**; **E**, compound **24**; **F**, compound **25**; **G**, compound **26**; **H**, compound **27**; **I**, compound **28**; **L**, compound **29**.

PAPER 4

Submitted

FLUORESCENT AMYLOID BETA PEPTIDE LIGAND DERIVATIVES AS POTENTIAL DIAGNOSTIC TOOLS FOR ALZHEIMER DISEASE

Cristina Airoldi,[1] Francisco Cardona,[1,2] Erika Sironi,[1] Laura Colombo,[3] Mario Salmona,[3] Ilaria Cambianica,[4] Francesca Ornaghi,[4] Giulio Sancini,[4] Francesco Nicotra,[1] Barbara La Ferla.[1]

[1]Department of Biotechnology and Biosciences, University of Milano – Bicocca, Piazza della Scienza 2, 20126 Milano, Italy; [2]Department of Chemistry, University of Aveiro, Campus Universitario de Santiago, 3810-193 Aveiro, Portugal; [3]Department of Molecular Biochemistry and Pharmacology, Mario Negri Institute for Pharmacological Research, Via La Masa 19, 20156 Milan, Italy; [4]Department of Experimental Medicine, University of Milano – Bicocca, via Cadore 48, 20052 Monza, MB, Italy.

Abstract

Aβ-peptide ligands based on a cis-glycofused benzopyran structure have been fluorescently labeled using coumarine derivatives. Compounds **3** and **4** conserved their binding ability to β-amyloid peptides, as shown by NMR experiments. Moreover, exploiting its fluorescent property, it was demonstrated that compound **3** was able to cross an *in vitro* model of blood brain barrier and to stain Aβ-deposits.

Introduction

Among the neurodegenerative diseases, Alzheimer disease (AD) is the most common and the principal cause of dementia in the elderly population.[1,2,3,4,5] One of the key pathological features of the disease is the abnormal production of β-amyloid peptides

[1] R. Brookmeyer, M. M. Corrada, F. C. Curriero and C. Kawas, *Archives of Neurology*, 2002, **59**, 1764-1767.
[2] R. Brookmeyer, S. Gray and C. Kawas, *American Journal of Public Health*, 1998, **88**, 1337-1342.
[3] C. L. Masters, R. Cappai, K. J. Barnham and V. L. Villemagne, *Journal of Neurochemistry*, 2006, **97**, 1700-1725.
[4] D. J. Selkoe, *Neuron*, 2001, **32**, 177-180

(Aβ) and their subsequent accumulation as aggregates in the forms of oligomers, fibrils and finally plaques which induce neurodegeneration.[6] In our previous work[7] we identified cis-glyco-fused benzopyran compounds as new Aβ-peptide ligands. These compounds maintained the aromatic feature which is present in a wide range of small molecules able to interact with Aβ-peptide and which seems to be crucial for the binding ability[8,9,10] and, at the same time, possess a glycofused entity which confers them ideal water solubility properties. Moreover, the glycidic moiety assures further possible derivatizations, such as conjugation to other molecular entities (nanoparticles, polymeric supports, etc.), which may be exploited as useful features for diagnostic and therapeutic purposes. The binding ability of these compounds to Aβ1-42 peptide, demonstrated by NMR experiments, represents a fundamental but not unique feature for the development of a potential diagnostic/therapeutic tool. In order to be useful such compounds should perform their action within the brain, therefore they have to be able to cross the blood brain barrier (BBB). The BBB is formed by the complex tight junctions between the endothelial cells of the brain capillaries and their low endocytic activity. This results in the capillary wall that behaves as a continuous lipid bilayer and prevents the passage of polar and lipid insoluble substances. Unlike the most of the tissue, the BBB prevents the paracellular passage, thus the small molecule should pass exploiting a transcellular mechanism. It is, therefore, the major obstacle to drugs that may combat diseases affecting the CNS.[11] Only few compounds with the correct hydrophilic/lypophilic balance have a greater chance to overcome the BBB through a diffusion mechanism.

---

[5] S. S. Sisodia and P. H. St George-Hyslop, *Nature Reviews Neuroscience*, 2002, **3**, 281-290.
[6] C. Airoldi, E. Sironi, B. La Ferla, F. Cardona, F. Nicotra, *Curr. Bioact. Compd*., 2011, **7**(3), 198-213
[7] C. Airoldi, F. Cardona, E. Sironi, L. Colombo, M. Salmona, A. Silva, F. Nicotra, B. La Ferla*, Chem Commun,* 2011, **47***,* 10266-10268
[8] F. Re, C. Airoldi, C. Zona, N. Quattrocchi, B. La Ferla, F. Nicotra, M. Masserini, *Curr. Med Chem*., 2010, **17**, 2990-3006
[9] C. Airoldi, C. Zona, E. Sironi, L. Colombo, M. Messa, D. Aurilia, M. Gregori, M. Masserini, M. Salmona, F. Nicotra, B. La Ferla, *J. Biotechnology,* 2010, **156**, 317-324
[10] C. Airoldi, L. Colombo, C. Manzoni, E. Sironi, A. Natalello, S.M. Doglia, G. Forloni, F. Tagliavini, E. Del Favero, L. Cantù, F. Nicotra, M. Salmona, *Org. Biomol. Chem*., 2011, **9**, 463-472.

The main mechanisms allowing the transport of drugs across the BBB account for (I) passive diffusion for small lipophilic drugs which may enter by penetrating the luminal and abluminal membranes, (II) active carrier-mediated, (III) receptor mediated transport, or (IV) via adsorption-mediated transcytosis, for non diffusible molecules. The net uptake of a drug by the brain via the BBB depends on the overall difference between the uptake and efflux processes. The uptake is controlled by several factors, including the systemic disposition of the drug and the properties of endothelial cells. The permeability of endothelial cells and their capacity to metabolize drugs actively control the amounts of drug crossing the BBB. Permeability is controlled by several properties of the endothelial cells. There is no paracellular movement of drugs because of the tight junctions linking the endothelial cells, but small lipophilic drugs (<600 Da) may enter the brain by penetrating the lipid membrane of the endothelial cells. The passive diffusion of a drug depends on its blood/brain concentration gradient and its lipid solubility, but it is inversely related to its degree of ionization and its molecular weight. Factors other than lipophilicity and molecular weight also modulate the transport of a drug across the BBB. Reducing the relative number of polar groups increases the transfer of a drug across the BBB.[11]

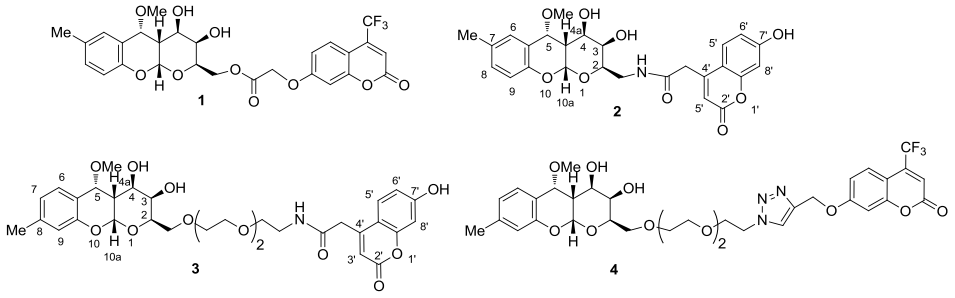

Figure 1: Fluorescent derivatives of Aβ-peptides ligands

In this work we designed and synthesized the fluorescent derivatives **1**, **2**, **3**, **4** (**figure 1**), in order to perform BBB passage studies. Moreover, the presence of the fluorophore

[11] J.M. Scherrmann, *Vascul Pharmacol*., 2002, **38**(6), 349-54.

allowed us to study the ligands' ability to stain Aβ deposits in Tg CRND8 mice. The choice of the fluorophore was done in order to modulate the hydrophilic properties of the molecule, maintaining the molecular weight low enough for a diffusion mechanism. For this reason we selected coumarine derivatives **7, 11** and **18** (**figure 2**). We exploited the primary hydroxyl group of the glycidic moiety to perform the linkage, since, as expected, previous binding studies confirmed that the sugar moiety was not or very poorly involved in the binding with the Aβ-peptide[7].

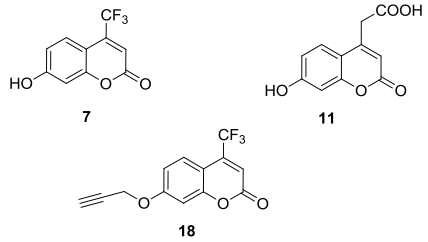

Figure 2: Coumarine derivatives.

Synthesis

Our first approach was focused on the direct conjugation of the fluorophore to the Aβ peptide ligand. Among the previously[7] identified ligands, compounds bearing the methyl substituent at position C7 and/or C8 of the aromatic ring showed the best binding properties, thus these compounds were used in the present work. For the synthesis of compound **1** (**scheme 1**), ligand **5** was regioselectively acylated with bromoacethylbromide at low temperature (-45°C) affording compound **6**, that was reacted with coumarine derivative **7** in basic conditions ($CsCO_3$) to afford the final product with a 20%, not optimized, overall yield. For the synthesis of compound **2** (**scheme 1**), we first converted the primary hydroxyl to the corresponding amine **10**, by a tosylation (TsCl, Py) followed by a nuclephylic azide substitution (NaN_3, DMF) and final reduction (H_2, Pd-Lindlar, MeOH). Compound **10** was then coupled with coumarine derivative **11,** using standard coupling conditions (DIC, HBTU, DIPEA, DMF dry) affording the final product **2**.

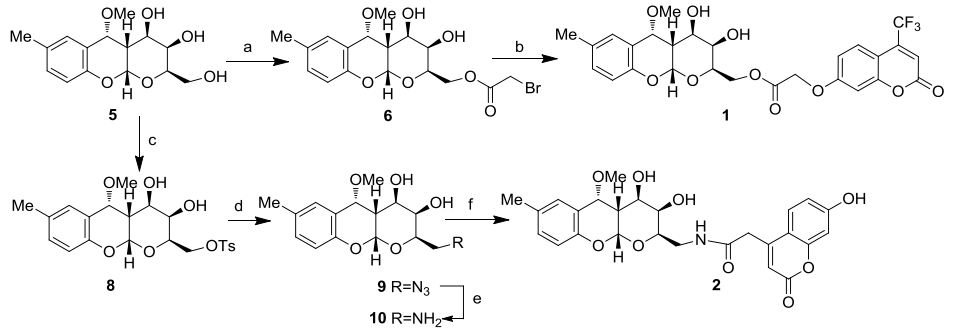

Scheme 1: reagents and conditions a) $BrCH_2COBr$, dry DMF, sym-collidine, -45°C, 40min., 54%; b) **7**, $CsCO_3$, dry DMF, r.t., 1h, 37%; c) TsCl, DMAP, dry Py, 0°C-r.t., 12h, 98%; d) NaN_3, dry DMF, 100°C, 12h, 60%; e) H_2, Pd- Lindlar, MeOH, r.t., 1h; f) **11**, DIC, HBTU, DIPEA, dry DMF, r.t., 47% (over two steps).

In order to verify the influence of the fluorophore on the binding properties to Aβ peptides, STD NMR experiments were carried out on both compounds.

Unfortunately, compound **1** resulted chemical unstable, as it is hydrolyzed immediately after dissolution in aqueous buffer (data not shown), probably because of the presence of the ether linkage in α position to the ester group.

Conversely, compound **2** resulted stable to hydrolysis and its interaction with Aβ1-42 was investigated by STD NMR experiments.[12]

NMR binding studies were carried out employing the same methodology previously described [7,9,10]. In particular, compound **2** ability to interact with Aβ1-42 oligomers was assessed by STD-NMR spectroscopy. STD-NMR experiments were performed using a ligand : peptide 10 : 1 mixture dissolved in deuterated PBS, pH 7.4, 37°C. The mixture was analyzed irradiating the sample at -1.0 ppm to achieve the selective saturation of

[12] a) M. Mayer, B. Meyer, *Angew. Chem*., *Int. Ed*., 1999, **38**, 1784–1788; b) B. Meyer, T. Peters, *Angew. Chem., Int. Ed*., 2003, **42**, 864–890; c) F. Peri, C. Airoldi, S. Colombo, S. Mari, J. Jimenez-Barbero, M. Martegani, F. Nicotra, *Eur. J. Org. Chem*., 2006, **16**, 3707-3720; d) C. Airoldi, A. Palmioli, A. D'Urzo, S. Colombo, M. Vanoni, E. Martegani and F. Peri, *ChemBioChem*, 2007, **8**, 1376–1379; e) A. Palmioli, E. Sacco, C. Airoldi, F. Di Nicolantonio, A. D'Urzo, S. Shirasawa, T. Sasazuki, A. Di Domizio, L. De Gioia, E. Martegani, A. Bardelli, F. Peri and M. Vanoni, *Biochem. Biophys. Res. Commun*., 2009, **386**, 593–597; f) C. Airoldi, S. Sommaruga, S. Merlo, P. Sperandeo, L. Cipolla, A. Polissi and F. Nicotra, *Chem.–Eur.*

some aliphatic resonances of Aβ oligomers. In general, the presence of NMR signals of the test molecule in the STD spectrum is a clear demonstration of the existence of interaction. Conversely, the absence of compound resonances in the STD spectrum indicates that the molecule is not an Aβ ligand. Different NMR resonances of compound **2** appeared in the STD spectrum recorded in the presence of Aβ oligomers (**Fig. 3**), thus showing its ability to recognize and bind Aβ1–42.

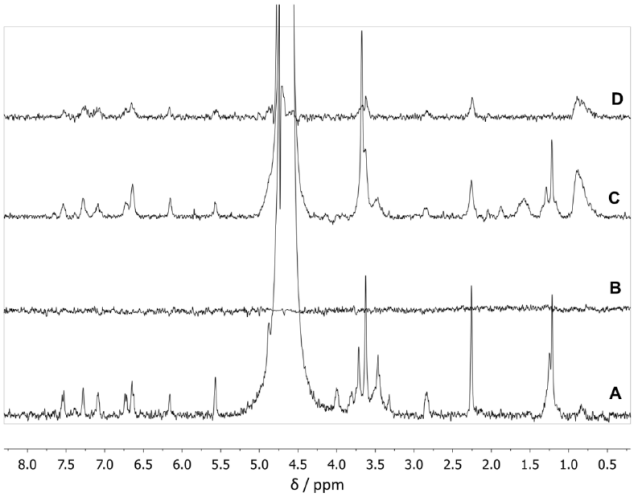

Figure 3. A) ^{1}H NMR spectrum of the compound **2** (0.5 mM) in PBS, pH 7.4, 37° C; B) blank STD-NMR spectrum of compound **2** acquired with a saturation time of 3.0 s and 2304 scans; C) ^{1}H NMR spectrum of the mixture containing the peptide Aβ1-42 (50 uM) and compound 2 (0.5 mM) in PBS, pH = 7.4, 37° C; D) STD-NMR spectrum acquired on the same mixture with a saturation time of 3.0 s and 2304 scans.

STD experiments evidenced the binding ability of compound **2**, even if its STD signals were rather low in intensity, probably due to solubility problems in physiological conditions. The poor quality of STD spectrum prevented the obtainment of a detailed epitope mapping and the acquisition of further NMR interaction experiments. In order to overcome the limitations encountered for derivatives **1** and **2**, we planned to

J., 2010, **16**, 1897–1902; g) R. Caraballo, H. Dong, J. P. Ribeiro, J. Jiménez-Barbero, O. Ramstrom, *Angew. Chem., Int. Ed*., 2010, **49**, 589–593; h) C. Airoldi, S. Giovannardi, B. La Ferla, J. Jiménez-Barbero, F. Nicotra, *Chem. Eur. J.,* 2011, **17**, 13395-13399.

introduce a triethylen spacer between the ligand and the fluorophore. This should increase both water solubility and chemical stability, avoiding the liable α-oxy ester group. For the preparation of this second set of derivatives we used Aβ peptide ligand **12** (**scheme 2**), that in our previous work showed the same binding properties of compound **5**, but a more straightforward preparation from commercially available reagents. Secondary hydroxyls were protected with an isopropyliden group (DMP, CH_3CN, CSA) and the free primary hydroxyl was reacted with triethylen derivative **14**[[13]] (NaH, DMF), to afford intermediate compound **15**. Removal of the protecting group (p-TsOH, H_2O:CH_3CN (0,5/1,5:v/v)), afforded derivative **16** bearing an azido functionality at the end of the triethylene moiety. For the synthesis of compound **3** the azido group was reduced (H_2, Pd-Lindlar) and the resulting amine **17** was coupled with coumarine derivative **11** (DIC, HBTU, DIPEA, DMF), while for the preparation of compound **4** the azido group was exploited in a chemoselective click cycloaddition reaction ($CuSO_45H_2O$, sodium ascorbate, t-BuOH:THF(1/1:v/v)) with the alkyne coumarine derivative **18**, obtained from **7** through propargylation of phenolic OH (supporting inf.).

[[13]] C. Tahtaoui, I. Parrot, P. Klotz, F. Guillier, J-L. Galzi, M. Hibert, B. Ilien, *J. Med. Chem*., 2004 , **47**(17), 4300 – 4315.

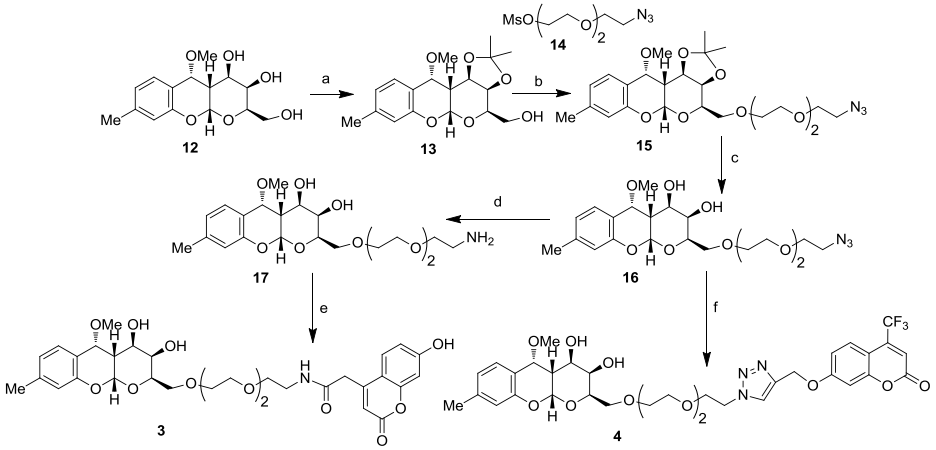

Scheme 2: reagents and conditions a) DMP, CSA, dry CH_3CN, r.t., 1h, 60% ; b) **14**, NaH 60%, dry DMF, 100ºC, 12h, 75%; c) p-TsOH, H_2O:CH_3CN (0,5/1,5:v/v), r.t., 30min., 90%; d) H_2, Pd-Lindlar, MeOH, r.t, 1h, 90%; e) **11**, DIC, HBTU, DIPEA, dry DMF, r.t., 12h, 20%; f) **18**, $CuSO_4 5H_2O$, sodium ascorbate, t-BuOH:THF(1/1:v/v), r.t., 12h, 55%.

As expected, the solubility of compound **3** in water allowed to perform both STD and trNOESY[9,10,12b,12c] NMR experiments. Both the techniques were applied on a sample containing Aβ1-42 and compound **3** dissolved in deuterated PBS, pH 7.4, 25°C at the final concentrations of 80 μM and 0.5 mM respectively. Figure 4 reports the STD spectra recorded with five different saturation times (**D**, 3.0 s; **E**, 2.0 s; **F**, 1.2 s; **G**, 0.7 s; **H**, 0.3 s).

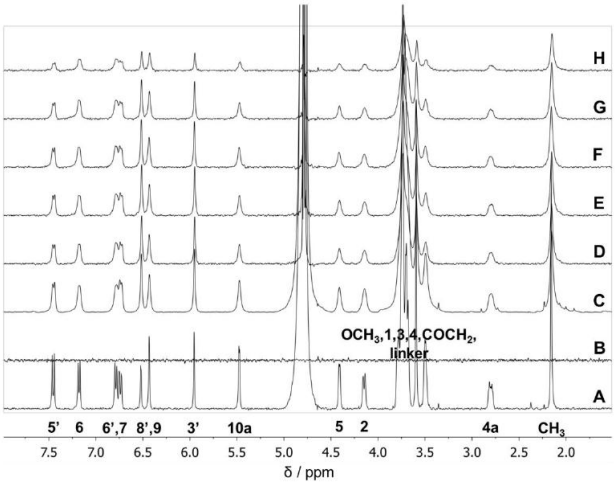

Figure 4. **A)** ^{1}H NMR spectrum of a solution of compound **3** (0.5 mM); **B)** blank STD-NMR spectrum of the same solution acquired with 3.0 s of saturation time; **C)** ^{1}H NMR spectrum of the mixture containing Aβ1-42 (80 uM) and compound **3** (0.5 mM) in PBS, pH=7.5, 25°C; **D**-**H)** STD-NMR spectra of the same mixture acquired with different saturation times. (**D**, 3.0 s; **E**, 2.0 s; **F**, 1.2 s; **G**, 0.7 s; **H**, 0.3 s).

STD spectra clearly demonstrated compound **3** ability to recognize and bind Aβ oligomers. The existence of interaction was also supported by the broadening of molecule **3** resonances when the compound was dissolved in the presence of the peptide (compare spectra **3 A** and **3 C**). This broadening reflects a decrease in proton relaxation times due to the formation of a receptor-ligand complex.

To map the ligand binding epitope, the STD spectrum acquired with a saturation time of 0.3 s was analysed to minimize the effect of relaxation on STD intensities[[14]]. **Figure 5** reports schematically the fractional STD effect for some ligand protons (or groups of protons), calculated as $(I_0 - I)/I_0*100$, where I is the intensity of the monitored signal in the STD spectrum and I_0 is the intensity of the same signal in a reference spectrum. The region of the ligand presenting the higher fractional STD effect (value around 40%), is the aromatic ring of the tricycline, thus resulting the ligand structural moiety mainly

[[14]] J. Yan, A. D. Kline, H. Mo, M.J. Shapiro, E.R. Zartler, *Journal of Magnetic Resonance*, 2003, **163**(2), 270–276.

involved in the interaction with Aβ, this achievement is in agreement with data obtained for the non-functionalized ligand[7]. Also the coumarine moiety participates to the interactions, but its contribution is less significant.

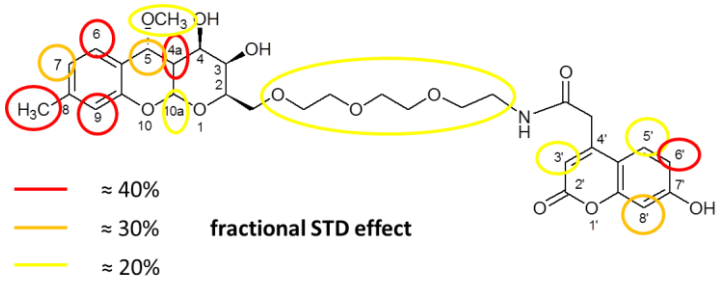

Figure 5. Fractional STD effects calculated for different protons of compounds **3**.

The binding was further assessed by trNOESY experiments. A blank NOESY spectrum of compound **3** was recorded in the absence of the Aβ1-42 peptide (**Figure 6A**). An inversion of the sign of its NOESY cross-peaks was observed between both spectra, passing from positive (red color), in the absence of Aβ1-42 peptide (**Figure 6A**), to negative (blue color) in the presence of Aβ1-42 peptide (**Figure 6B**). This change is due to an increase of the effective rotational motion correlation time of the molecule in the presence of the Aβ oligomers, that demonstrated the existence of a binding between the small molecule and Aβ aggregates.[10,12b]

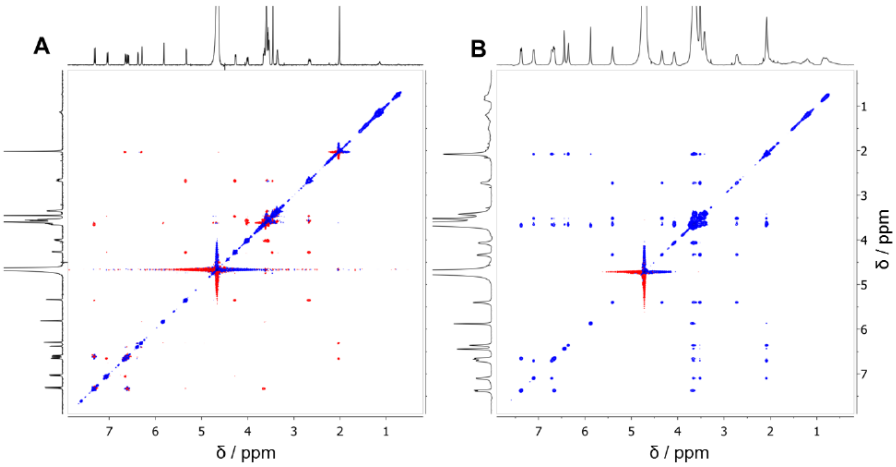

Figure 6 (A) 2D-NOESY spectrum of compound **3** dissolved in deuterated PBS, pH 7.5, 25°C, mixing time 0.9 s; (B) trNOESY of mixture containing Aβ1-42 (80 uM) and compound 3 (0.5 mM) dissolved in deuterated PBS, pH 7.5, 25°C, mixing time 0.3 s. Positive cross-peaks are red, negative ones blue.

The solubility of compound **4** in aqueous buffer was very poor. In particular, NMR binding experiments were performed on a sample containing the test molecule at a concentration of 0.5 mM in PBS, pH=7.5, 25°C, to which 5% of d^6-DMSO was added to promote its dissolution. Aβ1-42 peptide was added at a final concentration of 80 μM. In these conditions we obtained an STD spectrum of low quality (**Figure 7A-4**), but sufficient to assess the existence of interaction with Aβ1-42 peptide. The binding was further supported by the significant broadening of compound **4** ^{1}H resonances, observed when the molecule was dissolved in the presence of Aβ oligomers; this effect results evident from the comparison of the ^{1}H spectrum recorded in the absence (**Figure 7A-1**), with the spectrum acquired in the presence of Aβ1-42 peptide (**Figure 7A-3**). In addition, we could exploit the presence of the CF_3 substituent on the coumarine moiety, as a dramatic change also in its line width can be observed when the ^{19}F spectrum of the molecule alone (**Figure 7B-1**) is compared with the corresponding spectrum acquired on the ligand:receptor mixture (**Figure 7B-2**).

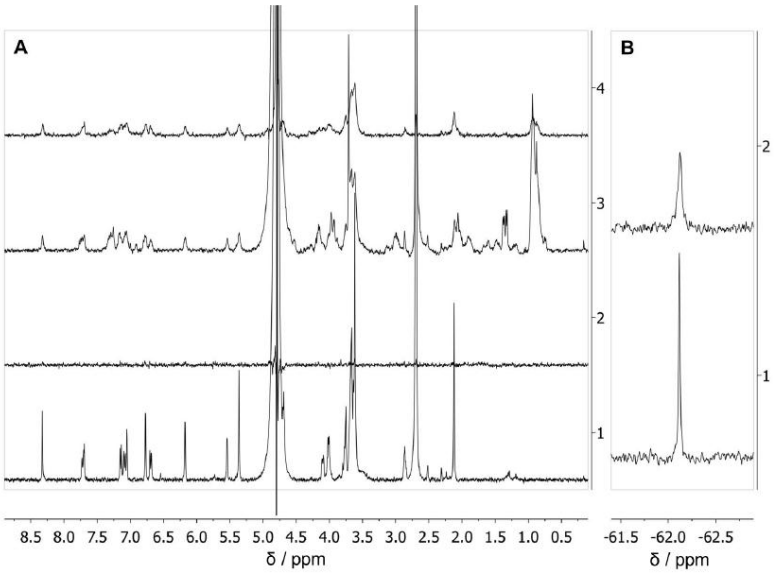

Figure 7. A-1) ^{1}H NMR spectrum of the compound **4** (0.5 mM); A-2) blank STD-NMR spectrum of compound **4** acquired with a saturation time of 2.0 s and 5200 scans; A-3) ^{1}H NMR spectrum of the mixture containing the peptide Aβ1-42 (80 uM) and compound **4** (0.5 mM); A-4) STD-NMR spectrum acquired on the same mixture with a saturation time of 2.0 s and 5200 scans. B) ^{19}F spectra of compound **4** dissolved in the absence (**1**) or in the presence (**2**) of Aβ oligomers. Samples were dissolved in PBS, pH=7.5, 25°C, adding 5% of d6-DMSO.

Transport Experiments

Evaluation of drug transport to the brain *in vitro* has usually been carried out by studying the transport of individual molecules across endothelial cell monolayers. Currently available *in vitro* models for BBB allow to evaluate quickly and in a reproducible way the predictive *in vivo* permeability of compounds and drugs under development.

The development of a cell culture system that mimics an *in vivo* BBB requires endothelial cells to be cultured on microporous supports. hCMEC/D3 cells (passages 25-35) were seeded on 12-well Transwell® inserts coated with type I collagen in a density of $5x10^{4}$ cells/cm^{2} and cultured with 0.5 mL and 1 mL of culture medium in the upper

and in the lower chamber, respectively as previously described.[15] Cells were treated with compound **3** when the trans-endothelial-electrical resistance (TEER) value was found to be highest.

The functional properties of monolayers were assessed by measuring the endothelial permeability of sucrose (between 0-180 min) as previously described.[16] 0.5mL of 9,4 and 94 µM compound **3** were added to the upper chamber and incubated between 0 and 180 minutes. After these periods of incubation, the fluorescence in the upper and lower chambers was measured (λex = 280 nm) to calculate the endothelial permeability (PE) across the cell monolayers, taking account of the passage of compound **3** through the filter without cells. [16] Each experiment was performed at least in triplicate. All the transport studies have been replicated in the presence of a paracellular marker, [^{14}C]-sucrose, in order to monitor potential toxic effects on the BBB exhibited by compound **3**.

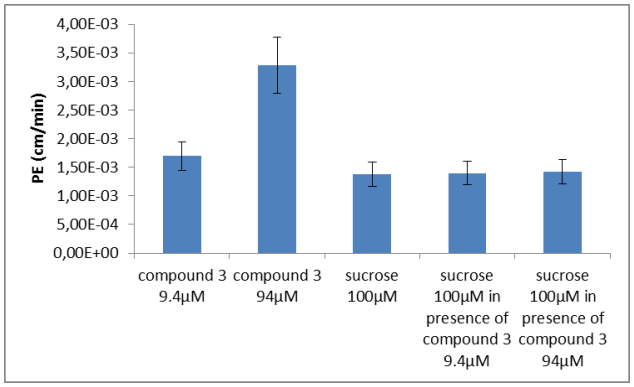

Figure 8: PE values across the hCMEC/D3 monolayers of compound **3** (9,4 and 94 µM) and PE values of sucrose (100µM) alone and in presence of compound **3**.

The amyloid β peptide ligand compound **3** does not affect the tightness of the hCMEC/D3 cell monolayer, since the TEER value (data not shown) and the permeability

[15] F. Re, I. Cambianica, C. Zona, S. Sesana, M. Gregori, R. Rigolio, B. La Ferla, F. Nicotra, G. Forloni, A. Cagnotto, M. Salmona, M. Masserini, G. Sancini. *Nanomedicine*, 2011, **7**(5), 551-559.

[16] R. Cecchelli, B. Dehouck, L. Descamps, L. Fenart, V. Buée-Scherrer, C. Duhem, S. Lundquist, M. Rentfel, G. Torpier , M. P. Dehouck, *Adv. Drug Deliver Rev.*, 1999, **36**, 165–178.

of [^{14}C]-sucrose did not change, within the experimental error (<3%), during hCMEC/D3 incubation with compound **3** (PE sucrose = 1.38±0,1x10-3 cm/min; PE sucrose = 1,40±0,1x10^{-3} in presence of derivative **3**) (**Figure 8**).

hCMEC/D3 cells, grown on transwell membrane inserts, were incubated with compound **3** on day 12, when the maximal TEER value was registered (68±8 Ω·cm2). Transport of [^{14}C]-sucrose was measured, with PE values of 1.38±0,2x10^{-3} cm/min in agreement with the values reported in literature.[^{17}] Compound **3,** at different concentrations (9,4 and 94 μM), has been added in the upper compartment and the amount in the lower compartment has been measured over time at 0, 60 and 180 min. The PE of compound **3** across the cell monolayers was 3,03±1.19x10^{-3}cm/min and 1,69±0,59x10^{-3} cm/min and these values were strictly correlated to the administered amount within the upper compartment respectively 94 μM *vs* 9,4 μM. The PE of compound **3** were closer of that of the transcellular marker propranolol, a reference point in term of lypofilic compound which can permeate the BBB [^{17}]. Taking together these preliminary results might account for passive diffusion as the main mechanism allowing the transport of compound **3** across the BBB. Further experiments are needed for deeply investigate this issue.

Staining

The ability of the compound **3** to bind amyloid deposits was tested in brain sections from Tg CRND8 mice. These animals carry a human APP with double mutations and accumulate Aβ deposits in brain parenchyma and at cerebrovascular level. Cryostatic sections of 20 μm were obtained from fresh tissue, mounted on gelatin coated microscope slides and used for a staining assay. Solutions of EtOH:water 50:50 (v/v) of test compound were layered on tissue sections. Fluorescent sections were viewed using fluoromicroscope equipped with FITC and DAPI filters. Thioflavin T (ThT) at 3 μM was

[^{17}] B.Poller, H.Gutmann, S. Krähenbühl, B. Weksler, I.Romero, P. O.Couraud, G.Tuffin, J.Drewe, J.Huwyler, *J.Neurochem*. 2008, **107**, 1358-1368.

used as a reference. Compound **3** was able to label amyloid plaques at a concentration of 6 µM, obtaining a result comparable to Thioflavin T staining. These results suggested that compound **3** is able to recognize the β-pleated sheet structure of amyloid fibrils similarly to ThT and without being involved in aspecific binding to tissue preparations (**Figure 9**).

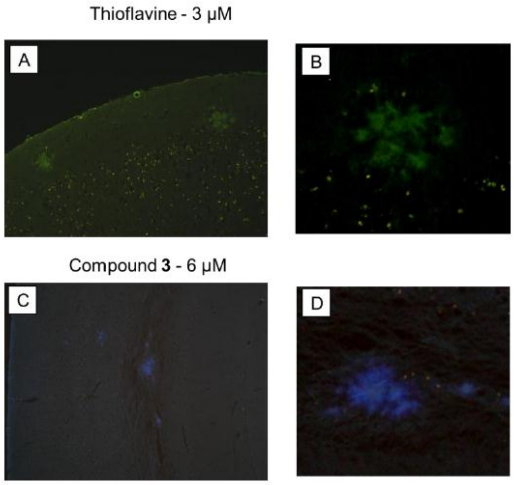

Figure 9. Brain sections of Tg CRND8 mice incubated with ThT (A-B) at 3 µM and compound **3** (C-D) at 6 µM. Fluorescent sections were viewed using fluoromicroscope FITC for ThT staining and DAPI for compound staining.

Conclusion

In conclusion, in this work we demonstrate through NMR experiments the preserved ability of derivatives **3** and **4** to bind Aβ peptides; moreover, fluorescency mesurements carried out with compound **3** indicate that its favorable physical–chemical properties, in terms of balanced hydrophylicity/lipophylicity, allow these compounds to permeate through the BBB, most probably exploiting a diffusion mechanism, and to stain amyloid plaques. These properties, taken together, suggest that these compounds could be very promising candidates for possible future applications both in the therapy and in the diagnosis of AD related diseases.

Acknowledgments

The research leading to these results has received funding from the European Community's Seventh Framework Programme (FP7/2007-2013) under grant agreement n° 212043 and from Regione Lombardia, Fondo per la promozione di accordi istituzionali, project no. 4779 ''Network Enabled Drug Design (NEDD)''. Francisco Cardona kindly acknowledges Fundaçao para a Ciencia e Tecnologia (FCT, Portugal) for the PhD grant (SFRH/44888/2008).

Supporting Information

Synthesis

General Remarks

All solvents were dried with molecular sieves for at least 24h prior to use. Thin layer chromatography (TLC) was performed on silica gel 60 F254 plates (Merck) with detection using UV light when possible, or by charring with a solution of concd. H_2SO_4/EtOH/H_2O (5:45:45) or a solution of $(NH_4)_6Mo_7O_{24}$ (21 g), $Ce(SO_4)_2$ (1 g), concd. H_2SO_4 (31 mL) in water (500 mL). Flash column chromatography was performed on silica gel 230-400 mesh (Merck). ^{1}H and ^{13}C NMR spectra were recorded at 25°C unless otherwise stated, with a Varian Mercury 400 MHz instrument. Chemical shift assignments, reported in ppm, are referenced to the corresponding solvent peaks. HRMS were recorded on a QSTAR elite LC/MS/MS system with a nanospray ion source. Optical rotations were measured at room temperature using an Atago Polax-2L polarimeter and are reported in units of 10^{-1} deg·cm2·g^{-1}.

General synthetic strategy for the synthesis of protected compounds **22** and **23:** (Airoldi, C.; Cardona, F.; Sironi, E.; Colombo, L.; Salmona, M.; Silva, A.; Nicotra, F.; La Ferla, B. *Chemical Communications* **2011**, *47*, 10266.)

A mixture containing the appropriate *O*-hydroxybenzaldehyde (**19-20**) (2.5 equiv.), trimethylorthoformiate (2.5 equiv.) and scandium triflate (3% mol) in CH_2Cl_2 is stirred at r.t. for 20 min. The mixture is then cooled at 0°C and tri-*O*-benzyl-D-galactal (**21**) is added. The reaction is then left stirring at r.t. for 30 min. The reaction is then diluted with CH_2Cl_2, washed with water, dried over Na_2SO_4, filtrated and the solvent is removed under reduced pressure. The crude is purified by flash chromatography, Toluene/AcOEt (9.75:0.25) to afford pure compounds **(22-23)**.

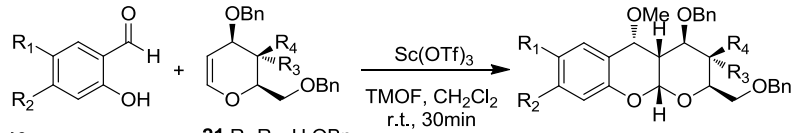

19 R_1,R_2= Me,H
20 R_1,R_2= H, Me

21 R_3,R_4=H,OBn

22 R_1,R_2,R_3,R_4= Me,H,H,OBn
23 R_1,R_2,R_3,R_4= H,Me,H,OBn

Compounds (22): yield 91%, C5 R/S 95/5

(22R)

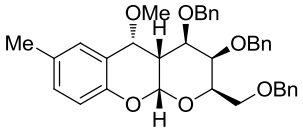

22R

^{1}H NMR (400 MHz, $CDCl_3$) δ 7.33 (d, *J* = 7.1 Hz, 1H, H6), 7.31 – 7.21 (m, 15H, Ar), 6.99 (d, *J* = 7.3 Hz, 1H, H8), 6.72 (d, *J* = 8.2 Hz, 1H, H9), 5.61 (d, *J* = 2.9 Hz, 1H, H10a), 4.96 (d, *J* = 11.4 Hz, 1H, OCH_2Ph), 4.74 (d, *J* = 4.5 Hz, 1H, H5), 4.62 – 4.33 (m, 5H, OCH_2Ph), 4.18 (t, *J* = 6.4 Hz, 1H, H2), 3.80 (s, 1H, H3), 3.66 (dd, *J* = 11.2, 2.6 Hz, 1H, H4), 3.61 (dd, *J* = 6.3, 4.1 Hz, 2H, CH_2O), 3.57 (s, 3H,OMe), 3.33 – 3.23 (m, 1H, H4a), 2.31 (s, 3H, Me). ^{13}C NMR (101 MHz, $CDCl_3$) δ 149.98, 139.05, 138.93, 138.16, 130.59, 129.64, 128.61, 128.43, 128.40, 128.36, 128.13, 127.97, 127.75, 127.52, 126.52, 121.97, 115.37, 97.63, 76.92, 76.33, 75.66, 75.16, 73.93, 73.71, 72.69, 71.65, 69.15, 57.1, 34.78, 20.99. $[\alpha]_D^{20}$= -5,2 (c=1, $CHCl_3$); MS: m/z calcd for $[M + H]^+$ = 567.3, $[M + Na]^+$ = 589.3, $[M + K]^+$ = 605.2; found $[M + H]^+$ = 567.6, $[M + Na]^+$ = 589.5, $[M + K]^+$ = 605.6.

(22S)

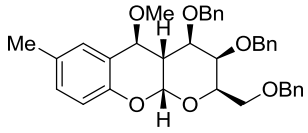

22S

^{1}H NMR (400 MHz, $CDCl_3$) δ 7.40 – 7.13 (m, 15H, Ar), 7.01 (dd, *J* = 8.3, 1.7 Hz, 1H, H8), 6.82 (s, 1H, H6), 6.75 (d, *J* = 8.3 Hz, 1H, H9), 5.66 (d, *J* = 3.2 Hz, 1H, H10a), 4.92 (d, *J* = 11.5 Hz, 1H, OCH_2Ph), 4.65 – 4.42 (m, 5H, OCH_2Ph), 4.37 – 4.30 (d, *J* = 2.0 Hz 1H, H5), 4.26 – 4.17 (m, 1H, H2), 3.98 (s, 1H, H3), 3.72 – 3.63 (m, 2H, CH_2O), 3.38 (s, 3H, ArOMe), 3.36 – 3.29 (dd, *J* = 2.38, 11.78 Hz, 1H, H4), 3.06 – 2.93 (m, 1H, H4a), 2.26 (s, 3H, Me). ^{13}C NMR (101 MHz, $CDCl_3$) δ 151.53, 138.81, 138.10, 137.77, 131.35, 131.03, 129.91, 128.64, 128.60, 128.54, 128.49, 128.26, 128.21, 128.01, 127.93, 127.82, 118.18, 116.64, 94.89, 75.00, 74.84, 74.80, 73.79, 71.55, 71.47, 71.35, 68.96, 56.42, 37.60, 29.93, 20.77. $[\alpha]_D^{20}$= -2,1 (c=1, $CHCl_3$); MS: m/z calcd for $[M + H]^+$ = 567.3, $[M + Na]^+$ = 589.3, $[M + K]^+$ = 605.2; found $[M + H]^+$ = 567.6, $[M + Na]^+$ = 589.5, $[M + K]^+$ = 605.6.

Compound (23): yield 45%, C5 R/S 100/0

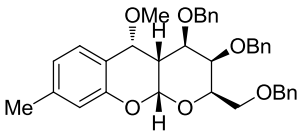

23

^{1}H NMR (400 MHz, $CDCl_3$) δ 7.42 (d, *J* = 7.8 Hz, 1H, H6), 7.37 – 7.20 (m, 15H, Ar), 6.81 (d, *J* = 7.8 Hz, 1H, H7), 6.66 (s, 1H, H9), 5.63 (d, *J* = 2.8 Hz, 1H, H10a), 4.97 (d, *J* = 11.4 Hz, 1H, OCH_2Ph), 4.74 (d, *J* = 4.2 Hz, 1H, H5), 4.62 – 4.34 (m, 5H, OCH_2Ph), 4.19 (t, *J* = 6.3 Hz, 1H, H2), 3.81 (s, 1H, H3), 3.66 (dd, *J* = 11.1, 2.6 Hz, 1H, H4), 3.62 (dd, *J* = 6.2, 4.6 Hz, 2H, CH_2O), 3.56 (s, 3H, OMe), 3.34 – 3.21 (m, 1H, H4a), 2.31 (s, 3H, Me). ^{13}C NMR (101 MHz, $CDCl_3$) δ 152.11, 139.20, 139.07, 139.00, 138.19, 128.61, 128.44, 128.41, 128.37, 128.12, 127.97, 127.94, 127.75, 127.51, 126.10, 122.28, 119.48, 116.04, 97.74, 76.22,

75.74, 75.16, 74.03, 73.70, 72.84, 71.69, 69.16, 57.06, 34.89, 21.41. $[\alpha]_D^{20}$= -6,2 (c=1, $CHCl_3$). MS: m/z calcd for $[M + K]^+$ = 605.2; found [$[M + K]^+$ = 605.2.

General synthetic strategy for the synthesis of compounds **5** and 1**2** (C5 R only): Airoldi, C.; Cardona, F.; Sironi, E.; Colombo, L.; Salmona, M.; Silva, A.; Nicotra, F.; La Ferla, B. *Chemical Communications* **2011**, *47*, 10266.

To a 6 mM solution of the protected compound in AcOEt/MeOH 1:1, previously degassed, $Pd(OH)_2$ 5% mol is added and the reaction mixture is stirred under H_2 atmosphere for 45min.-1.5 h. Then the catalist is removed by filtration and the solvent evaporated under reduced pressure to afford pure compounds (**5** and **12**)**.**

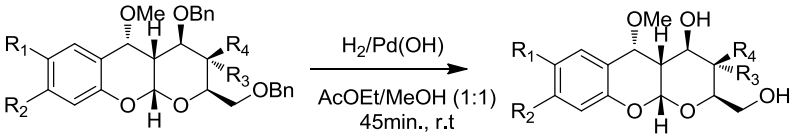

22 R_1,R_2,R_3,R_4= Me,H,H,OBn
23 R_1,R_2,R_3,R_4= H,Me,H,OBn

5 R_1,R_2,R_3,R_4= Me,H,H,OH
12 R_1,R_2,R_3,R_4= H,Me,H,OH

Compound (5): yield 95%

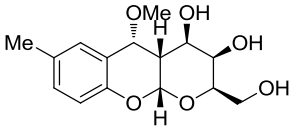

5

^{1}H NMR (400 MHz, CD_3OD) δ 7.24 (s, 1H, H6), 6.98 (d, *J* = 8.2 Hz, 1H, H8), 6.66 (d, *J* = 8.3 Hz, 1H, H9), 5.57 (d, *J* = 3.0 Hz, 1H, H10a), 3.98 (t, *J* = 6.0 Hz, 1H, H2), 3.83 – 3.78 (m, 2H, H3 and H4), 3.77 (dd, *J* = 6.0, 2.9 Hz, 2H, CH_2O), 3.68 (s, 3H, OMe), 2.96 – 2.89 (m, 1H, H4a), 2.26 (s, 3H, Me). ^{13}C NMR (101 MHz, CD_3OD) δ 150.14, 130.22, 129.54, 126.29, 120.97, 115.09, 96.65, 77.67, 72.66, 67.62, 67.37, 61.64, 57.73, 34.59, 19.57. $[\alpha]_D^{20}$= +13,3 (c=1, $CHCl_3$); MS: m/z calcd for $[M + Na]^+$ = 319.1, $[M + K]^+$ = 335.1; found $[M + Na]^+$ = 319.4, $[M + K]^+$ = 335.4.

Compound (12): yield 97%

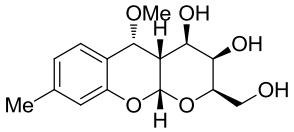

12

^{1}H NMR (400 MHz, CD_3OD) δ 7.29 (d,*J* = 7.8 Hz, 1H, H6), 6.76 (d, *J* = 7.8 Hz, 1H, H7), 6.60 (s, 1H, H9), 5.57 (d, *J* = 3.0 Hz, 1H, H10a), 4.85 (d, *J* = 4.7 Hz, 1H, H5), 3.98 (t, *J* = 5.9 Hz, 1H, H3), 3.83 – 3.73 (m, 4H, CH_2O, H2, H4), 3.67 (s, 3H, OMe), 2.96 – 2.85 (m, 1H, H4a), 2.25 (s, 3H, Me).

^{13}C NMR (101 MHz, CD_3OD) δ 156.14, 143.22, 133.19, 129.62, 125.66, 122.29, 119.72, 100.65, 81.54, 76.64, 71.24, 65.63, 61.61, 38.51, 23.91. $[\alpha]_D^{20}$= +8,3 (c=1, $CHCl_3$); MS: m/z calcd for $[M + Na]^+$ = 319.1; found $[M + Na]^+$ = 319.3.

Compound (6)

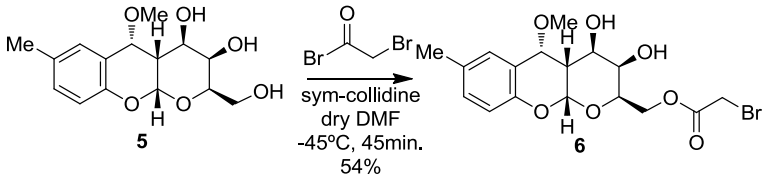

To a solution of compound **5** (90mg/0,303mmol) and 2,4,6-trimethylpyridine (0,424mmol/ 56uL) in dry DMF (1,68mL) with stirring at -45ºC a solution of Bromoacetyl Bromide (0,394mmol/34uL) in dry Toluene (200uL) was added. Stirring was continued for 40min. at -45ºC, and the the mixture was allowed to warm to room temperature. Toluene (12mL) was added, and the solids filtered off, and the filtrate concentrated. The residue was purified by flash chromatography Toluene/EtOAc (7:3) and EtOAc, affording 54% (68mg) of a white solid.

^{1}H NMR (400 MHz, $CDCl_3$) δ 7.22 (s, 1H, H6), 7.02 (d, *J* = 6.8 Hz, 1H, H8), 6.74 (d, *J* = 8.1 Hz, 1H, H9), 5.55 (d, *J* = 3.0 Hz, 1H, H10a), 4.81 (d, *J* = 4.7 Hz, 1H, H5), 4.50 (s, *J* = 5.3 Hz, 1H, CH_2), 4.49 (d, *J* = 1.2 Hz, 1H, CH_2), 4.28 (t, *J* = 5.3 Hz, 1H, H2), 4.04 – 3.95 (m,1H, H4),

3.95 – 3.84 (m, *J* = 7.2 Hz, 3H,CH_2Br and H3), 3.73 (s, 3H, OMe), 2.98 – 2.82 (m, 1H, H5a), 2.30 (s, 3H, CH_3).^{13}C NMR (101 MHz, CD_3OD) δ 171.71, 153.78, 134.36, 133.53, 130.41, 125.02, 119.10, 100.24, 81.30, 75.25, 74.11, 73.98, 68.85, 61.41, 52.39, 52.18, 51.96, 51.75, 51.54, 51.32, 51.11, 43.85, 29.27, 23.52.

Compound (1)

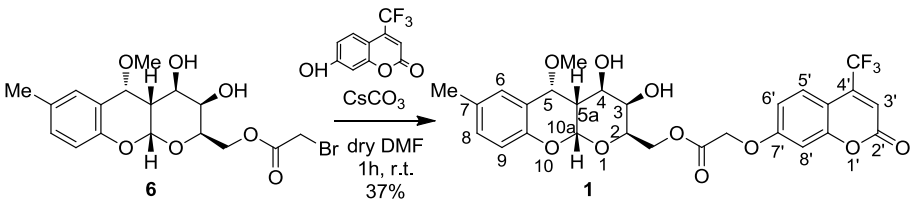

A solution of 7-hydroxycoumarin-4-trifluoromethyl (41mg/0,18mmol) in dry DMF (2mL) was added to a stirred solution of compound **6** (50mg/0,12mmol) in dry DMF (1mL). To the reaction mixture was added $CsCO_3$ (43mg/0,13mmol) and the resulting solution was stirred at r.t. for 1h, after which was poured into a solution of CH_2Cl_2-H_2O. The organic phase was washed with 1M NaOH solution and aqueous layer was washed with CH_2Cl_2. The combined organic layers were dried and concentrated under reduce pressure. The crude product was purified by flash chromatography Toluene/EtOAc (6:4), affording 37% (25mg) of a white solid.

^{1}H NMR (400 MHz, DMSO) δ 7.61 (d, J = 8.9 Hz, 1H, H5´), 7.25 – 7.12 (m, 2H, H8´,6), 7.09 (dd, J = 9.0, 2.3 Hz, 1H, H6´), 6.95 (d, J = 8.7 Hz, 1H, H8), 6.86 (s, 1H, H3´), 6.63 (d, J = 8.0 Hz, 1H, H9), 5.57 (d, J = 2.5 Hz, 1H, H10a), 5.03 (s, 2H, -OCOCH2-), 4.82 (d, J = 4.7 Hz, 1H, H5), 4.39 – 4.26 (m,1H, CH2), 4.30 – 4.2 (m,2H, CH2, H3), 4.10 – 3.98 (m, 1H, H2), 3.62 – 3.54 (m, 1H, H4), 3.53 (s, 3H, OMe), 2.90 – 2.76 (m, 1H, H5), 2.21 (s, 3H, Me).

Compound (8)

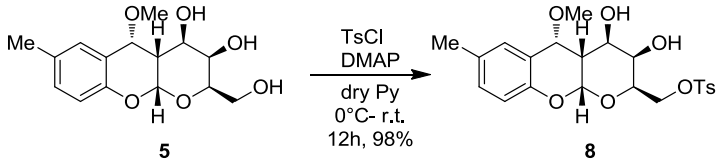

5 8

A solution of compound **5** (482mg/1,63mmol) in dry Pyridine (3,3mL) was cooled to 0ºC in a ice bath with stirring. A solution of p-toluensulfonyl chloride (574mg/3mmol) in dry Pyridine (3,8mL) was then added dropwise and stirring was continued at r.t. until the reaction seemed completed by TLC. After 12h, the solvent was then removed in vacuum to afford a crude product which was purified by flash chromatography, Petroleum Ether/ EtOAc (5:5), yielding 98% (719mg) of a white solid.

^{1}H NMR (400 MHz, $CDCl_3$) δ 7.83 (d, J = 8.2 Hz, 2H,ArOTs), 7.34 (d, J = 8.0 Hz, 2H, ArOTs), 7.19 (s, 1H,H6), 7.01 (d, J = 8.2 Hz, 1H, H8), 6.71 (d, J = 8.3 Hz, 1H, H9), 5.46 (d, J = 2.8 Hz, 1H, H10a), 4.76 (d, J = 5.0 Hz, 1H, H5), 4.39 - 4.21 (m, 2H, CH2O), 3.94 (m, 2H, H4 and H2), 3.83 (s, 1H, H3), 3.69 (s, 3H, OMe), 2.82 (m, 1H, H5a), 2.44 (s, 3H, Me), 2.29 (s, 3H, Me).^{13}C NMR (101 MHz, $cdcl_3$) δ 149.60, 145.05, 133.05, 131.06, 130.51, 130.05, 128.31, 126.68, 120.04, 116.11, 95.95, 78.50, 77.54, 77.22, 76.91, 69.55, 68.98, 66.88, 66.63, 59.64, 34.70, 21.85, 20.87. $[\alpha]_D^{20}$= +4,1 (c=1, CH_3CH_2OH); MS: m/z calcd for $[M + Na]^+$ = 473.5; found $[M + Na]^+$ = 473.1

Compound (9)

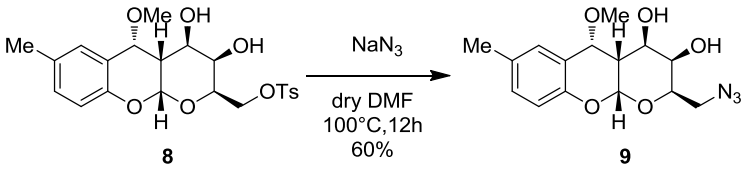

8 9

To a solution of compound **8** (100mg/0,22mmol) in dry DMF (1mL), a solution of NaN_3 (101mg/1,55mmol) in dry DMF (0,5mL) was added and stirring was continued at 100ºC for 12h. Upon cooling to r.t., the colorless precipitate was filtrate ad the solvent was

evaporated to dryness. The crude product was purified by flash chromatography, Petroleum Ether/EtOAc (6:4) affording 60% (42mg) of a white solid.

^{1}H NMR (400 MHz, $CDCl_3$) δ 7.22 (s, 1H, H6), 7.02 (d, J = 7.9 Hz, 1H, H8), 6.75 (d, J = 8.3 Hz, 1H, H9), 5.56 (d, J = 2.7 Hz, 1H, H10a), 4.80 (d, J = 5.0 Hz, 1H, H5), 4.16 (t, J = 6.4 Hz, 1H, H2), 3.98 (d, J = 2.9 Hz, 1H, H4), 3.83 (s, 1H, H3), 3.72 (s, 3H, OMe), 3.71 – 3.66 (m, 1H, CH_2O), 3.51 (dd, J = 12.7, 5.4 Hz, 1H, CH_2O), 2.93-2.84 (m, 1H, H5a), 2.30 (s, 3H,Me). ^{13}C NMR (101 MHz, $CDCl_3$) δ 149.67, 131.05, 130.53, 126.71, 120.06, 116.14, 96.06, 78.53, 77.57, 77.25, 76.93, 70.67, 67.25, 67.15, 59.72, 51.50, 34.69, 20.92. $[\alpha]_D^{20}$= -10,3 (c=1, CH_3CH_2OH); MS: m/z calcd for $[M + Na]^+$ = 344.3; found $[M + Na]^+$ = 344.1.

Compound (10)

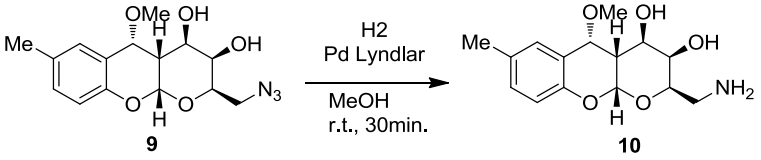

To a solution of compound **9** (30mg/0,093mmol) in MeOH (6mL) was added Lindlar catalyst (5%), and the mixture was hydrogenated at 1atm and r.t. for 30min. Filtration and concentration gave amine 10 in a quantitative yield.

^{1}H NMR (400 MHz, CD_3OD) δ 7.23 (d, J = 16.4 Hz, 1H, H6), 6.98 (d, J = 8.1 Hz, 1H, H8), 6.64 (dd, J = 8.2, 2.4 Hz, 1H, H9), 5.59 (d, J = 3.0 Hz, 1H, H10a), 4.86 (d, J = 5.0 Hz, 1H, H5), 3.95 (dd, J = 7.3, 4.8 Hz, 1H, H2), 3.88 – 3.77 (m, 1H, H4), 3.74 (dd, J = 9.7, 5.3 Hz, 1H, H3), 3.68 (s, 3H, OMe), 3.06 – 3.00 (m, 1H, CH_2O), 2.97 – 2.90 (m, 1H, H5a), 2.87 (dd, J = 13.3, 4.5 Hz, 1H, CH_2O), 2.29 – 2.23 (m, 3H, Me).

Compound (2)

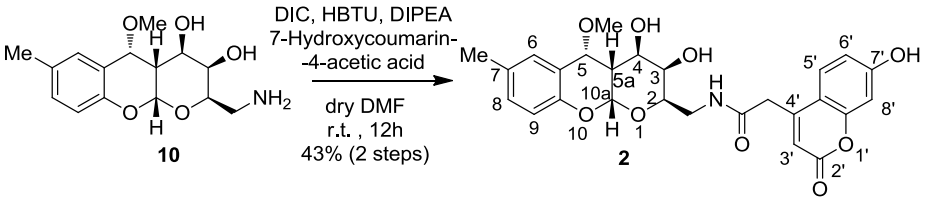

Working in anhydrous conditions, compound **10** (30mg/0,093mmol), 7-hydroxycoumarin-4-acetic acid (24,6mg/0,112mmol) and HBTU (53,1mg/0,14mmol) were dissolved in dry DMF (1,3ml). To this reaction mixture DIPEA (48µL/0,28mmol) was added at r.t. and after 10 min. DIC (0,14mmol/22µL) was added at 0ºC. The final reaction mixture was stirred at room temperature until the reaction seemed completed by TLC. After 12h, the solvent was then removed in vacuum to afford a crude product, which was purified by flash chromatography, $CHCl_3$/MeOH (9,5:0,5), yielding 43% (20mg) of a white solid.

^{1}H NMR (400 MHz, CD_3OD) δ 7.59 (d, J = 8.8 Hz, 1H, H5'), 7.23 (s, 1H, H6), 6.97 (d, J = 7.5 Hz, 1H, H8), 6.76 (d, J = 8.7 Hz, 1H, H6'), 6.63 (m, 2H,H9 and H8'), 6.16 (s, 1H, H3'), 5.54 (d, J = 2.8 Hz, 1H, H10a), 4.85 (d, J = 4.9 Hz, 1H, H5), 4.02 (s, 1H, H2), 3.81-3.71 (m, 3H, H4 and CH2C=O), 3.67 (s, 4H, OMe and H3), 3.57 (dd, J = 13.8, 4.5 Hz, 1H, CH2O), 3.44 (dd, J = 13.5, 8.5 Hz, 1H,CH2O), 2.88 (m, 1H, H5a), 2.26 (s, 3H, Me).^{13}C NMR (101 MHz, CD3OD) δ 170.35, 162.86, 156.03, 150.04, 130.21, 129.55, 126.27, 126.16, 120.88, 115.22, 114.65, 110.71, 110.37, 102.95, 96.59, 77.58, 70.49, 68.05, 67.12, 67.00, 57.64, 48.44, 48.23, 48.02, 47.81, 47.59, 47.38, 47.17, 40.72, 34.36, 29.59, 19.57. $[\alpha]_D^{20}$= +16,6 (c=1, CH_3CH_2OH); MS: m/z calcd for $[M + Na]^+$ = 520.5; found $[M + Na]^+$ = 520.2

Compound (13)

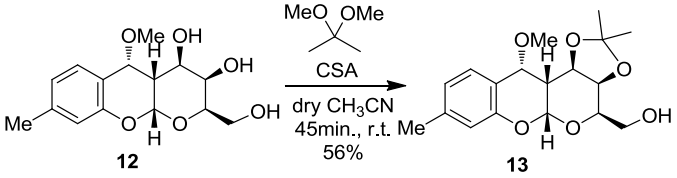

To a solution of compound **12** (500mg/1,69mmol) in dry CH_3CN (8,0mL), acetone dimetheylacetal (6,76mmol/0,4mL) and CSA (1%mmol) were added under argon. The reaction mixture remained under magnetic stirring for 45min. at room temperature, after which was added Et_3N to neutralize the CSA. The reaction was then concentrated under reduce pressure and the crude product purified by flash chromatography, Petroleum Ether/EtOAc (6:4) affording 56% (336mg) of a yellow solid.

^{1}H NMR (400 MHz, CD_3OD) 7.30 (d, *J* = 7.9 Hz, 1H, H6), 6.78 (d, *J* = 7.9 Hz, 1H, H7), 6.63 (s, 1H, H9), 5.52 (d, *J* = 3.8 Hz, 1H, H10), 4.68 (d, *J* = 5.2 Hz, 1H, H4), 4.31 (dd, *J* = 8.6, 3.7 Hz, 1H, H1), 4.15 (dd, *J* = 5.6, 2.4 Hz, 1H, H2), 4.12 – 4.06 (m, 1H, H3), 3.80 (dd, *J* = 6.1, 3.5 Hz, 2H, CH2), 3.54 (s, 3H,OMe), 2.79 – 2.66 (m, 1H,H4a), 2.26 (s, 3H,MeAr), 1.53 (s, 3H, Me), 1.29 (s, 3H,Me). ^{13}C NMR (101 MHz, CD_3OD) δ 152.12, 139.13, 127.03, 121.80, 118.72, 115.86, 108.61, 95.52, 75.27, 71.43, 70.87, 69.47, 61.45, 55.97, 48.21, 48.00, 47.78, 47.57, 47.36, 47.14, 46.93, 37.67, 26.92, 24.85, 19.75.MS: m/z calcd for $[M + Na]^+$ = 359.3; found $[M + Na]^+$ = 359.3.

Compound (15)

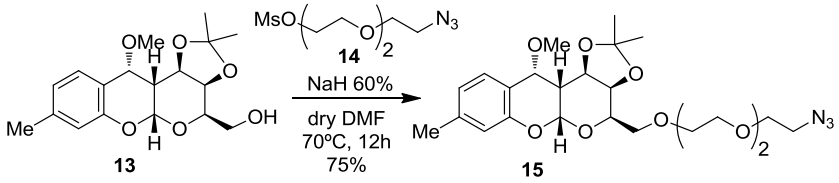

To a 60 % suspension of sodium hydride in oil (75 mg, 2,67mmol) an argon atmosphere dry DMF (10 mL) was added. The suspension was cooled to 0ºC with stirring and a solution of compound **13** (300mg/0,89mmol) in dry DMF (3 ml) and compound **14** (570mg/1,79mmo) in dry DMF (3ml) were added. The mixture was stirred at 70ºC for 12 h. After cooling to 0ºC, the reaction was quenched by slowly addition of MeOH (4 ml) and stirred for more 20 min. The reaction mixture was diluted with EtOAc, and washed with water, dried (NaSO4) and concentrated. The residue was purified by flash chromatography, Petroleum Ether/EtOAc (3:7), yielding 75% of a brownish oil.

^{1}H NMR (400 MHz, $CDCl_3$) δ 7.29 (d, *J* = 7.8 Hz, 1H, H6), 6.78 (d, *J* = 7.6 Hz, 1H, H7), 6.64 (s, 1H, H9), 5.57 (d, *J* = 2.28 Hz, 1H, H10a), 4,78 (d, J= 4.9, 3H, OCH_3), 4,19 (t, J = 5.4 Hz, 2H, 1H), 3,40 (t, J = 5.0 Hz, CH_2), 3,67 (s, 12H, trietileneglicole), 3.98-3.69 (m, 4H, H4, H3, H5, H2), 2.94 (m, 1H, H4a), 2.28 (s, 3H, Me), 1.66 (s, 3H, CH_3) e 1.24 (s, 3H, CH_3). ^{13}C NMR (400 MHz, $CDCl_3$) δ 149.18, 137.10, 123.49, 119.60, 115.04, 113.67, 93.76, 75.59, 74.76, 74.45, 74.13, 69.93, 68.25, 67.99, 67.93, 67.92, 67.75, 67.57, 64.57, 64.28, 56.63,

38.73, 34.33, 30.07, 32.05, 24.33, 18.59. MS: m/z calcd for $[M + Na]^+$ = 516.4; found $[M + Na]^+$ = 516.4.

Compound (16)

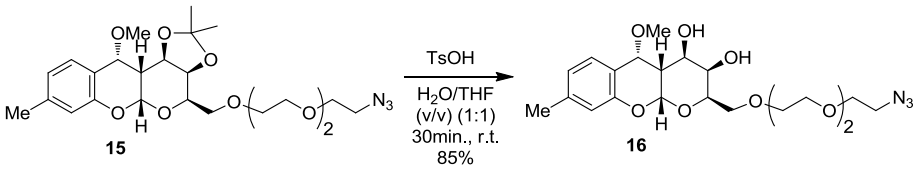

To a solution of compoud **13** (100mg/0,22mmol) in CH_3CN:H_2O (10:2) (10mL),p-toluenesulfonic acid (0,42mg/0,002mmol) was added. The final reaction mixture was stirred at room temperature until the reaction seemed completed by TLC. After 30min., Et_3N is added and the solvent was then removed in vacuum to afford a crude product which was purified by flash chromatography, Petroleum Ether/EtOAc (2:8), yielding 85% of a brownish oil.

^{1}H NMR (400 MHz, $CDCl_3$) δ 7.29 (d, *J* = 7.8 Hz, 1H, H6), 6.78 (d, *J* = 7.6 Hz, 1H, H7), 6.64 (s, 1H, H9), 5.57 (d, *J* = 2.28 Hz, 1H, H10a), 4,78 (d, *J*= 4.9, 3H, OCH_3), 4,19 (t, *J* = 5.4 Hz, 2H, 1H), 3,40 (t, *J* = 5.0 Hz, CH_2), 3,67 (s, 12H, triethylene glycol), 3.98-3.69 (m, 4H, H4, H3, H5, H2), 2.94 (m, 1H, H4a), 2.28 (s, 3H, Me). ^{13}C NMR (101 MHz, CDCl3) δ 149.18, 137.10, 123.49, 119.60, 115.04, 113.67, 93.76, 75.59, 74.76, 74.45, 74.13, 69.93, 68.25, 67.99, 67.93, 67.92, 67.75, 67.57, 64.57, 64.28, 56.63, 38.73, 32.05, 18.59. MS: m/z calcd for $[M + K]^+$ = 392.4; found $[M + K]^+$ = 392.4.

Compound (17)

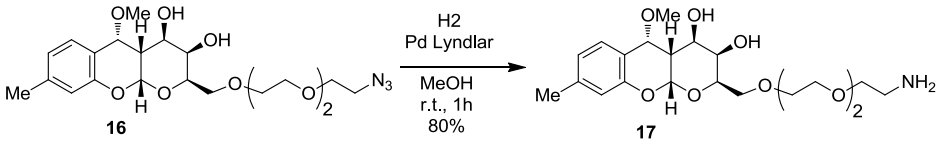

To a solution of compound **16** (80mg/0,20mmol) in $CHCl_3$:MeOH (1:1) (5mL) was added Lindlar catalyst (5%), and the mixture was hydrogenated at 1 atm and r.t. for 1h. Filtration and concentration gave amine 17 in 80% yield as a yellow oil.

^{1}H NMR (400 MHz, $CDCl_3$) δ 7.29 (d, J = 7.8 Hz, 1H, H6), 6.78 (d, J = 7.6 Hz, 1H, H7), 6.64 (s, 1H, H9), 5.57 (d, *J* = 2.28 Hz, 1H, H10a), 4,78 (d, *J*= 4.9, 3H, OCH_3), 4,19 (t, *J* = 5.4 Hz, 2H, 1H), 3,40 (t, *J* = 5.0 Hz, CH_2), 3,67 (s, 12H, triethylene glycol), 3.98-3.69 (m, 4H, H4, H3, H5, H2), 2.94 (m, 1H, H4a), 2.80 (s, 2H, CH_2-NH_2) 2.28 (s, 3H, Me). ^{13}C NMR (400 MHz, $CDCl_3$) δ 149.18, 137.10, 123.49, 119.60, 115.04, 113.67, 93.76, 75.59, 74.76, 74.45, 74.13, 69.93, 68.25, 67.99, 67.93, 67.92, 67.75, 67.57, 64.57, 64.28, 56.63, 38.73, 32.05, 18.59. MS: m/z calcd for $[M + H]^+$ = 428.5; found $[M + Na]^+$ = 428.5.

Compound (4)

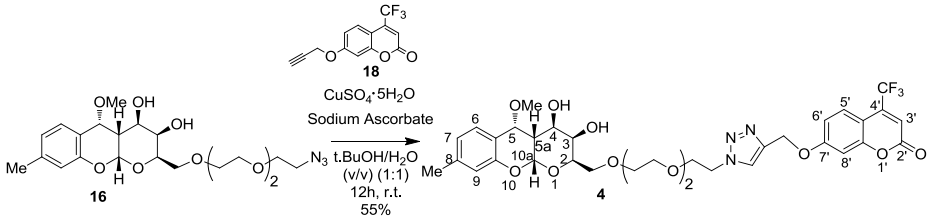

To a vigorously stirring suspension of compound **18** (72mg/0,27mmol) in 1:1 t-BuOH/H_2O, Copper(II) sulfate pentahydrate (9mg/0,035mmol) and sodium ascorbate (14mg/0,069mmol) were added. The reaction mixture was stirred for 10min at room temperture and then compound 16 (110mg/0,23mmol) was added. The suspension was stirred vigorously at r.t. for 12h. At this time TLC indicated completion of the reaction. Distilled water was added, and the aqueous layer was extracted with CH_2Cl_2. The combined extracts were dried, filtered and evaporated to afford a brownish oily solid. The product was then purified using column chromatography using $CHCl_3$ as eluant, which afforded the expected compound **4** as a brownish solid.

^{1}H NMR (400 MHz, CD_3OD) δ 8,25 (s, 1H, H8'), 7,63 (dd, J = 7.64 Hz, 1H, H14'), 7,24 (d, *J*= 7.8 Hz, 1H, H6), 7,13 (d, *J* = 2.5 Hz, 1H, H17'), 7,06 (dd, J= 9 e 2.5 Hz, 1H, H15'), 6,71 (d, *J* = 7.8 Hz, 1H, H7), 6,68 (s, 1H, H12'), 6,46 (s, 1H, H9), 5,51 (d, *J*= 3.0 Hz, 1H,H10a), 5,31 (s, 2H, H9'), 4,80 (d, J= 4.9 Hz, 1H, H5), 4,61 (m, 2H, H6'), 4,07 (t, J= 5.9 Hz,1H, H2'), 3,91 (m, 2H, H7'), da 3,77 a 3,57 (m, 15H, H3'', H4'', H5'', H1, H4, H3, H2, OCH_3) 2.84 (m, 1H, H4a), 2.80 (s, 2H, CH_2-triazole) 2.21 (s, 3H, CH_3). ^{13}C NMR (400 MHz, CD_3OD) δ

162.28, 156.17, 151.80, 142.19, 139.03, 125.96, 125.70, 125.46, 121.79, 112.24, 115.37, 113.56, 107.00, 102.22, 96.43, 76.35, 70.90, 70.51, 70.33, 70.40, 70.09, 70.04, 68.87, 67.41, 66.94, 66.90, 61.60, 61.62, 57.49, 50.17, 34.30, 19.76. ^{19}F NMR (400 MHz, CD_3OD) δ -72. MS: m/z calcd for $[M + H]_+$ = 721.67; found $[M + H]^+$ = 721.67.

Compound (3)

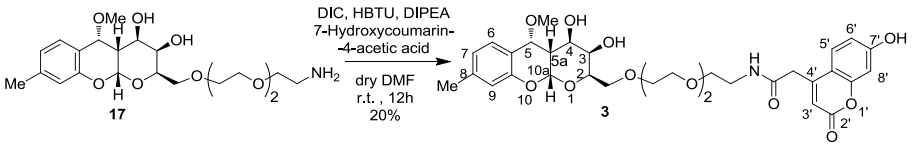

Working in anhydrous conditions, compound **17** (50mg/0,13mmol), 7-hydroxycoumarin-4-acetic acid (31mg/0,16mmol) and HBTU (68,26mg/0,20mmol) were dissolved in dry DMF (2ml). To this reaction mixture DIPEA (0,39mmol/67µL) was added at r.t. and after 10 min. DIC (0,20mmol/31µL) was added at 0ºC. The final reaction mixture was stirred at room temperature until the reaction seemed completed by TLC. After 12h, the solvent was then removed in vacuum to afford a crude product which was purified by flash chromatography, CH_2Cl_2/Acetone (5:5), yielding 20% (15mg) of a brown color solid.

^{1}H NMR (400 MHz, CD3OD) δ 7.29 (d, J = 7.8 Hz, 1H, H6), 6.78 (d, J = 7.6 Hz, 1H, H7), 6.64 (s, 1H, H9), 5.57 (d, *J* = 2.28 Hz, 1H, H10a), 4,78 (d, *J*= 4.9, 3H, OCH_3), 4,19 (t, *J* = 5.4 Hz, 2H, 1H), 3,40 (t, *J* = 5.0 Hz, CH_2), 3,67 (s, 12H, triethylene glycol), 3.98-3.69 (m, 4H, H4, H3, H5, H2), 2.94 (m, 1H, H4a), 2.80 (s, 2H, CH_2-NH_2) 2.28 (s, 3H, Me). ^{13}C NMR (400 MHz,CD3OD) δ 149.18, 137.10, 123.49, 119.60, 115.04, 113.67, 93.76, 75.59, 74.76, 74.45, 74.13, 69.93, 68.25, 67.99, 67.93, 67.92, 67.75, 67.57, 64.57, 64.28, 56.63, 38.73, 32.05, 18.59. MS: m/z calcd for $[M + H]^+$ = 428.5; found $[M + Na]^+$ = 428.5.

NMR binding studies

NMR experiments were recorded on a Varian 400-MHz Mercury. A batch of Aβ1-42 was selected that contained pre-amyloidogenic seeds highly toxic to N2a cells. Immediately

before use, lyophilized Aβ1-42 was dissolved in 10 mM NaOD in D_2O at a concentration of 160μM, then diluted 1:1 with 20 mM phosphate buffer, pH 7.4 containing one of the tested compounds. Compounds **2**, **3** and **4** were dissolved in PB, pH 7.4, and added to the peptide solution; for compound **4** 5% of d-DMSO was added. The pH of each sample was verified with a Microelectrode (Mettler Toledo) for 5 mm NMR tubes and adjusted with NaOD or DCl. All pH values were corrected for isotope effect. Basic sequences were employed for ^{1}H, ^{19}F, 2D-TOCSY, 2D-NOESY and STD experiments. For STD, a train of Gaussian-shaped pulses each of 50 ms was employed to saturate selectively the protein envelope; the total saturation time of the protein envelope was adjusted by the number of shaped pulses and was varied between 3 s and 0.3 s.

Sections staining

Brain tissue from Tg CRND8 mice encoding a double mutant form of amyloid precursor protein 695 (KM670/671NL + V717F) under the control of the PrP gene promoter (Chishti et al., 2001) were dissected and were fixed in Carnoy's and embedded in paraffin.

Procedures involving animals and their care were conducted in conformity with the institutional guidelines that are in compliance with national (D.L. No. 116, G.U. Suppl. 40, Feb. 18, 1992, Circolare No. 8, G.U., 14 Luglio 1994) and international laws and policies (EEC Council Directive 86/609, OJ L 358, 1 Dec.12, 1987; NIH Guide for the Care and use of Laboratory Animals, U.S. National Research Council, 1996). All efforts were made to minimize the number of animals used and their suffering.

Seven-micrometer-thick serial sections of paraffin-embedded blocks from the temporal cortex were mounted on gelatin coated microscope slides and used for staining. Paraffin sections were subjected to two incubations of 5 min in xylene, an incubation of 10 min each in 100% - 96% -70% EtOH for the complete dewaxing and two successive incubations of 5 min in water. Tissue sections were covered with a solution 3 μM of thioflavine T or 6 μM of compound **3** dissolved in water. After 30 min of

incubation, the sections were washed 3 times for 5 min in water and 5 min each in 70% - 96% - 100% EtOH. The sections were then incubated 5 min in xylene before adding the coverslip. Sections were visualized by fluorescent fluoromicroscope M-3204CCCD (OlympusBX61) equipped with the filters FITC (Ex 488 nm) for detecting thioflavine T and DAPI (Ex 405 nm) for detecting test compounds.

Transport Experiments

Trans-endothelial-electrical resistance (TEER) were measured by EVOMX meter, STX2 electrode, World Precision Instruments, Sarasota, Florida.

Fluorescence measurements were done using a Cary Eclipse spectrofluorimeter (Varian Inc., Palo Alto, California).

The radioactivity assay were achieved by means of a Tri-Carb 2200 CA Liquid Scintillation Analyzer (Packard Instrument Co. Inc., Rockville, MD).

The differences were evaluated for statistical significance using Student's t-test.

For transport experiments across a cell monolayer, hCMEC/D3 were seeded in a 12-well Transwell® inserts coated with type I collagen. 0.5 mL of cell suspensions containing 2.0 • 10^5cells were added to the upper (donor) chamber which was inserted into the lower (acceptor) chamber containing 1.0 mL of the culture medium. A cell monolayer was usually formed 14 days after seeding judged by three criteria: (1) the cells formed a confluent monolayer without visible spaces between cells under a light microscope; (2) the height of the culture medium in the upper chamber had to be at least 2 mm higher than that in the lower chamber for at least 24 h; and (3) a constant TEER (trans endothelial electrical resistance) value, measured using an EVOM Endohm chamber. Wells were used when TEER value was higher than 50 $\Omega \cdot cm^2$. Trans-endothelial permeability coefficient (PE) was calculated as reported by Bickel U. (*NeuroRx: The Journal of the American Society for Experimental NeuroTherapeutics* ,Vol. 2, 15–26, January 2005):

After adding the test substance to the donor compartment, repeated samples are taken from the donor compartment over the desired time course. The concentration measured in these samples and the known volumes of the compartments (V_{donor} and $V_{acceptor}$) are used to calculate the incremental clearance volumes ΔV_{Cl} for each time point:

$$\Delta V_{Cl} = C_{acceptor} \cdot V_{acceptor} / C_{donor}$$

As long as the concentration in the acceptor compartment is small and ΔV_{Cl} increases in linear manner, the slope of the line can be interpreted as the PS product for unidirectional transfer. With the known exchange surface, S, (filter area) the permeability may be obtained as P = PS/S. Finally, a correction needs to be made for the permeability of the cell-free filter:

$$1/P_{endothel} = 1/P_{totall} – 1(P_{filter})$$

With $P_{endothel}$ being equal to PE.

After adding the test substance to the upper compartment, samples were taken from the lower compartment at different times (0-60-180 min) for liquid scintillation counting (^{14}C sucrose) and for fluorescence assays (compound **3**). At the end of the experiments, TEER and [^{14}C]sucrose PE were re-determined in order to prove no occurrence of adverse effects on tight junction function due to sample application.

PAPER 5

*Chemistry, an Asian journal, **2012**, in press.*

NATURAL COMPOUNDS AGAINST ALZHEIMER'S DISEASE: MOLECULAR RECOGNITION OF SALVIA SCLAREOIDES EXTRACT AND ITS MAJOR COMPONENT, ROSMARINIC ACID, WITH AB1-42 PEPTIDE, AS INVESTIGATED BY NMR

Cristina Airoldi,[a] Erika Sironi,[a] Catarina Dias,[b] Filipa Marcelo,[b,c] Alice Martins,[b] Amélia Pilar Rauter,[b] Francesco Nicotra,[a] Jesus Jimenez-Barbero[a,c]

[a] Dr. C. Airoldi, E. Sironi, Prof. F. Nicotra, Prof. J. Jimenez-Barbero, Department of Biotechnology and Biosciences, University of Milano Bicocca, Piazza della Scienza, 2 – 20126 – Milano, Italy. Fax: +39 026448 3565.
E-mail: cristina.airoldi@unimib.it
[b] MSc C. Dias, Dr. A. Martins, Dr. F. Marcelo, Prof. A. P. Rauter, Centro de Quimica e Bioquimica, Departamento de Quimica e Bioquimica, Faculdade de Ciencias da Universidade de Lisboa, ED C8 5° Piso - 1749-016 - Lisboa, Portugal.
E-mail: aprauter@fc.ul.pt
[c] Dr. F. Marcelo, Prof. J. Jimenez-Barbero, Centro de Investigaciones Biologicas, C.S.I.C., Ramiro de Maetzu 9 - 28040 – Madrid , Spain.
E-mail: jjbarbero@cib.csic.es

Abstract

Amyloid peptides, Aβ1-40 and Aβ1-42, represent major molecular targets to develop potential drugs and diagnostic tools for Alzheimer's Disease (AD). In fact, oligomeric and fibrillar aggregates generated by these peptides are amongst the principal components of amyloid plaques found post-mortem in patients suffering from AD. Rosmarinic acid has been demonstrated to be effective in preventing the aggregation of amyloid peptides *in vitro* and to delay the progression of the disease in animal models. Nevertheless, no information is available about its molecular mechanism of action. Herein, we report the NMR characterization of *Salvia sclareoides* extract interaction and that of its major component rosmarinic acid with Aβ1-42 peptide, whose oligomers

have been described as the most toxic Aβ species *in vivo*. Our data shed light on the structural determinants of rosmarinic acid-Aβ1-42 oligomers interaction, allowing the elucidation of its mechanism of action. They also provide important information for the rational design of new compounds with higher affinity for Aβ peptides to generate new anti-amyloidogenic molecules and/or molecular tools for the specific targeting of amyloid aggregates *in vivo*. In addition, we identified methyl caffeate, another natural compound present in different plant and human diet, as a good ligand of Aβ1-42 oligomers, also showing anti-amyloidogenic activity. Finally, we demonstrated the possibility to exploit STD-NMR and trNOESY experiments to screen extracts from natural sources for the presence of Aβ peptide ligands.

Keywords: NMR spectroscopy · Alzheimer's disease · Aβ peptide · rosmarinic acid · caffeic acid · molecular recognition · NMR binding studies

Alzheimer's disease (AD) is the most widespread form of dementia worldwide. Senile amyloid plaques, vascular amyloidosis, neurofibrillary tangles of hyperphosphorylated tau protein and neurotrans-deficit represent the most characteristic pathological lesions found in AD patient brain.[1] These amyloid aggregates are formed by Aβ peptides of various aminoacid lengths derived from alternative processing of a membrane protein (amyloid precursor protein, APP).[2] The most abundant peptides are Aβ1–40 and Aβ1–42. In particular, Aβ1–40 is the prevalent fragment, while Aβ1–42 is the most amyloidogenic. Oligomeric and fibrillar aggregates generated by these peptides are amongst the principal components of amyloid plaques found *post-mortem* in patients suffering from AD.[3] Hence, they represent a target of choice for the development of new therapies and diagnostic tools for AD. A variety of natural and synthetic compounds have been reported to be effective in inhibiting the aggregation

[1] A. Nordberg, *Lancet. Neurol.* **2004***, 3*, 519–527.
[2] G. G. Glenner, C.W. Wong, *Biochem . Biophys. Res. Commun*. **1984**, *120*, 885–890.
[3] L. Fratiglioni, D. De Ronchi, H. Aguero Torres., *Drugs Aging* **1999**, *15*, 365-375.

of amyloid peptides *in vitro* and in delaying the progression of the disease in animal models.[4,5] Rosmarinic acid (RA, **Figure 1**) displays anti-aggregating activity against Aβ peptide[6] but its mechanism of action is still unknown.

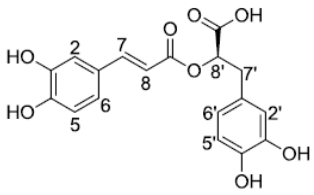

Figure 1. Rosmarinic acid structure and numbering.[7]

This molecular entity is a phenolic antioxidant carboxylic acid, present in many Lamiaceae species, commonly used as culinary herbs such as rosemary, lemon balm, peppermint, oregano, sage and thyme. As reported by Iuvone *et al.*,[8] RA reduces a number of events underlying AD associated pathological conditions, namely reactive oxygen species formation, lipid peroxidation, DNA fragmentation, caspase-3 activation, and *tau* protein hyperphosphorylation. In addition, it inhibits phosphorylated p38 mitogen-activated protein kinase. These data support the neuroprotective effect of sage against Aβ peptide neurotoxicity, which validates the traditional use of this spice in AD treatment. However, no information from the structural chemistry perspective is available about the molecular mechanism by which RA exerts its biological effects.

To bridge this gap, we have herein employed NMR spectroscopy to elucidate the structural features of RA binding to Aβ1-42 peptide. Very recently we have exploited Saturation Transfer Difference (STD)NMR[9] and trNOESY experiments[10] to

[4] H. Amijee, D. I. C. Scopes, *J. Alzheimers Dis.* **2009**, *17*, 33-47.
[5] a) F. Re, C. Airoldi, C. Zona, N. Quattrocchi, B. La Ferla, F. Nicotra, M. Masserini, *Curr. Med. Chem*. **2010**, *17*, 2990-3006; b) C. Airoldi , E. Sironi, B. La Ferla, F. Cardona, F. Nicotra, *Curr. Bioact. Compd*. **2011**, *7*, 198-213.
[6] T. Alkam, A. Nitta, H. Mizoguchi, A. Itoh, T. Nabeshima, *Behav. Brain Res.* **2007**, *180*, 139–145.
[7] Y. Lu, L. Y. Foo*, Phytochem.* **1999**, *51*, 91-94.
[8] T. Iuvone, D. De Filippis, G. Esposito, A. D'Amico, A. A. Izzo, *J. Pharmacol. Exp. Ther.* **2006**, *317*, 1143-1149.
[9] M. Mayer and B. Meyer, *Angew. Chem. Int. Ed.* **1999**, *38*, 1784-1788.
[10] B. Meyer and T. Peters, *Angew. Chem. Int. Ed.* **2003**, *42*, 864-890.

characterize the interaction of Aβ peptides with tetracycline and thioflavin T,[11] a small library of curcumine derivatives,[12] and a small pannel of glyco-fused benzopyran derivatives.[13] Thus, an analogous methodology has been applied herein to check the effect of *Salvia sclareoides* butanol extract and RA, one of its major components,[14] on the Aβ1-42 oligomer recognition process. Indeed, the key step was first to employ the global butanol extract from *Salvia sclareoides* rather than isolated and well characterized compounds. In this way, we could verify the ability of NMR recognition studies to detect the presence of Aβ ligands in extracts from natural sources.

The main goal in this work was the identification of the binding epitope of the key component in the extract for the interaction with Aβ1-42 peptide, as well as to elucidate the RA mechanism of action from the structural point of view. This kind of information can be exploited for the rational design of new Aβ ligands and for development of innovative therapies or diagnostic tools versus AD.

Results and Discussion

The ability of Saturation Transfer Difference (STD) and tr-NOESY NMR experiments to reveal the presence of Aβ1-42 oligomer ligands in the butanol extract of *Salvia sclareoides* was first investigated. A weighted amount (1 mg) of the *Salvia sclareoides* butanol extract*,* dissolved in PBS at pH 7.5, was added to a 80 μM solution of Aβ1-42 peptide dissolved in NaOD. Then, the pH was adjusted at the final value of 7.5. Under these experimental conditions, the peptide is present in oligomeric form, as previously demonstrated.[11] First of all, upon addition of Aβ1-42 oligomers to the NMR tube containing the extract solution, significant broadening of several ^{1}H NMR signals of the

[11] C. Airoldi, L. Colombo, C. Manzoni, E. Sironi, A. Natalello, S. M. Doglia, G. Forloni, F. Tagliavini, E. Del Favero, L. Cantu, F. Nicotra, M. Salmona, *Org. Biomol. Chem.* **2011**, *9*, 463-472.

[12] C. Airoldi, C. Zona, E. Sironi, L. Colombo, M. Messa, D. Aurilia, M. Gregori, M. Masserini, M. Salmona, F. Nicotra, B. La Ferla, *J. Biotechnol.* **2011**, *156*, 317-324.

[13] C. Airoldi, F. Cardona, E. Sironi, L. Colombo, M. Salmona, A. Silva, F. Nicotra, B. La Ferla, *Chem. Commun*. **2011**, *47*, 10266–10268.

[14] F. Marcelo, C. Dias, A. Martins, P. J. Madeira, T. Jorge, M. H. Florêncio, F. J. Cañada, E. J. Cabrita, J. Jiménez-Barbero, A. P. Rauter, *submitted*.

extract was observed (compare **Figures 2A** and **2C**), supporting the existence of interaction. Then, the STD experiment acquired on the mixture was analysed setting the on-resonance saturation frequency at -1.0 ppm. In this manner, saturation of most aliphatic resonances of the Aβ oligomers was achieved. The STD spectrum showed several NMR signals, belonging to molecules present into the extract (**Figure 2D**), this indicating the existence of their interactions with the Aβ1-42 oligomers.

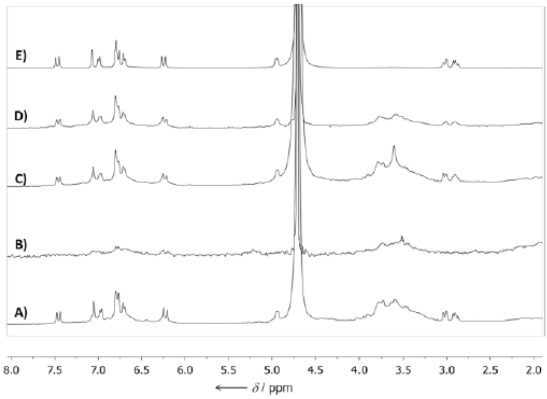

Figure 2. A) ^{1}H NMR spectrum of the 1 mg of the butanol extract of *Salvia sclareoides*; B) blank STD-NMR spectrum at 2s saturation time of the same sample; C) ^{1}H NMR spectrum of the mixture containing Aβ1-42 (80 uM) and 1 mg of the the butanol extract of *Salvia sclareoides*; D) STD-NMR spectrum of this mixture at 2s saturation time; E) ^{1}H NMR spectrum of 2 mM rosmarinic acid. All the samples were dissolved in deuterated PBS, pH 7.5, 25°C. The spectrometer frequency was 400 MHz.

The existence of interaction was further confirmed by trNOESY experiments acquired on the same ligand:peptide mixture (**Figure 3**). A blank NOESY spectrum of the extract solution was recorded in the absence of the Aβ1-42 peptide (**Figure 3A**). An inversion of the sign of the NOESY cross-peaks of the main component present in the extract was observed between both spectra, passing from positive (light grey color), in the absence of Aβ1-42 peptide, to negative (dark grey color) in the presence of Aβ1-42 peptide (**Figure 3B**). This change is due to an increase of the effective rotational motion correlation time of the molecule in the presence of the Aβ oligomers, strongly

supporting the existence of a binding between the small molecules present in the extract to a large molecular entity.[12] In this context, the macromolecule corresponds to the Aβ peptide oligomeric state.

A visual inspection of the shape and pattern of the observed signals in both the STD and trNOESY spectra suggested the presence of RA (**Figure 1**), known to be abundant in the butanol extract of *Salvia sclareoides*.[14] Indeed, the comparison between the ^{1}H NMR spectrum of the extract (**Figure 2A**) and that of pure RA, recorded under the same experimental conditions (**Figure 2E**) unequivocally supported this hypothesis. Using quantitative NMR methods, the amount of this metabolite was estimated as 40 milligrams per gram of *Salvia sclareoides* butanol extract.

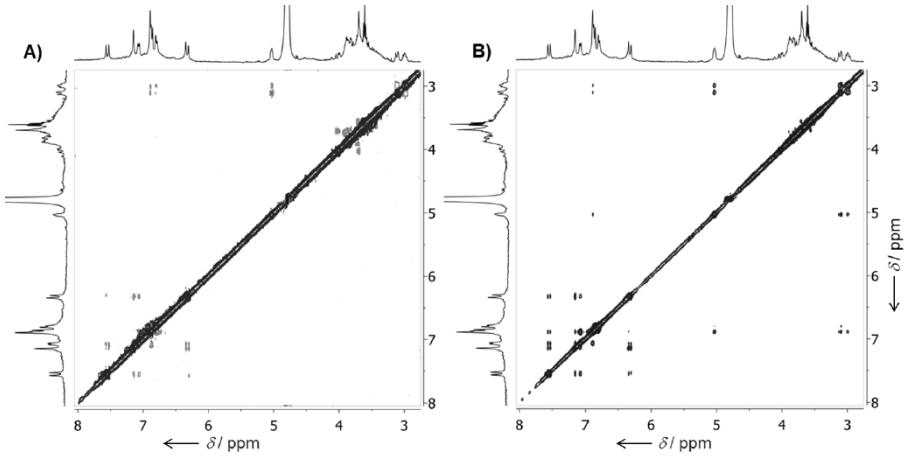

Figure 3. A) 400 MHz 2D-NOESY spectra of 1 mg of the butanol extract of *Salvia sclareoides*, with a mixing time of 0.8 s. B) trNOESY of the mixture containing Aβ1-42 (80 uM) and 1 mg of the butanol extract of *Salvia sclareoides*, with a mixing time 0.3 s. Both samples were dissolved in deuterated PBS, at pH 7.5 and 25°C. Positive cross-peaks are in light grey, negative in dark grey.

NMR characterization of rosmarinic acid binding to Aβ1-42 oligomers

To characterize the main features of the interaction of RA with Aβ oligomers, the same NMR experimental protocol was repeated on a mixture containing Aβ1-42 peptide and the pure compound. The STD and trNOESY experiments reported in Figures 4 and 6 unequivocally demonstrated that RA binds Aβ oligomers.

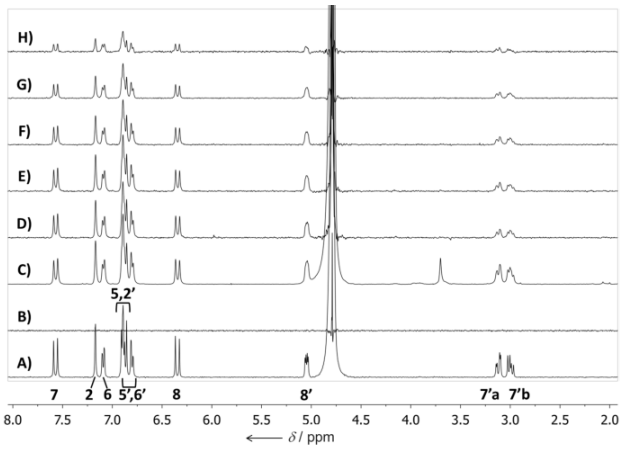

Figure 4. A) ^{1}H NMR spectrum of 2 mM RA; B) blank STD-NMR spectrum of the same sample acquired with a saturation time of 2s; C) ^{1}H NMR spectrum of the mixture containing 80 uM Aβ1-42 and 2 mM RA; D-H) STD-NMR spectra of the same mixture acquired with different saturation times. (D, 3.0 s; E, 2.0 s; F, 1.3 s; G, 0.8 s; H, 0.3 s). Both samples were dissolved in deuterated PBS, pH 7.5, 25°C. The spectra were recorded at 400 MHz. The key resonances are highlighted in spectrum 4A in the bottom part; assignments are consistent with published data.[7]

The STD intensities (**Figure 4**) clearly indicated that the aromatic protons are mostly involved in the binding. **Figure 5** reports schematically the fractional STD effect for RA protons, calculated as $(I_0 - I)/I_0$, where I is the intensity of the monitored signal in the STD spectrum and I_0 is the intensity of the same signal in a reference spectrum. The aromatic protons show the highest percentage of fractional STD effect.

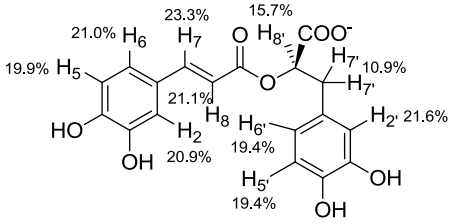

Figure 5. Fractional STD effects calculated for RA protons. Higher is the value for a specific proton, lower is its distance from the receptor protons.

The trNOESY spectrum recorded at 25°C (**Figure 6B**) provided an additional evidence of the existence of interaction. When the NOESY spectrum of the free ligand (**Figure 6A**) was compared to the trNOESY spectrum (in the presence of Aβ1-42), the presence of additional cross peaks was evident (**Figure 6**). In fact, close contacts between the olefinic protons and protons at both aromatic rings suggest the existence of a folded conformation of RA in the bound state, that is much less populated in the free state. In the free state these NOEs are absent, thus expecting an extended conformation in solution for RA (**Figure 1S**). In fact, different geometries of RA would account for the experimental NMR data after using molecular mechanics calculations with the MM3 force field,[15,16] as implemented in the MacroModel program (Maestro Suite).[17] The two major folded conformations in the bound state, deduced using this protocol, are depicted in **Figure 7**.

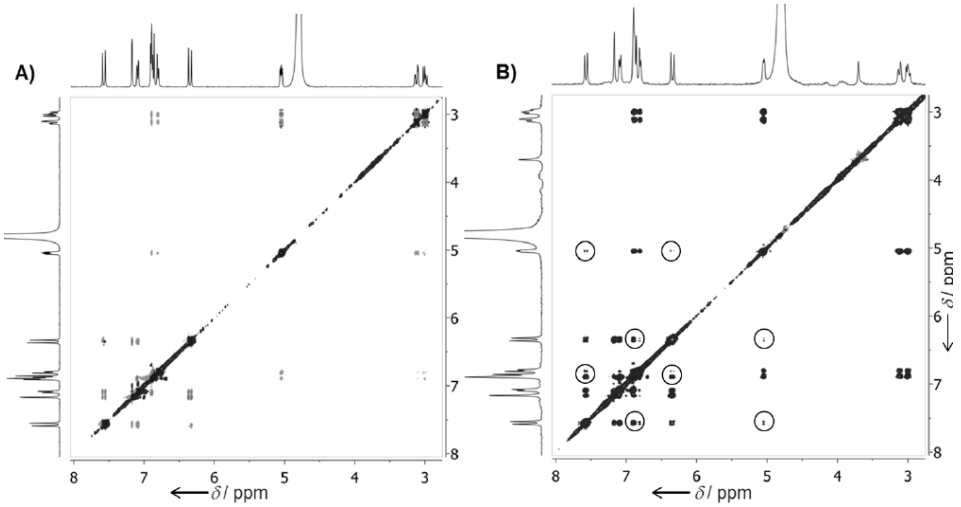

Figure 6. A) 400 MHz 2D-NOESY spectrum of 2 mM RA with a mixing time of 0.8 s. B) trNOESY of the mixture containing Aβ1-42 (80 uM) and 2 mM RA, with a mixing time of 0.3 s. Both samples were dissolved in deuterated PBS, at pH 7.5 and 25°C. Positive cross-peaks are in light grey, negative in dark grey. Additional cross-peaks present in the trNOESY spectrum are circled.

[15] N. L. Allinger, Y. H. Yuh and J. H. Lii, *J. Am. Chem. Soc.* **1989**, *111*, 8551-8566
[16] M. Martín-Pastor, J. F. Espinosa, J. L. Asensio, J. Jiménez-Barbero, *Carbohydr. Res.* **1997**, *298*, 15-49.
[17] MacroModel, 9.6 ed., Schrödinger, LLC **2008**, New York.

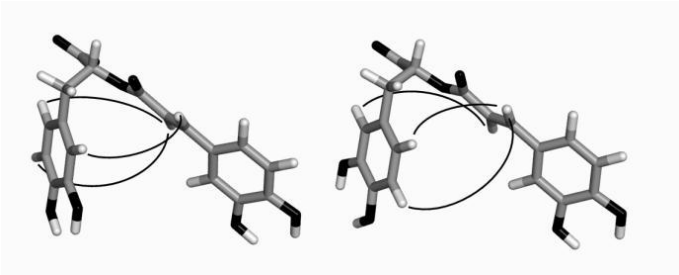

Figure 7. Two possible folded conformations calculated by MM3* for RA on the basis of trNOESY distance constrains. The arrows indicate the NOEs between olefinic protons H7 and H8 and the aromatic ring justifying the presence of a folded conformation.

Although merely speculative, we could guess that this hairpin-like structure would allow RA to intercalate into the Aβ oligomer structure, at the interface between monomers, inducing the disruption of the aggregates. Unfortunately, the lack of knowledge about the structure of Aβ oligomer prevented us to test this hypothesis. To further dissect the contribution of the two aromatic entities of RA to Aβ1-42 recognition and binding, we subdivided its structure into two parts, according to **Scheme 2**. The two obtained entities correspond to methyl caffeate (**1**) and to dihydrocaffeic acid (**2**). The methyl group of methyl caffeate was chosen to keep the ester function present in RA, introducing the alkoxy group as small as possible. Methyl caffeate and dihydrocaffeic acid are nonflavonoid catecholic compounds present in many plants and in the diet, as part of fruits, tea, coffee, and wine [[18]] and are known for their antioxidant activity. Recently, methyl caffeate has also been described for its antidiabetic effect. [[19]]

[[18]] a) J. V. Buren, L. D. Vos, W. Pilnik, *J. Food Sci.* **1973**, *38*, 656–658; b) B. C. Challis, C. D. Bartlett, *Nature* **1975**, *254*, 532–533.
[[19]] G. R. Ghandi, S. Ignacimuthu, M. G. Paulraj, P. Sasikumar, *Eur. J. Pharmacol.*, **2011**, 670, 623-631.

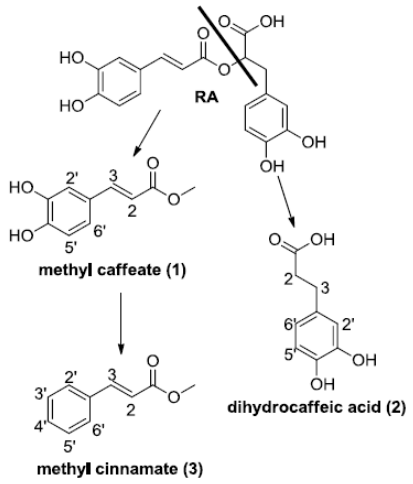

Scheme 2. Structure and numbering of compounds employed for NMR interaction studies.

Methyl caffeate and dihydrocaffeic acid were prepared starting from caffeic acid by methyl esterification and hydrogenation, respectively (see the experimental section for details). Then, their interaction with Aβ1-42 was verified by STD and trNOESY experiments, employing the same experimental protocol used for RA. STD experiments revealed that methyl caffeate retained the ability to recognize and bind Aβ oligomers. Indeed, the STD spectrum acquired in the presence of Aβ1-42 peptide contained the corresponding resonance signals (**Figure 8D** and **Supporting Information – Figure 2S**). The existence of this interaction was also supported by the line broadening of the methyl caffeate signals (**Figure 8C**) and trNOESY experiment (**Supporting Information – Figure 3S**) acquired in the presence of Aβ oligomers.

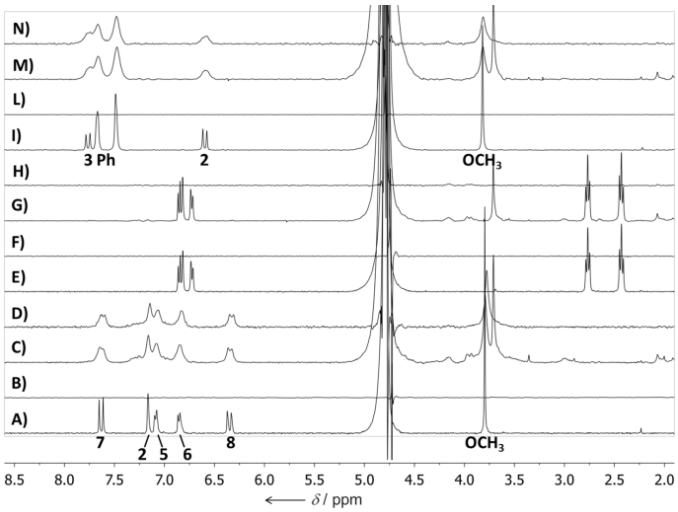

Figure 8. A) ^{1}H NMR spectrum of 1mM methyl caffeate; B) Blank STD-NMR spectrum of the same sample acquired with a saturation time of 2s; C) ^{1}H NMR spectrum of the mixture containing 80 uM Aβ1-42 and 1mM methyl caffeate; D) STD-NMR spectrum of the same mixture in C acquired with a saturation time of 2 s;E) ^{1}H NMR spectrum of 1mM dihydrocaffeic acid; F) Blank STD-NMR spectrum of the same sample acquired with a saturation time of 2 s; G) ^{1}H NMR spectrum of the mixture containing 80 uM Aβ1-42 and 1mM dihydrocaffeic acid; H) STD-NMR spectrum of the same mixture in G acquired with a saturation time of 2 s. I) ^{1}H NMR spectrum of 1 mM methyl cinnamate; L) Blank STD-NMR spectrum of the same sample acquired with a saturation time of 2s; M) ^{1}H NMR spectrum of the mixture containing 80 uM Aβ1-42 and 1 mM methyl cinnamate; N) STD-NMR spectrum of the same mixture in M acquired with a saturation time of 2 s All the samples were dissolved in deuterated PBS, pH 7.5, 25°C. The spectra were recorded at 400 MHz. The key resonances for methyl caffeate are highlighted in spectrum 8A in the bottom part; assignments are consistent with published data;[20] The key resonances for methyl cinnamate are highlighted in spectrum 8I in the bottom part.

On the other hand, dihydrocaffeic acid was not an Aβ ligand. In fact, the STD recorded on the mixture containing Aβ1-42 and this compound only showed peptide resonances (**Figure 8H**). We can speculate that the presence of the conjugated double bond that makes planar the structure of methyl caffeate can be an important molecular feature for the recognition and binding processes. At the same time, the higher polarity of

[20] M. Hoeneisen, J. Alarco, P. Aqueveque, M. Bittner, J. Becerra, M. Silva, J. Jakupovic, *Z. Naturforsch. D.* **2003**, *58c*, 39-41.

dihydrocaffeic acid could also affect the interaction. Furthermore, to investigate the role of the hydroxyl groups on the aromatic ring, we decided to test methyl cinnamate as potential Aβ peptide ligand. Also methyl cinnamate is a natural compound found in a variety of plants, including fruits, like strawberry, and some culinary spices, such as Sichuan pepper and some varieties of basil.[21] Methyl cinnamate resonances appeared in STD spectra recorded in the presence of Aβ oligomers (**Figure 8N** and **Supporting Information – Figure 4S**). In addition, a broadening of methyl cinnamate signals and a change in the NOE cross-peak sign occurred when compound was incubated with Aβ1-42 (**Supporting Information – Figure 5S**). All these data clearly demonstrated that methyl cinnamate indeed interacts with oligomers. In the light of these results, the presence of the hydroxyl groups are irrelevant for the existence of binding. Nevertheless, an accurate inspection of samples containing Aβ1-42 and methyl cinnamate revealed that, a few hours after incubation, the material started to precipitate on the bottom of the NMR tube (see below). This behavior was not observed for samples containing mixtures of the peptide with RA, methyl caffeate or dihydrocaffeic acid. These additional data led us to hypothesize that the molecules under study could have different effects on the peptide aggregation.

RA and methyl caffeate promote the disaggregation of Aβ aggregates

The effect of RA, methyl caffeate and methyl cinnamate on Aβ peptide aggregation was then evaluated with the Thioflavin T (ThT) assay.[22] ThT fluorescence increases after its binding to amyloid aggregates, and thus can be exploited to monitor the peptide aggregation process. First, we verified that RA, methyl caffeate and methyl cinnamate did not quench ThT fluorescence. Then, Aβ peptide was incubated in PBS, pH 7.5, for 72h, with and without an equimolar concentration of each test compound. A small amount was collected for each sample at different times, ThT was added to a

[21] A. Viña, E. Murillo, J. Braz. *Chem. Soc*. **2003**, *14*, 744-749.
[22] H. LeVine, *Protein Sci*. **1993**, *2*, 404–410.

concentration of 20 µM and its fluorescence was measured. **Fig. 9** shows the results of the ThT assay.

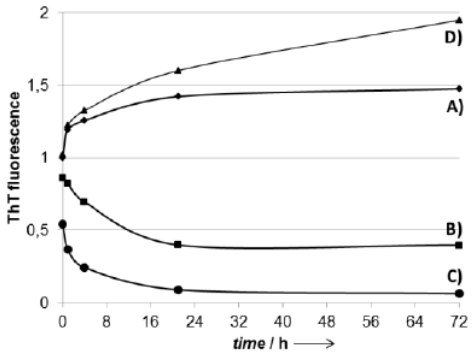

Figure 9. Effects of RA, methyl caffeate and methyl cinnamate on the kinetics of Aβ peptide aggregation, followed through ThT assay. The reaction mixtures containing 100 µM Aβ, PBS, pH 7.5, 50 mM PO_4^{2-},100 mM NaCl alone (A) or an equimolar amount of RA (B), methyl caffeate (C) or methyl cinnamate (D) were incubated at 37°C for the indicated times and ThT fluorescence was measured. Each curve shows a representative pattern of three independent experiments. Fluorescence values were normalized respect to the value measured for the sample containing the peptide alone at t0.

As expected, ThT fluorescence increased over time for the sample containing the peptide alone (**Figure 9A**), as a consequence of Aβ aggregation. Conversely, a fluorescence decrease was observed for the samples incubated with RA (**Figure 9B**) and methyl caffeate (**Figure 9C**), meaning that these molecules not only inhibit the aggregation, but also play a disaggregating activity. In particular, methyl caffeate exerts the stronger effect, as deduced from the lower fluorescence values measured. Indeed, the fluorescence rose over time, also for the mixture containing methyl cinnamate (**Figure 9D**). The increase was higher than for the peptide alone, suggesting that this compound promoted Aβ aggregation. This result is in agreement with the previous observation about the tendency of the sample to precipitate under the NMR conditions. In fact, Aβ aggregate solubility in water decreases with the increase in size of the aggregates themselves.

Conclusion

The potential of NMR approaches for the screening of natural product mixtures obtained from plant extracts has been already described.[23] Nevertheless, to the best of our knowledge, no examples in this context concerning the identification of substances able to interact with amyloid aggregates has been provided. The results here reported demonstrate that NMR spectroscopy, in particular STD and trNOESY experiments, are a powerful tool to screen extracts from natural sources for the presence of Aβ peptide ligands. The availability of new screening methods is strategic. In fact, due to AD severe impact on patients and their families' quality of life, its massive economic burden, and the lack of effective therapies and diagnostic tools, there is an urgent need for effective molecules for AD treatment. In this work, exploiting NMR techniques we were able to reveal the binding of RA, a major component of the butanol extract of *Salvia sclareoides*, to Aβ oligomers. RA has been previously identified as the mainly responsible molecule for the neuroprotective effect of sage against Aβ peptide neurotoxicity.[8] In this context, the characterization of the Aβ oligomer recognition and binding processes is crucial for the rational design of new ligands with higher affinity for Aβ aggregates, suitable for the development of innovative tools for both the therapy and the diagnosis of AD. Through the study of the RA binding mode, this information has been gathered, also allowing to identify two natural compounds, methyl caffeate and methyl cinnamate, as good ligand of Aβ1-42 oligomers. In addition, their effect on Aβ aggregation has been studied, getting evidences of methyl caffeate disaggregating properties. The significance of this result increases in the light of the recent discovery about the methyl caffeate antidiabetic activity,[19] that fits with the accumulation of amyloid fibrils in type 2 diabetes.[24] This fact suggests that this compound could be effective against both pathologies. Our

[23] a) M. Politi, M. I. Chávez, F. J. Cañada, J. Jiménez-Barbero, *Eur. J. Org. Chem.* **2005**, 1392-1396; b) M. Politi, J. Alvaro-Blanco, P. Groves, A. Prieto, J. Antonio Leal, F. J. Cañada, J. Jiménez-Barbero, *Eur. J. Org. Chem.* **2006**, 2067–2073; c) Politi M, Silipo A, Siciliano T, Tebano M, Flamini G, Braca A, Jiménez-Barbero *J. Phytochem. Anal.* **2007**, *18*, 33-41.

experimental results provide a further demonstration of the great relevance of NMR spectroscopy in the drug discovery field. Moreover, due to the growing interest in nutraceutical and functional food sciences, NMR can be also validated as a key tool for new and alternative therapeutic approaches.

Experimental Section

Plant material and extraction

Aerial parts of *S. sclareoides Brot.* (*Labiatae*), collected at the Lizandro Estuary, Mafra, Portugal in May, were identified in the Herbarium Joao Carvalho Vasconcelos (LISI), Instituto Superior de Agronomia, Universidade Tecnica de Lisboa, Portugal, where a voucher specimen was deposited.

The air-dried and finely powdered aerial parts (100 g) of the plant were macerated with dichloromethane overnight, at room temperature (rt). After filtration of the macerate, the plant was then extracted first with methanol, which was filtered off, and then with a 50% methanol aqueous solution. Methanol was evaporated and the aqueous phase was extracted with *n*-butanol, to give the butanol extract (3 g).

Standards and reagents

Rosmarinic acid, thionyl chloride and all the solvents used for synthesis were purchased from Sigma Aldrich. Palladium on activated carbon and caffeic acid were purchased from Fluka.

Synthesis

Preparation of methyl caffeate [IUPAC name: (2*E*)-3-(3,4-dihydroxyphenyl)prop-2-enoate] **(1)**. Caffeic acid (50 mg, 0,277 mmol) was dissolved in dry methanol (2,5 mL), and $SOCl_2$ (0,03 mL, 0,4 mmol) was added to the solution. The reaction mixture was stirred at room temperature under argon atmosphere for 18 hours. The solvent was evaporated and the crude purified by flash chromatography on silica gel (eluent

[24] C. Glabe, Neurobiol. *Aging* **2006**, *27*, 570–575.

petroleum ether/ethyl acetate/methanol=7/3/0,5) affording caffeic acid methyl ester as a yellow powder (yield = 97%). ^{1}H NMR (400 MHz, Methanol-d4) δ 7.53 (d, J = 15.9 Hz, 1H, H13), 7.03 (d, J = 2.1 Hz, 1H, H15), 6.92 (dd, J = 8.2, 2.1 Hz, 1H, H16), 6.77 (d, J = 8.2 Hz, 1H, H17), 6.24 (d, J = 15.9 Hz, 1H,H14), 3.74 (s, 3H, CH3). ^{13}C NMR (101 MHz, Methanol-d4) δ 169.67, 149.51, 146.86, 127.62, 122.85, 116.41, 115.04, 114.76, 51.92.

Preparation of 3-(3,4-dihydroxyphenyl)propanoic acid **(2)**. Caffeic acid (50 mg, 0,277 mmol) was dissolved in degassed methanol (4 mL) and palladium on activated carbon was added as catalyst. The reaction mixture was stirred at room temperature under hydrogen atmosphere for 3 hours. The mixture was filtered to remove the catalyst and the solvent was evaporated. The crude was purified with flash chromatography on silica gel (eluent petroleum ether/ethyl acetate/methanol=7/3/0,5) affording saturated caffeic acid as a yellow powder (yield = 83%). ^{1}H NMR (400 MHz, Methanol-d4) δ 6.70 – 6.61 (m, 2H, Ar), 6.52 (dd, J = 8.0, 2.0 Hz, 1H, Ar), 2.75 (t, J = 7.7 Hz, 2H, CH2), 2.51 (t, J = 7.7 Hz, 2H, CH2). ^{13}C NMR (101 MHz, D_2O) δ 177.08, 146.12, 144.52, 133.75, 120.41, 116.27, 110.07, 37.24, 31.47.

NMR spectroscopy binding studies

NMR experiments were recorded on a Varian 400-MHz Mercury instrument. Aβ1-42 was purchased from Anaspec, methyl cinnamate from Sigma-Aldrich. Immediately before use, lyophilized Aβ1-42 was dissolved in 10 mM NaOD in D_2O at a concentration of 160μM, then diluted 1:1 with 10 mM phosphate buffer saline, pH 7.4 containing 100 mM NaCl (PBS) and butanol extract of *Salvia sclareoides* or one of the tested compounds. In particular, the final concentrations/quantities of Aβ1-42, RA, compound **1**, compound **2**, compound **3** and the butanol extract of *Salvia sclareoides* in the samples were 80 uM, 1 mM, 1 mM, 1 mM and 1 mg respectively. The pH of each sample was verified with a Microelectrode (Mettler Toledo) for 5 mm NMR tubes and adjusted with NaOD and/or DCl. All pH values were corrected for isotope effect. The basic VARIAN sequences were employed for 2D-TOCSY, 2D-NOESY, ^{13}C-HSQC, DOSY and STD experiments. For STD, a train of Gaussian-shaped pulses each of 50 ms was employed to saturate selectively the protein envelope; the total saturation time of the

protein envelope was adjusted by the number of shaped pulses and was varied between 3 s and 0.3 s. For the quantitative NMR experiment, 1 mg of butanol extract of *Salvia sclareoides* was dissolved in 550 µL of D_2O and DSS was added to the final concentration of 0.4 mM. A ^1H spectrum was acquired with a recycle delay of 60 s to achieve the complete relaxation of all the resonances at each scan. The quantification was performed by comparing the DSS methyl resonance integral with the RA aromatic resonance integrals.

Molecular Mechanics (MM) calculations

Molecular mechanics were conducted with MacroModel 9.8.2078 as implemented in version 9.1.207 of the Maestro suite, using the MM3* force field.[25] A systematic variation of the torsional degrees of freedom of the molecules permitted generating different starting structures that were further minimized to provide the corresponding local minima. The continuum GB/SA solvent model was employed and the general PRCG (Polak–Ribiere Conjugate Gradient) method for energy minimization was used. An extended cut-off was applied.

Thioflavin T (ThT) assay

Aβ1-42, dissolved at a concentration of 100 µM in PBS, pH=7.5, was incubated for 74 h at 37°C under gentle shaking, with and without an equimolar concentration of RA, methyl caffeate or methyl cinnamate. For each fluorescence measurement, ThT was added at a final concentration of 20 µM to 150 µL of the samples. Fluorescence spectra were acquired with a Varian Cary Eclipse Fluorescence Spectrophotometer (exc. wavelength: 450 nm; emission wavelength = 482 nm).

Acknowledgements

The research leading to these results has received funding from Regione Lombardia, Fondo per la promozionedi accordi istituzionali, Progetto no. 4779 ‘‘Network Enabled Drug Design (NEDD)’’. The authors also thank FCT-Portugal for a post-doc research

grant (SFRH/BPD/65462/2009) and for the financial support of CQB Strategic Project PEst-OE/QUI/UI0612/2011. The group at Madrid thanks MINECO of Spain (grant CTQ2012-32025), Comunidad de Madrid (MHit project), and EU (GlycoHit and Glycopharm projects, and COST actions CM1102 and BM1003)

Supporting Information

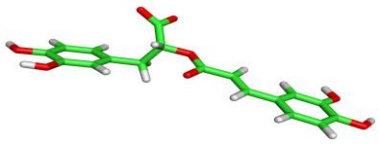

Figure 1S. Extended conformations calculated by MM3* for RA.

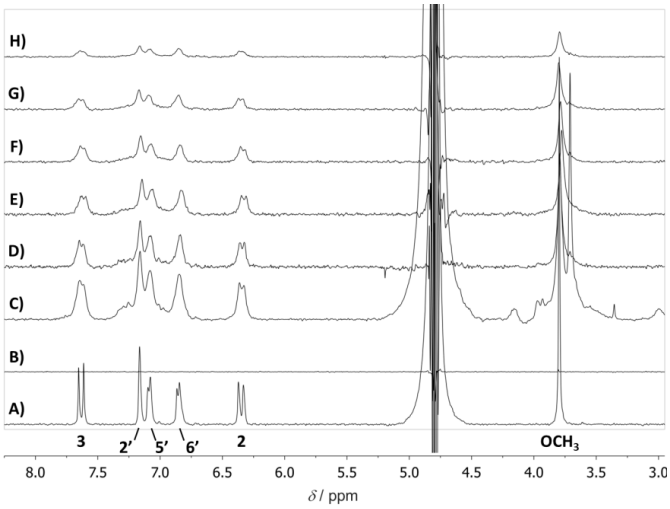

Figure 2S. A) ^{1}H NMR spectrum of 1 mM methyl caffeate; B) blank STD-NMR spectrum of the same sample acquired with a saturation time of 2s; C) ^{1}H NMR spectrum of the mixture containing 80 uM Aβ1-42 and 1 mM methyl caffeate; D-H) STD-NMR spectra of the same mixture acquired with different saturation times. (D, 3.0 s; E, 2.0 s; F, 1.3 s; G, 0.8 s; H, 0.3 s). Both samples were dissolved in deuterated PBS, pH 7.5, 25°C. The spectra were recorded at 400 MHz.

---

[25] N. L. Allinger, Y. H. Yuh and J. H. Lii, *J. Am. Chem. Soc.* **1989**, *111*, 8551-8566.

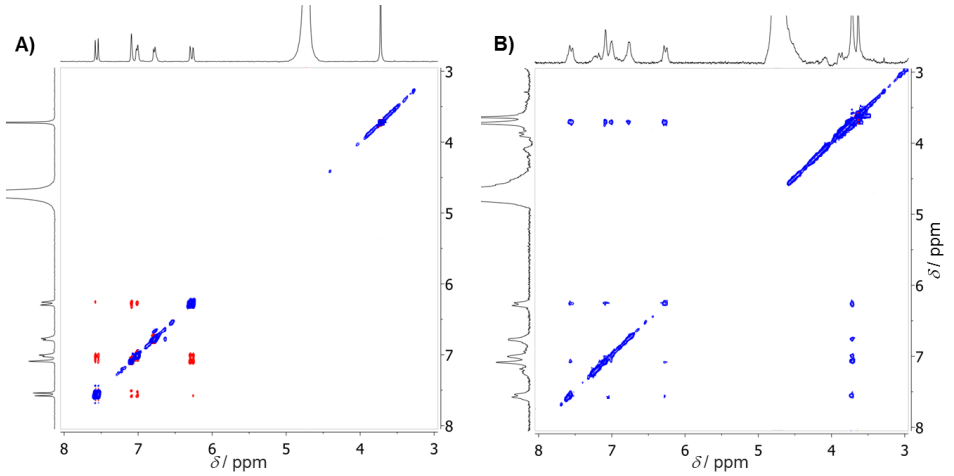

Figure 3S. A) 400 MHz 2D-NOESY spectrum of 1mM methyl caffeate with a mixing time of 0.9 s. B) trNOESY of the mixture containing Aβ1-42 (80 uM) and 1mM methyl caffeate, with a mixing time of 0.3 s. Both samples were dissolved in deuterated PBS, at pH 7.5 and 25°C. Positive cross-peaks are in red, negative in blue.

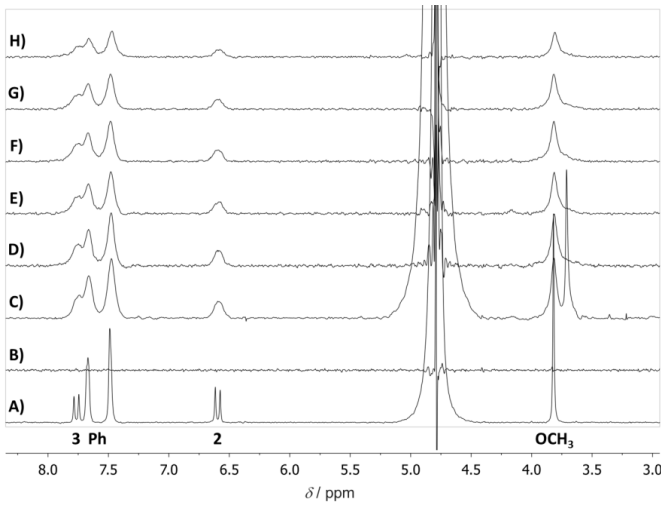

Figure 4S. A) ^{1}H NMR spectrum of 1mM methyl cinnamate; B) blank STD-NMR spectrum of the same sample acquired with a saturation time of 2s; C) ^{1}H NMR spectrum of the mixture containing 80 uM Aβ1-42 and 1mM methyl methyl cinnamate; D-H) STD-NMR spectra of the same mixture acquired with different saturation times. (D, 3.0 s; E, 2.0 s; F, 1.3 s; G, 0.8 s; H, 0.3 s). Both samples were dissolved in deuterated PBS, pH 7.5, 25°C. The spectra were recorded at 400 MHz.

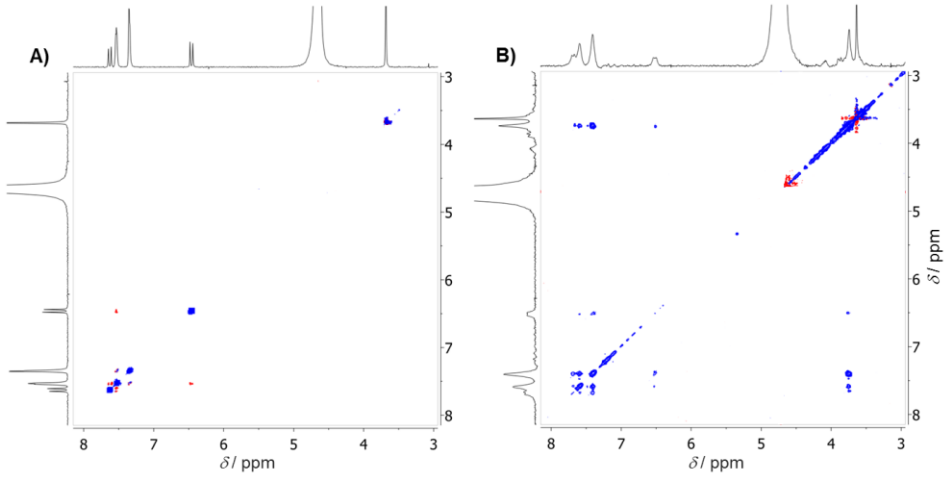

Figure 5S. A) 400 MHz 2D-NOESY spectrum of 1mM methyl cinnamate with a mixing time of 0.9 s. B) trNOESY of the mixture containing Aβ1-42 (80 uM) and 1mM methyl cinnamate, with a mixing time of 0.3 s. Both samples were dissolved in deuterated PBS, at pH 7.5 and 25°C. Positive cross-peaks are in red, negative in blu

Conclusions and Remarks

This work allowed the development of NMR experimental protocols useful for the screening of potential anti-amyloidogenic compounds and for the characterization of their binding to Aβ oligomers.

In particular the interaction of tetracycline, curcumin, rosmarinic acid and some derivatives of them was investigated.

For all these compounds, the aromatic moieties were identified as the binding epitope, essential for the interaction.

Some glycofused tricyclic derivatives were then synthesized as tetracycline analogues with better characteristics in terms of chemical stability and solubility respect to tetracycline, and their binding to Aβ peptides was confirmed. A further derivatization of the best tricyclic ligands allowed the production of fluorescent Aβ ligands, able to cross an *in vitro* model of blood brain barrier and stain Aβ deposits in brain sections. These molecules represent potential diagnostic tools for Alzheimer's Disease.

Curcumin derivatives more stable and soluble in water, and functionalized for conjugation with nanoparticles, were also synthesized. Their binding to Aβ oligomers was confirmed by STD-NMR experiments, and their ability to stain Aβ deposits verified by fluorescence microscopy.

The interaction of Aβ oligomers with rosmarinic acid present in *Salvia sclareoides* extracts was releaved, demonstrating the potential of NMR spectroscopy to perform the screening of natural product mixtures for the identification of substances able to interact with amyloid aggregates. NMR studies on the purified molecule allowed the detection of a bound conformation of rosmarinic acid different from that of the free molecule in solution. Moreover methyl caffeate, a rosmarinic acid derivative, was identified

as a compound able to bind Aβ peptides, also displaying disaggregating properties.

Other Papers:

1. Barbara La Ferla, Cristina Airoldi, Cristiano Zona, Alexandre Orsato, Francisco Cardona, Silvia Merlo, Erika Sironi, Giuseppe D'Orazio and Francesco Nicotra "Natural glycoconjugates with antitumor activity" *Nat. Prod. Rep.*, **2011**, 28, 630-648
2. Cristina Airoldi, Erika Sironi, Barbara La Ferla, Francisco Cardona, Francesco Nicotra "Abeta monomers, oligomers and fibrils: structural features", Current Bioactive Compounds, **2011**, 7, 198-213.
3. Claudia Manzoni; Laura Colombo; Paolo Bigini; Valentina Diana; Alfredo Cagnotto; Massimo Messa; Monica Lupi; Valentina Bonetto; Mauro Pignataro; Cristina Airoldi; Erika Sironi; Alun Williams; Mario Salmona "The molecular assembly of amyloid Abeta controls its neurotoxicity and binding to cellular proteins", PlOsOne, **2011**, vol. 6, issue 9, e24909.
4. Cristina Airoldi, Silvia Merlo, Erika Sironi, Francesco Nicotra, Jesus Jimenez-Barbero "NMR Tools For Protein-Ligand Interaction Studies under Non-Homogeneous Conditions: A Model For Artificial Lectin-Carbohydrate Recognition", Journal of Material Science and Engineering, in press, **2012**
5. Cristina Airoldi, Silvia Merlo, Erika Sironi, "NMR molecular recognition studies for the elucidation of protein and nucleic acid structure and function" in e-Book Series on Application of NMR Spectroscopy in Molecular Identification, in press, **2012**

Patents:

1. Italian patent "Nuovi tricicli glicofusi quali ligandi del peptide beta-amiloide", (RM2011A000264), inventors: Francesco Nicotra (19%), Barbara La Ferla (19%), Cristina Airoldi (19%), Francisco Cardona (19%), Erika Sironi (19%), Massimo Masserini (5%).

Oral Communications:

1. Sironi E., Airoldi C., Cardona F., La Ferla B., Colombo L., Manzoni C., Salmona M., Nicotra F., "NMR characterization of the interaction between Abeta peptides and small ligands for the development of new anti-Alzheimer's drugs", Italian-Spanish Joint Workshop CARIPLO project 2008-3175, April 22, **2010**, Milan, Italy.

2. Sironi E., Airoldi C., Cardona F., La Ferla B., Zona C., Nicotra F. "New Aβ peptide ligands for the diagnosis and therapy of Alzheimer's Disease" NAD 3rd Annual Meeting & Conference in combination with Satellite Event to the EuroNanoForum 1-3rd June **2011**, Budapest, Hungary.

Other Communications:

1. Airoldi C., Sironi E., Colombo L., Manzoni C., Natalello A., Del Favero E., Cantù L., Doglia M.S., Nicotra F., Salmona M. "NMR characterization of Abeta peptide-tetracycline interaction". EUROMAR **2009**, Goteborg (Svezia), 5-9 luglio.

2. Russo L., Shaikh N., Airoldi C., Merlo S., Sironi E., Bini D., Gabrielli L., Cipolla L., Nicotra F., "Design of Smart Biomaterials, Chemical Tools for Molecular Recognition studies: Synthesis and NMR Characterization of Bioactive Molecules", Italian-Spanish Joint Workshop CARIPLO project 2008-3175, April 22, **2010**, Milan, Italy.

3. Zona C., La Ferla B., Airoldi C., Aurilia D., Sironi E., Nicotra F., "Design and synthesis of molecular device for therapy and diagnosis of Alzheimer's Disease", Italian-Spanish Joint Workshop CARIPLO project 2008-3175, April 22, **2010**, Milan, Italy.

4. La Ferla B., Cardona F., Sironi E., Airoldi C., Silva A., Nicotra F.," Glycofused polycycles as beta-amyloid peptides ligands", XII Convegno-Scuola sulla Chimica dei Carboidrati, 20-23 Giugno **2010**, Pontignano (SI).

5. Cardona F., La Ferla B., Sironi E., Airoldi C., Silva A., Nicotra F., "Synthesis and NMR interaction studies of glycofused tricycles as beta-amyloid peptides ligands", XII Belgian Organic Synthesis Symposium, July 11-16, **2010**, Namur, Belgium.

6. Airoldi C., Sironi E., Colombo L., Manzoni C., Salmona M., Nicotra F., "Abeta peptide-small molecule interaction studies as a tool for the development of new anti-Alzheimer's drugs", 14th International Biotechnology Symposium and Exhibition, Biotechnology for the Sustainability of Human Society, September 14-18, **2010**, Rimini, Italy.

7. Airoldi C., Sironi E., Merlo S., Macchi E., Nicotra F., Jimenez-Barbero J.," New NMR tools for the study of receptor-ligand interactions in non-homogenous media", 14th International Biotechnology Symposium and Exhibition, Biotechnology for the Sustainability of Human Society, September 14-18, **2010**, Rimini, Italy.

8. Zona C., La Ferla B., Airoldi C., Aurilia D., Sironi E., Nicotra F., "Design and synthesis of ligands and nanoparticles for therapy and diagnosis of Alzheimer's Disease", 14th International Biotechnology Symposium and Exhibition, Biotechnology for the Sustainability of Human Society, September 14-18, **2010**, Rimini, Italy.

9. Airoldi C., Merlo S., Sironi E., Macchi E., Nicotra F., Jimenez-Barbero J., "Novel NMR applications for characterizing ligand-receptor interactions under non-homogeneus conditions", V GERMN Bienal Meeting, September 26-29, **2010**, Bilbao, Spain.

10. Nicotra F., La Ferla B., Airoldi C., Sironi E., Cardona F., Zona C. " Aβ-Peptide Ligands for the Therapy and Diagnosis of Alzheimer's Disease", GAFHI 2011, May 26-29, **2011**, Goslar, Germany.

11. Nicotra F., Cardona F., La Ferla B., Sironi E., Airoldi C., Silva A. "Glycofused tricycles as beta-amyloid peptide ligands for the diagnosis

and therapy of Alzheimer's Disease", 16th European Carbohydrate Symposium July 3-7, **2011**, Naples, Italy.

12. Sironi E., Airoldi C., Cardona F., La Ferla B. and Nicotra F., "NMR characterization of glycofused tricycles as new Abeta peptide ligands for the diagnosis and therapy of Alzheimer's Disease", SMASH, Chamonix, 18-21 September **2011.**

13. Merlo S., Airoldi C., Sironi E., Nicotra F., Jimenez Barbero J., "NMR Characterization of Osteogenic Growth Peptide Interaction with alfa2-macroglobulin", SMASH, Chamonix, 18-21 September **2011**.

14. Airoldi C., Merlo S., Sironi E., Macchi E., Nicotra F., Jimenez Barbero J. "NMR Tools for Protein-Ligand Interaction Studies Under Non-Homogeneous Conditions: The Example of Lectin - Carbohydrate Recognition", SMASH, Chamonix, 18-21 September **2011**.

15. Sironi E., Airoldi C., Cardona F., La Ferla B., Colombo L., Messa M., Nicotra F. "Synthesis and NMR characterization of glycofused tricycles as new Abeta peptide ligands for the diagnosis and therapy of Alzheimer's Disease", International Carbohydrate Symposium, Madrid, 22-26 July **2012**.

16. Merlo S., Airoldi C., Sironi E., Macchi E., Nicotra F.; Jimenez-Barbero J. "A model for lectin-carbohydrate recognition exploited for NMR interaction studies in heterogeneous systems ", International Carbohydrate Symposium, Madrid, 22-26 July **2012**.

17. Airoldi C., Merlo S., Sironi E., La Ferla B., Nicotra F., Jiménez-Barbero J. "Improving saturation transfer difference NMR experiments of membrane proteins in living cells: the interaction of the SGLT1 cotransporter with its ligands", International Carbohydrate Symposium, Madrid, 22-26 July **2012**.

18. Sironi E., Merlo S., Airoldi C., Cardona F., La Ferla B., Messa M., Colombo L., Salmona M., Nicotra F. “NMR characterization of glycofused tricycles as ligand for amyloidogenic peptides: going towards the development of new tools for the diagnosis and therapy of neurodegenerative disorders”, XLI National Congress on Magnetic Resonance, Pisa, 17-19 September **2012**.

19. Sironi E., Airoldi C., Jimenez-Barbero J., Nicotra F. “Natural compounds against Alzheimer’s Disease: NMR investigation on the interaction between rosmarinic acid and amyloid beta peptides” , XLI National Congress on Magnetic Resonance, Pisa, 17-19 September **2012**.

20. Airoldi C., Merlo S., Sironi E., La Ferla B., Jimenez-Barbero J., Nicotra F. “Improving saturation transfer difference NMR experiments of membrane proteins in living cells with HR-MAS NMR” , Pisa, 17-19 September **2012**.

21. Merlo S., Airoldi C., Sironi E., Macchi E., Nicotra F., Jimenez-Barbero J. “Recognition processes in non-homogeneous media by HR-MAS NMR: artificial lectin interaction with carbohydrates”, Pisa, 17-19 September **2012**.

22. Airoldi C., Sironi E., Merlo S., Cardona F., La Ferla B., Colombo L., Messa M., Salmona M., Nicotra F. “Towards the development of new tools for the diagnosis and therapy of neurodegenerative diseases: NMR characterization of glycofused tricycles as new amyloidogenic peptide ligands, Convegno Nazionale della divisione di chimica dei sistemi biologici, Naples, 24-25 September **2012.**